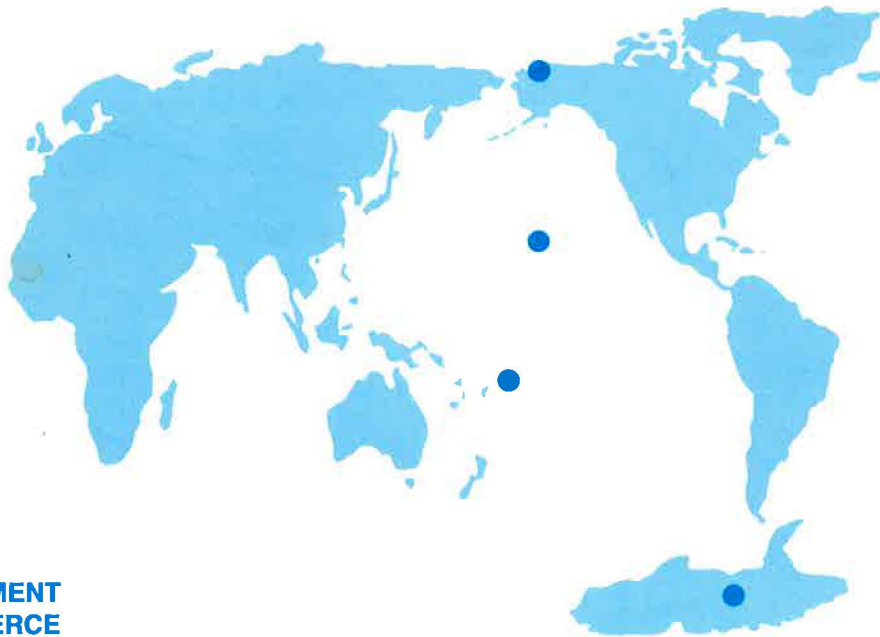


Climate Monitoring and Diagnostics Laboratory

No. 21

Summary Report 1992



U.S. DEPARTMENT
OF COMMERCE

NATIONAL
OCEANIC AND
ATMOSPHERIC
ADMINISTRATION

ENVIRONMENTAL
RESEARCH
LABORATORIES





Climate Monitoring and Diagnostics Laboratory No. 21

Summary Report 1992

James T. Peterson, Editor
Rita M. Rosson, Assistant Editor

Boulder, Colorado

December 1993

U.S. DEPARTMENT OF COMMERCE

Ronald H. Brown, Secretary

National Oceanic and Atmospheric Administration
D. James Baker, Under Secretary for Oceans and Atmosphere/Administrator
Environmental Research Laboratories
Alan R. Thomas, Director

NOTICE

Mention of a commercial company or product does not constitute an endorsement by NOAA Environmental Research Laboratories. Use for publicity or advertising purposes of information from this publication concerning proprietary products or the tests of such products is not authorized.

Contents

CMDL Staff, 1992	vi
CMDL Station Information	vii
1. Observatory Operations Division	1
1.1. Mauna Loa	1
1.1.1. Operations	1
1.1.2. Programs	1
1.2. Barrow	7
1.2.1. Operations	7
1.2.2. Programs	7
1.3. Samoa	9
1.3.1. Operations	9
1.3.2. Programs	10
1.4. South Pole	12
1.4.1. Operations	12
1.4.2. Programs	13
1.5. References	15
2. Carbon Cycle Division.....	16
2.1. Continuing Programs	16
2.1.1. In Situ Carbon Dioxide Measurements	16
2.1.2. Flask Sample Carbon Dioxide Measurements	17
2.1.3. In Situ Methane Measurements	19
2.1.4. Flask Measurements of Methane	20
2.1.5. In Situ Carbon Monoxide Measurements.....	22
2.1.6. Flask Measurements of Carbon Monoxide.....	23
2.2. Reference Gas Standards	24
2.2.1. Carbon Dioxide.....	24
2.2.2. Carbon Monoxide.....	25
2.3. New Measurement Programs	26
2.3.1. Measurements of Carbon Dioxide on a Very Tall Tower.....	26
2.3.2. Flask Samples From Aircraft.....	27
2.4. Data Management.....	28
2.5. References	29
3. Aerosols, Radiation, Ozone, and Water Vapor Division.....	30
3.1. Continuing Programs	30
3.1.1. Surface Aerosols	30
3.1.2. Lidar Observations of Aerosols	34
3.1.3. Total Ozone Observations	34
3.1.4. Umkehr Observations.....	36
3.1.5. Calibration of CMDL Dobson Spectrophotometers	36
3.1.6. Validation of TOMS and Satellite Instrument Ozone Data	39
3.1.7. Tropospheric Ozone	39
3.1.8. Ozonesonde Observations	40
3.1.9. Stratospheric Water Vapor	41
3.1.10. Surface Radiation.....	42
3.1.11. Solar Radiation Facility	45
3.1.12. Atmospheric Trajectory Analysis	46

3.2.	Special Project - A Decrease in Arctic Haze at BRW.....	47
3.3.	References	49
4.	Acquisition and Data Management Division	51
4.1.	Continuing Programs	51
4.1.1.	Station Climatology	51
4.1.2.	Data Management	58
4.2.	Reference	58
5.	Nitrous Oxide and Halocarbons Division	59
5.1.	Continuing Programs	59
5.1.1.	Flask Samples	59
5.1.2.	RITS Continuous Gas Chromatograph Systems at CMDL Baseline Stations and Niwot Ridge	59
5.1.3.	Low Electron Attachment Potential Species (LEAPS).....	61
5.1.4.	Alternative Halocarbon Measurements.....	61
5.1.5.	Gravimetric Standards.....	65
5.2.	Special Projects	67
5.2.1.	Aircraft Measurements of the CFCs	67
5.2.2.	Ocean/Atmosphere Exchange of Trace Compounds	69
5.2.3.	Software Development.....	73
5.3.	References	74
6.	Director's Office	76
6.1.	Introduction.....	76
6.2.	Methods.....	76
6.3.	Results.....	77
6.3.1.	Stratospheric Aerosol Optical Depth	77
6.3.2.	Stratospheric Aerosol Measurements.....	77
6.4.	Discussion	79
6.5.	References.....	80
7.	Cooperative Programs	81
	Antarctic Ultraviolet Spectroradiometer Monitoring Program: South Pole and Barrow Contrasts in UV Irradiance <i>C.R. Booth, T. B. Lucas, J.R. Tusson IV, J.H. Morrow, and T. Mastechkina</i>	81
	Lidar Observations of Volcanic Aerosol Layers and Polar Stratospheric Clouds at South Pole, 1990, 1991, and 1992 <i>M. Cacciani, P. DiGirolamo, A. DiSarra, G. Fiocco, D. Fuà, P. Colagrande, and G. Panegrossi</i>	84
	Fine Sulfur Concentrations at the Mauna Loa Observatory and Other Hawaiian Sites <i>T.A. Cahill</i>	86
	Artificial Windshielding of Precipitation Gauges in the Arctic <i>G.P. Clagett</i>	92
	A Comparison of Aerosol Size Distributions and Nephelometer Measurements at Mauna Loa Observatory <i>A. Clarke and B. Bodhaine</i>	93
	Improved MFOV Performance at Mauna Loa <i>P.F. Hein, J.M. Davis, and S.K. Cox</i>	97
	Atmospheric Methane at Cape Meares, Oregon <i>M.A.K. Khalil and R.A. Rasmussen</i>	100
	Radioactivity in the Surface Air at BRW, MLO, SMO, and SPO during 1992 <i>R.J. Larsen and C.G. Sanderson</i>	102

Tomsk-7 Debris at BRW: Detection and Transport <i>H.N. Lee, R.J. Larsen, and C.G. Sanderson</i>	104
Ultrahigh Resolution Infrared Solar Spectra from Mauna Loa Observatory <i>F.J. Murcray, S.J. David, R.D. Blatherwick, A. Goldman, and D.G. Murcray</i>	106
Advanced Global Atmospheric Gases Experiment (AGAGE) <i>R.G. Prinn, R.F. Weiss, F.N. Alyea, D.M. Cunnold, P.J. Fraser, L.P. Steele, and P.G. Simmonds</i>	108
The ¹³ C/ ¹² C of Atmospheric Methane <i>P. Quay, J. Stutsman, and D. Wilbur</i>	111
Non Seasalt Sulfate to Methanesulfonate Ratios at American Samoa <i>D.L. Savoie and J.M. Prospero</i>	112
USGS Barrow Observatory <i>J. Townshend</i>	115
Separation of Local From Distant Pollution at MLO Using PB-212 <i>S. Whittlestone, S.D. Schery, and Y. Li</i>	116
Recent Interannual Variations in CO ₂ in Both Hemispheres <i>T.P. Whorf, C.D. Keeling, and D.M. Wahlen</i>	119
8. International Activities, 1992	123
9. Publications and Presentations by CMDL Staff, 1992	126
10. Acronyms and Abbreviations	129

CMDL Staff, 1992

Director's Office

Eldon Ferguson, Director
James T. Peterson, Deputy Director
Donna Leise, Administrative Officer
Sandra Howe, Administrative Assistant
Carole Brandes, Secretary
Ellen Hardman, Secretary
Rita Rosson, Editorial Assistant
Denise Theede, Program Clerk

Special Projects

Howard Bridgman, Visiting Scientist
M. Kiskey, CIRES
Craig Quincy, CIRES
Mark Serreze, CIRES
Patrick Sheridan, CIRES
Spencer Shiotani, Physical Science Aid
Ludmilla Sokolik, NRC Post Doctorate

Aerosols, Radiation, Ozone & Water Vapor Division

David Hofmann, Chief
Jill Foose, Secretary
Jennifer Barnett, Physical Science Aid
Barry Bodhaine, Meteorologist
Paul Chilson, Physical Science Aid
John DeLuisi, Meteorologist
Ellsworth Dutton, Meteorologist
Robert Evans, CIRES
Jason Gingerich, Physical Science Aid
Robert Grass, CIRES
Rudy Haas, Mathematician
Bradley Halter, CIRES
Joyce Harris, Physical Scientist
Todd Idler, Physical Science Aid
Gloria Koening, Computer Programmer
Walter Komhyr, Physicist
Thomas Kotsines, Physical Science Aid
Jeffrey Lathrop, Physical Scientist
Kent Leonard, CIRES
David Longenecker, CIRES
Donald Nelson, Meteorologist
John Ogren, Physical Scientist
Samuel Oltmans, Physicist
Micheal O'Neill, CIRES
Greg Orleans, Physical Science Aid
Gina Palmer, Physical Science Aid
Frank Polacek, III, Meteorological Technician
Gayland Pounder, Physical Science Aid
Dorothy Quincy, CIRES
Scott Sanberg, Electronic Technician

Scott Sio, Physical Science Aid
Robert Stone, CIRES
David Theisen, Physical Science Aid
Holger Vömel, CIRES
Byron Wells, Physical Science Aid
James Wendell, Electronic Technician

Acquisition and Data Management Division

Gary Herbert, Chief
Sheri Cox, Secretary
Mark Bieniulis, CIRES
Thomas Mefford, CIRES
Kenneth Thaut, Electronic Technician

Carbon Cycle Division

Pieter Tans, Chief
Carol Brandes, Secretary
Trey Moody, Secretary
Peter Bakwin, CIRES
Phillipe Ciais, NRC
Thomas Conway, Research Chemist
Wyatt Coy, CIRES
Mario DiCino, Physical Science Aid
Edward Dlugokencky, CIRES
Douglas Guenther, CIRES
Duane Kitzis, CIRES
Patricia Lang, Physical Scientist
Terry Lesoing, CIRES
Martin Manning, Visiting Scientist
Kenneth Masarie, CIRES
Paul Novelli, CIRES
Aaron Patton, CO-OP
Norman Sitter, Physical Science Aid
Michael Stavish, CO-OP
Kirk Thoning, Physicist
Michael Trolier, INSTAAR
Lee Waterman, Research Chemist
Ni Zhang, CIRES
Conglong Zhao, CIRES

Nitrous Oxide and Halocarbons Division

James Elkins, Chief
Carol Brandes, Secretary
Trey Moody, Secretary
Thomas Baring, Physical Science Aid
James Butler, Research Chemist
Scott Cummings, CIRES
Jennie Dolan, C.U. Work Study
Andrew Duang, C.U. Work Study
Geoffrey Dutton, CIRES
Timothy Gilpin, NRC

Arnold Hayden, CIRES Student
Garry Holcomb, Electronic Engineer
Kristen Kauffman, C.U. Work Study
Jürgen Lobert, CIRES
Richard Myers, Physical Science Technician
Steve Montzka, Research Chemist
Jae W. Nam, C.U. Work Study
Phuong Nguyen, CIRES Student
Matthew Nowick, C.U. Work Study
William Sturges, CIRES
Thomas Swanson, CIRES
Thayne Thompson, Physicist
Tina Waller, C.U. Work Study

Observatory Operations Division

Bernard Mendonca, Chief
Sheri Cox, Secretary

Daniel Endres, Station Chief, Barrow
Christopher Churylo, Electronic Engineer
Bradley Halter, Physical Scientist

Russell Schnell, Director, Mauna Loa
Judith Pereira, Program Support Technician
John Chin, Physicist
Thomas DeFoor, Electronic Engineer
Melody Keaunui, Clerk
Darryl Kuniyuki, NOAA Jr. Fellow
Steven Ryan, Physical Scientist
Robert Uchida, Electronic Technician
Alice Wall, Physical Science Aid
Alan Yoshinaga, Chemist

Carl Farmer, Station Chief, Samoa
Mark Winey, Electronic Engineer

Dale Tysor, NOAA Corps, South Pole
David Gaines, Electronic Engineer
Katherine, McNitt, NOAA Corps,
Raymond Dunn, Electronic Engineer
Carl Groeneveld, NOAA Corps
Thomas Jacobs, NOAA Corps

CMDL Station Information

Name:	Barrow (BRW)	Mauna Loa (MLO)
Latitude:	71.323	19.539
Longitude:	156.609	155.578
Elevation:	8 m	3397 m
Time Zone:	GMT -9	GMT -10
Office Hours:	8:00 am-5:00 pm	8:00 am-5:00 pm
Telephone		
Office hours:	(907) 852-6500	(808) 961-3788
Fax:	(907) 852-4622	(808) 961-3789
Postal Address:	Officer in Charge NOAA/ERL/CMDL Pouch 8888 Barrow, AK 99723	U.S. Dept. of Commerce NOAA - Mauna Loa Observatory P.O. Box 275 Hilo, HI 96720
Freight Address:	Same as above	U.S. Dept. of Commerce NOAA - Mauna Loa Observatory 154 Waianuenue Ave. Hilo, HI 96720
Name:	Samoa (SMO)	South Pole (SPO)
Latitude:	-14.232	-89.997
Longitude:	170.563	-102.0
Elevation:	77 m	2841 m
Time Zone:	GMT -11	GMT +12
Office Hours:	8:00 am-5:00 pm	8:00 am - 5:00 pm
Telephone:		
Office hours:	011 (684) 622-7455	Relayed through CMDL Boulder
After hours:	011 (684) 699-9953	
Fax:	011 (684) 699-4440	
Postal Address:	U.S. Dept. of Commerce NOAA - CMDL Samoa Observatory Pago Pago, American Samoa 96799	Officer in Charge NOAA/CMDL Clean Air Facility S-257 PSC 468 Box 402 FPO AP 96598-5402
Freight Address:	Same as above	Same as above

1. Observatory Operations Division

1.1. MAUNA LOA OBSERVATORY

R. C. SCHNELL

1.1.1. OPERATIONS

Two, month-long MLOPEX intensive study periods and the MLO electrical upgrade dominated the non-routine MLO activities during 1992. MLOPEX is an NCAR-organized free troposphere photochemistry experiment focusing on odd-nitrogen, odd-oxygen, and odd-hydrogen chemistry. The study utilized instruments mounted in four large ocean shipping containers; the equipment was operated by up to 25 scientists and support crew. Additional instruments for the study were mounted on the MLO meteorological tower. The AEC building was used by NCAR as a communication and data analysis center. Study periods occurred in April and July after which the instruments and containers were removed from the MLO site. It is expected that the results from the MLOPEX studies will provide valuable information on the sources, ages, and recent flow histories of air masses enveloping MLO in various seasons.

The MLO electrical upgrade consisted of re-installing all of the outdoor power distribution and data transmission cables into buried conduits. In addition, all buildings, the meteorological and air sampling towers, and the HAO facility were connected into a single, well-built grounding network. This construction began in April and lasted throughout the year.

A major upgrade of our computing facility occurred at the Hilo facility with the acquisition and installation of a VAX 4000 computer (provided by the NDSC program), three 486 PC's, and a high-capacity laser printer. All of the computers and printers in the Hilo offices have been connected with an Ethernet LAN, including the third floor office and basement labs.

MLO will be host to a Network for the Detection of Stratospheric Change (NDSC) facility to be built east of the observatory. NDSC is a set of high-quality, remote-sounding research stations for observing and understanding the physical and chemical state of the stratosphere. Plans for the ≈ 5000 ft² building and land acquisition were essentially completed in 1992.

Siting plans were developed for the future installation of the Global Oscillation Network Group (GONG) facility designed to study the core of the sun. This 5-year project by the National Solar Observatory, Tucson, Arizona, will include the installation of an unmanned trailer and solar tracker.

In 1992 MLO was visited by 393 signed-in guests. This number was influenced (on the high side) by the MLOPEX

activities. Few of the visitors coming to MLO are opportune walk-ins. Instead, most are knowledgeable in science and have MLO as their destination. About 50% of our visitors in 1992 were from Europe or Asia.

1.1.2. PROGRAMS

Three new CMDL programs were added in 1992: column water vapor, continuous CO, and UVB at 280-320 nm. Smaller changes in programs included discontinuing 3-L evacuated flasks for CO₂, CH₄, CO, ¹³C, ¹⁸O of CO₂ at MLO and increasing the size of flasks from 0.5 L to 3.0 L for the same gases at Cape Kumukahi. These programs have added 15% and one mountain staff day per week to the MLO workload over 1991.

Table 1.1 summarizes the programs in operation at MLO during 1992. Details of some of the programs are as follows:

Carbon Dioxide

The CMDL Siemens Ultramat-3 IR CO₂ analyzer and the SIO Applied Physics IR CO₂ analyzer were operated in parallel without major problems throughout the year. Routine maintenance and calibrations were undertaken on both instruments as scheduled.

The preliminary average MLO CO₂ concentration for 1992 was 356.2 ppm. The CO₂ annual growth rate between 1991 and 1992 was approximately 0.75 ppm. Compared to the previous year's growth rate of 1.3 ppm per year, this is a significant difference, a 42% drop.

Outgassing from the volcanic vents at the Mauna Loa caldera and along the northeast rift zone at Mauna Loa continued to cause periodic observable disturbances in some of the CO₂ data record. As in prior years, these venting events occurred mostly between midnight and 0800 LST of the following day, during the down slope wind regime. The erratic concentrations in the data resulting from venting events were easily identified by visually scanning chart records or by utilizing a computerized data screening procedure, and thus they have been separated from the clean-air record without difficulty. Such venting episodes were detected mainly on the basis of criteria for CO₂ concentration, CO₂ variability, and wind sector. The criterion for the CO₂ standard deviation screening was 1.0 ppm, which is the value suggested by *Thoning et al.* [1989].

The frequency of monthly occurrences of observable outgassing from volcanic vents on Mauna Loa for 1992 are listed in Table 1.2, and the annual number of events for the past 5 years are listed in Table 1.3.

The weekly CO₂, CH₄, and other gas sampling programs, using flasks at MLO and at Cape Kumukahi, were carried out according to schedule throughout the year, without problems.

TABLE 1.1. Summary of Measurement Programs at MLO in 1992

Program	Instrument	Sampling Frequency
<i>Gases</i>		
CO ₂	Siemens Ultramat-3 IR analyzer 3-L glass flasks†	Continuous 1 pair wk ⁻¹
CO	0.5-L glass flasks, through analyzer Trace Analytical RGA ³ reduction gas analyzer no. R5	1 pair wk ⁻¹ Continuous (5/92)
CO ₂ , CH ₄ , CO, ¹³ C, ¹⁸ O of CO ₂	0.5-L glass flasks, MAKS pump unit (MLO) 3-L glass flasks (Kumakahi)	1 pair wk ⁻¹
CH ₄	Carle automated GC no. 6	1 sample (24 min) ⁻¹
Surface O ₃	Dasibi ozone meter	Continuous
Total O ₃	Dobson spectrophotometer no. 76	3 day ⁻¹ , weekdays
O ₃ profiles	Dobson spectrophotometer no. 76 (automated Umkehr method) Balloonborne ECC sonde	2 day ⁻¹ 1 wk ⁻¹
CFC-11, CFC-12, N ₂ O	300-mL stainless steel flasks	1 pair wk ⁻¹
CFC-11, CFC-12, N ₂ O, CCl ₄ , CH ₃ CCl ₃ , CFC-113	HP5890 automated GC	1 sample (h) ⁻¹
CH ₃ Br, HCFC-22, CFC-113 CCl ₄ , CH ₃ CCl ₃ , CFC-113 Halon-1211, Halon-1301	0.8-L stainless-steel flasks	Monthly
N ₂ O	Shimadzu automated GC1	1 sample(h) ⁻¹
Radon	Two-filter system	Continuous integrated 30-min samples
<i>Aerosols</i>		
Condensation nuclei	Pollak CNC TSI CNC*	1 day ⁻¹ Continuous
Optical properties	Four-wavelength nephelometer*: 450, 550, 700, 850 nm	Continuous
Stratospheric and upper tropospheric aerosols	Lidar, 694.3 nm	1-3 profiles wk ⁻¹
Black carbon	Aethelometer	Continuous
Total suspended particles	High-volume sampler	2 samples (mo) ⁻¹
<i>Solar Radiation</i>		
Global irradiance	Eppley pyranometers with Q, OG1, and RG8 filters	Continuous
Direct irradiance	Eppley pyrliometer (2) with Q filter Eppley pyrliometer with Q, OG1, RG2, and RG8 filters	Continuous 3 day ⁻¹
Diffuse irradiance	Eppley/Kendall active cavity radiometer Eppley pyrgeometer with shading disk and Q filter*	1 mo ⁻¹ Continuous
Turbidity	J-202 and J-314 sunphotometers with 380-, 500-, 778-, 862-nm narrowband filters PMD three-wavelength sunphotometer*: 380, 500, 778 nm; narrowband	3 day ⁻¹ , weekdays Continuous
Ultraviolet radiation	Robinson-Berger UV radiometer (erythema)	Continuous
UV solar radiation (ARL)	Yankee Environmental UVB, pyranometer (280-320 nm)	Continuous (10/92)
Column water vapor	2 wavelength tracking sunphotometer	Continuous (4/92)
<i>Meteorology</i>		
Air temperature	Aspirated thermistor*, 2- and 40-m heights Max.-min. thermometers, 2-m height Hygrothermograph	Continuous 1 day ⁻¹ Continuous
Temperature gradient	Aspirated thermistors*, 2- and 40-m heights	Continuous
Dewpoint temperature	Dewpoint hygrometer*, 2-m height	Continuous
Relative humidity	Hygrothermograph	Continuous

TABLE 1.1. Summary of Measurement Programs at MLO in 1992—Continued

Program	Instrument	Sampling Frequency
<i>Meteorology - Continued</i>		
Pressure	Capacitance transducer* Mercurial barometer	Continuous 5 wk ⁻¹
Wind (speed and direction)	Bendix Aerovane*, 8.5- and 40-m heights	Continuous
Planetary boundary layer meteorology (PBL MET)	Wind vane, cup anemometer, and aspirated RTD thermometer (direction, speed, temperature at 3, 5, 10, 20, 30, and 40 m levels)	Continuous
Precipitation	Rain gauge, 8-in Rain gauge, 8-in‡ Rain gauge, tipping bucket*	5 wk ⁻¹ 1 wk ⁻¹ Continuous
Total perceptible water	Foskett IR hygrometer*	Continuous
<i>Precipitation Chemistry</i>		
pH	pH meter	Daily
Conductivity	Conductivity bridge	Daily
Chemical components	Ion chromatograph	As needed
<i>Cooperative Programs</i>		
CO ₂ (SIO)	Applied Physics IR analyzer	Continuous
CO ₂ , ¹³ C, N ₂ O (SIO)	5-L evacuated glass flasks†	1 pair wk ⁻¹
CO ₂ , CO, CH ₄ , ¹³ C/ ¹² C (CSIRO)	Pressurized glass flask sample	1 mo ⁻¹
Total suspended particles (DOE)	High-volume sampler (1 filter wk ⁻¹)	Continuous
CH ₄ (¹³ C/ ¹² C) (Univ. of Washington)	35-L evacuated flask	1 mo ⁻¹
Ultraviolet radiation (Smithsonian)	8-wavelength UV radiometer: 290-325 nm; narrowband	Continuous
Solar aureole intensity (CSU)	Multi-aperture tracking photometer: 2, 5, 10, 20, 30° fields of view	Continuous
Precipitation collection (DOE)	Exposed collection pails	Integrated monthly sample
Precipitation collection for organic acid analysis (Univ. of Virginia)	Aerochemetric automatic collector	Collection after each rain event
Wet-dry deposition (ISWS, NADP)	Aerochemetric automatic collector and weighing-bucket rain gauge	Integrated 7-day sample
Aerosol chemistry, upslope-downslope discrimination (Univ. of Washington)	Nuclepore filters	Inactive
Aerosol chemistry (Univ. of Calif.-Davis)	Programmed filter sampler	Integrated 3-day sample 1 continuous and 1 down-slope sample (3 days) ⁻¹
Various trace gases (OGIST)	Stainless steel flasks†	1 set wk ⁻¹ (3 flasks)
Sulfate, nitrate, aerosols (URI)	Filter system	Daily, 2000-0600 LST
Radon (ANSTO)	Aerosol scavenging of Rn daughters	Continuous; integrated 30-min samples
Formation of ³ He (WHOI)	Closed cylinder	Continuous 12-mo ambient exposure from 1/90
Solar spectra (Univ. of Denver)	FTIR spectrometer	1 wk ⁻¹
O ₂ /N ₂ (NCAR)	Three 5-L glass flasks	1 wk ⁻¹

All instruments are at MLO unless indicated.

*Data from this instrument recorded and processed by CAMS.

†MLO and Kumukahi.

‡Kulani Mauka

TABLE 1.2. Estimated Mauna Loa Venting Episodes (Total Time in Hours) at MLO in 1992*

Jan.	Feb.	March	April	May	June	July	August	Sept.	Oct.	Nov.	Dec.	Year
0	0	2	2	0	2	1	6	4	0	3	3	23

*Criteria: CO₂ SD ≥1.0 ppm; wind direction sector 135°-225°; wind speed ≥1.35 m s⁻¹.

TABLE 1.3. CO₂ Venting Events From 1988 Through 1992

Year	Total Time (Hours)
1988	200
1989	84
1990	48
1991	26
1992	23

Methane

The Carle automated GC system, "Carle 6," was in continuous operation throughout the year providing CH₄ data on the basis of a grab air sample being taken every 24 minutes. The instrument functioned well during the year.

The CH₄ data continued to show clearly defined cycles of varying frequencies. The typical diurnal cycle was well correlated with up- and downslope winds, with the marine boundary layer air having the higher CH₄ concentrations. There were also multi-day or synoptic scale CH₄ cycles observed that apparently relate to different air mass source regions. The MLO CH₄ measurements show CH₄ lost its upward trend in 1992 compared with 1991's gradual increase. The MLO 1992 monthly average CH₄ value was ~1725 ppb with the maximum occurring in March (~1735 ppb). There were decreases in CH₄ concentrations below the annual average in August (to ~1710 ppb), September (to ~1720 ppb) and October (to ~1720 ppb).

Carbon Monoxide

A Trace Analytical RGA3 reduction gas analyzer for the continuous measurement of CO mixing ratios was installed in May. System operations and chromatographic data logging are handled by an HP3396A integrator. The system has worked well since installation.

Ozone Monitoring

The 1992 MLO ozone monitoring program consists of three measurement phases: continuous MLO surface ozone monitoring using a Dasibi model 1003-AH UV absorption ozone monitor; daily total and Umkehr ozone profile measurements using a computer-based automated Dobson instrument (Dobson no. 76); and ozone profile measurements based on weekly ascents of balloon-borne

ECC ozonesondes released from the NWS station at the Hilo airport. In addition to the daily automated Umkehr measurements and 5-day-a-week total ozone measurements, five special early morning AD-CD direct sun observations were completed in 1993. The Dasibi ozone monitor performed in a fully satisfactory manner and provided a continuous, high-quality record of station-level ozone concentrations for the entire year. The weekly ozonesonde flights were coordinated with lidar observations to provide further opportunities to study the effects of the Pinatubo aerosol cloud on ozone chemistry.

Halocarbons and Nitrous Oxide

The RITS system had its annual major maintenance in February 1992. During this time a Best UPS was installed, valves were replaced or serviced on the HP-GC, leaking solenoids were replaced, older plastic (pneumatic) lines on the valves were replaced, and a back-flush needle valve was installed on the HP-GC. In addition, the low value reading was adjusted on the Shimadzu GC, and the air lines on the tower were fitted with beaker cover protectors. During this maintenance operation, the computer crashed and a replacement was shipped from Boulder (a bad power supply and back plane were replaced). The keyboard was also sent back to Boulder later for repair.

Comparison air supply option tests were conducted from April 17 to May 4 for various pump, tower air line, and aluminum stack configurations. From these tests, a minor leak problem was detected in the 41E1 valve in conjunction with the Valco valve in the stream select unit. This was repaired. In June the mid-tower air line was installed as AIR2 and the aluminum stack pump unit was disconnected from the system. In July the Best UPS frequency windows were expanded to allow greater flexibility for incoming power. Prior to this expansion, preset values were too narrow for the Helco power delivered to the station.

In general, the RITS computer experienced problems throughout the year before and after the UPS installation. It was hoped that the UPS installation would alleviate some of the earlier computer "glitch" problems as it did with the power problems to the entire system. This was not the case, as computer hang ups continued through 1992. The ASCII conversion program, which allows MLO personnel to look at the data more closely, had some problems in early 1992 but was successfully modified at MLO in late 1992.

Aerosol Monitoring

The TSI unit is a continuous expansion CNC in which condensation occurs in a butyl alcohol vapor chamber and single particle counting statistics are used as a basis for the CN concentration calculations. The instrument has continued to display higher counts than the Pollak since its return from the company in 1991. This instrument will be compared to a second TSI in early 1993.

The aethalometer performed satisfactorily during 1992. There was some local contamination of the data during the latter half of the year when the observatory electrical upgrade contractor was using diesel equipment at MLO.

The 4-wavelength nephelometer went down on January 17 because of a faulty automatic air/filter valve. While awaiting arrival of a replacement valve from Boulder, maintenance was performed on the circuitry. The system was brought back in service on February 26. The system performed without any problems the remainder of the year.

Radon

The CMDL/DOE radon program completed its second year of operation, collecting quality data 87% of the total hours in 1992. Experiments with a sister instrument at the DOE/EML lab in New York in the fall of 1992 isolated the source of thoron contamination as being in the welds in the aluminum chamber and housings. A thick coating of epoxy was applied to the MLO instrument welds in December that completely eliminated the thoron contamination. This brought the instrument sensitivity down from more than 50mBq/m³ to less than 15mBq/m³ for a 30-minute sample.

Results from the first 30 months of operation are summarized in Figures 1.1 and 1.2. A strong seasonal cycle is seen at MLO. Downslope March monthly averages are highest at 300mBq/m³ with a minimum in October of less than 10mBq/m³. Radon emanating from soils at lower altitudes on Hawaii is typically transported in the daytime upslope winds, with concentrations averaging over 100mBq/m³.

Solar Radiation

Two water-vapor meters built by the University of Arizona were put on the solar dome spar on April 2. The instruments measure narrow-band solar radiation at 870 nm and 940 nm. The station pyranometer was replaced on October 27. The solar dome controller and related sensors were damaged when the building was being rewired as part of the station electrical upgrade; this caused loss of automated operation for the remainder of 1992.

Fifty-seven hand-held sunphotometer instrument calibrations were performed during the year. The broadband atmospheric transmission factor increased from 0.86 in January to 0.90 in December as the Pinatubo aerosol continued to fall out of the atmosphere.

The old Robertson-Berger erythema meter, in use for many years at MLO, was replaced with a newer model 500 RB meter. An IBM PC is now being used as a data acquisition system for the newer R-B meter.

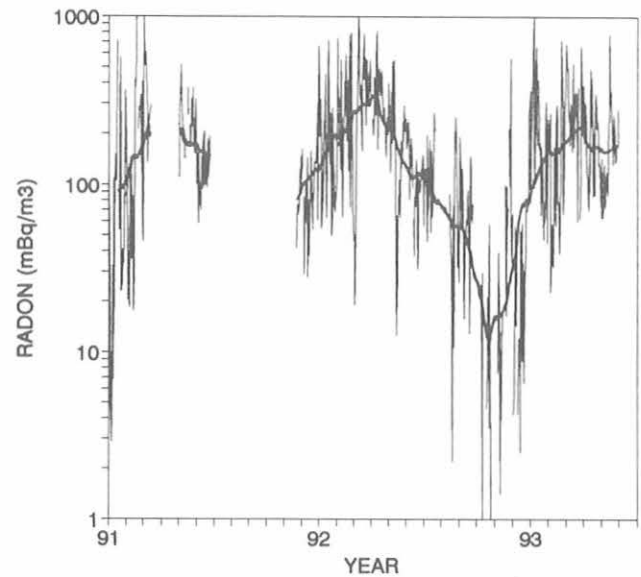


Fig. 1.1. Nightly average radon concentrations between 00 and 07 LST measured by the CMDL/DOE radon instrument at MLO during its first 30 months of operation. The heavy solid line is a 60-day running geometric mean. Synoptic-scale variability is primarily caused by changes in air trajectories coming from continental sources.

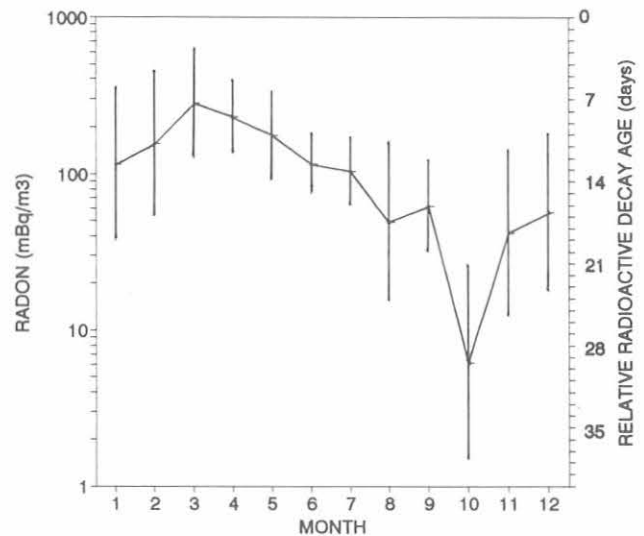


Fig. 1.2. Seasonal representation of Figure 1.1 data, shown by monthly geometric means $\pm 1\sigma$. The right-hand scale (with arbitrary zero) relates radon loss to the 3.8 day radon half-life. All else being equal, this suggests that continental air reaches MLO 2 to 3 weeks faster during the spring Asian dust season than in the fall. Only 7 days' data were averaged for October.

A Yankee Environmental UVB instrument was installed on September 17 and connected to CAMS ASR channels 6 and 7. This UVB pyranometer measures global solar UVB irradiance from 280 nm to 330 nm.

Computers/Network

A VAX 4000 computer was installed in November and an Ethernet LAN set up to connect all the PC's in the Hilo office. A network printer was connected to the system. A dial-in modem connection to the VAX and a 486 PC was put in place so MLO staff can call in and work on the system from home. We are now waiting for a NASA Internet connection to establish a network between Boulder and MLO.

MLO Database

Subsequent to the addition of the VAX computer, several large, integrated data bases were created along with utility programs to convert the data and read the data bases for analysis. More data bases are being added on a monthly basis. The data bases currently stored in the VAX along with the period covered: mlohrsall - all hourly data from 1985 until 1999 (contains all CAMS data, RITS, CH₄, black carbon, radon, Scripps CO₂, and other future projects up to 100 parameters (master. hrs); mlominmsd - minimum data from solar dome (only when dome is open); mlo3mnall - 3-minute data for solar radiation data (or other parameters); mlo30mall - 30-minute data; mlohrshis - data starting January 1, 1958; mlowkyall - weekly data; and mlowkyprofile data (ozonesonde, lidar, and NWS soundings).

Meteorology

A Planetary Boundary Layer System (PBL) was installed and activated January 15, 1992. The system measures wind speed, wind direction, and temperature at the 3, 5, 10, 20, 30, and 40 meter levels. Sensors are scanned by a 386 computer at 1-second intervals, and 1-minute averages are displayed and stored by the computer. Frequent anemometer problems were experienced in the early stages, but the system has operated trouble-free after all the sensors were overhauled.

There were no changes in the standard meteorological observations program. The routine monitoring of wind speed, wind direction, temperatures, dew point, and atmospheric pressure was carried out during the year without major problems. The mercury barometer was moved to a more stable location in the middle of the MLO building on November 9. Weekly dewpoint and temperature comparisons and semi-annual calibrations revealed no discrepancies in the data.

Precipitation Chemistry

The MLO modified program of precipitation chemistry collection and analyses continued throughout 1992 within the basic MLO operational routine. This program consists of a weekly integrated precipitation sample from the

Hilo NWS station and the collection of precipitation event samples at MLO. Analyses of these samples are undertaken in the Hilo Laboratory for pH, conductivity, and several ions using currently available equipment.

Lidar

Lidar operations continued on a regular weekly basis up to November 4 on which date a major electrical breakdown occurred during an observation. The lidar was out of service until February 1, 1993. As shown in Figure 1.3, stratospheric aerosols from the June 15-16, 1991, eruption of Mt. Pinatubo continued to decrease over the year with a more rapid decline beginning in mid-October.

Cooperative Programs

The cooperative programs continued without any major changes from 1991 except for the University of Washington's aerosol chemistry program that went into inactive status due to malfunctions in the control system. No replacement was received in 1992. The O₂/N₂ flask sampling program (NCAR) matured in 1992 having passed through a shakedown period in late 1991. The NCAR flask program did not send any flasks in 1992 and was subsequently discontinued. Weekly sunrise solar spectra FTIR measurements (University of Denver) were conducted throughout the year. A second staff member has been fully trained in the FTIR spectrometer operation. This program has also now settled into a mature phase.

MLO cooperative programs are listed in Table 1.1. It is the consensus of the MLO staff that cooperative program activities now consume 50% of MLO non-administrative staff time.

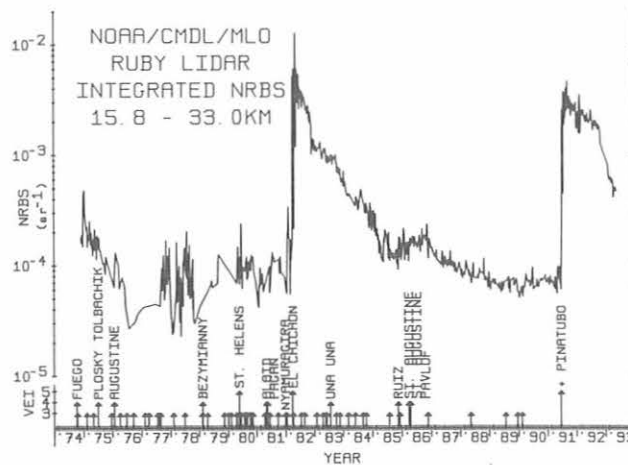


Fig. 1.3. Stratospheric column aerosol backscatter record from the MLO lidar. The El Chichon and Pinatubo aerosols are the most significant inputs in the past two decades. Note the rapid decrease in the Pinatubo aerosols beginning in October 1992.

1.2. BARROW OBSERVATORY

D. ENDRES

1.2.1. OPERATIONS

January 1992 marked the start of the 20th year of data collection at BRW.

BRW serves as part of the training for the CMDL SPO crew each year. This year the NOAA Corps officer was in BRW for training during February and March and again during June and July. The electronics technician was here during July and August.

A new third-party support agreement with the DEW Line site was negotiated this year with a greatly reduced road maintenance schedule.

A gate for the observatory road is being planned to control the increased traffic on the observatory road. On several occasions the station was used as a starting point for 4-wheel drive vehicles to gain access to the tundra.

In October the electronics technician left for a new position and was replaced in November.

Polar bears were seen in record numbers during the fall with as many as 30 bears sighted at the dump on several occasions.

During the winter of 1992-1993 the road was left drifted with snow due to the extreme cost of snow removal. Station personnel started skiing to the station when there were no known bears in the area. The road closure helped to keep traffic off the road.

Last year an offshore exploratory oil rig was stationed east of the station about 32 km out. ARCO Alaska moved it during the summer of 1992. To date, no effects have been noted in the BRW data set.

With the help of the MASC Engineering Office in Boulder, plans for a new BRW Observatory building were completed. The plans call for about a 50% increase in building size, with the old observatory building to be used for warm storage and/or co-op projects. Funds for the construction of a new observatory have not yet been obtained. A standing request to secure funds from the Department of Commerce NOAA Capital Improvement Appropriations is pending.

The 1985 Chevy Suburban was returned to GSA in Anchorage and a 1992 Ford pick-up was issued to BRW. The DEW Line allowed us access to a stall in their garage. This gave us a place to park the truck during the day with enough room left on the side for the snow machines. The snow machines are particularly useful during the winter when access to the observatory by car can become difficult. All vehicles ran fine during the year with normal maintenance.

The bathroom in Apartment A was remodeled by station personnel during April to finish the government housing upgrade. A problem in the apartment occurred when a broken pipe was found in the wall that called for extensive repair to the plumbing. In spite of the break, no structural

damage was found to the house. In a separate incident, a pipe under the house, about 3.6 m long, froze and cracked in several places. Station personnel replaced and re-plumbed the pipe and installed insulation to correct the situation.

1.2.2. PROGRAMS

Table 1.4 summarizes the 1992 measurement programs at BRW. Operational highlights are as follows:

Aerosols

The nephelometer ran well all year with only minor maintenance required. Aerosol backscatter, as measured by the nephelometer, showed the typical springtime high with no substantial deviation from the past record.

The Tygon tubing on the inlet to the TSI CNC was replaced with copper tubing. It was decided to keep the diameter of the tubing at 3/8 inch (9.525 mm) i.d. There is less particle loss due to static electricity in the copper tubing than in the Tygon tubing.

The lamp was replaced in the aethalometer when the data began to show erratic values. The problem was cleared up and the aethalometer continues to collect black carbon data. A very good correlation has been shown between black carbon and CO₂ data [Hansen, 1989].

Solar Radiation

The first sunrise of the year occurred on January 23. For the first few weeks of the solar year the elevation angle is too low for quality direct sun observations. All global instruments were returned to service at sunrise and worked well throughout the year.

Backlash in the rack and pinion gears for the solar tracker was adjusted and the tracker experienced no problems this year.

The quartz and the RG8 pyranometers, along with the pyrheliometer, were returned to Boulder during November for calibration. The FWNIP was calibrated.

Carbon Cycle

CO₂ NDIR. The Barrow CO₂ mixing ratio reached a high this year of over 360 ppm. A peak is seen each spring with a summer minimum occurring during September and October. During the fall of 1991 the CO₂ system was upgraded to a Siemens Ultramat 5E [Ferguson and Rosson, 1991]. The Siemens NDIR ran fine all year with minimal downtime.

CH₄. Batteries were changed in the CH₄ UPS. The local utilities co-op experienced problems with the generators that caused several outages late in 1991. During April a member of the CMDL Carbon Cycle Division arrived to upgrade the system by replacing the gas chromatograph. Several modifications were made to the internal plumbing of the GC along with program updates. Late in the year there was a problem with noisy data. Changing the diaphragm in the air sample pumps apparently

TABLE 1.4. Summary of Measurement Programs at BRW in 1992

Program	Instrument	Sampling Frequency
<i>Gases</i>		
CO ₂	Siemens Ultramat 5E analyzer 3-L glass flasks	Continuous 1 pair wk ⁻¹
CO ₂ , CH ₄ , CO	0.5-L glass flasks, through analyzer	1 pair wk ⁻¹
CH ₄	0.5-L glass flasks, P ³ pump unit	1 pair wk ⁻¹
Surface O ₃	Carle automated GC	1 sample (12 min) ⁻¹
Total O ₃	Dasibi ozone meter	Continuous
CFC-11, CFC-12, CFC-113, N ₂ O	Dobson spectrophotometer no. 91	3 day ⁻¹
H1211, H1301, HCFC-22	300-mL stainless steel flasks	1 pair wk ⁻¹
CFC-11, CFC-12, CFC-113, N ₂ O, CCl ₄ , CH ₃ CCl ₃	800-mL stainless steel flasks	1 pair month ⁻¹
N ₂ O	HP5890 automated GC	1 sample (0.5 h) ⁻¹
CO	Shimadzu automated GC Trace Analytical GC	1 sample (0.5 h) ⁻¹ 1 sample (6 min) ⁻¹
<i>Aerosols</i>		
Condensation nuclei	Pollak CNC	1 day ⁻¹
Optical properties	T.S.I. CNC	Continuous
Black carbon	Four-wavelength nephelometer Aethalometer	Continuous Continuous
<i>Solar and Terrestrial Radiation</i>		
Global irradiance	Eppley pyranometers with Q and RG8 filters	Continuous
Direct irradiance	Tracking NIP	Continuous
	Eppley pyrhelimeter with Q, OG1, RG2, and RG8 filters	Discrete
Terrestrial (IR) radiation	Eppley pyrgeometer	Continuous
Albedo	Eppley pyranometer and pyrgeometer	Continuous
<i>Meteorology</i>		
Air temperature	Thermistor, 2 levels Max.-min. thermometers	Continuous 1 day ⁻¹
Dewpoint temperature	Dewpoint hygrometer	Continuous
Pressure	Capacitance transducer Mercurial barometer	Continuous Discrete
Wind (speed and direction)	Bendix Aerovane	Continuous
Precipitation	Rain gauge, tipping bucket	
<i>Cooperative Programs</i>		
Total surface particulates (DOE)	High-volume sampler (1 filter wk ⁻¹)	Continuous
Precipitation gauge (USDA)	Wyoming shielded precipitation gauge. Nipher shield, Alter shield, 2 buckets	1 mo ⁻¹
Magnetic fields (USGS)	3-Component fluxgate magnetometer and total field proton magnetometer	Continuous
Various trace gases (OGIST)	Stainless steel flasks	1 set wk ⁻¹ (3 flasks set ⁻¹)
¹³ C, ¹⁸ O, CO ₂ (CSIRO)	5-L glass flasks	1 pair (2 wk) ⁻¹
CO ₂ , ¹³ C, N ₂ O (SIO)	5-L evacuated glass flasks	1 pair wk ⁻¹
CH ₄ (Univ. of Calif., Irvine)	Various stainless steel flasks	1 set (3 mo) ⁻¹
Earthquake detection (Univ. of Alaska)	Seismograph	Continuous, check site 1 wk ⁻¹
¹³ CH ₄ (¹³ C/ ¹² C) (Univ. of Washington)	35-L stainless steel flasks	1 (2 wk) ⁻¹
Ultralow frequency waves (Univ. of Tokyo)	Magnetometer	Continuous
UV monitor (NSF)	UV spectrometer	1 scan per 0.5 hour
Magnetic fields (NAVSWC)	³ He sensors	Continuous
O ₂ in air (Univ. of Rhode Island)	3-L glass flasks	1 pair (2 wk) ⁻¹

cleared up the problem. The system ran fine the rest of the year.

CO. Another member of the CMDL Carbon Cycle Division came to BRW to upgrade the CO system. The CO detector uses HgO to reduce CO to CO₂ and Hg. Mercury vapor absorbs UV light and produces a signal proportional to levels of CO. The system ran fine all year.

Flask Samples. Flasks were exposed on a weekly basis. CO₂, CH₂, and CO are measured from the flask samples. An offset between the CMDL 3-L flasks and the MAKS flasks was noted and is currently under investigation by CMDL Boulder personnel.

Meteorology

Winds as high as 96.5 km ph (60 mph) were recorded during a blizzard in November. During December a series of six low-pressure cells moved across the Arctic raising temperatures to as high as -6°C (+20°F). All instrumentation ran fine during the year. Aerovane and temperature probe calibrations were performed at 6-month intervals with no drift in calibration found.

Ozone

Surface Ozone. Barrow O₃ measurements are a two-part program with surface level measurements made by the Dasibi ozone meter. Springtime data often show a minimum and have been seen to reach levels down to zero. The most likely cause is the build up of Br in ocean water during the winter and when it is released into the atmosphere and undergoes photochemical disassociation during spring break up destroying ozone in the process. On a longer time scale, an overall increase in average surface ozone amounts has been shown for BRW and it may be the by-product of NO emissions from the Prudhoe Bay oil fields [Jaffe, 1991].

Total Ozone. Ozone observations began in late February when the sun angle became high enough to produce reliable signals. A possible problem with high humidity was discussed and it was decided to build and install a dryer system. With the dryer system, air is pushed through a desiccant and blown through the Dobson. Whenever practical, zenith observations were taken in conjunction with direct sun observations to produce a data set for analysis of the difference between the data from direct sun and zenith observations.

The observational year was concluded on October 8 when the sun angle decreased to levels too low for observations.

Halocarbons

In situ measurements. Problems with the GC data acquisition system locking up continue to plague the station. Generally good data was collected except for the episodes of unexplained failures. A power down reset was the only thing that would work to restart the system after lockups.

BRW data along with that from other remote long-term CMDL monitoring sites, show a decrease in the rate of increase in global CFC's. The seasonal cycle of CFC mixing ratios was still seen in the BRW data set.

Flask samples. When flasks were available, they were exposed on a weekly basis and returned to Boulder for analysis. Measured compounds included CFC's, HCFC'S, and the LEAPS gases.

Cooperative Programs

Only programs with problems or unusual occurrences are mentioned in this section.

The DOE began preliminary discussions with BRW and UIC/NARL regarding the possibility of using the BRW Observatory and surrounding area as part of the ARM/CART site. The ARM program is part of an effort by the DOE to resolve uncertainties about global climate change and the role of clouds on any possible change. Instrumentation will collect data to determine the interactions of sunlight, radiant energy, and clouds on temperature, weather, and climate. A 10-year project is being planned.

USDA/SCS Snow Survey gages froze again during the winter of 1991-1992 because the fluid used could not handle the cold temperatures. During the summer of 1992 a switch was made to a different type of solution that has a lower freezing point.

The University of Rhode Island began collecting flask samples of ambient air in BRW for analysis of O₂/N₂ and CO₂. O₂ fluxes mirror those of CO₂. By measuring O₂ concentrations, important information about the fate of fossil fuel CO₂ can be gained as well as the information regarding the fertility of the ocean.

Several new projects are being planned for BRW in the coming year. The University of Washington is planning to have high-pressure cylinders filled at BRW for analysis of ¹⁴C in CO at the University of Washington. The measurements will provide information about photochemical influences on tropospheric OH radical concentrations.

A project is being planned by the U.S. Interagency Arctic Buoy Program to set up and calibrate ice buoys at BRW .

1.3. SAMOA

C. FARMER

1.3.1. OPERATIONS

The past year at the observatory was spent doing many of the hurricane recovery chores that were not completed immediately following Hurricane Val. Most measurement programs were continued during the year without any major difficulties. It was the middle of the year before all of the main CMDL programs were back to normal with the replacement of the CO₂ sampling mast at the point area.

The only item that still needed attention was the replacement of the Hi-Vol sampling enclosure for EML and the maximum/minimum temperature shelter.

There were more problems with the generator during the year. The starter shorted out and in doing so caused many other problems, the most serious of which required the replacement of the radiator that had been replaced just 1 year earlier and the replacement of the injectors that were damaged due to water getting in the fuel. The old radiator was returned to Caterpillar in hopes that they would replace it under warranty but they did not. The starter burned out and also had to be replaced. Most of these repairs and modifications were performed by the observatory personnel.

Much of the hurricane damage on the island went unrepaired for the year, especially the roads. The condition of the road to the observatory worsened further with the passage of a period of unusually heavy rain in April of more than 580 mm (23 inches) and the passage of a hurricane near the islands during the last week in December when again heavy rains and flooding occurred.

Because the batteries were no longer holding a charge, the PV array was disconnected during August. New batteries were requested but because of their high replacement cost, they could not be purchased and were not in place by the end of the year. This created few problems for the CAMS and other equipment that normally used the solar PV power, until the end of the year when the island power began going off and on quite often. Because of the degradation of the island power, the data acquisition units had a high failure rate. They began experiencing many autorestarts, the bram lost messages, and several circuit board failures occurred with all units. This problem was finally dealt with by running extension cords to the Ekto building and using the UPS power available there.

We had a small problem with the new chief in Tula village when the rent payments for March and April were delayed in the mail. He threatened to change all of the locks at the observatory. Luckily the check for April arrived in time for the Station Chief to persuade him not to lock us out.

1.3.2. PROGRAMS

Table 1.5 summarizes the programs at SMO for 1992. Further descriptions of some of the programs follow.

Carbon Dioxide

The sampling mast that was broken during Hurricane Val was replaced during July. Until that time the temporary sampling mast that was configured after Hurricane Ofa had been in use since early January. There appeared to be little difference in the CO₂ data when the winds were within the clean air sector except possibly there was a slight decrease in the standard deviations of the hourly averages.

A shortage of working tanks occurred near the end of the year. The new tanks were supposed to arrive in early December but failed to make the ship. The system was kept running by switching in old working tank standards for about 1 week at a time, working the remaining pressure levels of the working tanks to lower than normal levels before they were shipped back to Boulder for final concentration level checks.

The flask sampling program continued throughout the year without any major difficulties. The only significant change to the regular flask sampling program was the switch to the 2.5-L flasks for the MAK5 unit and the discontinuance of the 3-L flasks.

Surface Ozone

There were many problems with this program during the year. A new instrument was shipped in February to the observatory only to develop immediate problems because of its newer design it ran cooler, causing a condensation problem that eventually led to its return to Boulder. The old instrument was refurbished in Boulder, was returned to Samoa, and was put back into service. There were also problems with the chart recorder hanging up on several occasions and it was finally replaced. There was also a great deal of data lost due to the continued failure of the ozone board in the data acquisition unit. This problem worsened when the PV array had to be shut down.

Total Ozone

There were no serious difficulties with the operation of Dobson spectrophotometer no. 42 during the year. An expanded program was started in March to include zenith observations after each direct sun observation to improve the algorithm to convert the zenith observations to ozone values. This program was continued through the end of the year.

Halocarbons and Nitrous Oxide

There were problems during the year with the halocarbon and N₂O gas chromatographs. However, loss of data was kept to a minimum in most circumstances. These problems included the loss of a power supply in the computer, the continued problem of the water removal system getting plugged up, problems with the air compressor, and a temperature control problem with the N₂O gas chromatograph. The source of the fine powdery substance that was plugging up the water removal system was determined to be the traps themselves, although the presence of the material upstream of the traps seems to contradict this. New stainless-steel traps were installed and appeared to be working well; however, there was eventually a problem with them plugging up as well. To keep the system from being affected by the regular low voltages experienced during the evening hours and power outages, the UPS continued to work without difficulty. Several other minor problems were encountered during the year.

TABLE 1.5. Summary of Measurement Programs at SMO in 1992

Program	Instrument	Sampling Frequency
<i>Gases</i>		
CO ₂	Siemens Ultramat-5E analyzer	Continuous
CO ₂ , CH ₄	3-L glass flasks	1 pair wk ⁻¹
	0.5-L glass flasks, through analyzer	1 pair wk ⁻¹
	2.5-L glass flasks, MAKS pump unit	1 pair wk ⁻¹
Surface O ₃	Dasibi ozone meter	Continuous
Total O ₃	Dobson spectrophotometer no. 42	4 day ⁻¹
CFC-11, CFC-12, N ₂ O	300-mL stainless steel flasks	1 pair wk ⁻¹
CFC-11, CFC-12, N ₂ O, CCl ₄ , CH ₃ CCl ₃	HP5890 automated GC	1 sample (h) ⁻¹
N ₂ O	Shimadzu automated GC	1 pair mo ⁻¹
LEAPS Gases H-1301, H-1211, CFC-113, CFC-22	1-L stainless-steel flasks	1 pair mo ⁻¹
HC00H, CH ₃ C00H, HC1, HNO ₃ , CH ₃ SO ₃ H	Condensation sampling with ion chromatographic analysis	Discrete
<i>Aerosols</i>		
Condensation nuclei	Pollak CNC	1 day ⁻¹
	G.E. CNC	Continuous
<i>Solar Radiation</i>		
Global irradiance	Eppley pyranometers with Q and RG8 filters	Continuous
Direct irradiance	Eppley pyrhelimeter with Q filter	Continuous
	Eppley pyrhelimeter with Q, OG1, RG2, and RG8 filters	Discrete
<i>Meteorology</i>		
Air temperature	Thermistors (2)	Continuous
	Max.-min. thermometers	1 day ⁻¹
Dewpoint temperature	Polished mirror	Continuous
Pressure	Capacitance transducer	Continuous
	Mercurial barometer	1 wk ⁻¹
Wind (speed and direction)	Bendix Aerovane	Continuous
Precipitation	Rain gauge, weighing bucket	Continuous
	Rain gauge, tipping bucket	Continuous
	Rain gauge, plastic bulk	1 day ⁻¹
	HASL Chemetrics wet/dry collector	1 day ⁻¹
<i>Precipitation Chemistry</i>		
pH	Fisher model 805 meter	1 day ⁻¹ (CMDL); 1 wk ⁻¹ (NADP)
Conductivity	Beckman model RC-16C meter	1 day ⁻¹ (CMDL); 1 wk ⁻¹ (NADP)
Anions (NO ₃ ⁻ , SO ₄ ⁻)	Dionex QIC ion chromatograph	1 day ⁻¹ (CMDL)
<i>Cooperative Programs</i>		
CO ₂ , ¹³ C, N ₂ O (SIO)	5-L evacuated glass flasks	3 flasks wk ⁻¹
GAGE project: CFC-11, CFC-12, N ₂ O, CH ₃ CCl ₃ , CCl ₄ (SIO)	HP5880 gas chromatograph	1 h ⁻¹
Various trace gases (OGIST)	Stainless steel flasks	3 flasks wk ⁻¹ (3 flasks set ⁻¹)
Wet deposition (NADP)	HASL Chemetrics wet-dry collector	1 wk ⁻¹
Bulk deposition (EML)	Plastic bucket	Continuous (1 bucket mo ⁻¹)
Hi-vol sampler (EML)	High-volume sampler	Continuous (1 filter wk ⁻¹)
Hi-vol sampler (SEASPAN Project)	High-volume sampler	Continuous (1 filter wk ⁻¹)
CH ₄ , (¹³ C/ ¹² C ratio) (Univ. of Wash.)	30-L pressurized cylinder	Biweekly
Light hydrocarbons (UCI)	1-L evacuated stainless steel flasks	3-4 flasks qtr ⁻¹

Flask air sampling continued on a weekly basis when flasks were available. Either 300-ml (weekly) or 1-L (monthly) flasks were used.

Aerosols

The aerosol program continued at the observatory with the addition of a TSI condensation nucleus counter. There were several problems initially encountered with the unit and the acquisition of the data from it, but it was up and running by May. The other component of the aerosol program, the GE condensation nucleus counter, ran throughout most of the year experiencing problems typical of past years.

Solar Radiation

This program had few problems during the year. There was some difficulty with the tracking NIP staying aligned during the middle of the year, the reason for which was never clear.

Meteorology

After Hurricane Val destroyed the weather shelter, the maximum/minimum thermometers remained underneath the carport for the entire year. This obviously was not an ideal location for the thermometers, but without a shelter, this temporary site was required. One result of this temporary location was that during the year many people who came up to the observatory after hours began taking or breaking the thermometers due to their conspicuous location. All the other meteorological-shelter instruments performed well during the year.

Problems with the Aerovane were suspected when the measured wind speed was not as high as it appeared to be. The Aerovane readings were checked against a hand-held anemometer to verify that the measured wind speeds were below expected values. The problem was due to the degaussing of the magnet in the instrument. Later in the year during the passage of a hurricane near the island, the direction was affected causing the direction to shift by about +20°. Later tests have verified this to be the case.

Precipitation Chemistry

When it rained, daily precipitation samples continued to be collected during the year. All analyses were performed at the observatory. Samples are no longer being shipped to MLO for further analyses. Analysis is performed using a Dionex QIC ion chromatograph on loan from the University of Washington.

Cooperative Programs

The cooperative program that again involved the most time during the year was the gas chromatographs operated by SIO. All problems were dealt with and the system ran well throughout most of the year. Most all other programs operated without difficulty for the year. The National Acid Deposition Program was discontinued during the year with the last sample being taken in October.

1.4. SOUTH POLE OBSERVATORY

D. TYSOR

1.4.1. OPERATIONS

CMDL's most remote baseline observatory is located at the Amundsen-Scott South Pole Station (SPO). The SPO is located 200 m from the geographic South Pole on the polar plateau at an elevation of 2835 m. The extreme environment of the polar plateau adds to the remoteness of the station. With an average year-round temperature of -49°C, planes can land only during a short summer season (approximately November 1-February 15). This report will cover dates from November 1, 1991-November 1, 1992, a time-frame consistent with the rotation dates for incoming and outgoing observatory staff.

The SPO is housed in the Clean Air Facility (CAF), a building located several hundred meters grid northeast of the main dome structure of the United State's Antarctic station. This location is optimal for the sampling of atmospheric constituents because the wind blows from a clean air sector a large percentage of the time.

While most of the CMDL SPO operations are located at the CAF, the SPO balloon programs were carried out in the Balloon Inflation Tower located "down wind" of the station. Antarctic Support Associates (ASA) computer facilities located in the main dome, were also used by the CMDL program.

NSF is the United States' agency tasked with managing all of our country's Antarctic science projects. NSF funds provide the base support for research, transportation, and logistics for university and government agencies as well as for the civilian contractors, ASA, to help develop, maintain, and improve America's presence on the continent.

This year's support facilities that had an impact or future impact on CMDL's program included the following:

A ceilometer (for measuring cloud base heights) was purchased by the U.S. Navy and installed on the roof of CAF. Although the instrument is to be operated and maintained by ASA, software was written that allowed CMDL to collect raw data from this instrument. This data may be able to contribute to several of NOAA's programs including solar radiation (radiation budget), aerosols (tropospheric/surface), as well as for its intended purpose for meteorology (cloud base heights).

The upgrades on the station power plant continued during the 1991-1992 season. In previous years, power has been a problem at the Pole when blackouts and brownouts were quite common. The station is perhaps one season away from completing the power plant upgrade, but during the year station power was very clean and there were only a few unscheduled blackouts. During the summer, a new two-story building on stilts was constructed in an area known as "summer camp." This structure and others like it represent the future design of new buildings at the Pole and as such could eventually be used as the next CAF. The

current CAF is over 15 years old and is scheduled to be replaced in the next few years.

CMDL scientific data from the Pole is sent out via the ATS-3 satellite. This satellite was also used for phone traffic into the United States via Malabar, Florida. When available, the LES-8 and LES-9 satellites were used to transmit additional data from the Pole. The SPO data ranks second in the priority list of all project data currently being transmitted from the Pole, so data transmittal went smoothly.

1.4.2. PROGRAMS

Table 1.6 is a summary of the measurement programs at SPO during 1992. The following is a short discussion of the various programs.

Aerosols

Most of the aerosol equipment functioned well during the year. The aethalometer performed well in its task of measuring carbon aerosols, but was returned to Boulder in December 1991 for refurbishing.

The 4-wavelength nephelometer measures the optical properties of aerosols and ran well except during high winds. For some unexplained reason, all four channels would drop out when winds exceeded 30 knots. When the wind speed decreased, the instrument would automatically begin collecting data again.

The TSI condensation nuclei counter (CNC) also performed poorly during high winds exhibiting erratic behavior. A blown driver card was the only hardware replacement required for the TSI. The instrument functioned perfectly during low wind conditions.

The Pollak CNC observations took several days to stabilize after the instrument was watered, but after the Pollak had time to dry out, the results began to agree with the TSI CNC.

CAMS

Data is collected for the various programs using the Control and Monitoring System (CAMS). The CAMS units all functioned very well during low wind conditions. However, during high winds especially in the winter, the CO₂ unit had one autorestart and the ASR (Aerosol, Solar Radiation) unit had numerous ones.

Carbon Dioxide

The Siemans IR analyzer that measures in situ baseline CO₂ concentrations worked without fail for the entire year. The chart recorder failed on occasion, but was easily fixed with the replacement of a few electronic components.

The through-analyzer flask program samples the same air that is analyzed by the Siemans equipment. The flasks were saved throughout the winter and were returned to Boulder in the summer for analysis and comparison with the Siemans' data. A second CO₂ flask program involved the use of a portable MAKS unit. Samples are collected

outside simultaneously with the SIO program flasks and the MAKS flasks are shipped back to Boulder in the summer along with the through-analyzer flasks. All CO₂ flasks compared well with the Siemans analyzer data.

Dobson Ozone Spectrophotometer

The Dobson ozone spectrophotometer measures the total ozone in a column of air. The measurements are normalized to ozone concentrations in a vertical column over the station. This equipment is normally operational in the summertime when the sun is several degrees above the horizon and in the wintertime when the moon is full. The instrument was operational 100% of the operational window. Missed observations were usually due to poor weather conditions, i.e., blowing snow or thick overcast skies.

Meteorology

Meteorology equipment includes instruments to measure temperature, pressure, frost-point temperature, and wind speed and direction as well as the CAMS units for recording all of the data. After replacing the CAMS anemometer board early in the season, the meteorology equipment functioned well throughout the rest of the year.

NOAH - Halocarbons

The gas chromatograph system that measures CFC's in the atmosphere, was reworked during the summer and ran almost continuously for the rest of the year. Minor computer problems and valve realignments account for the small amount of down-time in the winter. The flask sampling program ran smoothly.

Ozonesonde Balloons

This program was the year's most challenging. Extensive data was collected on stratospheric ozone even though there was a telemetry reception problem with the ground equipment. Balloons were launched in high winds with greater success than in previous years.

Solar Radiation

The side-by-side comparison of Soviet versus American solar radiation instruments was completed in the summer. The Soviet equipment was removed and returned to Boulder. The tracker for the normal incidence pyrheliometer had a few problems, but the data still compared well with the manually operated instrument. No pyrgeometer data was collected after both instruments malfunctioned in the winter.

Water Vapor Balloons

Like the ozonesonde program, this balloon program suffered from the telemetry problems mentioned earlier. Other problems included faulty timers that are supposed to fire, causing a slow descent for the balloons. The correct functioning of the timers is particularly important as the most valuable water vapor data is collected during descent.

TABLE 1.6. Summary of Measurement Programs at SPO in 1992

Program	Instrument	Sampling Frequency
<i>Gases</i>		
CO ₂	Siemens IR analyzer	Continuous
CO ₂ , CH ₄	0.5-L glass flasks, through analyzer	1 pair twice mo ⁻¹
	0.5-L glass flasks, MAKs pump unit	1 pair twice mo ⁻¹
Surface O ₃	Dasibi ozone meter	Continuous
Total O ₃	Dobson spectrophotometer no. 82	2 day ⁻¹
Ozone profiles	Balloonborne ECC sonde	1 wk ⁻¹ , summer, autumn, winter; 1 (3 day) ⁻¹ , spring
CFC-11, CFC-12, CFC-113, N ₂ O, CH ₃ CCl ₃ , CCl ₄	Shimadzu automated mini-2 GCs	1 sample (2 h) ⁻¹
CFC-11, CFC-12, N ₂ O, CFC-113, CCl ₄ , CH ₃ CCl ₃	300-mL stainless steel flasks	3 pair mo ⁻¹ , summer
CFC-11, CFC-12, N ₂ O, CFC-113, CCl ₄ , CH ₃ CCl ₃	850-mL stainless steel flasks	1 pair mo ⁻¹ , summer, winter
H-1301, H-1211, F-22, F113		
Water vapor	Balloonborne sonde	6 times yr ⁻¹
<i>Aerosols</i>		
Condensation nuclei	Pollack CNC	1 day ⁻¹
	TSI CNC	Continuous
Optical properties	Four-wavelength nephelometer	Continuous
Carbon aerosols	Aethalometer	Continuous, summer
<i>Solar and Terrestrial Radiation</i>		
Global irradiance	Eppley pyranometers with Q and RG8 filters	Continuous, summer
	Eppley pyranometer with Q filter	Continuous, summer
	Net radiometer	Continuous, summer
Direct irradiance	Eppley pyrhemliometer with Q, OG1, RG2, and RG8 filters	Discrete, summer
	Eppley pyrhemliometers with Q and RG8 filters	Continuous, summer
Albedo	Eppley pyranometers with Q and RG8 filters filters, downward facing	Continuous, summer
<i>Terrestrial Radiation</i>		
Global irradiance	Eppley pyrgeometer	Continuous
Albedo	Eppley pyrgeometer, downward facing	Continuous
<i>Meteorology</i>		
Air temperature	Platinum resistor, 2- and 20-m heights	Continuous
Pressure	Capacitance transducer	Continuous
	Mercurial barometer	1 time wk ⁻¹
Wind (speed and direction)	Bendix Aerovane	Continuous
Frost-point temperature	Hygrometer	Continuous
<i>Cooperative Programs</i>		
CO ₂ , ¹³ C, N ₂ O (SIO)	5-L evacuated glass flasks	2 mo ⁻¹ (3 flasks sample ⁻¹)
Total surface particulates (DOE)	High-volume sampler	Continuous (4 filters mo ⁻¹)
Various trace gases (OGIST)	Stainless-steel flasks	1 week ⁻¹ (2 flasks set ⁻¹)
¹⁴ C (ARL)	3,000 psi spheres	500 psi day ⁻¹ , summer
Interhemispheric ¹³ C/ ¹⁴ C (CSIRO)	5-L glass flasks	1 or 2 flasks mo ⁻¹
Polar stratospheric clouds (Univ. of Rome)	Optical lidar	1 week ⁻²
O ₂ , N ₂ (NCAR)	Air sampling pump and flasks	1 mo ⁻¹ (3 flasks set ⁻¹), summer

Cooperative Programs

The Commonwealth Scientific and Industrial Research Organization (CSIRO) and the Oregon Graduate Institute of Science and Technology (OGIST) flask sampling programs, which sample for various trace gases, both ran smoothly.

The flasks for the Scripps Institute of Oceanography (SIO) CO₂ program lost their vacuum after the 1990-1991 season. This resulted in contaminated flask samples early in the summer. The program had no problems after new flasks were shipped in. The Department of Energy (DOE)

pump ran flawlessly. Filters were collected that were later sampled for total surface particulates.

The NOAA Air Resources Laboratory (ARL) ^{14}C pump had no problems, but was removed in the early summer. This long-term project was terminated at the request of the P.I. who decided to end the program in Antarctica.

The NCAR air sampling pump was subject to leaks, but several samples were able to be collected. These flask samples were later analyzed for oxygen to nitrogen ratios. This program to determine global oxygen concentrations in the atmosphere was started this year as a feasibility study. Depending on the initial results, the program may be continued into the future years.

The University of Rome lidar project was given its own project number (S-256), but NOAA continued assisting with the collection of data for this project. During the summer, a more powerful laser was installed. The instrument ran with no problems during the year.

In summary, the CMDL programs ran well over the year. The ozone and solar radiation measurements gave pertinent data that helped to quantify and describe ozone depletion over Antarctica and the volcanic dust veil from Mt.

Pinatubo and Mt. Hudson that spread globally and warmed the stratosphere while slightly cooling the troposphere. All the trace gas measurements continued to exhibit the buildup in the atmosphere but at a slower rate for the halocarbons.

REFERENCES

- Ferguson, E.E., and R.M. Rosson (Eds.), *Climate Monitoring and Diagnostics Laboratory No. 19: Summary Report 1990*, 133 pp., NOAA Environmental Research Laboratories, Boulder, Colorado, 1991.
- Hansen, A.D.A., T.I. Conway, L.P. Steele, B.A. Bodhaine, K.W. Thoning, P. Tans, and T. Novakov, Correlations among combustion effluent species at Barrow, Alaska: Aerosol black carbon, carbon dioxide, and methane, *J. Atmos. Chem.*, *9*, 283-299, 1989.
- Jaffe, D.A., R.E. Honrath, J.A. Herring, S.-M. Li, and J.D. Kahl, Measurements of nitrogen oxides at Barrow, Alaska during spring: Evidence for regional and northern hemispheric sources of pollution, *J. Geophys. Res.*, *96*, 7395-7405, 1991.
- Thoning, K.W., P.P. Tans, W.D. Komhyr, Atmospheric carbon dioxide at Mauna Loa Observatory, 2, Analysis of NOAA GMCC Data 1974-1985, *J. Geophys. Res.*, *94(D6)*, 8549-8565, 1989.

2. Carbon Cycle Division

P.P. TANS (EDITOR), P.S. BAKWIN, T.J. CONWAY, E.J. DLUGOKENCKY, D.W. GUENTHER,
P.M. LANG, K.A. MASARIE, P.C. NOVELLI, K.W. THONING, AND L.S. WATERMAN

2.1. CONTINUING PROGRAMS

2.1.1. IN SITU CARBON DIOXIDE MEASUREMENTS

The mixing ratio of atmospheric CO₂ was measured with continuously operating NDIR analyzers at the four CMDL observatories during 1992 as in previous years. Monthly and annual mean CO₂ mixing ratios [in the WMO 1985 mole fraction scale (X85)] are given in Table 2.1. These values are provisional, pending final calibrations of station standards. Preliminary selected daily average CO₂ mixing ratios for 1992 are plotted versus time for the four observatories in Figure 2.1.

The CO₂ in-situ systems operated during 1992 from a low of 93.5% at SMO to a high 98.5% of the year at MLO. BRW operated 97.8% of the time and SPO 95.0%. This is based on the number of valid hourly averaged CO₂ mixing ratios that were calculated for the year, taking into account missing data due to reference gas calibrations during the year. The major loss of data at SPO was due to temperature instability in the Clean Air Facility, which affected the stability of the CO₂ NDIR analyzer. A failure of the SMO CAMS unit in December resulted in 4 days of lost data. In December 1991, typhoon Val struck SMO, damaging the CO₂ intake mast at the point. A temporary intake line was erected on the point so that CO₂ monitoring could resume. Power outages in January accounted for 5 days of lost data. In July, a new, stronger 23-m high mast was installed.

TABLE 2.1. Provisional Monthly Mean CO₂ Mixing Ratios From Continuous Analyzer Data (ppmv, Relative to Dry Air WMO X85 Mole Fraction Scale)

	BRW	MLO	SMO	SPO
Jan.	361.62	356.02	354.20	353.05
Feb	362.21	356.79	354.56	352.80
March	362.48	357.60	354.78	352.68
April	362.55	358.75	354.58	352.90
May	362.77	359.33	354.63	353.25
June	360.42	359.15	354.87	353.65
July	353.58	356.68	355.35	354.09
Aug.	347.09	354.74	355.31	354.47
Sept.	347.69	352.76	354.96	354.66
Oct.	353.66	353.16	355.05	354.67
Nov.	357.24	354.09	354.78	354.49
Dec.	361.05	355.34	355.25	354.22
Year	357.70	356.20	354.86	353.74

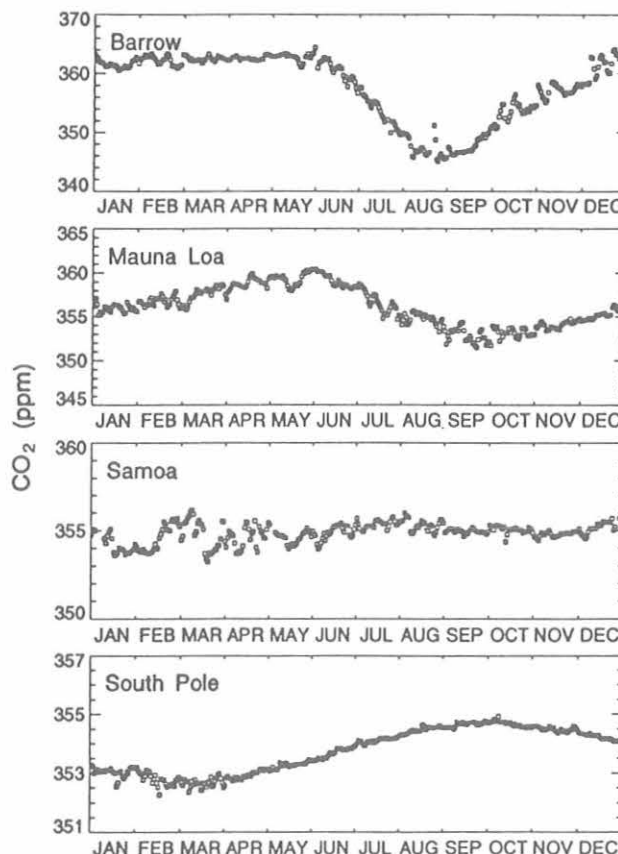


Fig. 2.1. Preliminary selected daily mean mixing ratios at the four CMDL observatories.

The growth rate of CO₂, as measured by the observatory systems, was smaller than average in 1991 and 1992. Figure 2.2 shows the instantaneous growth rate with the annual cycles removed at the four CMDL observatories for the years 1980 through 1992. These curves were obtained using methods similar to Thoning *et al.* [1989]; they are the derivative of a curve that is a combination of a function consisting of a quadratic polynomial, four annual harmonic terms, and low pass filtering of the residuals to remove high frequency variations. Annual cycles were removed by not including the derivatives of the four annual harmonic terms. The BRW growth rate, which typically has greater fluctuations than the other sites, appeared to be negative for most of 1992. The low growth rate at BRW is also apparent when comparing the annual mean difference between BRW and SPO. In 1991, this difference was 5.1 ppm, but for 1992 it was only 4.0 ppm.

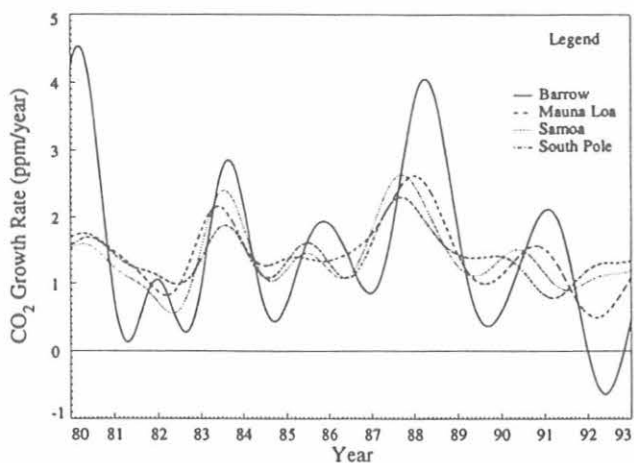


Fig. 2.2. The variation of the CO₂ growth rate for the period 1980-1992. The curves are the time derivatives of the deseasonalized, smoothed daily mean data for the four CMDL observatories.

2.1.2. FLASK SAMPLE CARBON DIOXIDE MEASUREMENTS

Measurements of the global distribution of atmospheric CO₂ by flask sampling continued in 1992. Table 2.2 lists 33 sites of the CMDL cooperative flask sampling network where flask samples were collected in 1992. Carbon dioxide mixing ratios (as well as CH₄, CO, and isotopic ratios) were measured in the CMDL Boulder laboratories. Provisional annual mean CO₂ mixing ratios for 1992 and revised values for 1990 and 1991 are given in Table 2.2. The first annual means for the recently started programs at Izaña, Canary Islands; Mace Head, Ireland; Qinghai, China; and Ulaan Uul, Mongolia are included in Table 2.2. Flask sampling at Heimaey, Iceland, was also begun in late 1992. The Iceland site was chosen to replace Ocean Station M which is expected to cease operation in the next year.

Sampling on regular voyages of the containerships *Southland Star* and *Wellington Star* continued in 1992. Since the ships sample similar regions of the Pacific Ocean, the annual mean CO₂ mixing ratios for 1990 through 1992 from both ships were combined into 5-degree latitude bins centered on latitudes from 30°N to 35°S (Table 2.3).

The flask sampling program in the South China Sea, begun in 1991, continued in 1992. Flask samples are collected at 3-degree latitude intervals from 3°N to 21°N on regular voyages of the Chevron refined product carrier *Carla A. Hills*. It is hoped that this intensive sampling program (averaging more than one sample per day) will help quantify the large CH₄ source due to rice production in southeast Asia. Annual mean CO₂ mixing ratios for 1992, the first complete year of sampling, are presented in Table 2.4.

The conversion of the flask sampling network to the 2.5-L Teflon O-ring stopcock flasks and the MAKS sampler continued in 1992. These changes, together with an

TABLE 2.2. Provisional 1990-1992 Annual Mean CO₂ Mixing Ratios From Network Sites

Code	Station	CO ₂ (ppm)		
		1990	1991	1992
ALT	Alert, N.W.T., Canada	355.5	357.2	357.5
AMS	Amsterdam Island	352.5	[]	[]
ASC	Ascension Island	352.9	353.9	355.1
AZR	Terceira Island, Azores	353.2	355.8	[]
BME	Bermuda (east coast)	355.2	356.1	357.0
BMW	Bermuda (west coast)	355.1	356.6	356.3
BRW	Barrow, Alaska	356.0	357.6	357.5
CBA	Cold Bay, Alaska	355.3	357.3	357.3
CGO	Cape Grim, Tasmania	351.6	352.8	353.5
CHR	Christmas Island	354.3	355.4	356.4
CMO	Cape Meares, Oregon	355.4	356.7	356.3
GMI	Guam, Mariana Islands	354.2	356.1	356.3
HBA	Halley Bay, Antarctica	[]	[]	[]
IZO	Izaña Observatory, Tenerife		[]	356.2
KEY	Key Biscayne, Florida	355.9	356.5	357.3
KUM	Cape Kumukahi, Hawaii	354.3	355.8	356.3
MBC	Mould Bay, Canada	356.0	357.6	357.4
MHT	Mace Head, Ireland		[]	356.1
MID	Midway Island	355.2	357.0	356.8
MLO	Mauna Loa, Hawaii	354.1	355.5	356.4
NWR	Niwot Ridge, Colorado	354.7	356.1	356.8
PSA	Palmer Station, Antarctica	351.9	353.2	354.2
QPC	Qinghai Province, China		[]	356.6
RPB	Ragged Point, Barbados	354.7	355.9	355.9
SEY	Mahé Island, Seychelles	353.3	353.9	354.8
SGI	South Georgia Island	[]	[]	[]
SHM	Shemya Island, Alaska	355.0	356.7	357.1
SMO	American Samoa	352.8	354.2	354.9
SPO	South Pole, Antarctica	351.8	353.1	354.1
STM	Ocean Station M	354.8	356.5	356.5
SYO	Syowa Station, Antarctica	352.3	353.3	354.2
TAP	Tae-ahn Peninsula, S. Korea	[]	359.8	360.6
UUM	Ulaan Uul, Mongolia			356.3

Square brackets indicate insufficient data to calculate annual mean.

increased emphasis on face-to-face training, have resulted in a significant increase in sample quality. An objective criterion for successful flask sample collection is that the two members of the sample pair, collected in series, agree to within 0.5 ppm. Figure 2.3 shows the percentage of samples meeting this criterion ("good pairs") for all sites during 1987-1992. The percentage of good pairs has increased from ~75% to 90%, if the shipboard flasks are excluded. The somewhat lower percentage of good pairs for shipboard sampling is probably due to the use of evacuated flasks rather than the MAKS sampler (for the convenience of the ship personnel) and the presence of contamination sources on the ships.

The most notable feature of the 1992 CO₂ flask data is a decrease in the CO₂ growth rate, particularly in the northern hemisphere. The flask data from Mould Bay, Canada (76° 15'N, 119° 21'W) and Cold Bay, Alaska (55° 12'N, 162° 43'W) are shown in Figures 2.4 and 2.5 as

TABLE 2.3. Provisional 1990-1992 Annual Mean CO₂ Mixing Ratios From the *Southland Star* and *Wellington Star* Shipboard Flasks

Latitude	CO ₂ (ppm)		
	1990	1991	1992
30°N	354.6	356.5	357.1
25°N	354.4	356.1	357.0
20°N	354.9	356.0	356.8
15°N	354.7	356.0	356.9
10°N	355.0	356.2	357.1
5°N	354.9	355.9	356.9
Equator	354.9	355.7	356.4
5°S	354.9	355.4	356.1
10°S	354.1	355.0	355.6
15°S	353.0	354.4	355.4
20°S	352.5	353.8	354.9
25°S	352.5	353.7	354.5
30°S	352.3	353.4	354.4
35°S	352.1	353.7	354.5

examples. The trend curves for both sites (dotted lines) show that the increase in CO₂ levelled off in late 1991, and essentially no CO₂ increase was observed in 1992.

The spatial distribution of the 1992 CO₂ growth rate anomaly is shown in Table 2.5. The mean growth rates for 1981-1992 and 1991-1992 were calculated from annual averages based on flask data smoothed in space and time. The global CO₂ growth in 1991-1992 was less than half of the 1981-1992 mean. From 30° to 90°N, CO₂ did not increase from 1991 to 1992. From the CO₂ data alone it is difficult to explain the 1992 CO₂ growth rate anomaly. Although 1992 fossil fuel CO₂ emission data are not yet available, it is extremely unlikely that fossil fuel CO₂ emissions decreased enough to account for the observed northern hemisphere results. An increased CO₂ sink in the terrestrial biosphere is a possible explanation, and is supported by deeper than usual CO₂ drawdowns during the summer of 1992, observed at several flask network sites.

TABLE 2.4. Provisional 1992 Annual Mean CO₂ Mixing Ratios From the *Carla A. Hills* Shipboard Flasks

Latitude	CO ₂ (ppm)
3°N	357.6
6°N	357.0
9°N	357.2
12°N	357.6
15°N	358.2
18°N	358.5
21°N	359.1

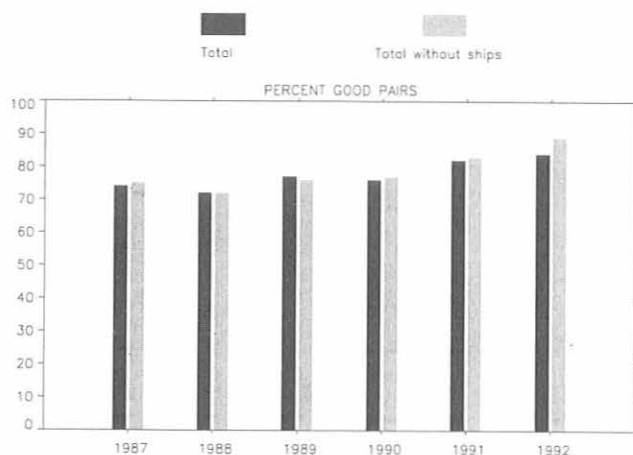


Fig. 2.3. The percentage of flask samples collected each year from 1987 to 1992 meeting the good pair criterion for CO₂ (difference between flasks flushed and filled in series less than 0.5 ppm). The shaded bar represents the percentage of good pairs from both land-based and shipboard samples, and the solid bar represents only the land-based samples.

Similarly, an increase in the flux of atmospheric CO₂ into the oceans could have occurred as a result of cooler sea surface temperatures. The cooling is due to the aerosol cloud produced by the eruption of Mt. Pinatubo. Work is currently being done to improve on these speculations using a 2-D model to calculate the latitude distribution of CO₂ sources and sinks. In addition, the measurements of ¹³C/¹²C in CO₂ from flask network sites begun in 1990 should be extremely valuable in distinguishing between marine and terrestrial effects.

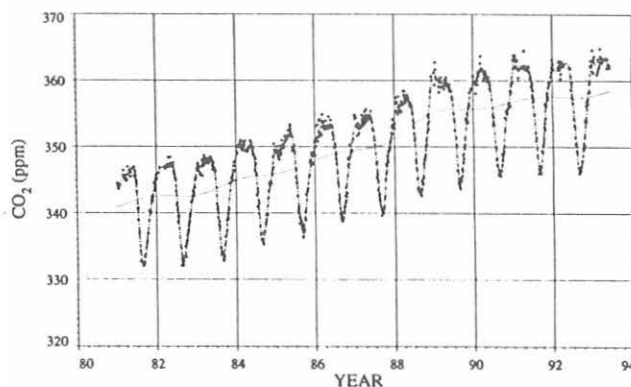


Fig. 2.4. Flask sample CO₂ data for Mould Bay, Canada, 1981-1993. Each square symbol represents the average of a retained pair or a retained single flask. The dashed-dot curve is a combination of curve fits to and digital filtering of the data that shows both low and high frequency variability in the data. The dotted curve shows only the long-term trend with the mean seasonality removed. Note the absence of an increase in CO₂ from 1991 to 1992 (dotted curve).

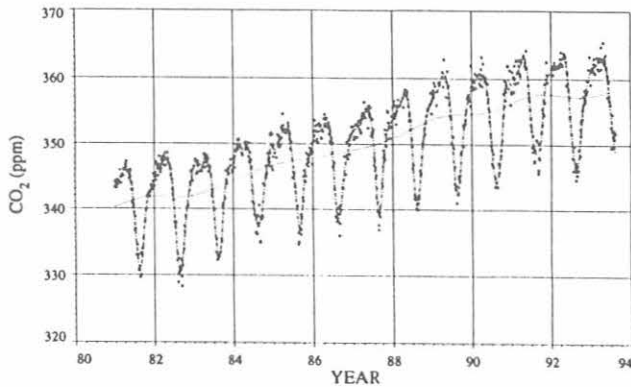


Figure 2.5. Flask sample CO₂ data for Cold Bay, Alaska, 1981-1993. The symbols and curves are the same as in Figure 2.4. Again, note the absence of an increase in CO₂ from 1991 to 1992 (dotted curve).

TABLE 2.5. Comparison of 1981-1992 and 1991-1992 CO₂ Growth Rates (ppm yr⁻¹)

	Global	30°S-90°S	30°S-0	0-30°N	30°N-90°N
1981-1992	1.43	1.38	1.42	1.45	1.47
1991-1992	0.59	0.91	0.87	0.58	0.03

2.1.3. IN SITU METHANE MEASUREMENTS

Semi-continuous measurements of atmospheric CH₄ continued at BRW and MLO in 1992. As before, the sampling frequency was 60 samples per day.

A rebuilt GC, designated Carle 5, was installed at BRW on May 14, 1992. It included modifications designed to make the GC system more robust and easier to maintain, and to improve the measurement precision. Carle 5 was modified in Boulder and then installed at BRW. In Boulder the catalyst used to convert CO and CO₂ to CH₄ in a stream of H₂ and a 4-port, 2-position valve used to divert the gas flow to the catalyst were removed from the GC. This change greatly simplified the procedure for balancing the carrier gas flow rate at the FID for the two positions of the sampling valve. The GC framework was extensively modified to install a Valco Instruments 10-port sample valve instead of the factory equipped Carle valve. Compared with Carle valves, Valco valves are easier to align and maintain, and they are more robust. The sample loop was increased from about 3 mL (STP) to about 6 mL (STP). A 10-mL (STP) sample loop was experimented with, but this amount of sample overloaded the columns. The final important modification was a switch from a column sequence reversal chromatographic method to a backflush of the silica gel pre-column. The combined result of these changes was an improvement in measurement precision from about 0.2% to 0.1% (reported as 1σ of the mean of 20 replicate measurements).

As before, a rule-based expert system (AMIE) was used to evaluate the quality of the in situ measurements [Masarie *et al.*, 1991]. During 1992, 5.7% of the data from BRW and 11.3% of the data from MLO were flagged by AMIE. Daily averaged dry air CH₄ mixing ratios for 1992 in ppb (where 1 ppb = 1 part in 10⁹) are shown in Figure 2.6a for BRW and Figure 2.6b for MLO. The daily means exclude all values flagged by AMIE, but they are not constrained by wind speed or direction.

General features in the data are similar to previous years. At BRW, large CH₄ mixing ratios are observed when the wind direction is outside the clean air sector (defined as 020 to 110), as air masses elevated in CH₄ due to anthropogenic activities pass over the site. Much of the noise in the data is removed when the data are constrained to wind directions within the clean air sector. At MLO, large variability (up to 50 ppb in 2 days) in the CH₄ mixing ratio occurring on synoptic time scales has been attributed to transport affects by Harris *et al.* [1992]. Air masses rapidly transported from Asia to MLO in about a week elevate the CH₄ mixing ratio at MLO compared with air masses that have resided over the tropical Pacific Ocean.

At MLO a diurnal cycle in the CH₄ mixing ratio related to the local meteorology is seen also. After sunrise, the mountain warms which results in air being drawn up from the boundary layer to the sampling site. With this air comes CH₄ mixing ratios that are ≈30 ppb higher than during nighttime when air representative of the free troposphere is sampled. The effects of the upslope/downslope phenomenon on the mixing ratio of CH₄ are shown in Figure 2.7a for August 19 to 21, 1992. The same pattern is observed for the dew point temperature in

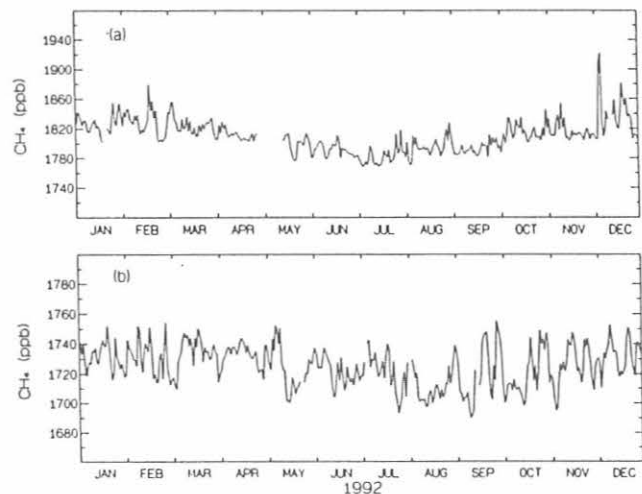


Fig. 2.6. Unselected, daily mean CH₄ mixing ratios for 1992: (a) BRW and (b) MLO. Gaps in the data are due to instrument malfunction. Please note the change in vertical scale between (a) and (b).

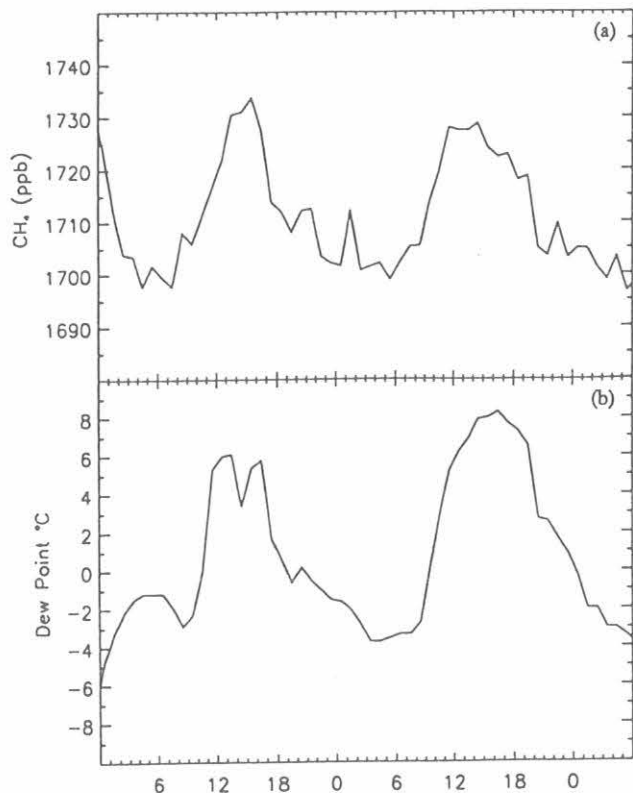


Fig. 2.7. Hourly averaged values for CH₄ (a) and dew point (b) for MLO spanning the period August 19 to 21, 1992. The diurnal cycle results from differences in vertical transport between day and night at the observatory.

Figure 2.7b; higher dewpoints are indicative of moist air moving up from the marine boundary layer to the sampling site.

2.1.4 FLASK MEASUREMENTS OF METHANE

During 1992, the determination of the global distribution of atmospheric CH₄ continued. Measurements of CH₄ were made covering all or part of 1992 from samples collected at 34 sites and three ships participating in the CMDL Carbon Cycle Division cooperative air sampling network. Sampling was started at three new sites during the year: Vestmannaeyjar, Iceland (October), Grifton, North Carolina (July), and Ulaan Uul, Mongolia (January). At the time of writing, no samples were received for 1992 from Halley Bay, Antarctica, and South Georgia Island, and only part of 1992 was covered for Azores (January) and Crozet (January to June). Provisional annual mean values are shown for sites in the cooperative air sampling network in Tables 2.6, and 2.7.

We continued to determine CH₄ mixing ratios from both flasks of a sample pair using the Carle 7 analysis system. In 1992, 6300 flasks were analyzed for atmospheric CH₄.

The average pair difference, based on 2481 pairs, was (0.3 ± 5.0) ppb.

MLO and Cape Kumukahi, Hawaii (KUM) are two sampling sites on the Island of Hawaii approximately 90 km apart, with MLO at an elevation of 3394 m and KUM at sea level. These sites provide a unique opportunity to look for vertical differences in the mixing ratios and seasonal cycles. The annual mean CH₄ mixing ratios for 1984 to 1992 are, on average, (16.0 ± 4.5) ppb larger at KUM than MLO (where the uncertainty is 1σ of the mean). A detailed examination of the data suggests that the vertical gradient averaged over the measurement period varies with the time of year from ≈ 20 ppb during fall, winter, and spring to ≈ 6 ppb during summer. Detrended, seasonal cycles determined from the flask sample data and averaged over the period 1983 through 1992 are shown in Figure 2.8 for MLO and KUM. As shown in the figure, the seasonal cycles at both sites have roughly the same phase, reaching their minima at nearly the same time, but the amplitude of the seasonal cycle at KUM is ≈ 12 ppb (or 40%) larger than at MLO. The appearance of the minima at similar times is

TABLE 2.6. Provisional 1992 Annual Mean CH₄ Mixing Ratios From the Flask Network Sites

Code	Station	CH ₄ (ppm)
ALT	Alert, N.W.T., Canada	1802.1
ASC	Ascension Island	1677.2
AZR	Terceira Island, Azores	[]
BME	Bermuda (east coast)	1769.8
BMW	Bermuda (west coast)	1760.9
BRW	Barrow, Alaska	1806.5
CBA	Cold Bay, Alaska	1794.3
CGO	Cape Grim, Tasmania	1666.2
CHR	Christmas Island	1692.4
CMO	Cape Meares, Oregon	1776.5
GMI	Guam, Mariana Islands	1726.2
HBA	Halley Bay, Antarctica	[]
IZO	Izaña Observatory, Tenerife	1746.8
KEY	Key Biscayne, Florida	1755.0
KUM	Cape Kumukahi, Hawaii	1741.5
MBC	Mould Bay, Canada	1802.8
MHT	Mace Head, Ireland	1782.2
MID	Midway Island	1756.5
MLO	Mauna Loa, Hawaii	1724.0
NWR	Niwot Ridge, Colorado	1756.2
PSA	Palmer Station, Antarctica	1667.6
QPC	Qinghai Province, China	1765.8
RPB	Ragged Point, Barbados	1729.2
SEY	Mahé Island, Seychelles	1689.0
SGI	South Georgia Island	[]
SHM	Shemya Island, Alaska	1795.0
SMO	American Samoa	1668.7
SPO	South Pole, Antarctica	1666.9
STM	Ocean Station M	1793.8
SYO	Syowa Station, Antarctica	1667.7
TAP	Tae-ahn Peninsula, S. Korea	1829.3

Square brackets indicate insufficient data to calculate annual mean.

TABLE 2.7. Annual Mean CH₄ Mixing Ratios From Shipboard Air Sampling

Latitude	CH ₄ (ppb)
<i>Southland Star and Wellington Star</i>	
35°S	1672.2
30°S	1669.3
25°S	1668.3
20°S	1668.3
15°S	1670.0
10°S	1672.7
5°S	1682.8
Equator	1690.7
5°N	1702.1
10°N	1721.6
15°N	17347
20°N	1749.4
25°N	1758.8
30°N	1769.7
<i>Carla A. Hills</i>	
3°N	1719.9
6°N	1723.7
9°N	1727.7
12°N	1738.4
15°N	1739.0
18°N	1746.3
21°N	1762.1

likely due to the fact that the CH₄ sink (reaction with hydroxyl radical, OH) occurs throughout the atmosphere. This is unlike CO₂, where the minimum at KUM precedes the minimum at MLO by about 3 weeks because the drawdown in CO₂ is due to photosynthesis which occurs

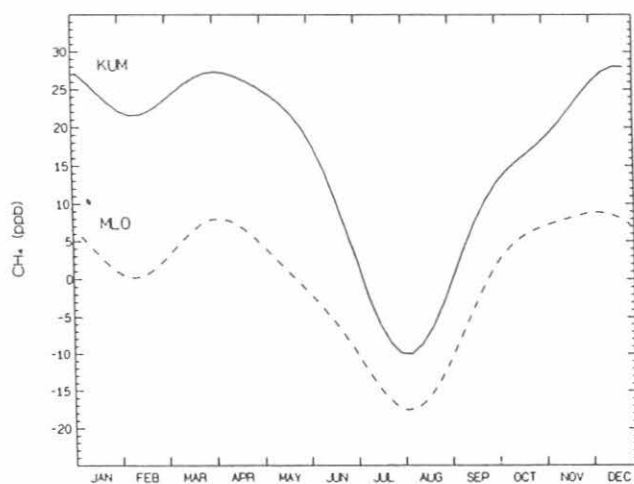


Fig. 2.8. Average, detrended seasonal cycles for MLO (dashed line) and KUM (solid line) determined from the flask data. The curves are based on data from the period 1983 to 1992.

entirely at the surface, within the atmospheric boundary layer. Although it is not surprising that the amplitudes of the seasonal cycles at these two sites are different, a model of atmospheric chemistry and transport is necessary to quantitatively explain the observations.

New air sampling sites located near important CH₄ source regions are being used to place better constraints on regional sources and sinks of CH₄. CH₄ data from one of these sites, Tae-ahn Peninsula in South Korea (TAP), are shown in Figure 2.9 for 1991 and 1992. The important features in the time series are the lack of a seasonal cycle in the average CH₄ mixing ratio and the near-simultaneous appearance of the highest and the lowest values during the summer. Analysis of atmospheric trajectories shows that the lowest values observed during the summer are associated with southeasterly flow off the tropical Pacific Ocean. Values observed at TAP at such times are typical of values observed at KUM. During June to August, northwesterly flow from the peat-rich wetlands located in the maritime provinces of the former Soviet Union elevate CH₄ at TAP by about 80 ppb above the annual mean. Analysis of the TAP observations using a 3-D atmospheric CH₄ model (in collaboration with I. Fung and Y. Chung) suggests that CH₄ emissions from the Far East Russian wetlands may be about two times those of Alaskan wetlands. Also using the 3-D model, the data were used to constrain the global CH₄ emissions from rice cultivation to $\approx 100 \text{ Tg CH}_4 \text{ yr}^{-1}$.

The flask sample data were smoothed using techniques described in Steele *et al.* [1992] to obtain biweekly, zonally averaged data used to study CH₄ trends on large spatial scales (e.g. global, hemispheric, or semihemispheric). Time series of global and hemispheric values are shown in Figure 2.10. The lines approximate the trends. The main features in the data are the strong latitudinal gradient with values in the northern hemisphere always higher than those

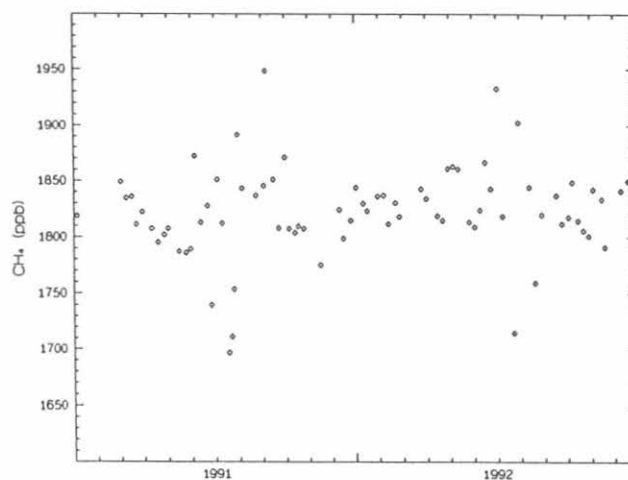


Fig. 2.9. Methane mixing ratios (ppb) for TAP from air samples collected as part of the CMDL cooperative air sampling network.

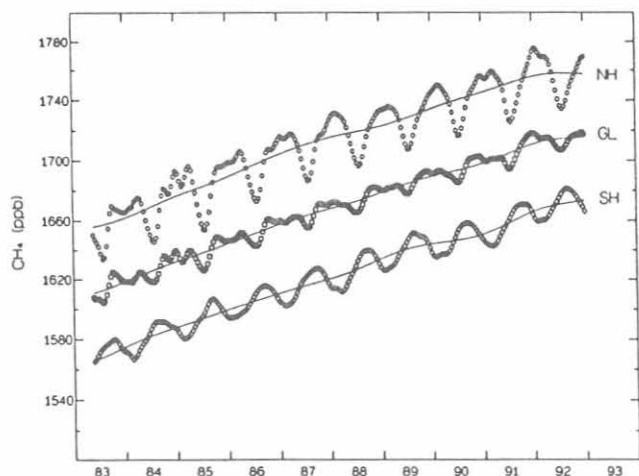


Fig. 2.10. Biweekly CH_4 mixing ratios (symbols) for global and northern and southern hemispheres determined from zonally smoothed flask network data. The line represents the long-term trend in atmospheric CH_4 .

in the southern hemisphere, the seasonal variation in both hemispheres, and the long-term trend. The globally averaged values show a seasonal cycle which is a combination of the seasonal cycles in the two hemispheres. Based on these surface measurements, the global burden of atmospheric CH_4 undergoes a seasonal variation of about 43 Tg CH_4 , where 1 Tg = 10^{12} g. The regular seasonal cycle in the southern hemisphere is due to the seasonality in the photochemical oxidation of CH_4 by OH. The more complex seasonal cycle in the northern hemisphere arises through interactions between seasonal sources and sinks.

A decrease in the global growth rate of atmospheric CH_4 over the period of these measurements from about 14 ppb yr^{-1} in 1984 to less than 10 ppb yr^{-1} in 1992 was observed. It is confidently observed that the decrease is not related to measurement or sampling problems. In Figure 2.11, the instantaneous growth rate curves for semihemispheres obtained using methods as described by Steele *et al.* [1992] are shown for 1983 to 1992. The semihemispheres represent the latitude regions HNH = 30-90°N, LNH = 0-30°N, LSH = 0-30°S, and HSH = 30-90°S. While the rates of decrease of the growth rates for the semihemispheres LSH, LNH, and HSH are somewhat similar, the growth rate in the HNH has fallen off about a factor of 3 faster than the others. The growth rate is affected by both sources and sinks of CH_4 . The observation that the growth rate is falling off much more rapidly in the high latitudes of the northern hemisphere, where most of the industrialized world lives, suggests to us that changes in emissions of anthropogenic sources are largely responsible for the change in the CH_4 growth rate. In particular, the component of the global methane source that is most amenable to rapid reductions by human intervention is that associated with fossil fuel exploitation.

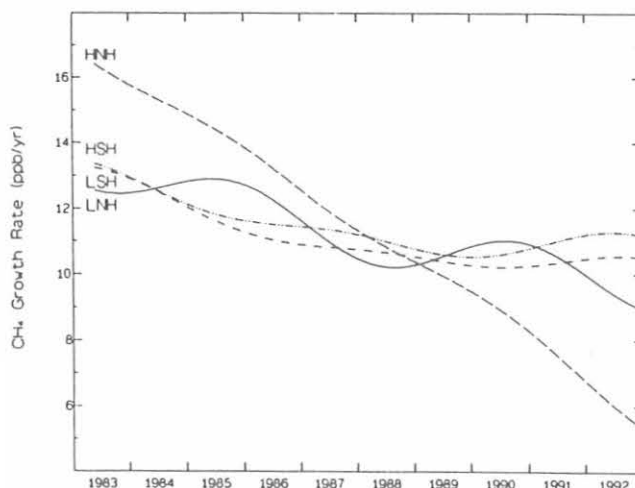


Fig. 2.11. Growth rate variations for four semihemispheres, each containing equal volumes of the atmosphere. The figure highlights the more rapid decrease in the CH_4 growth rate in the high latitudes of the northern hemisphere than in the other semihemispheres.

2.1.5. IN SITU CARBON MONOXIDE MEASUREMENTS

In 1992 quasi-continuous in situ measurements of CO were made at BRW using a Trace Analytical RGA installed at the observatory in September 1991. The analysis, gas chromatography followed by mercuric oxide reduction detection, requires about 3 minutes. Chromatographic data were stored on a diskette, and mixing ratios were calculated from the raw data using a 2-point, linear calibration scheme (standards had mixing ratios of 75.3 and 178.8 ppb CO). The standards were referenced to the CMDL CO-standard scale. The instrument was operational 93% of the time; in March 1992 components of the chromatograph and detector were replaced.

Preliminary hourly-averaged CO mixing ratios for 1992 are shown Figure 2.12a. The data were not constrained for wind speed or direction. The time series shows higher CO mixing ratios in the winter, and lower levels in the summer, which is a seasonal cycle typical of CO. The in situ time series exhibits periods of low variability in CO levels punctuated by short-term increases or decreases. Comparison of CO to CO_2 for January 1992 (Fig. 2.12b, c) shows the mixing ratios of both gases often change rapidly at the same time; these episodes are called "events." In winter, events classified as originating from very distant sources (based upon wind direction) had CO/ CO_2 ratios (ppb/ppm) of between 6 and 10 (r^2 from 0.8 to 0.9); higher ratios of between 6 and 22 (r^2 from 0.6 to 0.8) were observed, and, based upon wind direction, were attributed to local emissions. It has been suggested that in winter, trace gases and aerosols from non-local sources at BRW originate largely from Western Russia and Eastern Europe [Lowenthal and Rahn, 1985; Halter *et al.*, 1985]. In the absence of significant sinks for either gas, CO/ CO_2 ratios

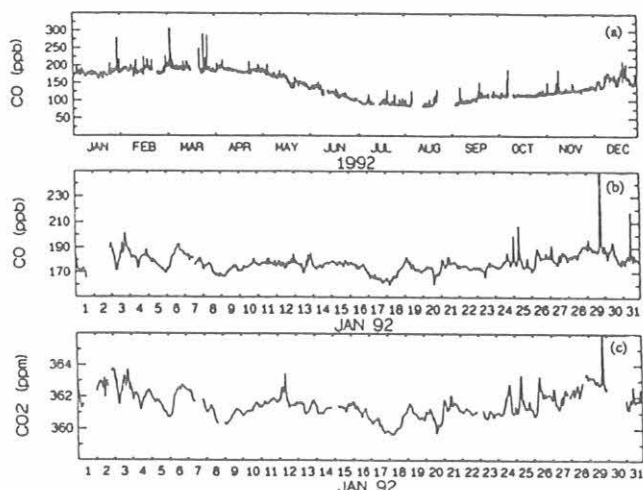


Fig. 2.12. (a) In situ hourly average CO mixing ratios at BRW for 1992. (b) In situ hourly average CO mixing ratios at BRW for January 1992. (c) In situ hourly average CO₂ mixing ratios at BRW for January 1992.

may represent emission ratios from these areas. The average wintertime ratio for events within the designated clean air sector was 8.5. These ratios are about a factor of 2 lower than those estimated for the Northeastern United States and Western Europe [P. Bakwin *et al.*, manuscript in preparation]. The lower value may reflect a number of differences between the United States/Western Europe and Eastern Europe/Russia, including population densities, differences in fossil fuel usage, or a source of CO₂ not sufficiently accounted for (wintertime respiration). In summer the situation is quite different. The CO/CO₂ ratios at Barrow are lower than in winter and show much less correlation (r^2 ranges from 0.1 to 0.9). In summer, CO is lost to oxidation by OH, and CO₂ is certainly depressed due to photosynthesis. As a result, the CO/CO₂ ratio can be both positive and negative.

A CO analysis system, similar to that operating at BRW, was installed at MLO in June 1992. Five to six mixing ratios were calculated every hour using a piecewise linear calibration scheme. The three standards used were referenced to the CMDL scale and had mixing ratios of 81.6, 124.6, and 185.6 ppb. Beginning in July 1992, the system was operating 92% of the time. Figure 2.13 shows

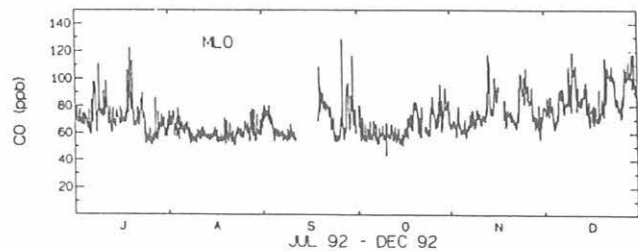


Fig. 2.13. In situ hourly average CO mixing ratios at MLO.

preliminary data collected during 1992. Mixing ratios at MLO are, as expected from previous studies [Novelli *et al.*, 1992, among others], lower than those observed at BRW. In winter the background CO levels reach about 130 ppb; in summer levels of 65 ppb are found.

2.1.6. FLASK MEASUREMENTS OF CARBON MONOXIDE

Carbon monoxide mixing ratios were measured in a subset of flasks collected as part of the cooperative air sampling program. Measurements were made only in air from sites where glass flasks with Teflon O-ring stopcocks were used. Table 2.8 provides the fixed sites where CO was measured in 1992, the date of the first sample collected for CO, and where possible, the 1992 annual mean value for the site. Samples for CO were also collected during crossings of the Pacific Ocean by ships of the Blue Star Line and on the South China Sea between Singapore and Hong Kong on board the tanker *Carla A. Hills* of the Chevron Shipping Company. Analysis of air from all of these flask samples for CO and H₂ was made on a semi-automated Trace Analytical RGA, which shared a common flask sampling carousel, data collection and analysis system, and valve switching control with the gas chromatograph used for the flask measurements of methane. CH₄, CO, and H₂ analyses used a common reference gas. From January to March, the reference gas standard AAL-17269 (118.5 ppb) was used and from May to December, the reference gas AAL-17270 (112.9 ppb) was used. Both standards consisted of chemically dried (using phosphorous pentoxide on an inert support) air collected at Niwot Ridge, Colorado, and both were calibrated against the CMDL CO secondary standards. Hydrogen was referenced to an arbitrary scale awaiting the preparation of accurate standards. The precision of the CO method, estimated as the difference of mixing ratios determined for each flask in a (near-) simultaneously collected pair of flasks, was typically 2 ppb or better.

The response characteristics of the instrument used for flask analysis were non-linear from 0 to 250 ppb. Therefore, CO mixing ratios were calculated using a multi-point calibration curve. A suite of 6-8 standards, and one sample of zero air passed through a CO scrubber (Schutze reagent), were analyzed twice monthly, and all standard response data were normalized to the response of a single flask analysis standard (AAL-17269 or AAL-17270). These response ratios were fit using a polynomial function. CO in flask samples was determined by first calculating the ratio of the area of the sample to that of the standard. Using the calibration curve and these ratios, a mixing ratio for each sample was calculated.

The annual mean CO values were calculated for stations that had a complete data set for 1992 (Table 2.8). These mean values were calculated from a curve fit to the measurements [Thoning *et al.*, 1989] that reduces the effects of short-term variability of the individual samples and of inhomogeneous sampling density through the year. Annual means for 1992 were plotted versus station latitude

TABLE 2.8. Flask Network Sites for CO Analysis and Preliminary Annual Mean CO Levels (ppb)

Code	Station	Latitude	First Sample*	Annual Mean†
ALT	Alert, N.W.T., Canada	82°N	April 1992	
ASC	Ascension Island	8°S	Feb. 1989	80.8 (1.8)
BAL	Baltic Sea Cruises	55°N	Aug. 1992	
BME	Bermuda (east coast)	32°N	June 1991	135.5 (2.5)
BMW	Bermuda (west coast)	32°N	July 1991	132.6 (2.3)
BRW	Barrow, Alaska	71°N	July 1988	139.4 (1.1)
CBA	Cold Bay, Alaska	55°N	April 1992	
CGO	Cape Grim, Tasmania	41°S	June 1991	54.5 (0.4)‡
CHR	Christmas Island	2°N	Dec. 1989	72.9 (0.8)‡
CMO	Cape Meares, Oregon	45°N	Jan. 1992	139.4 (3.0)
GMI	Guam, Mariana Islands	13°N	Oct. 1989	98.5 (1.6)
ICE	Iceland	63°N	Oct. 1992	
ITN	Griffon, N. Carolina Tower	35°N	July 1992	
IZO	Izaña Observatory, Tenerife	28°N	Nov. 1991	110.8 (1.2)
KEY	Key Biscayne, Florida	25°N	Aug. 1991	120.6 (2.4)
KUM	Cape Kumukahi, Hawaii	20°N	June 1989	105.0 (1.7)
MBC	Mould Bay, Canada	76°N	Feb. 1992	
MHT	Mace Head, Ireland	54°N	June 1991	133.8 (2.9)
MID	Midway Island	28°N	Jan. 1992	120.6 (1.9)
MLO	Mauna Loa, Hawaii	20°N	July 1989	96.4 (1.7)
NWR	Niwot Ridge, Colorado	40°N	Dec. 1988	125.8 (1.8)
PSA	Palmer Station, Antarctica	65°S		
QPC	Qinghai Province, China	36°N	July 1991	135.9 (3.8)
RPB	Ragged Point, Barbados	13°N	March 1993	
SEY	Mahé Island, Seychelles	4°S	Sept. 1990	84.3 (1.4)
SMO	American Samoa	14°S	Sept. 1988	57.0 (0.5)
TAP	Tae-ahn Peninsula, S. Korea	36°N	Nov. 1990	285.5 (24)
UUM	Ulaan Uul, Mongolia	44°N	Jan. 1992	181.4 (2.0)§

*The month and year air samples were first collected in a glass flask fitted with Teflon O-ring stopcocks and analyzed for CO.

†Preliminary 1992 mean mixing ratios and the standard error are taken from a smooth curve fit to the measured CO in flask samples as described in *Novelli et al.*, 1991.

‡Mean value for 11 months of data; no samples available for 1 month.

§Mean value from 10 months of data; no samples available for 2 months.

to evaluate the latitudinal variation of CO (Figure 2.14). Generally CO values decreased from north to south. However there were some interesting exceptions. The greatest annual mean CO levels were observed in the mid- and high-northern latitudes. Annual mean CO mixing ratios were about the same from 71°N (Barrow) to 32°N (Bermuda). Further south, carbon monoxide levels decreased to about 55 ppb at 40°S (SMO, CGO). The lifetime of tropospheric CO varies widely with season and latitude. At high latitudes CO is largely conserved in winter and is destroyed by reaction with OH during the

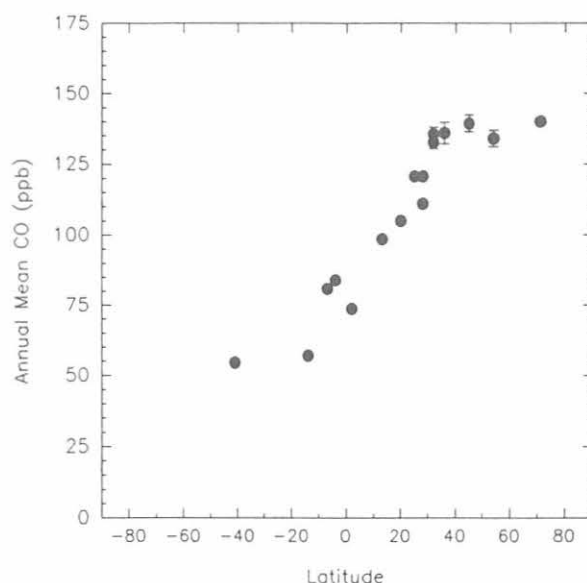


Fig. 2.14. Latitudinal distribution of CO. Annual means for 1992 were calculated by taking weekly values from a smoothed curve fit to the data, then calculating monthly means, and annual means from the monthly means as described by *Novelli et al.* [1992].

summer. In the tropics CO has a lifetime of 1-2 months due to the high OH radical concentration. The latitudinal distribution reported here would suggest there are large regions of the troposphere that are relatively well mixed on time scales comparable to CO lifetimes. However, a comparison of annual mean CO values at stations with similar latitude and different longitude (for example Key Biscayne, Florida, Midway Island, and Izaña Observatory, Tenerife at about 25°-28°N, or Tae-ahn Peninsula, S. Korea and Qinghai Province, China at 36°N) sometimes shows substantial longitudinal variations in CO. These differences probably reflect regional scale anthropogenic impacts on CO levels at some locations. Similarly, biomass burning in Africa may directly impact CO levels at some downwind sites (e.g., Ascension Island and Mahé Island, Seychelles, but not Christmas Island).

2.2. REFERENCE GAS STANDARDS

2.2.1. CARBON DIOXIDE

The calibrations of CO₂-in-air reference gas tanks continued in 1991; on 154 days, 308 tanks were calibrated. The filling of high-pressure cylinders with dry air from Niwot Ridge for use as reference gases continued in 1991. The set of 15 reference gases stored in large aluminum cylinders, which will eventually become the CMDL primary CO₂ standards, were calibrated by the Scripps Institute of Oceanography (SIO) in 1992. The NOAA secondary CO₂-in-air standards were also shipped to SIO for calibration in 1992.

The transfer calibration system was revised in 1992 to allow more calibrations to be performed using the same amount of standard reference gases. Figure 2.15 shows the new system. A Valco 16-port stream selection valve replaced an array of eight solenoid valves for switching the appropriate gas to the NDIR analyzer. The number of unknown gas tanks being calibrated was increased from two to four, while still using four known standards. Now either two or four unknowns can be calibrated at one time, with the time for each calibration being 2 hours and 24 minutes and 3 hours and 12 minutes respectively.

Construction of a system for making manometric measurements of the mole fraction of CO₂ in standard gases continued in 1992. Extensive modifications to the system were made. Tests showed unstable adsorption effects from the small amounts of polymers used in the system, even when using dry air, which created instability in the measurement of the volumes containing the air sample and the CO₂ sample. Based on this, it was decided to replace all the polymer parts with glass. This involved installing standard greased stopcocks in place of metal valves. These stopcocks are connected to an air-driven

rotary actuator, which turns the handle of the stopcock 90 degrees.

Some small changes in the response of the Ruska quartz-spiral pressure gauge were observed but unexplained. A deadweight pressure gauge purchased by the Carbon Cycle Division in 1992 was used to calibrate the pressure gauges in the system. A history of calibrations was begun so that the long-term stability of the gauge calibration can be observed.

2.2.2. CARBON MONOXIDE

The CMDL primary CO standards were prepared gravimetrically and were propagated to a set of secondary CO-in-air standards [Novelli *et al.*, 1991]. These secondaries were used to calibrate a set of tertiary standards. These make up the CMDL working standards. In March 1992 three CO-in-air standards were prepared by the CMDL NOAA Division using gravimetric methods (mixing ratios of 48.0, 99.9 and 147.2 ppb). The secondary and tertiary standards were then calibrated using the new gravimetric standards. The CO values assigned to

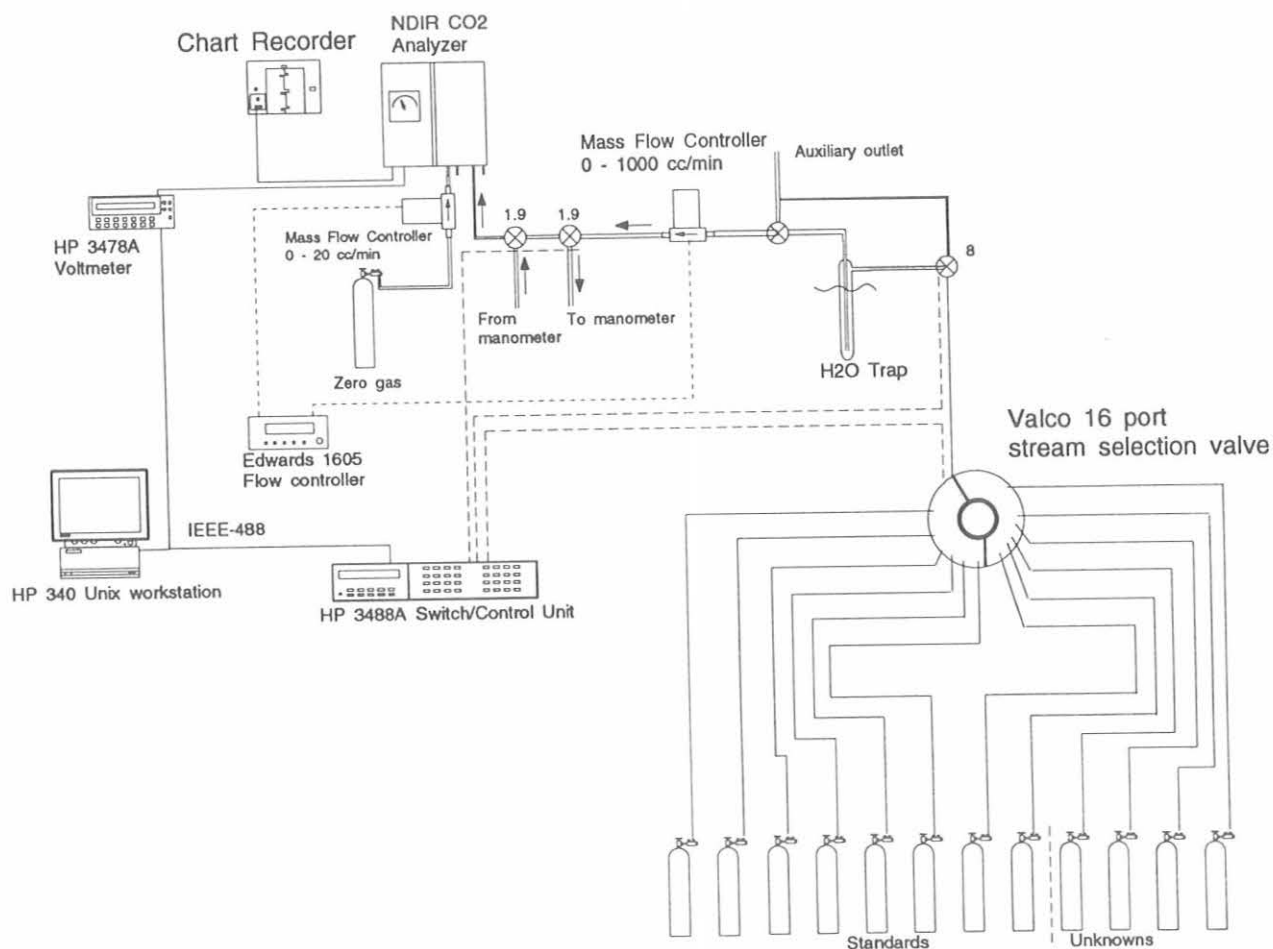


Fig. 2.15. Diagram of CO₂ transfer calibration system.

TABLE 2.9. CO Mixing Ratios* Assigned to Standards Based Upon Different Calibration Procedures

Cylinder ID	Type Fill Date†	GravI (ppb)‡	Second (ppb)§	GravII (ppb)**
AAL-17269	NWR, Nov. 1987	118.5 (0.6)	117.6 (0.9)	117.0 (0.6)
CC68734	NWR, Dec. 1988	159.7 (1.5)	159.5 (1.0)	160.1 (1.8)
CC61344	NWR, Dec. 1988	181.5 (1.5)	182.3 (1.3)	181.5 (1.7)
CC73110	NWR, Jan. 1990	202.4 (0.9)	200.7 (2.1)	202.6 (1.9)
CC73198	NWR, Jan. 1990	179.3 (1.7)	178.8 (0.9)	179.3 (1.7)
CC89259	SM, Jan. 1990	34.9 (1.9)	31.9 (1.7)	32.2 (1.5)
CC89580	SM, June 1990		50.7 (1.1)	49.9 (0.6)
CC71607	NWR, Sept. 1991		133.8 (2.0)	134.4 (1.4)

*Mixing ratios are in units of parts per billion by mole fraction (ppb). Values represent the mean of several calibrations; the standard deviations of the means are presented in parentheses.

†Type of air in tank and fill date. NWR indicates the cylinder was filled at Niwot Ridge, Colorado; SM indicates the standard was purchased from Scott Marrin, Inc.

‡GravI = Mixing ratios assigned based upon calibration against the 17 gravimetric standards prepared 1989-1990 as described by *Novelli et al.*, 1991.

§Second = Mixing ratios assigned to cylinders based solely upon calibration against other secondary standards using CO values based upon GravI.

**GravII = Mixing ratios assigned to cylinders based upon calibration against the gravimetric standards prepared in March 1992.

standards using either a 1-, 2- or multi-point calibration, and using either the primary, secondary or new gravimetrics show no significant difference (Table 2.9.). The intercalibrations of the CMDL working standards show that the reference values assigned to the standards were propagated with a precision of at least 1%. Comparison of gravimetric standards made at different times, with different materials, and by different people suggests an accuracy of 1%. In general, the working standards appear stable with respect to CO over time scales of at least several years.

2.3. NEW MEASUREMENT PROGRAMS

2.3.1. MEASUREMENTS OF CARBON DIOXIDE ON A VERY TALL TOWER

Measurements of CO₂ on a 610-m tall television and radio transmitter tower in a rural area of eastern North Carolina (35° 21' 55" N, 77° 23' 38" W, 9 m above sea level) began in June 1992. Use of the tower and space in the transmitter building for our analytical and data acquisition equipment were donated free of charge by American Family Broadcasting, Inc.

Tubes for trace gas sampling were mounted on the tower with inlets at 51, 123, and 496 m height, and sensors for wind speed and direction, temperature and humidity were placed at the same three levels. Three CO₂ analyzers are located within the transmitter building at the base of the tower, with an analyzer dedicated to continuous sampling from each altitude. Flask samples are collected weekly from the 496 m level for analysis for CH₄, CO₂, CO and δ¹³C in CO₂. In addition, concentrations of radon-222 are being measured by scientists from the University of North Carolina. Radon-222 originates in the soil from decay of radium-226 and has a half-life of 3.8 days, making it an

excellent tracer for soil/atmosphere gas exchange and for continental air masses. Sampling and calibration sequences are controlled and data are read and pre-processed using a PC. One-half hour averages of the data are computed and transmitted to Boulder each day by modem.

Figure 2.16 shows the mean diurnal cycle for CO₂ at each height for periods of several days in June 1992 and January 1993. In summer the concentration gradient is positive upwards in the afternoon because of vigorous photosynthetic uptake of CO₂ at the surface. At night a shallow inversion forms, and concentrations at 51 m rapidly increase because of plant and soil respiration and industrial emissions, often reaching in excess of 400 ppm. Radon-222 concentrations also build up near the surface at night. The diurnal cycle is damped at higher altitudes; the magnitude is typically 7-10 ppm at 496 m in summer. A morning pulse of CO₂ is evident at 123 and 496 m as CO₂ stored in the nocturnal stable layer is mixed upward with the onset of convection. The nocturnal build-up at low altitudes is reflected in 10-20 ppm higher daily mean CO₂ concentrations at 51 m than at 496 m in summer. In winter the biologically driven surface sources and sinks are much smaller and the diurnal variation at all altitudes is greatly reduced. Clearly, biological activity dominates industrial CO₂ sources at this rural site in summer.

A time series of the daily minimum CO₂ concentration at 496 m is shown in Figure 2.17. The daily minimum, which generally occurs in late afternoon, may reasonably approximate the average for the daytime convective boundary layer (e.g., 2-3 km depth), since vertical gradients above 496 m are likely to be small. The time series of daily mean concentrations shows a similar pattern, but the values are typically 2-8 ppm higher. Monthly statistics for the daily minimums and means are given in Table 2.10.

Day-to-day changes in the daily minimums (or means) are large, as much as 15-20 ppm in the summer, probably

reflecting changes in air-mass back trajectory and the vigor of vertical mixing. Also in summer, the biological source and sink strengths are strongly dependent on meteorological parameters such as temperature and illumination. The monthly medians change smoothly, confirming that these data will be useful for comparison with the CMDL "background" (remote) sites. The magnitude of the seasonal cycle is about 15 ppm, with a sharp minimum in August and a broad maximum in January-April. Starting in about the last week of April, concentrations begin to drop rapidly as photosynthetic activity increases towards summer levels.

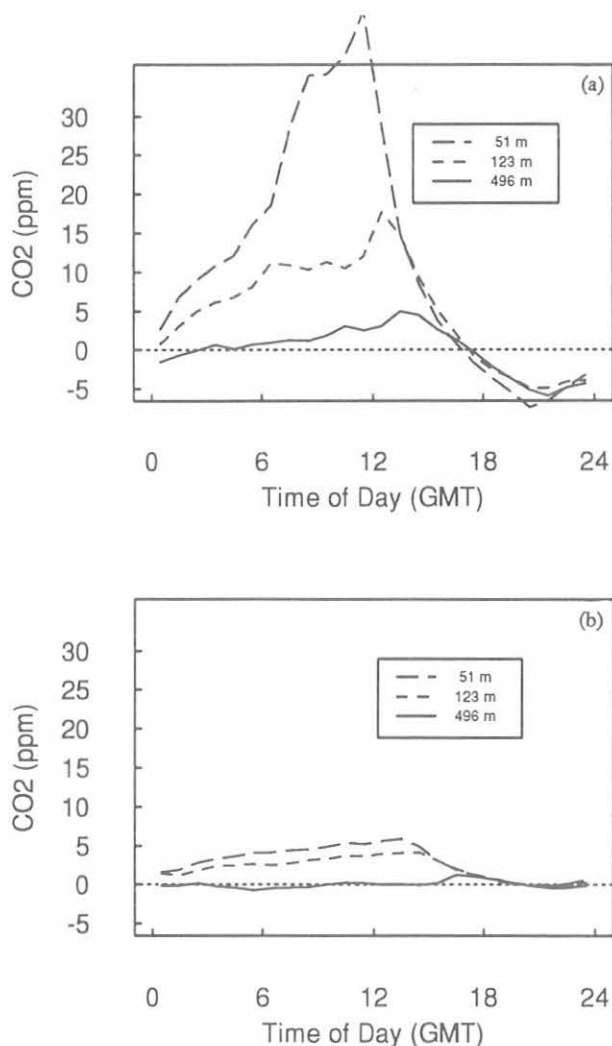


Fig. 2.16. Mean diurnal cycles of CO_2 at 51, 123, and 496 m above the ground on the tower in eastern North Carolina for (a) June 14-21, 1992, (b) January 18-February 1, 1993. The daily mean at 496 m for each day has been subtracted from the data and the data were binned in 1-hour intervals. Time is given as GMT, which is 5 hours ahead of local standard time.

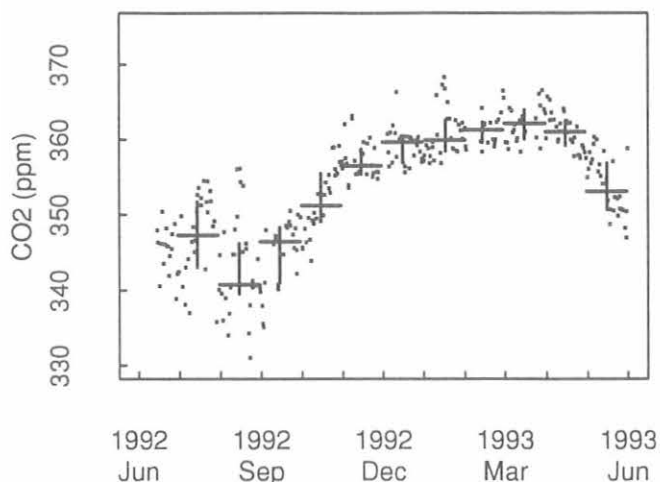


Fig. 2.17. Daily minimum CO_2 mixing ratios at 496 m above the ground on the North Carolina tower for June 14, 1992, to May 31, 1993. Medians and the upper and lower quartiles for each month are also shown (and are summarized in Table 2.10).

2.3.2 FLASK SAMPLES FROM AIRCRAFT

This year marked the beginning of operation of the Aircraft Sampling Project. The intent of this project is to measure biweekly profiles of CO_2 , CH_4 , and CO in the troposphere over continental sites to determine vertical mixing rates and identify trace gas sources and sinks. The operation may also be useful for studying boundary layer dynamics and species ratios of anthropogenic sources.

To make sample collection economically feasible, the project relies on a highly automated sampling system that requires a minimum of labor to operate and can be flown on inexpensive and available aircraft. The current system consists of two aluminum cases, each about 25 cm \times 50 cm \times 75 cm and each weighing about 30 kg. One case contains compressors and batteries, making the system completely self-powered and operable up to 12000 m. The other case contains 20 1-L glass sampling flasks and a microcontroller to actuate the sample valves at pre-programmed altitudes, based on inputs from a Global Positioning System receiver and a barometric altimeter. The system can be installed in a light aircraft by one person in less than 15 minutes and operates unattended or with minimal pilot interaction. After a sampling flight, the flask case is plugged into an automated analysis system, which sequentially measures the samples with no further operator intervention.

Our first sampling site using this system is located over Carr, Colorado, about 100 km north of Boulder (40.9°N, 104.8°W). Test flights began in March, and regularly scheduled twice-monthly flights commenced in November. A low-cost single-engine plane was used to take samples up to 7600 m. Figure 2.18 shows a typical CO_2 profile. The combined sampling and analysis method yields a precision of about 0.07 ppm CO_2 , 5 ppb CH_4 and 3 ppb CO . After a

TABLE 2.10. Monthly Statistics for Daily Minimum and Mean CO₂ (ppm) 496 m Above the Ground on the North Carolina Tower

Month	Year	Daily Minimum						Daily Mean					
		Mean	Std. Dev.	N	Median	LQ	UQ	Mean	Std. Dev.	N	Median	LQ	UQ
July	1992	347.00	5.62	31	347.38	343.02	351.71	353.86	4.42	25	353.96	351.22	356.84
Aug.	1992	342.85	6.42	31	340.70	338.96	346.44	348.77	6.47	29	349.14	343.15	354.09
Sept.	1992	345.37	4.46	22	346.99	342.19	348.55	349.83	4.44	18	351.10	346.47	352.54
Oct.	1992	352.12	4.08	31	351.24	349.23	355.48	356.29	5.19	30	354.99	352.31	359.71
Nov.	1992	357.26	2.58	27	356.55	355.47	358.88	361.40	4.32	29	360.45	358.11	363.29
Dec.	1992	359.11	2.24	29	359.68	357.20	360.32	361.88	3.12	29	361.33	359.80	363.66
Jan.	1993	360.89	3.21	29	360.07	358.45	362.57	364.06	3.78	28	363.21	361.60	366.03
Feb.	1993	361.28	2.21	17	361.28	359.56	362.31	364.76	2.83	17	364.08	362.53	367.61
March	1993	362.02	2.41	23	362.00	359.87	364.03	365.51	3.48	23	364.58	362.90	368.64
April	1993	360.91	2.28	30	360.99	359.04	362.44	363.61	2.94	27	363.34	361.76	365.19
May	1993	353.71	3.66	31	353.10	350.67	356.88	357.77	3.53	30	358.35	354.58	361.08

year of sampling and a full seasonal cycle of data has been obtained, the vertical mixing rate and seasonal averages for CO₂, CH₄, and CO can be estimated.

2.4. DATA MANAGEMENT

Considerable effort was made in 1992 to define and implement a long-term Carbon Cycle Division flask data management strategy. Annually, more than 5500 air samples are collected in glass flasks from over 30 different locations and shipped to Boulder where they are analyzed for several trace gas species. Air collected into a single 2.5-L glass flask is currently analyzed for CO₂, CH₄, CO, H₂ within our lab, and for C¹⁸O₂ and ¹³CO₂ by the Stable Isotope Laboratory at the Institute of Arctic and Alpine Research (INSTAAR, University of Colorado). Future flask measurement projects include N₂O by CMDL and ¹³CH₄ by INSTAAR. Each flask has a unique sample history that includes sampling location, date and time, flask identification number, sample collection method, and sampling wind speed and direction. Each analysis produces a mixing ratio or isotopic ratio, a flag, and additional analysis information. The proliferation of flask data from the various measurement projects has lead us to consider a data management strategy that (1) will allow timely comparisons of ambient mixing ratios or isotopic ratios of the measured species; (2) will easily accommodate all existing and future trace gas measurements made from air collected in flasks; (3) will continue to provide the individual measurement programs the independence necessary to best maintain their data; (4) will require minimal software modifications; and (5) can be maintained by a primary and secondary database manager. After considering several strategies, including commercially available relational database management packages, management software that could provide the necessary flexibility with relatively little disruption to the projects and minimal modifications to existing software was developed in-house.

The strategy adopted is simple and features a search key that is common to all files containing analysis results for

an air sample collected in a flask. For a given air sample, results will exist in one daily analysis file and one processed site file for each project analyzing the sample. Search keys used by relational database packages are often non-repeating consecutive integers. To satisfy the above mentioned requirements, a key that uniquely identifies a flask sampling event was built. This 31-character key includes the sampling location, GMT date and time, flask id number, and sample collection method as shown below for an air sample collected at MLO.

MLO 1992 12 18 20 07 2340-66 P

The only condition required of current and future flask measurement projects is that analysis results residing in the daily analysis files and processed site files must be preceded by the 31-character search key. Once this condition is satisfied, the primary task becomes one of

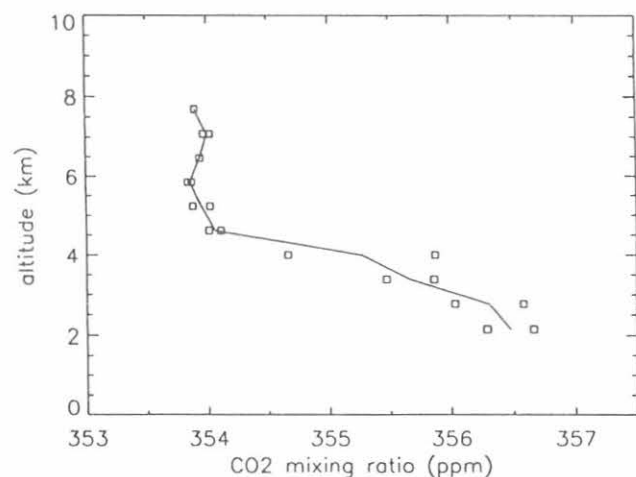


Fig. 2.18. Vertical profile for CO₂ over Carr, Colorado, from December 10, 1992. (Altitude is in km above sea level.) Square symbols represent individual flask measurements. The solid line is drawn through the average of two samples collected in succession at each altitude.

ensuring that the integrity of the 31-character search key is maintained everywhere it exists. This is accomplished by restricting access to the search key.

The search key is created by one (and only one) software package within the Carbon Cycle Division. Before an air sample is analyzed, the flask must proceed through a check-in procedure. This procedure is semi-automatic and has two primary functions. The first function is to maintain a flask inventory, i.e., tracking when, where, and how each flask was shipped from and returned to Boulder. The second function is to introduce each flask's sampling history into a computer data base; it is here that the 31-character search key is created. During a measurement, the analysis software simply requests the flask identification code, and upon entry, receives the search key from the database. This software then uses the search key in creating the data files resulting from the analysis. The search key is propagated to the various measurement projects as the air sample is analyzed. At no time may the individual measurement projects modify the search key. If an error in the search key is suspected, then the original sample sheet is annotated and the problem is resolved at a later time.

The search key may be edited by one (and only one) software package within the Carbon Cycle Division. Every 2 weeks the original sample sheets of flasks analyzed during this period are collected and collated. The sample history from each sample sheet is compared with the history recorded during the check-in procedure; annotations made during analyses are also addressed at this time. Any necessary changes to the search key are made at this time by the primary database manager using a single software package. This package replaces the incorrect search key with the edited key everywhere that the key exists and documents each action in a log file. All personnel responsible for maintaining the various measurement databases are automatically notified of the changes made by the database manager by electronic mailing of the log file.

This flask data management strategy has been fully implemented. The benefits of this strategy are already

quite clear. The various measurement project data bases remain independent, but are easily related by the search key. The integrity of the search key is maintained by restricting access to both personnel and software. New measurement programs can develop independently but integrate easily by satisfying the single design constraint based on the search key. Considerable time is saved when search-key errors are corrected everywhere by the data base manager. And finally, software written for the statistical and graphical analysis of flask data can be species-independent, providing powerful analysis tools to a greater number of flask measurement programs.

2.5. REFERENCES

- Halter, B.C., J.M. Harris, and K.A. Rahn, A study of winter variability in carbon dioxide and Arctic haze aerosols at Barrow, Alaska, *Atmos. Environ.*, 19, 2033-2037, 1985.
- Harris, J.M., P.P. Tans, E.J. Dlugokencky, K.A. Masarie, P.M. Lang, S. Whittlestone, and L.P. Steele, Variations in atmospheric methane at Mauna Loa Observatory related to long-range transport, *J. Geophys. Res.*, 97, 6003-6010, 1992.
- Lowenthal, D.H., and K.A. Rahn, Regional sources of pollution aerosol at Barrow, Alaska, during winter 1979-80 as determined from elemental tracers, *Atmos. Environ.*, 19, 2011-2024, 1985.
- Masarie, K.A., L.P. Steele, P.M. Lang, A Rule-based expert system for evaluating the quality of long-term, in situ, gas chromatographic measurements of atmospheric methane, NOAA Tech. Memo, ERL CMDL-3, Boulder, CO, 1991.
- Novelli, P.C., L.P. Steele, and P.P. Tans, Mixing Ratios of Carbon Monoxide in the Troposphere, *J. Geophys. Res.*, 97, 20,731-10,750, 1992.
- Novelli, P.C., J.W. Elkins, and L.P. Steele, The development and evaluation of a gravimetric reference scale for measurements of atmospheric carbon monoxide, *J. Geophys. Res.*, 96, 13,109-13,121, 1991.
- Steele, L.P., E.J. Dlugokencky, P.M. Lang, P.P. Tans, R.C. Martin, and K.A. Masarie, Slowing down of the global accumulation of atmospheric methane during the 1980s, *Nature*, 358, 313-316, 1992.
- Thoning, K.W., P.P. Tans, and W.D. Komhyr, Atmospheric carbon dioxide at Mauna Loa Observatory 2. Analysis of the NOAA GMCC data, 1974-1985, *J. Geophys. Res.*, 94, 8549-8565, 1989.

3. Aerosol, Radiation, Ozone, and Water Vapor Division

B. BODHAINE, E. DUTTON, R. EVANS, R. GRASS, J. HARRIS, D. HOFMANN, W. KOMHYR,
D. NELSON, J. OGREN, AND S. OLTMANS

3.1. CONTINUING PROGRAMS

3.1.1. SURFACE AEROSOLS

3.1.1.1. BASELINE OBSERVATIONS

Operations

The aerosol monitoring program at BRW, MLO, SMO, and SPO continued during 1992 as in previous years. Condensation nucleus (CN) concentration was measured continuously with TSI (butanol-based) CN counters at BRW, MLO, SMO, and SPO. Daily calibration points were provided by Pollak CN counters at all stations. TSI CN counters have been operated at BRW since March 1990, MLO since May 1988, SMO since May 1992, and SPO since January 1989. After TSI CN counter installation at each station, G.E. CN counter operation was continued for a 1-year comparison, and then G.E. CN counter operation was terminated. At the end of 1992 all G.E. CN counters had been discontinued. Aerosol scattering extinction coefficient (σ_{sp}) at 450-, 550-, 700-, and 850-nm wavelengths was measured continuously at BRW, MLO, and SPO with four-wavelength nephelometers. Aerosol absorption coefficient has been measured continuously using aethalometers at BRW since April 1988, MLO since April 1990, and at SPO during December 1986-December 1991. Table 3.1 shows the time periods of operation of the CN counters and nephelometers at the four baseline stations.

Figure 3.1 shows daily geometric means of CN concentration (lower portion of each plot), σ_{sp} (middle portion of each plot), and Ångström exponent (upper portion of each plot) at the CMDL stations for 1992. Two independent values of Ångström exponent (α) were calculated from the 450-, 550-, and 700-nm channels of σ_{sp} data using the relation $\alpha = -\Delta \log \sigma_{sp} / \Delta \log \lambda$, where α is

Ångström exponent and λ is wavelength. These averages were calculated only if data for all three wavelengths were available. The interpretation of α in terms of aerosol size distribution was discussed by *Bodhaine and DeLuigi* [1985]. Monthly geometric means of the 1991 aerosol data are listed in Table 3.2. A graphical presentation of the monthly geometric means of the entire data record for the four stations is shown in Figure 3.2.

Discussion

The BRW data in Figure 3.1 show a σ_{sp} maximum of about $3 \times 10^{-5} \text{ m}^{-1}$ during spring, typical of the well-known Arctic Haze. Minimum values of σ_{sp} below 10^{-6} m^{-1} occurred in July-August. The BRW long-term record shown in Figure 3.2 clearly shows this annual cycle in σ_{sp} , with springtime monthly means of about 10^{-5} m^{-1} and summertime monthly means of about 10^{-6} m^{-1} . The BRW CN record shows a more variable semiannual cycle with a maximum that usually coincides with the maximum in σ_{sp} and another maximum in late summer or early fall. The 1992 annual geometric mean for CN is 228 cm^{-3} and the annual mean for σ_{sp} (550 nm) is $4.62 \times 10^{-6} \text{ m}^{-1}$. Note that the G.E. counter CN record is shown as a solid line and the TSI counter CN record is shown as a dashed line. The individual squares plotted on the CN graph are monthly means of Pollak counter observations. These are shown separately because the TSI and Pollak counter give independent data sets, whereas the G.E. counter was calibrated using the Pollak counter data. Numerous gaps in the data are apparent because of the averaging process excluding data if local pollution is evident or if winds are not from the clean air sector. The BRW aerosol data set was presented by *Quakenbush and Bodhaine* [1986].

The MLO σ_{sp} data shown in Figure 3.1 are typical with the highest values in April and May and lower values in fall and winter. Large events are apparent in the springtime, caused by the long-range transport of Asian desert dust in the upper troposphere to the vicinity of Hawaii. As discussed in the *1988 Summary Report* [*Elkins and Rosson*, 1989], σ_{sp} values were generally higher since the installation of the new nephelometer in 1985 and have not reached the low values expected in winter. The MLO CN record shown in Figure 3.1 is typical, giving an annual geometric mean concentration of 375 cm^{-3} ; the annual mean of σ_{sp} (550 nm) is $8.58 \times 10^{-7} \text{ m}^{-1}$. Note that all MLO aerosol data presented here are in the form of geometric means during 0000-0800 HST (1000-1800 UT) in order to include data for nighttime downslope wind conditions only. The MLO data set was presented by *Massey et al.* [1987].

TABLE 3.1. Operation of Aerosol Instrumentation at BRW, MLO, SMO, and SPO

Station	Pollak CN	G.E. CN	TSI CN	4- λ Neph.
BRW	May 1976- Present	May 1976- Mar. 1991	March 1990- Present	May 1976- Present
MLO	Jan. 1974- Present	Jan. 1974- June 1989	June 1988- Present	Jan. 1974- Present
SMO	June 1977- Present	June 1977- Dec. 1992	May 1992- Present	June 1977- Mar. 1991
SPO	Jan. 1974- Present	Jan. 1974- Dec. 1989	Jan. 1989 Present	Jan. 1979- Present

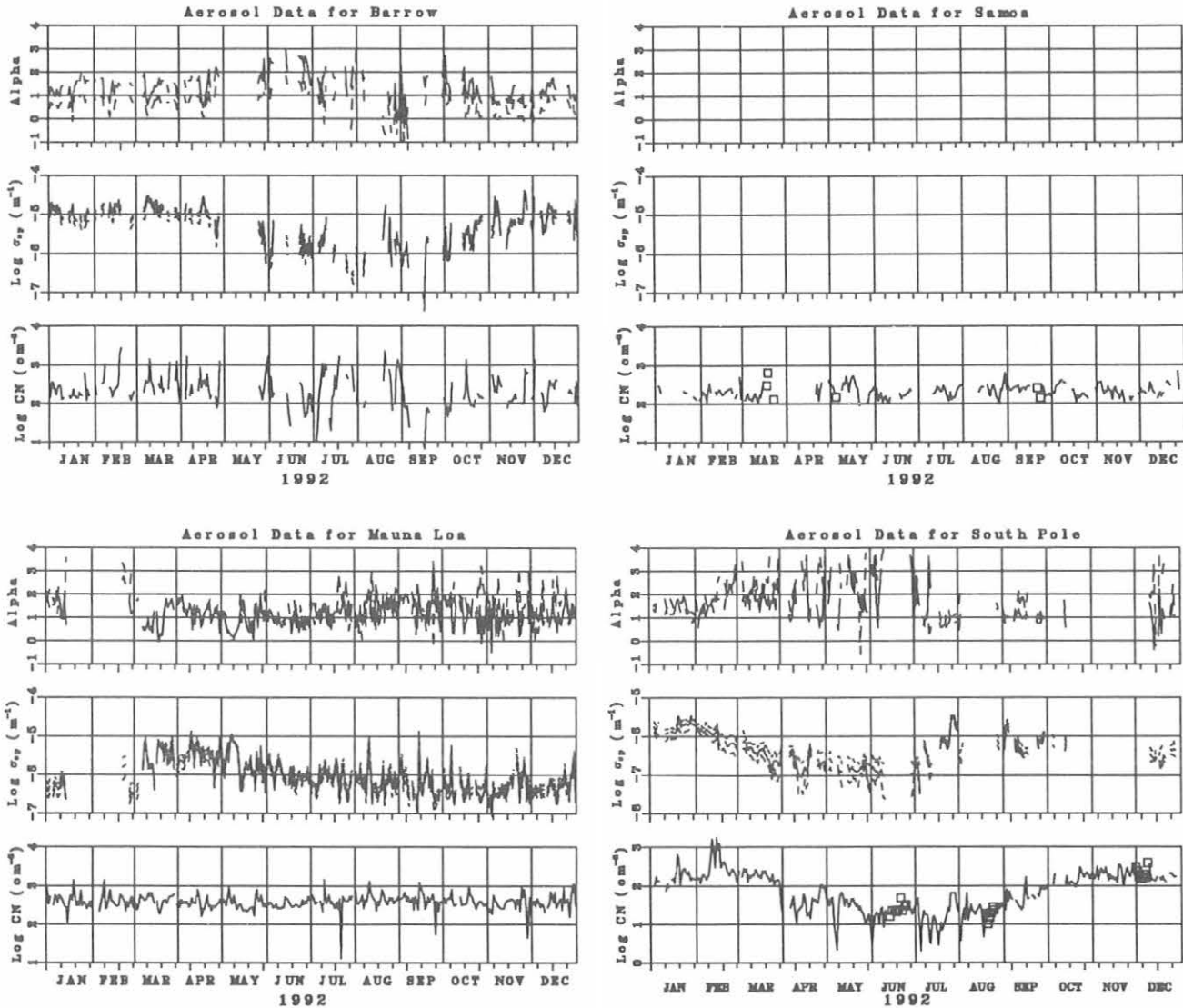


Fig. 3.1. Daily geometric means of σ_{sp} and CN data at BRW, MLO, SMO, and SPO for 1992. Data for MLO are included only for 0000-0800 LST. For each station, CN concentration (lower) is shown as a solid line, and daily mean Pollak counter data are shown as small squares. The σ_{sp} data (middle) are shown for 450 (dotted), 550 (solid), and 700 nm (dashed). Ångström exponents (alpha) were calculated from 450- and 550-nm (dotted) and 550- and 700-nm (solid) σ_{sp} data.

The SMO CN data continue as in previous years with no significant annual cycle or long-term trend. The SMO 1992 annual mean is about 207 cm^{-3} for CN concentration, representative of the background marine boundary layer in that region. The SMO nephelometer was removed from service in March 1991. The SMO data record was presented by *Bodhaine and DeLuisi* [1985].

The SPO σ_{sp} and CN data are shown in Figure 3.1. These data show a strong annual cycle reaching a maximum in the austral summer and a minimum in the winter, similar to previous years. The σ_{sp} data show fairly clean values in the fall and events resulting from the transport of sea-salt particles in July and September.

Because of instrument problems, some data are missing in the winter and fall. Referring to the long-term data set for SPO shown in Figure 3.2, the σ_{sp} data generally show intermediate values in the austral summer and fall, and large events, sometimes exceeding 10^{-6} m^{-1} , in late winter. These large aerosol events are caused by the transport of sea salt in the upper troposphere from stormy regions near the Antarctic coast to the interior of the continent. The SPO 1992 annual means are about 69 cm^{-3} for CN and $4.41 \times 10^{-7} \text{ m}^{-1}$ for σ_{sp} (550 nm). Analyses of the SPO data were presented by *Bodhaine et al.* [1986, 1987]. The complete data set was presented by *Bodhaine and Shanahan* [1990].

TABLE 3.2. Monthly Geometric Means of CN concentration (cm^{-3}) and σ_{sp} (m^{-1}) at 450, 550, and 700 nm for BRW, MLO, SMO, and SPO During 1992

	Jan.	Feb.	March	April	May	June	July	Aug.	Sept.	Oct.	Nov.	Dec.
<i>BRW</i>												
CN	204	354	346	263	338	100	363	354	83	162	245	208
σ_{sp} (450)	1.17-5	1.48-5	1.70-5	1.15-5	3.63-6	2.57-6	1.62-6	2.04-6	1.62-6	4.57-6	9.55-6	1.02-5
σ_{sp} (550)	1.05-5	1.29-5	1.48-5	9.77-6	2.75-6	1.95-6	1.35-6	1.86-6	1.05-6	3.89-6	9.33-6	9.33-6
σ_{sp} (700)	7.76-6	9.33-6	1.07-5	6.92-6	1.7-6	1.12-6	9.55-7	1.55-6	7.24-7	2.88-6	7.76-6	6.92-6
<i>MLO</i>												
CN	398	380	407	338	309	380	380	436	426	354	331	380
σ_{sp} (450)	7.08-7	1.15-6	3.8-6	4.07-6	2.4-6	1.35-6	1.00-6	8.32-7	6.61-7	5.13-7	6.17-7	6.17-7
σ_{sp} (550)	5.13-7	7.08-7	3.09-6	3.24-6	2.04-6	1.07-6	7.76-7	6.17-7	5.01-7	3.63-7	5.01-7	4.57-7
σ_{sp} (700)	3.55-7	4.17-7	2.45-6	2.45-6	1.70-6	8.51-7	5.89-7	4.37-7	3.39-7	2.82-7	3.72-7	3.55-7
<i>SMO</i>												
CN	213	190	151	263	251	154	208	218	223	223	194	229
<i>SPO</i>												
CN	181	275	154	34	22	22	13	25	53	162	213	169
σ_{sp} (450)	2.40-6	1.35-6	5.25-7	3.55-7	2.45-7	2.29-7	7.24-7	1.10-6	7.76-7	9.12-7		4.79-7
σ_{sp} (550)	1.86-6	9.77-7	3.31-7	2.14-7	1.38-7	1.23-7	5.75-7	8.32-7	5.89-7	6.31-7		3.16-7
σ_{sp} (700)	1.29-6	5.89-7	1.95-7	1.29-7	8.13-8	6.17-8	4.37-7	6.03-7	4.68-7	5.25-7		2.51-7

A compact exponential format is used for σ_{sp} such that $1.78-5 = 1.78 \cdot 10^{-5}$.

3.1.1.2. REGIONAL OBSERVATIONS

In order to address questions concerning climate forcing by anthropogenic aerosol particles [Charlson *et al.*, 1992; Penner *et al.*, 1993], CMDL is establishing a network of four regional aerosol monitoring stations. Two of the stations are located in marine locations and two in continental locations; for each category one site is relatively free of anthropogenic influences and the other is frequently perturbed by anthropogenic aerosols. Table 3.3 lists the four sites, their characteristics, and their current status (June 1993). Each station operates in close collaboration with a local university or government agency that provides on-site support for the measurements.

The scientific questions that define the context of the measurements at these sites include:

- What are the sign, mechanism, magnitude, uncertainty, and spatial distribution of the climate forcing by anthropogenic aerosol particles?
- What are the physical and chemical processes, including their rates and spatial distributions, leading to formation and removal of the particles responsible for the forcing, and how do these processes determine the size and chemical-composition distributions of the particles?
- What is the sensitivity of the forcing and its spatial distribution to changes in these parameters?

- How has the forcing changed in the past, and how will it change in the future?

Clearly, ground-based measurements at a few sites will provide answers to only a few of these questions. Recognizing this, the strategy of the CMDL regional aerosol measurement program is to determine means, variability, and possible trends of key optical, chemical, and microphysical properties for a number of important aerosol types.

The measurements will provide ground-truth for satellite measurements and global models, as well as key aerosol parameters for global-scale models (e.g., scattering efficiency of sulfate particles, hemispheric backscattering fraction). An important aspect of this strategy is that the chemical measurements are linked to the physical measurements through simultaneous, size-selective sampling and thermal analysis, which allows the observed aerosol properties to be connected to the atmospheric cycles of specific chemical species.

When the sites are fully operational, continuous measurements will include the total particle number concentration (N_{tot}), the cloud condensation nucleus number concentration (N_{ccn}), aerosol optical depth (δ), and components of the aerosol extinction coefficient (total scattering σ_{sp} , backwards hemispheric scattering σ_{bsp} , and absorption σ_{ap}). Size-resolved impactor and filter samples

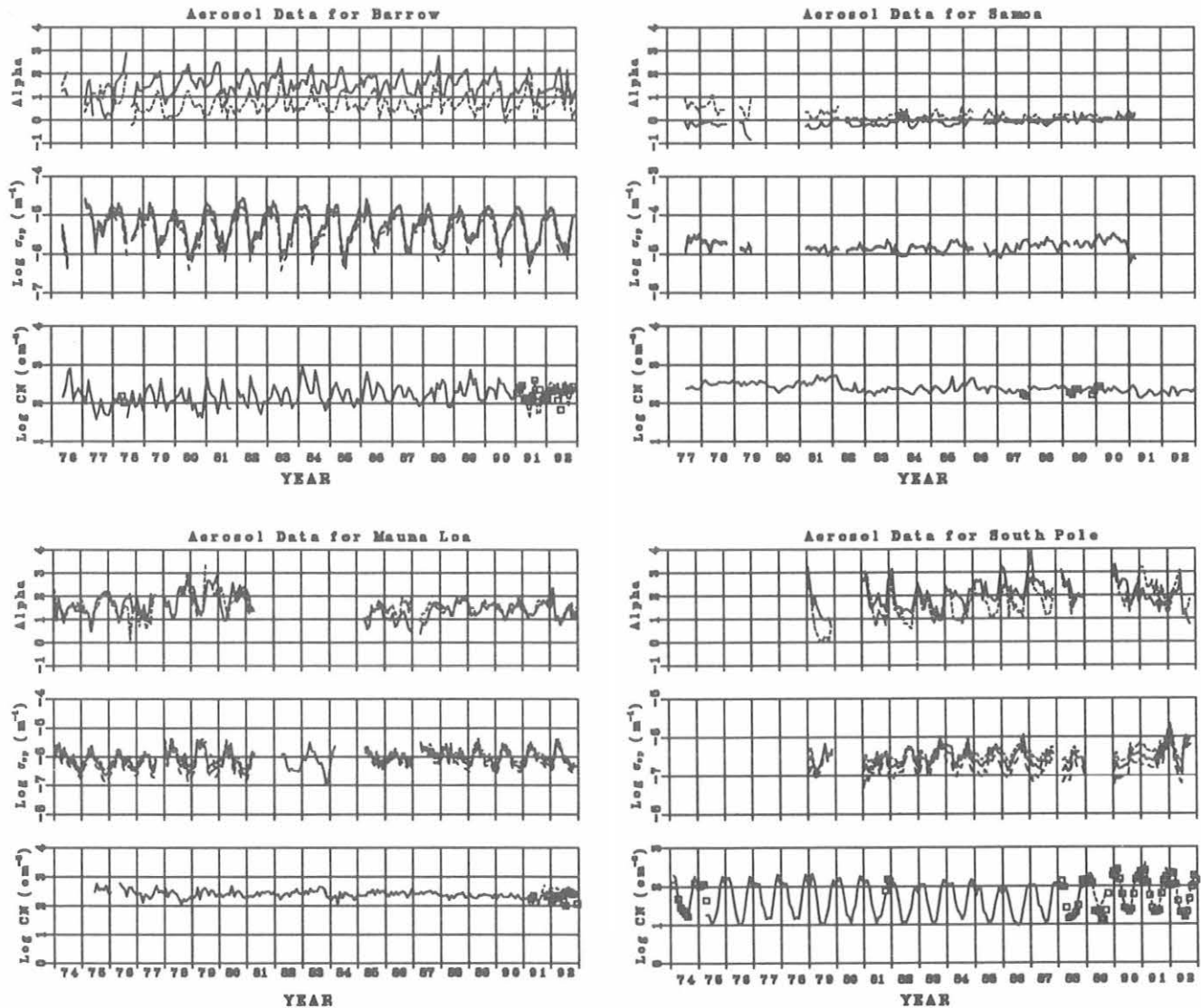


Fig. 3.2. Monthly geometric means of σ_{sp} and CN data for the entire data record. Data for MLO are included only for 0000-0800 LST. The σ_{sp} data (middle) are shown for 450 (dotted), 550 (solid), and 700 nm (dashed). Ångström exponents (alpha) were calculated from 450- and 550-nm (dotted), and 550- and 700-nm (solid) σ_{sp} data. Note that G. E. CN counter data are shown as a solid line, TSI CN counter data are shown as a dashed line, and Pollak CN counter data are shown as small squares.

TABLE 3.3. CMDL Regional Aerosol Monitoring Sites

Category	Perturbed Marine	Perturbed Continental	Clean Continental	Clean Marine
Location	Sable Island, Nova Scotia, Canada	Bondville, Illinois	Laramie, Wyoming	Cheeka Peak, Washington
Collaborating institute	Atmospheric Environ- ment Service, Canada	University of Illinois, Illinois State Water Survey	University of Wyoming	University of Washington
Status	Operational August 1992	Planned for operations late-1993	Site feasibility measure- ments began April 1993	Operational, May 1993
Current measure- ments (June 1993)	N_{tot} , σ_{sp} (3 λ), size- resolved), δ (4 λ), size- resolved chemical composition	N_{tot} , σ_{sp} (3 λ), size- resolved), δ (5 λ), size- resolved chemical composition	N_{tot} , σ_{sp} (3 λ)	N_{tot} , σ_{sp} and σ_{bsp} (1 λ), size- resolved), δ (4 λ), size- resolved chemical composition

(submicrometer and supermicrometer size fractions) will be obtained for gravimetric and chemical (ion chromatographic) analyses. All size-selective sampling, as well as the measurements of the components of the aerosol extinction coefficient, will be performed at a low, controlled relative humidity (40%) to eliminate confounding effects because of changes in ambient relative humidity.

Because of the early developmental state of the regional aerosol measurement program, the limited amount of monthly-averaged data obtained in 1992 will be included in the 1993 CMDL Summary Report. An example of the size-resolved measurements of the aerosol light scattering coefficient at Sable Island is shown in Figure 3.3. The Sable Island site was chosen to allow characterization of anthropogenically-perturbed marine aerosols, but air mass trajectories from clean marine and clean continental areas are also frequently encountered at the site. Clean marine air was encountered at the beginning of the period shown in Figure 3.3, resulting in low particle number concentrations and light scattering coefficients. The contributions to σ_{sp} of the sub- and super-micrometer size fractions were about equal. The large peaks on September 12 are due to contamination by local sources on the island; a automatic control algorithm in the sampling system prevents contamination of the filter samples during such periods. After several days the air trajectories came from northeastern Canada, causing higher particle number concentrations but similar levels of σ_{sp} . Air trajectories bringing polluted air from the eastern United States were observed at the end of the period, yielding much higher values of N_{tot} and σ_{sp} . Submicrometer particles dominated the light scattering coefficient, although a substantial increase of light scattering from supermicrometer particles was also observed.

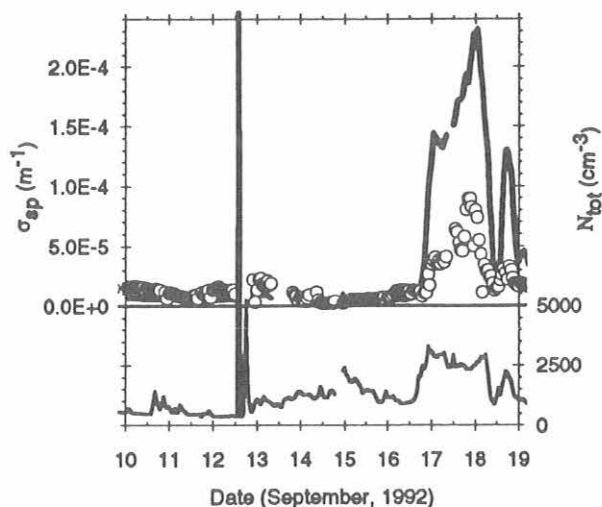


Fig. 3.3. Observed total particle number concentration (lower pane) and size-resolved aerosol light scattering coefficient (upper pane, 550 nm wavelength, solid line for 0-1 μm diameter particles, circles for 1-10 μm particles) at Sable Island, Canada, September 10-19, 1992.

3.1.2. LIDAR OBSERVATIONS OF AEROSOLS

(See 1.1.2. for report on Mauna Loa lidar data.)

3.1.3. TOTAL OZONE OBSERVATIONS

Total ozone observations continued throughout 1992 at 15 of 16 stations that comprise the U.S. Dobson spectrophotometer network (Table 3.4). Of the 15 stations, 5 were operated by CMDL personnel, 4 by the NWS, 2 are domestic cooperative stations, and 4 are foreign cooperative stations. The Dobson spectrophotometer, operated at Florida State University in Tallahassee until November 1989, was relocated in 1992 to the Municipal Airport in Tallahassee. NWS staff made routine total ozone observations at Tallahassee beginning in March 1993.

The Poker Flat Research Range instrument failed in May and the instrument was shipped to Boulder for repair and re-calibration. In early June the instrument was returned, but problems in the computer system driving this automated instrument and problems with the operations at the Range in general kept the instrument from making any useful observations through the rest of the year. At the end of the summer, the instrument and shelter were moved to the roof of the Geophysical Institute, University of Alaska, for installation early in 1993.

A semi-automated method of operation for the Dobson ozone spectrophotometer was developed by CMDL. The system uses an encoder and a counter to read the R-dial position and a computer to guide the operator through the observations and record the data. The operator is given a total ozone value at the end of the observation. The advantage is that the data is in a format ready for processing or transmission by electronic mail. Instrument no. 82 was equipped with this system at SPO where the need for the system was greatest as all the data are transmitted by satellite to CMDL.

Provisional daily 1992 total ozone amounts applicable to local apparent noon for stations listed in Table 3.4 were archived at the World Ozone Data Center (WODC), 4905 Dufferin Street, Downsview, Ontario M3H 5T4, Canada, in *Ozone Data for the World*. Table 3.5 lists mean monthly total ozone amounts measured at the various stations. (Monthly means are derived for stations where observations were made during at least 10 days each month.) Ozone values shown for MLO for July-October may be too high by about 2.5%; more work is needed to assess the exact measurement errors. Ozone values in the table are expressed in the Bass-Paur [1985] ozone absorption coefficient scale [Komhyr et al., 1993a], adopted for use by the WMO beginning January 1, 1992. The Bass-Paur coefficients yield ozone amounts 0.9743 times as large as those derived from the use of the Vigroux [1957] ozone absorption coefficients.

Because of the need for "ground truth" validation of satellite instrument ozone data and the desirability of obtaining reliable information on ozone trends during past decades, the NOAA National Environmental Satellite, Data,

TABLE 3.4. U.S. Dobson Ozone Spectrophotometer Station Network for 1992

Station	Period of Record	Instrument No.	Agency
Bismarck, North Dakota*	Jan. 1, 1963-present	33	NOAA
Caribou, Maine*	Jan. 1, 1963-present	34	NOAA
Wallops Is., Virginia*	July 1, 1967-present	38	NOAA; NASA
SMO*	Dec. 19, 1975-present	42	NOAA
Tallahassee, Florida*	May 2, 1964-Nov. 30, 1989; Nov. 1, 1992-present	58	NOAA; Florida State University
Boulder, Colorado*	Sept. 1, 1966-present	61	NOAA
Poker Flat, Alaska	March 6, 1984-present	63	NOAA; University of Alaska
Lauder, New Zealand	Jan. 29, 1987-present	72	NOAA; DSIR
MLO*	Jan. 2, 1964-present	76	NOAA
Nashville, Tennessee*	Jan. 2, 1963-present	79	NOAA
Perth, Australia	July 30, 1984-present	81	NOAA; Australian Bureau Meteorology
SPO	Nov. 17, 1961-present	82	NOAA
Haute Provence, France	Sept. 2, 1983-present	85	NOAA; CNRS
Huancayo, Peru	Feb. 14, 1964-present	87	NOAA; IGP
BRW	June 6, 1986-present	91	NOAA
Fresno, California*	June 22, 1983-present	94	NOAA

*Stations where total ozone data were tentatively re-evaluated.

TABLE 3.5. Provisional 1992 Monthly Mean Total Ozone Amounts (m-atm-cm)

Station	Jan.	Feb.	March	April	May	June	July	Aug.	Sept.	Oct.	Nov.	Dec.
Bismarck, ND	337	346	354	347	331	328	321	302	297	272	307	320
Caribou, ME	353	364	375	384	346	354	335	311	278	293	285	302
Wallops Is., VA	314	323	337	331	338	322	299	293	278	284	254	262
SMO	251	249	247	237	234	235	233	238	240	239	248	249
Tallahassee, FL	-	-	-	-	-	-	-	-	-	-	-	-
Boulder, CO	324	325	336	318	308	299	296	287	276	270	290	285
Poker Flat, AK	-	423	404	397	333	-	-	-	-	-	-	-
Lauder, New Zealand	290	284	278	266	309	-	-	[358]	367	350	318	289
MLO	236	255	265	279	284	279	(267)	(266)	(258)	(250)	(241)	(230)
Nashville, TN	303	317	327	319	333	318	297	303	284	288	268	262
Perth, Australia	282	274	271	273	[277]	-	-	-	324	318	307	290
SPO	278	262	-	[286]	[254]	[260]	[244]	[257]	-	185	180	269
Haute Provence, France	296	332	329	362	346	340	[331]	[286]	285	291	262	292
Huancayo, Peru	242	245	241	235	227	221	224	237	247	245	248	248
BRW	-	[260]	417	416	384	330	291	301	314	325	-	-
Fresno, CA	310	321	346	309	315	325	301	297	281	270	263	278

Monthly mean ozone values in square brackets are derived from observations made on fewer than 10 days per month. Values in parentheses may be too high by about 2.5%.

and Information Service, in cooperation with the WMO, embarked on an international project to optimize the quality of Dobson spectrophotometer data of the global Dobson instrument network in 1991. To this end, a "Dobson Data Re-evaluation Handbook" [Komhyr *et al.*, 1993b] was prepared outlining procedures to be followed in re-evaluating the data. For Dobson instruments that were periodically calibrated throughout the years relative to World Primary Standard Dobson Instrument 83, as have been the instruments of the U.S. station network, the "Handbook" specifies procedures for correcting the data for instrument spectral calibration changes arising from aging of optical components, optical contamination, cobalt filter

corrosion by humidity, and optical wedge calibration changes.

Reevaluation of the U.S. data began in 1991. To date, data from 9 of 16 stations identified in Table 3.4 were tentatively reprocessed. The method involved use of updated initial and final calibrations (relative to Dobson instrument 83) as well as the determination, from quasi-simultaneous direct-sun and zenith-sky observations, of corrections to empirical charts, from which total ozone amounts are derived from observations on the clear or cloudy zenith sky. Resulting data are improved compared with those originally archived at the WODC, with monthly means generally differing from the archived values on

average by not more than about $\pm 2\%$. Portions of the records, however, are subject to additional refinement. Maximum errors within these data portions are estimated not to exceed $\pm 2\%$.

Figure 3.4 plots 1979-1992 ozone anomaly data (i.e., monthly mean ozone deviations from monthly normals) for 14 of the 15 operating CMDL ozone stations. Data used in the analysis are the tentatively re-evaluated data for 8 of the 14 stations (see Table 3.4), but provisional data as archived at the WODC for the remaining 6 stations. The plots exhibit several interesting features. The two most northerly stations, e.g., Point Barrow and Poker Flat, Alaska, show downward ozone trends of -0.38 and -0.47% yr^{-1} , respectively, based on sparse data obtained during springtime seasons of the years when observations were made. (The trend at Poker Flat is not statistically significant at the 95% confidence interval [t-statistic]). Stations on the U.S. mainland (Caribou, Bismarck, Boulder, Wallops Island, and Nashville) with complete 1979-1992 records show downward ozone trends ranging from -0.33 to -0.46% yr^{-1} . Data from Fresno, also on the U.S. mainland, exhibit a non-statistically significant downward trend of -0.22% yr^{-1} over the 9-year record of observations. At Haute Provence Observatory, the 9-year record yields a large downward trend of -0.62% yr^{-1} , primarily because of unusually low ozone that occurred there in the spring of 1990 and in 1992. Smaller trends, ranging from 0.03 to -0.20% yr^{-1} are evident for the near-equatorial stations of MLO, Huancayo, and SMO. The two southern hemisphere stations of Perth and Lauder exhibit positive ozone trends that likely result, at least in part, from the shortness of the records.

Monthly mean total ozone amounts measured at SPO during October 15-31 time intervals of 1962-1991 are plotted in Figure 3.5. (Mid-October is when Dobson spectrophotometer total ozone observations first become possible at SPO following the polar night.) The October 1992 mean ozone value of 185 DU was higher than the corresponding 1991 value of 162 DU. This larger ozone amount resulted most likely from the relative proximity to SPO of the polar vortex boundary in 1992 than in 1993. The SPO November 1992 mean total ozone (180 DU) was considerably lower in 1992 than in 1991 (289 DU).

The CMDL Dobson spectrophotometer observations show low ozone values in 1992, similar to those reported for the TOMS satellite instrument *Gleason et al.* [1993]. While the TOMS total ozone record is relatively short, allowing comparison of recent decreases in ozone with ozone amounts measured only since 1978, the CMDL Dobson instrument data date back for a number of the stations to the 1960s and 1970s, a time when atmospheric ozone destruction was minimal due to anthropogenic chlorofluorocarbons. Recent and past Dobson instrument total ozone data from the six contiguous U.S. stations of Nashville, Fresno, Wallops Island, Boulder, Bismarck, Caribou, and from MLO in Hawaii and SMO in the South Pacific, are compared in Figure 3.6. The solid lines in the plots are percent decreases in 1992 monthly mean total

ozone amounts relative to long-term normal monthly means for the eight stations. For all stations except Fresno, the normal monthly means were derived from data obtained at the stations through 1985 (see Table 3.4). For the shorter Fresno record, the monthly normals were obtained from 1984-1991 data. Dashed lines in Figure 3.6 represent standard deviations ($\pm 1\sigma$) of the normal monthly means.

Note that nearly all monthly means fall below long-term normal ozone levels to values as low as about -10% . The mean 1992 ozone deficiency for the eight stations is 4.7% . For the record as a whole, the monthly mean ozone values fell below one standard deviation of the normal monthly means 66% of the time and below two standard deviations 38% of the time.

3.1.4. UMKEHR OBSERVATIONS

Umkehr observations with automated Dobson ozone spectrophotometers continued during 1992 at Boulder, Haute Provence, Lauder, MLO, Perth, and Poker Flat. Table 3.6 lists the number of observations attempted and the number that yielded useful data. Observations with excessive cloud interference were not useful. Umkehr data quality during 1992 was adversely affected by aerosol particles still remaining in the stratosphere following the June 1991 eruption of Mt. Pinatubo in the Philippines. Umkehr observations at Poker Flat were only made during March and April 1992. An instrument mechanical failure, followed by multiple failures in the controlling computer system, kept the station out of operation. The instrument and shelter were moved to the Geophysical Institute at the University of Alaska, Fairbanks, for observations starting in 1993. Both Lauder and Perth missed many weeks of observations in June, July, and August while the instruments were in Boulder for recalibration. Umkehr data for 1991 has not been archived at the WMO World Ozone Data Center, since a correction for the interference from the Mt. Pinatubo aerosols has not been determined.

3.1.5. CALIBRATION OF CMDL DOBSON SPECTROPHOTOMETERS

Three Dobson ozone spectrophotometers of the CMDL network and three others were calibrated during 1992. Table 3.7 lists all the instruments calibrated and the resulting calibration difference expressed as a percent ozone difference. This percentage difference is calculated between measurements from the test instrument and the standard instrument with the ADDSGQP observation type at a μ value of 2, and a total ozone value of 300 DU, before any repair or calibration adjustment is made. All calibrations were performed in Boulder relative to the NOAA world primary standard Dobson spectrophotometer 83 and to secondary standard Dobson spectrophotometer 65.

Instrument 63 from Poker Flat Research Range had a failure of one of the bands holding the optical wedge in place. The instrument was repaired with an attempt to

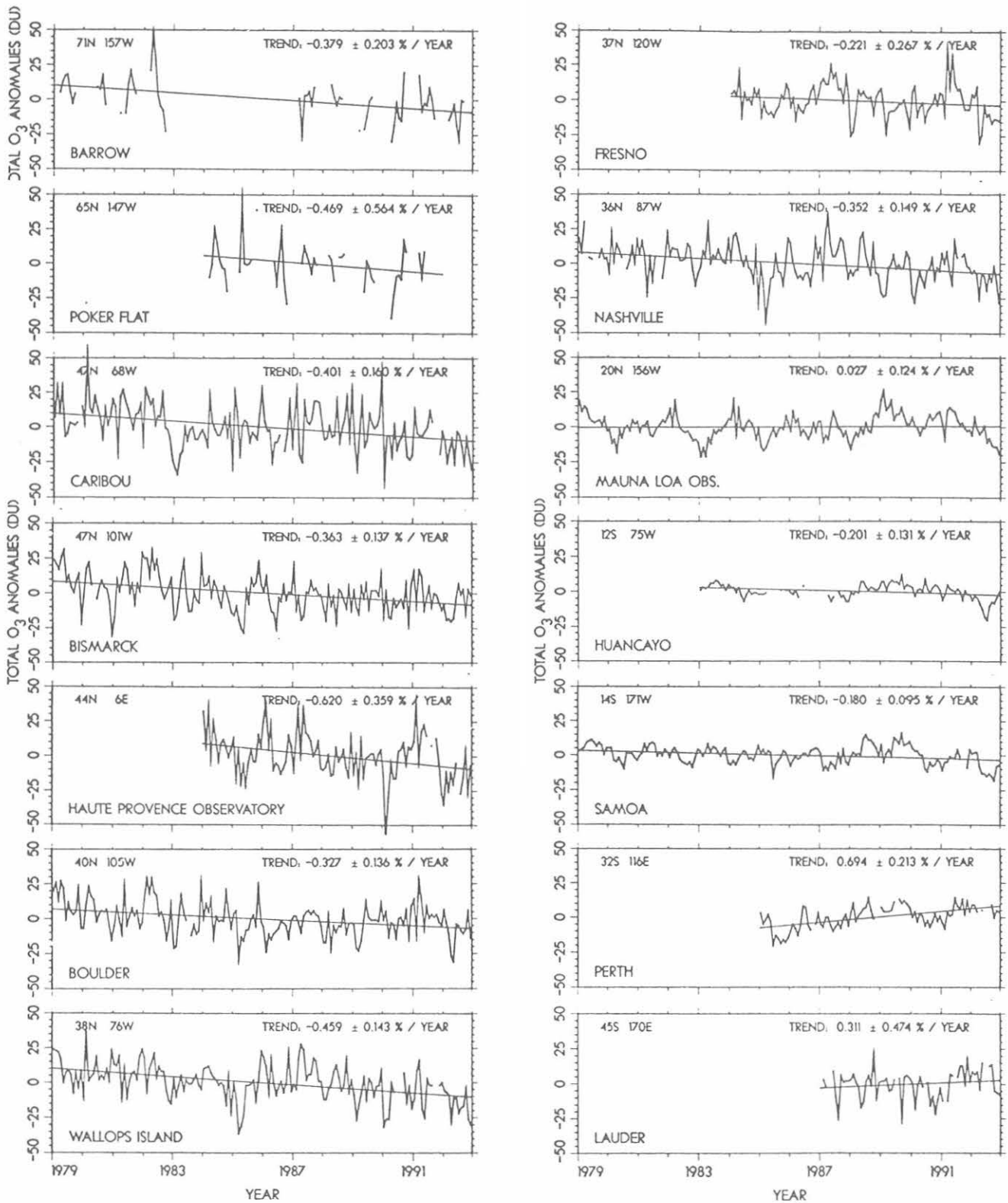


Fig. 3.4. Total ozone anomaly data derived from Dobson spectrophotometer observations. Least-squares linear regression lines have been fitted to the data obtained through 1992. Uncertainties in indicated ozone trends are 95% confidence intervals (t-statistic).

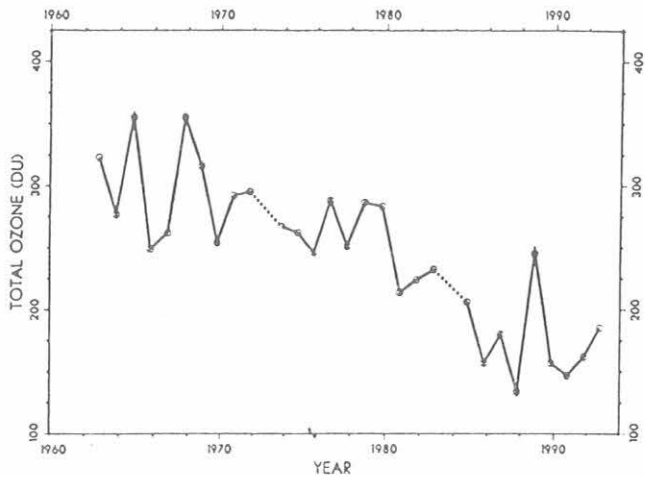


Fig. 3.5. SPO mean total ozone amounts for October 15-31 time intervals of 1962-1992.

replace the wedge back into the correct position, based on the results of standard lamp tests, before the comparison with a standard. A wedge calibration after the comparison showed that the wedge had been replaced very close to the original position, based on the observation that after the wedge was cleaned, the wedge density curve was the same as the 1989 curve. Instrument 81 from Perth, Australia, had worn bearings in the wedge drive assembly replaced. Instrument 72 from Lauder, New Zealand, was accidentally damaged by oil on the optical wedge, thus the result in Table 3.7 is misleading. A wedge calibration defined the problem completely, and an interim calibration could be applied to the data for the period when the oil was on the wedge. This time period was known to the day.

Three non-CMDL instruments were calibrated by CMDL in 1992. The results are listed in Table 3.7. Instrument 99 from Argentina was sent to Boulder after the instrument was damaged by a fall that resulted in a broken band on the wedge. A repair was attempted on site, but the correct

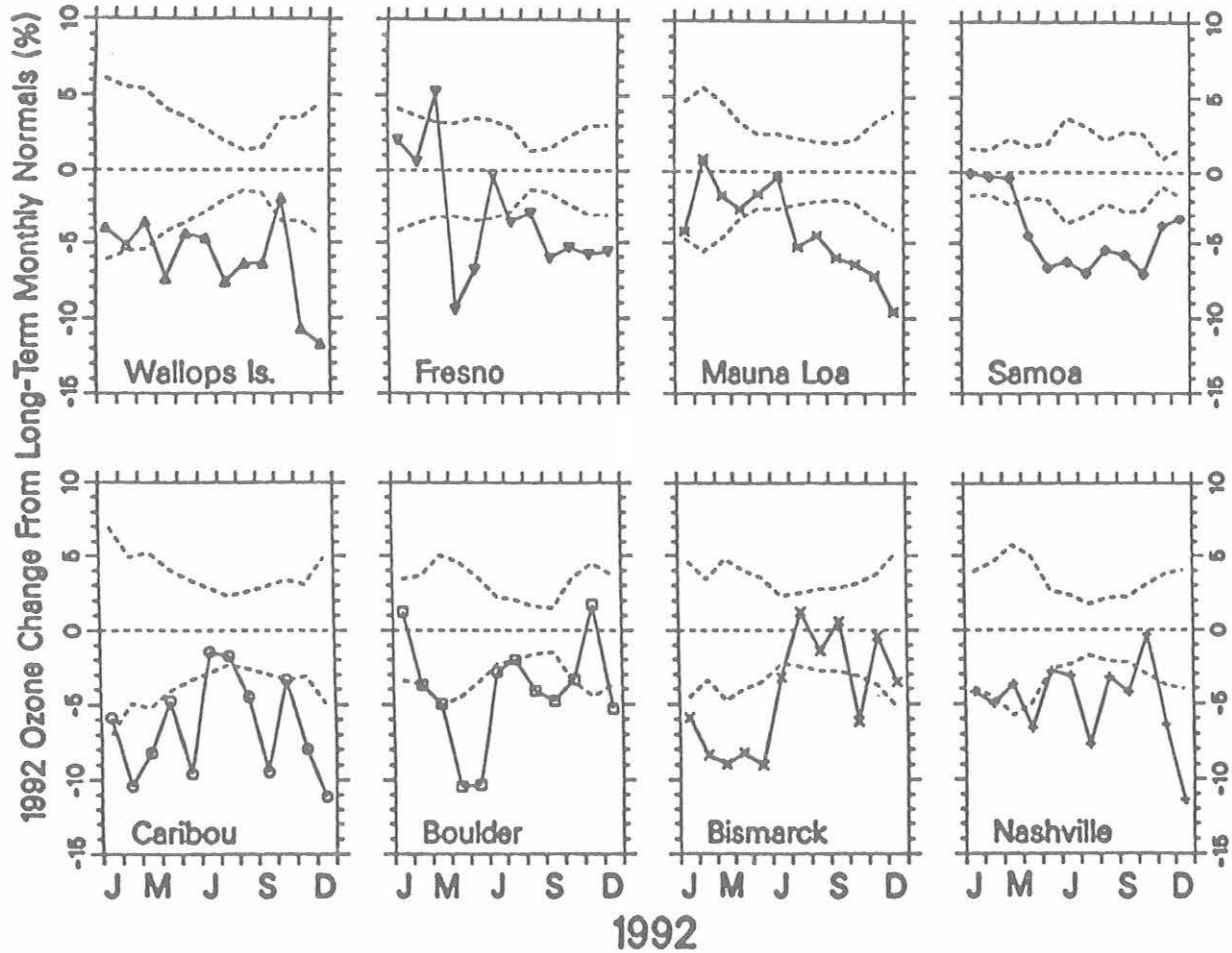


Fig. 3.6. January 1992-May 1993 percent decreases in monthly mean total ozone amount at six contiguous U.S. stations and in Hawaii and Samoa relative to long-term normal monthly means. Dashed lines are standard deviations (1σ) of the normal monthly means.

TABLE 3.6. Umkehr Observation Frequency During 1992

Station	Station Coordinates	Total No. Obs. Made	Total No. Useful Obs.
Boulder	40°N, 105°W	532	200
Haute Provence	43°S, 170°E	445	215
Lauder	45°S, 170°E	511	158
MLO	20°N, 156°W	580	413
Perth	32°S, 116°E	427	199
Poker Flat	65°N, 147°W	77	22

TABLE 3.7. Dobson Ozone Spectrophotometers Calibrated in 1992

Station	Instrument Number	Calibration Date	Calibration Corr. Needed (%)*
Poker Flat (now UAF)	63	May 15	-1.3
Perth Airport, Australia	81	June 19	-0.8
Lauder, Australia	72	July 14	-1.4
Argentina	99	July 27	-0.5
Melbourne, Australia	105	June 19	-0.8
Tsukuba, Japan	116	June 28	-0.5

*Applicable to $\mu = 2$ and 300 DU ozone

band was not available. The results in the table are, therefore, less reliable when considering existing data. Instrument 105 is a WMO regional standard owned and operated by the Australian Bureau of Meteorology in Melbourne. Instrument 116 is the standard for the Japanese network and is operated by the Aerological Observatory, Tsukuba, Japan.

The calibration of instrument 82 was verified and the instrument sent to SPO as a replacement for instrument 80. While both instruments were on station, observations were made with both instruments in overlapping time periods. The results showed that both instruments produced ozone values that agreed within 1%.

A Shimadzu-built copy of the Dobson ozone spectrophotometer, owned by the WMO, was rebuilt in Boulder for subsequent use in Lagos, Nigeria. As most of this instrument's construction was different than that of the British-built Dobson instrument, a great amount of ingenuity was used to get the optical parts aligned correctly. The instrument calibration was excellent after rebuilding.

CMDL developed a semi-automated version of a two-lamp wedge calibrator that increased the speed of a wedge calibration from 2 days to one-half day.

3.1.6. VALIDATION OF TOMS AND SATELLITE INSTRUMENT OZONE DATA

World primary standard Dobson instrument 83, maintained by CMDL, operated in June-August 1992 at MLO in an ongoing program to assess its calibration and to

provide "ground-truth" data for verification of ozone measurements made by the NASA TOMS and SBUV instruments from aboard the Nimbus 7 satellite. While large differences were observed between Dobson instrument 83 and TOMS data prior to 1987, development of a wavelength pair justification technique [Herman *et al.*, 1991] has rendered data from the two kinds of instruments highly compatible. TOMS corrected (Version 6) data and Dobson instrument 83 data for 1979-1992 are compared in Figure 3.7, showing agreement to within about $\pm 0.5\%$. The long-term ozone measurement precision of Dobson instrument 83 is currently estimated to be $\pm 1\%$.

3.1.7. TROPOSPHERIC OZONE

The CMDL network of surface ozone measurements includes the four baseline observatories; three AEROCE sites (Bermuda, Barbados, and Mace Head, Ireland); Niwot Ridge; and Westman Islands, Iceland. The station at Reykjavik, Iceland, continues operation under the direction of the Icelandic Meteorological Office. The data from this site are heavily influenced by its in-city location and the data are more difficult to interpret as regionally representative. Figure 3.8 shows the diurnal cycle (shown as deviations from the daily mean) for Reykjavik (a) and Westman Islands (b). At Reykjavik, there is a large variation with minimum values in the day and highest values very early in the morning. At Westman Islands, on the other hand, there is no significant diurnal cycle that is consistent with the fact that it is removed from local or regional pollution sources on a small island south of the main island of Iceland. At Reykjavik, the diurnal cycle appears to be driven by daily automobile traffic patterns and the titration of ozone by nitric oxide (NO) [Oltmans and Levy, 1993].

Interestingly, at Reykjavik the average concentration for 0307 LST is very similar to the daily average at Westman Islands indicating that for relatively unpolluted conditions the broad scale patterns determine important features such as the seasonal variation [Oltmans and Levy, 1993]. The long-term trend patterns reported last year [Ferguson and Rosson, 1992] for the four observatories are not altered by the addition of the 1992 data. A fuller discussion of the surface ozone measurements can be found in Oltmans and

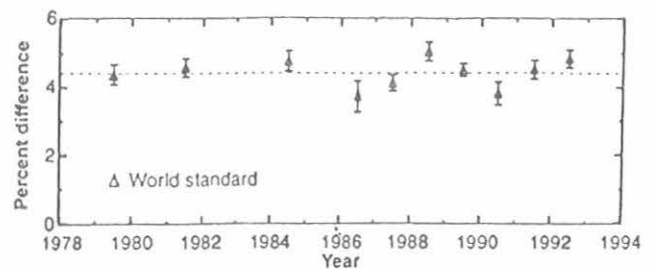


Fig. 3.7. Percent differences between TOMS and World Standard Dobson Instrument 83 total ozone amounts measured at MLO during months of June-August 1979-1992.

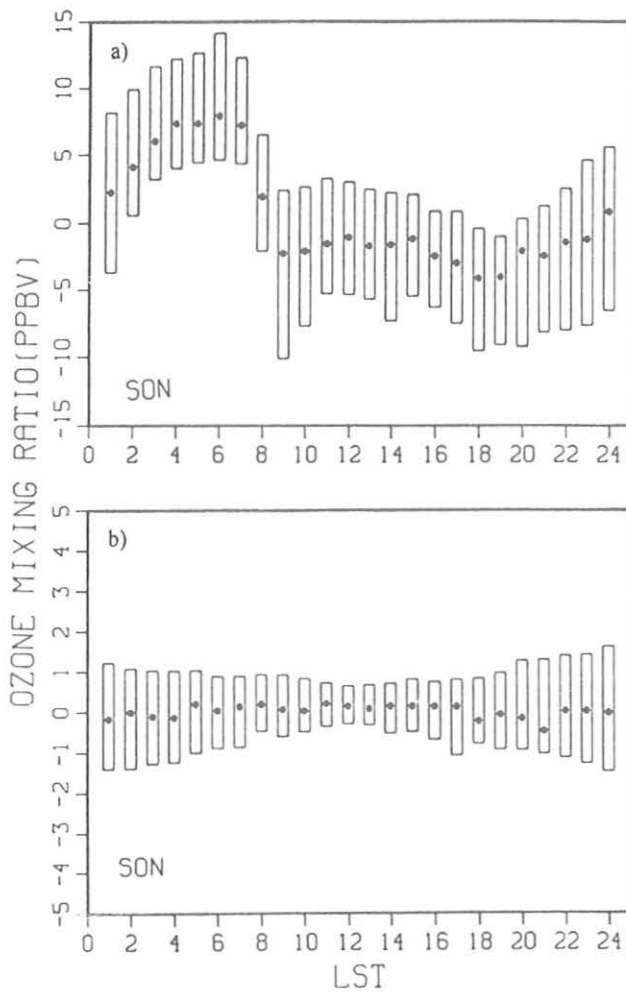


Fig. 3.8. Average hourly departures from the daily mean of the surface ozone mixing ratio (ppbv) for the 3 months of September, October, and November at (a) Reykjavik and (b) Westman Islands, Iceland.

Levy [1993]. The monthly mean mixing ratios from each site are summarized in Table 3.8. For MLO, the averages are based on the period from 00-08 LST (downslope flow) and at Reykjavik for 03-07 LST.

3.1.8. OZONESONDE OBSERVATIONS

After reestablishing weekly ozone vertical profile measurements at Hilo, Hawaii, and Boulder, Colorado, in 1991, in response to the eruption of Mt. Pinatubo, the sounding program was continued at these sites as well as SPO in 1992.

Two significant effects of the Mt. Pinatubo eruption on stratospheric ozone were found. At SPO there was additional springtime ozone depletion in 1992, particularly in the lower stratosphere. Figure 3.9 shows the vertical profile of the ozone partial pressure over South Pole at a date near the minimum in column ozone amount for the years 1986-1992. In 1992 (the open stars), there is significantly less ozone in the layer from 10-15 km than in previous years. In addition, in the region from 14-17 km, ozone has essentially been completely destroyed in 1992. In 1990, similar near complete ozone loss in this region was also seen but the lower stratospheric destruction was not. Evidence of unusual ozone loss was also seen in 1991 in the lowest part of the stratosphere. The 1991 reduction in this region was attributed to the enhanced ozone destroying effects of volcanic aerosol from the Mt. Hudson (46°S) eruption in August 1991 [Hofmann *et al.*, 1992]. The presence of enhanced aerosols, cold polar stratospheric temperatures (but not cold enough to form polar stratospheric clouds at 10-15 km), and high levels of chlorine from human manufactured chlorofluorocarbons allowed ozone destruction in a region where it had not previously been seen. By winter 1992 the volcanic aerosol from Mt. Pinatubo, which was ejected to much higher altitudes than that from Mt. Hudson, had settled into the 10-18 km region over Antarctica [Cacciani *et al.*, 1993]. In 1991 the Mt. Pinatubo aerosol probably did not penetrate the Antarctic polar vortex at these levels. In late winter and spring 1992, ozone declined more rapidly than in previous years. The course of this decline is shown in Figure 3.10 which shows profiles from late August through the minimum value achieved on October 11. The column amount of 105 DU, obtained by integrating the data from the profile measurements, is the lowest ever measured over South Pole and may well represent the lowest column amount measured anywhere [Hofmann and Olimans, 1993].

TABLE 3.8. Monthly Mean Surface ozone Mixing Ratios (ppbv) During 1992

Station	Jan.	Feb.	March	April	May	June	July	Aug.	Sept.	Oct.	Nov.	Dec.
BRW	29.5	28.4	23.3	15.7	17.1	19.7	18.6	19.0	24.2			
Reykjavik, Iceland	35.6	35.2	39.8	41.4	36.5	30.9	20.7	24.9				
Westman Is., Iceland									(33.5)	33.6	39.1	38.6
Mace Head, Ireland	28.2	37.7	40.8	41.0	43.8	36.2	27.9	30.9	30.9	32.9	36.1	30.5
NWR	44.6	45.4	48.7	52.4	47.1	47.0	44.1	41.9	41.5	39.1	35.8	38.2
Bermuda	42.9	42.4	52.0	48.0	35.4	26.6	23.8	24.1	27.9	39.5	34.2	35.9
MLO	40.1	42.7	53.4	60.9	46.8	49.4	38.8	30.6	26.3			
Barbados	23.3	23.3	22.8	19.5	16.4	16.0	16.6		18.2			
SPO	8.3	18.0	17.4	21.8	23.0	31.2	32.3	31.4	27.7	24.3	25.2	28.1

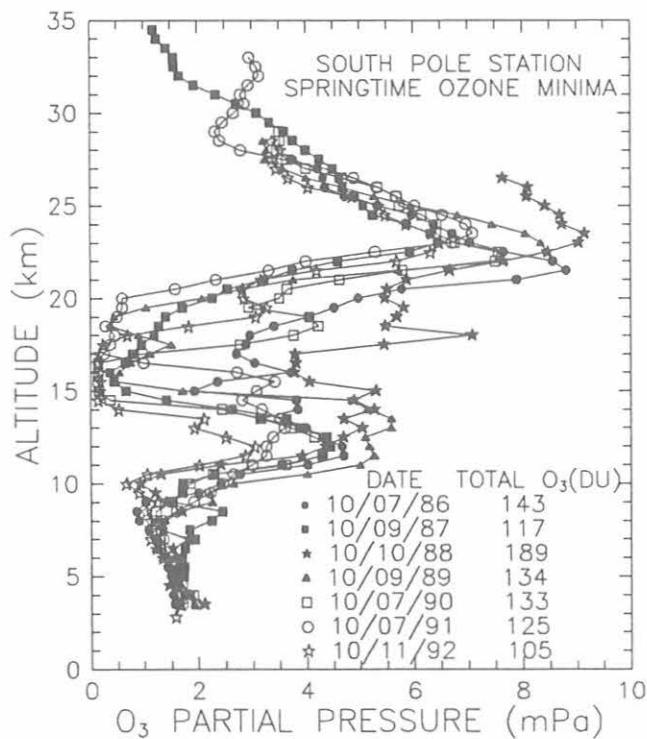


Fig. 3.9. Profile of ozone partial pressure over South Pole on the date nearest the minimum in column ozone each year in the period 1986-1992.

This represents a 60% decline from late August to mid-October. Twenty years earlier, ozone actually increased during this portion of the year [Olmans *et al.*, 1993].

At Hilo and Boulder, ozone profiles have remained perturbed late into 1992 from the effects of the Mt. Pinatubo eruption 1.5 years earlier (Figure 3.11). This perturbation is primarily seen as a displacement of the ozone profile with lower ozone amounts in the lower stratosphere and enhanced concentrations above the maximum. Overall, there has been a decline in the total column amounts for the period following the eruption [Hofmann *et al.*, 1993]. In the subtropical (or high tropical) latitude and mid-latitude cases represented by Hilo and Boulder, the poleward transport of ozone poor air in the lower stratosphere and enhanced ozone amounts higher in the stratosphere, resulting from the lofting of the tropical ozone column following the volcanic eruption, is consistent with the patterns shown in Figure 3.10. The lifting of the column results from the heating by absorption from the upwelling long-wave radiation and an enhanced vertical and horizontal circulation in the tropics [Brasseur and Granier, 1992]. It appears that the persistent nature of these anomalies well into 1992 is at least partially related to the timing of the eruption relative to the shift in the phase of the tropical stratospheric quasi-biennial wind oscillation (QBO) from its easterly to westerly regimes

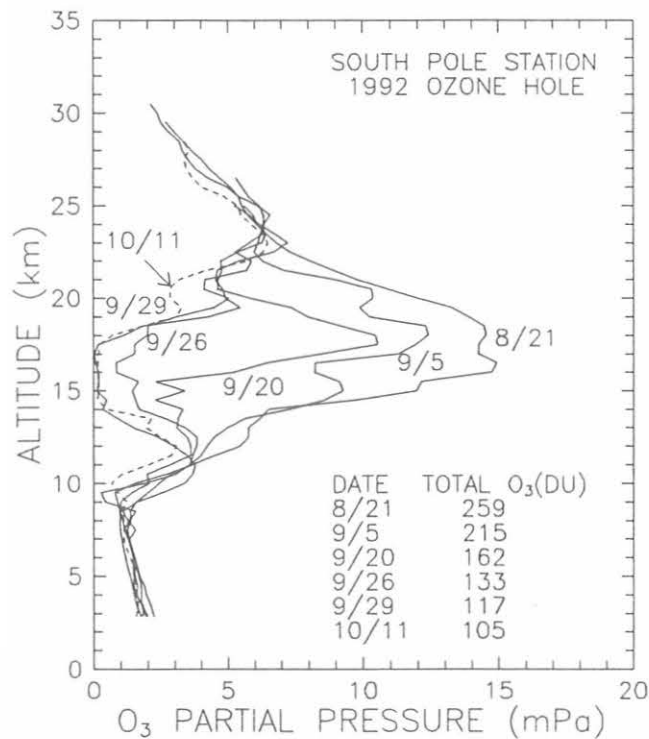


Fig. 3.10. Ozone vertical profiles at South Pole from August 21-October 11, 1992, showing the spring decline in stratospheric ozone.

[Hofmann *et al.*, 1993], although chlorine-catalyzed ozone depletion, related to the increase in volcanic aerosol particle surface area, is probably also involved.

3.1.9. STRATOSPHERIC WATER VAPOR

In addition to the continuing monthly water vapor profile measurements carried out at Boulder, upper tropospheric and stratospheric measurements were done in Hilo, Hawaii; Barstow, California; Lauder, New Zealand; McMurdo and South Pole, Antarctica; and Kiruna, Sweden. Most of the soundings were carried out as part of the UARS correlative measurements program.

The 12-year record of over 110 water vapor profiles obtained in Boulder during 1981-1992 were recently re-analyzed. Two kilometer layer averages were calculated for the stratosphere and upper troposphere between 10-26 km (Table 3.9). A linear least-squares trend was computed for the time series of approximately monthly balloon soundings (Figure 3.12 and Table 3.9). Significant increasing water vapor concentrations were found in the lower stratosphere with the largest increase of $\sim 1\%$ yr⁻¹ in the 18-20 km layer. Since the primary source of water vapor in the stratosphere is the oxidation of CH₄ [LeTexier *et al.*, 1988], the rising concentrations of atmospheric CH₄ [Steele *et al.*, 1992] are expected to lead to rising

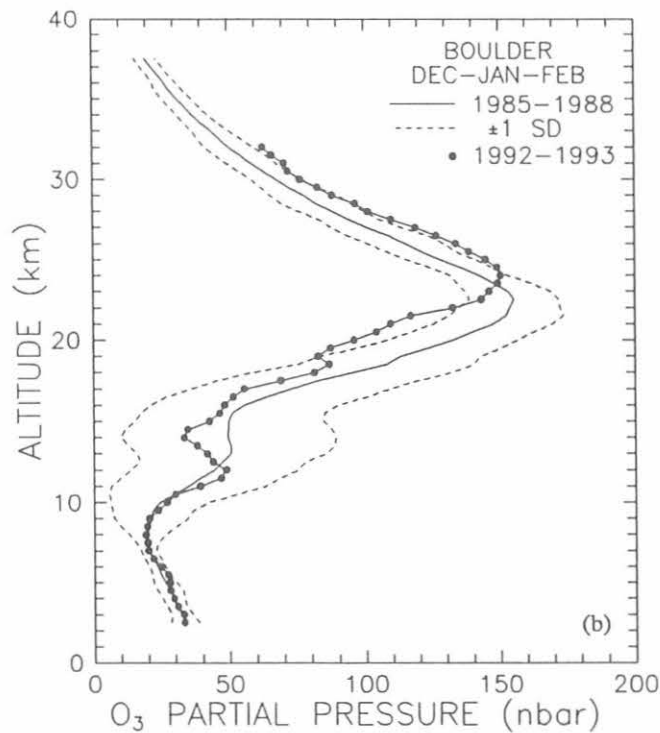
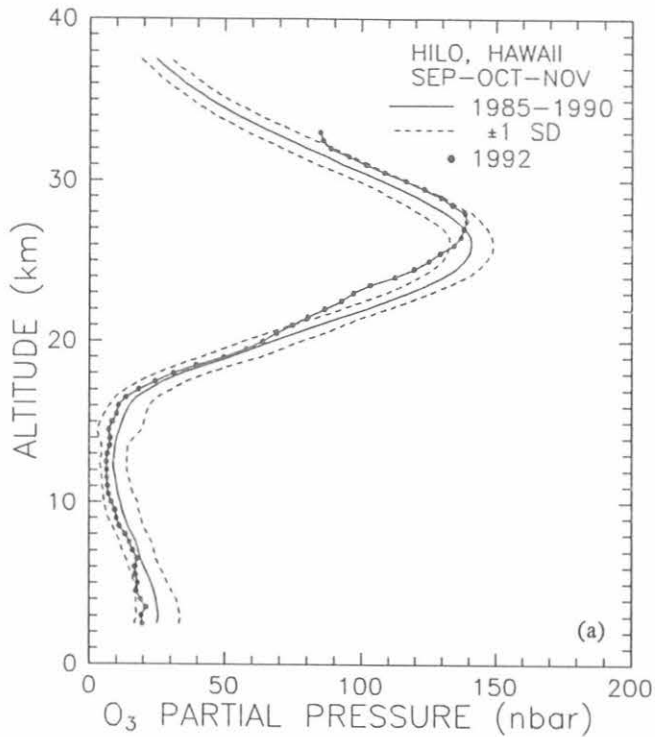


Fig. 3.11. (a) Autumn 1992 average ozone profile (thick line) compared to the 1985 average for this season (thin line) at Hilo, Hawaii, and (b) winter 1992-1993 ozone profile at Boulder compared to the 1985-1988 winter average.

TABLE 3.9. Water Vapor Mixing Ratios Over Boulder, Colorado, During 1981-1992

Level (km)	Mean (ppmv)	Std. Dev. (ppmv)	Number Obs.	Trend (% yr ⁻¹)	95% Confidence Interval (% yr ⁻¹)
10-12	59.15	48.67	113	1.63	3.27
12-14	12.18	9.02	113	1.01	2.77
14-16	4.59	1.71	113	.38	1.11
16-18	3.83	.65	113	.75*	.67
18-20	3.82	.35	112	1.05*	.49
20-22	4.08	.31	105	.90*	.41
22-24	4.21	.30	101	.54*	.38
24-26	4.28	.30	84	.29	.41

The trends are computed for deseasonalized values. The 95% confidence interval is based on students t-distribution.

*Significant at 95% confidence level.

stratospheric water vapor concentrations as well. The measured increase is somewhat larger than that expected from rising CH₄ amounts alone. This may indicate another source of increasing water vapor in the lower stratosphere such as an increase in the troposphere resulting from rising tropospheric temperatures.

3.1.10. SURFACE RADIATION

Solar and Terrestrial Atmospheric Radiation

Surface based radiation monitoring projects continue at eight CMDL locations: Barrow, Alaska; Erie and Boulder (BAO and BLD), Colorado; Bermuda (BRM); Mauna Loa, Hawaii; Kwajalein, Marshall Islands (KWJ); American Samoa; and the South Pole. The long-term continuous measurements at these sites include broadband downward solar irradiances, and several sites (BRW, BAO, BRM, KWJ, and SPO) also measure downward thermal infrared irradiances. At sites where the measurements were determined to have a representative surface (BRW, BAO, and SPO), upward solar and infrared irradiance measurement projects are also maintained. The surface radiation budget (SRB) is a basic and critically important climate variable that has long been inadequately observed because of insufficient global coverage and inherent instrumental limitations. The more extensive observations are made at CMDL sites where the measurements are more areally representative, especially with respect to land surface and cloudiness. In order to make the CMDL data more available to the general scientific community, irradiances observed at those representative sites (BRW, BAO, KWJ, BRM, and SPO) are being incorporated into an international data base sponsored by the WMO and NASA under the Baseline Surface Radiation Network (BSRN). All data from CMDL sites are also maintained as part of the long-term CMDL surface radiation record which exists for the past 15 years at four of the sites (BRW, MLO, SMO, and SPO). Previous CMDL and GMCC Summary

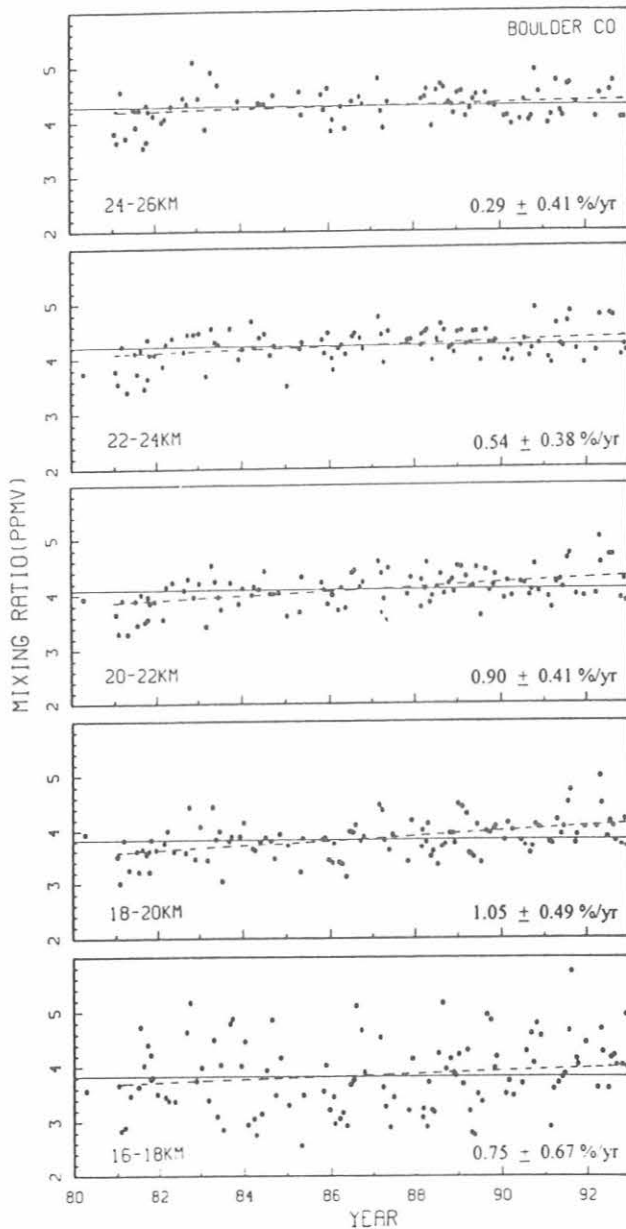


Fig. 3.12. Time series of water vapor mixing ratios in 2-km intervals for individual profile measurements at Boulder, Colorado, during 1980-1992. The solid line is the mean for each 2-km interval. The dashed line is the linear fit to the deseasonalized data.

Reports have discussed the wide ranging and useful applications of these data to scientific questions. Recently completed projects utilizing the radiation observational results from the CMDL field sites are as follows: the detection of a long-term decrease in arctic haze [Bodhaine and Dutton, 1993]; comparison of satellite- and BAO-derived SRB under clear and cloudy conditions [Cess et al., 1991, 1993]; the effects of snow surfaces on atmospheric absorption [Nemesure et al., 1993]; detection of intermediate-term trends in cloudiness related to radiation

perturbations [Dutton et al., 1991; Schnell et al., 1991]; a technique for monitoring long-term climate variability using surface albedo records [Dutton and Endres, 1991; Foster et al., 1992]; identification of a strong statistical coherence between the QBO and the MLO long-term transmission record [Dutton, 1992a]; a surprisingly good agreement between modeled and observed thermal infrared irradiances over the range of globally extreme conditions [Dutton, 1993]; and a determination of the radiative effects of the Mt. Pinatubo volcanic eruption [Dutton and Christy, 1992; Russell et al., 1993; Dutton et al., 1993]. Numerous additional requests were made and fulfilled for CMDL radiation data for a variety of research applications.

Figure 3.13 shows updated results on the late summer cloudiness and irradiance trends at SPO reported by Dutton et al. [1991]. As suggested by Dutton et al. [1991], the previously observed trends during January and February until 1988, did not project into the future. The current SPO irradiance level suggest a return to previous levels.

The MLO atmospheric transmission record updated through 1992, is shown in Figure 3.14. The effects of the eruptions of Pinatubo and El Chichon are most obvious and are enlarged and compared in the inset of the figure. Frequent updates of this data are submitted to the NOAA Climate Analysis Center monthly *Climate Diagnostic Bulletin*.

Snowmelt date at Barrow, Alaska, is defined as the last date each year that any significant snow remains on the ground, but considerable differences between the National Weather Service observations within the village of Barrow and out on the tundra were noted in Figure 3.15. The CMDL albedo data continue to suggest that there has been no significant change in the annual date of spring snowmelt near Barrow since the 1940s.

Observatory operations continued during the year showing only a few significant changes that can be an important attribute of a long-term measurement effort. Newly available blowers were added to the upward facing pyranometer and pyrgeometer at BRW. The new units are very effective in keeping frozen precipitation and condensation off the filter domes. Additional blower units will be acquired as funds allow for implementation at other sites. All continuous data logging at all eight sites now have 3-minute-or-better resolution recorded and permanently stored. Data sampling times range from 1 to 2 seconds at all sites except Boulder where it is 10 seconds in order to accommodate a large number, nearly 100, A/D channels on one data logger. Many current data loggers (BAO, BLD, BRM, and KWJ) have integrating A/D channels, and all other sites will be converted to this capability in the next couple of years. A critical requirement of the radiation project is to make stable and accurate micro-volt level measurements to ensure that the potential voltage measurement error is small compared to other sources of error.

Data processing for the three newer sites (KWJ, BAO, and BRM) was largely incorporated into the system used to process raw data from the other older sites. Incoming data

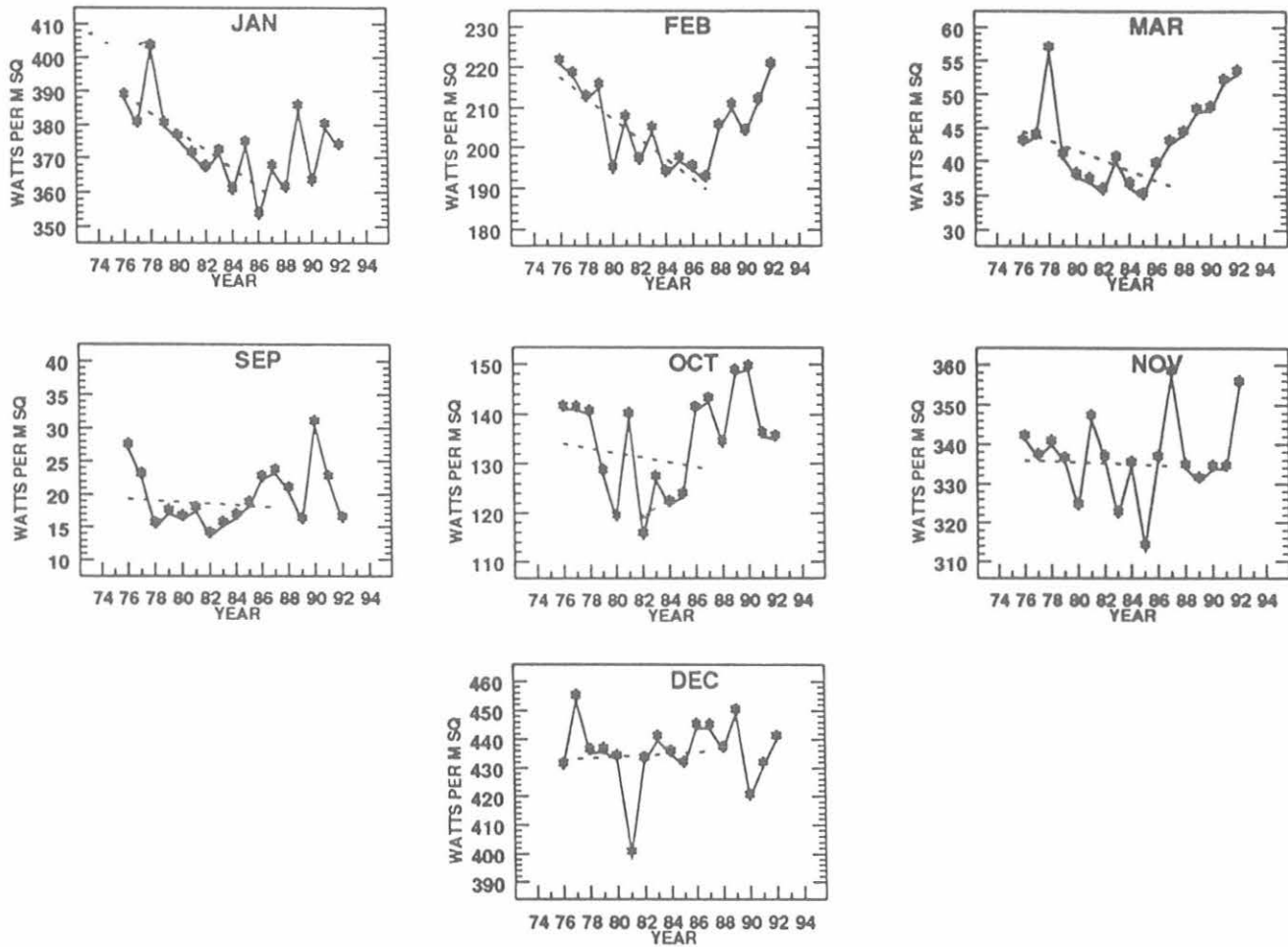


Fig. 3.13. Monthly mean total (direct plus diffuse) solar irradiance at SPO. The plotted lines are for linear least-squares fits for 1976-1987.

are presently processed and edited as received from the site within 2–4 weeks. Data received from the sites is being delayed by as much as 3 weeks as data tapes are filled and transmitted. Final processing is completed about 1 calendar year after the data are first available for processing. Final assignment of calibration information is ongoing as updated radiometer calibration data are made available. Data editing, processing, and final storage have all been moved to medium-sized and personal computers directly under the control of CMDL, thereby eliminating the dependence of outside computer expertise and resources. Data processing is evolving towards a system where real-time interrogation of the field data is possible, and preliminary analysis of the data can be completed in the Boulder offices the day after the data are collected. Several sites (KWJ, BAO, BLD, and BRM) currently operate in that mode.

Remote Sensing of Aerosol Optical Properties and Water Vapor

Other than clouds, aerosols and water vapor are the main contributors to thermal-infrared and solar radiation

variations and subsequent radiative climate forcing. The potential climate variations resulting from such factors are extensive and varied. The observed and potential radiative variations may be due to either anthropogenic causes: increased industrial production of aerosols and water vapor feedback resulting from increasing greenhouse gases, or from natural causes; i.e., volcanic, biogenic, or surface wind-generated aerosols and inherently varying water vapor. CMDL has a long history of exploratory and operational projects relating to the remote sensing of aerosols and water vapor as related to climate variations. Wide-band spectral observations of direct solar irradiance using a filter wheel NIP at BRW, MLO, SMO, and SPO were used to infer aerosol optical depth and column water vapor amounts since 1977. These measurements have proven to be durable and stable over time, thereby extending monitoring efforts even though their accuracy is less than can be obtained by more sophisticated but less robust instrumentation. Additional and exceptional effort has been put into high-precision narrow spectral band optical depth measurements at MLO. Here, several narrowband (0.005 μm) sunphotometers are routinely

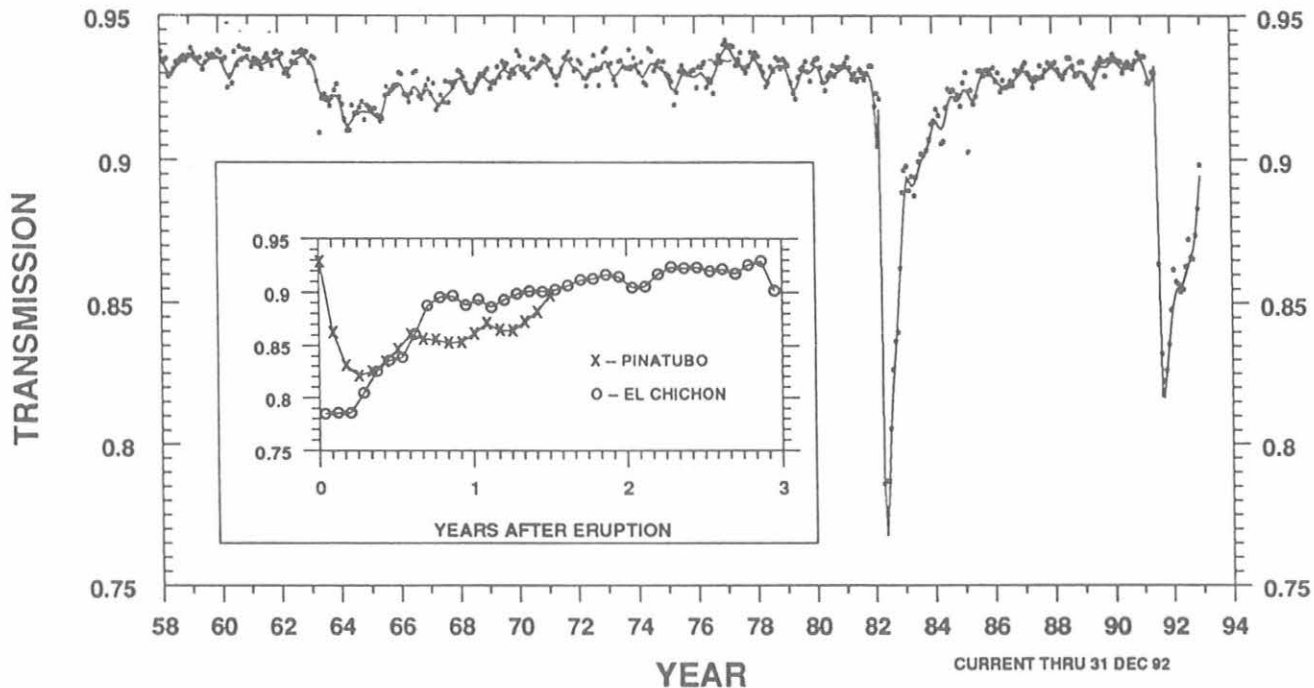


Fig. 3.14. Monthly mean "apparent" atmospheric transmission as determined from broadband direct solar beam observations at MLO.

operated and, because of the nearly ideal atmospheric conditions and the existence of automated observing platforms, have produced reliably consistent long-term data sets. Results from the MLO aerosol optical depth measurement project are reported by *Dutton et al.* [1993], *Russell et al.* [1993], and in previous CMDL Summary Reports. Two additional aerosol optical-depth measurement series were begun in 1992, one uses handheld J-series sunphotometers at Sable Island, Nova Scotia. The other at

MLO was a short-term (6-month) comparison of a commercially available automatic four-channel sunphotometer (from EKO, Japan) that is operated in the automated solar dome. The Sable Island measurement series is a part of a new, comprehensive, surface-based CMDL aerosol sampling project described elsewhere in this report.

3.1.11. SOLAR RADIATION FACILITY

An observational broadband radiation plan for the Department of Energy Southern Great Plains Clouds and Radiation Testbed site (SGP/CART) located near Lamont, Oklahoma, was developed during the first half of the year. A site plan incorporating measurement capability for solar diffuse, direct, and global radiation, plus longwave radiation using pyrometers, was completed. The solar diffuse and IR pyrometer incorporated an SRF-designed tracking disk system to occult the sun during operation. Use of tracking disks has resulted in improved accuracy in solar diffuse determination and, in the case of the pyrometers, minimizes the corrections to data due to sensor dome heating effects. A preliminary suite of these broadband sensors was prepared and transported to Lamont during early June 1992. Personnel from the CMDL Solar Radiation Facility (SRF) were on site at SGP/CART to erect a temporary measurement array consisting of a pyranometer, tracking-disk-equipped pyranometer for diffuse sky radiation measurements, tracking-disk-equipped pyrometer for IR measurements, and a pyrheliometer mounted on an automatic solar tracker. A data acquisition system for this suite of sensors was also built and

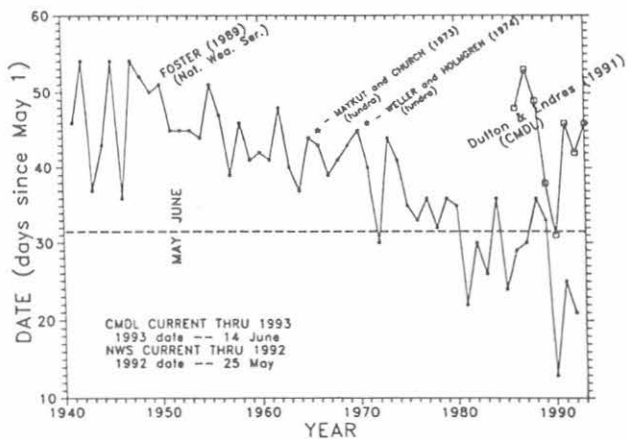


Fig. 3.15. Date of annual spring snowmelt as determined by various researchers in and around Barrow, Alaska. The downward trend indicated by the Foster (NWS) curve is believed to be due to "urbanization" in Barrow.

acquisition software was developed by CMDL personnel. This preliminary suite of sensors remained operational until the permanent site plan could be implemented.

The SRF took delivery of two automated absolute cavity systems. These units will result in more accurate determinations of the solar beam data used in calibration modes and, hence, enable more accurate transfers of the absolute scale to CMDL field sensors. The units are also capable of all weather operation and thus have the potential for becoming an operationally continuous measurement system. Continuous measurements have beneficial potential for CMDL field sites, particularly MLO, with its long history of solar beam measurements that are the basis of the MLO transmission record. The development, operation, and performance of the automated cavity system is described in *Hickey et al.* [1992, 1993].

Calibration and characterization activities of the SRF continued during the year. During the second half, a review of all CMDL field sensors was completed and an updated inventory of sensors by serial number, calibration history, and deployment history was created using a database management program. A total of over 90 different sensors were deployed over the past 20 years at the original GMCC and now CMDL sites, and the new database package will enable better management of this large group of sensors.

During the year, standards activities consisted of establishing the relationship of the new automated cavities to existing SRF reference units. This was accomplished through side-by-side comparisons and computation of ratios. Excessive cloudiness during the summer and fall of 1992 prevented the collection of as much data as desirable, but these activities are a regular part of the SRF operations, and eventually comparison histories will be created for traceability to historical NOAA SRF reference units. Collaboration with other laboratories was also maintained, and, in particular, standards comparisons were continued with the National Renewable Energy Laboratory in Golden.

3.1.12. ATMOSPHERIC TRAJECTORY ANALYSIS

During the past year, the computing environment for the trajectory programs has improved since the acquisition of a Sun Sparc-II workstation, which has provided significantly more memory and computing speed than the old Cyber computer. The workstation has allowed the use of a " θ chooser" that automatically picks θ for a given location, time, and elevation or pressure. It has also permitted modifications to the isentropic program to make it more usable and realistic in the lower atmosphere.

Input to θ chooser includes beginning and ending dates, destination identifier, destination latitude and longitude, limits of the data grid, and either the required pressure or elevation for the θ surface at the destination. The θ chooser outputs a line for each date with its calculated θ upon arrival.

Usually θ chooser can find θ within several tens of meters of the requested elevation. If the θ surface is strongly tilted with respect to the surrounding pressure surfaces, and the destination does not lie on or near a grid point, a difference of a few hundreds of meters could occur in arrival height of the trajectory versus the requested height. The error occurs due to spatial interpolation on the isobaric and isentropic surfaces. When the θ chosen results in an elevation that differs from the requested elevation by more than 50 m, a 1° adjustment is made to θ , and the elevation is recomputed and rechecked against the requested elevation. This procedure may have to be iterated several times until the actual and the requested elevations differ by fewer than 50 m.

Theta chooser is a tool that is helpful when the potential temperature of the trajectory is not known. In the future it will also be used to adjust the θ surface as its elevation changes in response to synoptic and seasonal variations of temperature and pressure. This is important for the construction of long-term climatologies because it will produce trajectories that arrive at approximately the same elevation each day.

In the past, there were problems associated with using the isentropic model below about 1500 m msl and over mountainous terrain. Trajectories would often "crash" into the ground because the θ surfaces were bumpy or traveled through mountains. Although isentropic trajectories are not always suitable in the near-surface layer, air traveling to this altitude may encounter significant vertical motions along the way; for example, as a result of travel around a high-pressure system or transport from colder regions at higher latitudes. It is recognized that isobaric trajectories used in the past to model air flow at lower altitudes, are not the best solution under these conditions because they do not take into account the vertical motions that transport the air parcels to these lower altitudes. Experimental changes to the isentropic model are aimed at solving these problems. With these changes, trajectories are calculated on a given isentropic surface until they come within 100 m of the topography. At this point, trajectories are promoted by winds averaged in the layer 100-600 m above the ground which is assumed to be representative of the mixed boundary layer above the friction layer. If 100 m msl is below 1000 hPa, winds at 1000 hPa are used as the lower limit of the surface layer. It is known that the air does not simply stop when the potential temperature surface becomes undefined or when it approaches a mountain barrier. By using surface layer winds as an approximation of air movement when the isentropic surface becomes undefined, the usefulness of the trajectory model can be extended.

Figure 3.16 shows trajectories arriving at BRW on January 15, 1985. The plot of vertical motion at the bottom indicates that air parcels descended about 1 km in 5 days as they approached BRW. Theta levels of 257.8K for 00 UT and 256.2K for 12 UT were selected by the θ chooser in the

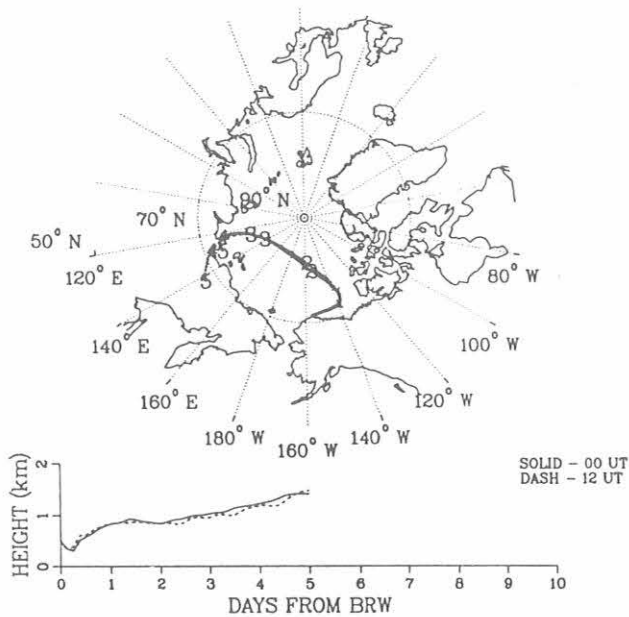


Fig. 3.16. Hybrid trajectories arriving at BRW on January 15, 1985, at 500 m elevation (see text).

previous step so that trajectories arrive at 500 m. Figure 3.17 depicts trajectories for February 2, 1985. The θ surfaces were adjusted to 265.6K for 00 UT and 265.9K for 12 UT to be 500 m elevation at BRW. The trajectories show flow from the southeast over mountainous terrain (the Brooks Range and the Alaskan Range). The European Centre for Medium-Range Weather Forecasts supplied the

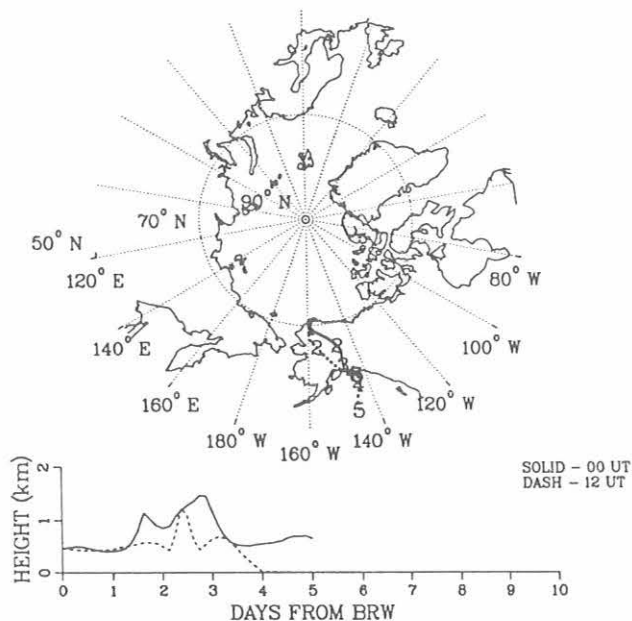


Fig. 3.17. Hybrid trajectories arriving at BRW on February 2, 1985, at 500 m elevation (see text).

2.5° gridded data of winds, temperature, and height used in the trajectory calculations. Topography is smoothed over a 2.5° grid. Air traveling in the boundary layer mode rather than the isentropic mode is assigned pressure, temperature, and height of the surface, interpolated bilinearly from the four surrounding grid points. During transitions of mode, some interpolations in space and time may use data from both modes.

These modifications to the trajectory program are still considered experimental. If all goes well, after further review and refinement, a similar hybrid version of the trajectory program will be used to construct a near surface pseudo-isentropic flow climatology for BRW.

3.2. SPECIAL PROJECT - A DECREASE IN ARCTIC HAZE AT BRW

Introduction

The "Arctic haze" as an Arctic-wide phenomenon has been the subject of intense interest since the first aerosol chemical analyses of Barrow samples by *Rahn et al.* [1977], although the phenomenon was first discussed in the literature by *Mitchell* [1957]. Excellent reviews of the subject were provided by *Barrie* [1986] and *Shaw and Khalil* [1989].

Continuous aerosol measurements were initiated at BRW in May 1976 [*Bodhaine*, 1989] with the installation of a CN counter for the measurement of the particle number concentration and a four-wavelength nephelometer for the measurement of aerosol scattering extinction coefficient (σ_{sp}). Optical depth (τ) measurements were initiated in 1976 using wideband spectral pyrheliometers [*Dutton and Christy*, 1992]. Surface-based aerosol and τ measurements at BRW were presented by *Bodhaine et al.* [1984, 1989] and *Dutton et al.* [1984, 1989].

The purpose of this brief report is to show statistically significant long-term decreases since 1982 of March-April σ_{sp} and τ measurements. March-April is the time of year when the Arctic haze caused by long-range transport is most evident in the vicinity of Barrow [*Bodhaine and Dutton*, 1993].

Instrumentation

Aerosol scattering extinction is measured continuously at BRW with an MRI four-wavelength nephelometer similar to the design of *Ahlquist and Charlson* [1969]. A rotating filter wheel in front of the photodetector allows continuous measurements at 450, 550, 700, and 850 nm. This instrument can measure aerosol scatter as low as about 10^{-7} m^{-1} (about 1% of Rayleigh scatter by air molecules) at an averaging time of about 1 hour. The nephelometer is calibrated every 2 months by filling it with CO_2 gas and adjusting the output of the instrument to give the known scattering coefficients of CO_2 . The accuracy of nephelometer data is generally accepted to be about $\pm 20\%$.

The direct solar beam has been measured at BRW since 1976 using a FWNIP with wide-band Schott glass cutoff

filters. The τ data for the 0.3-0.69 μm wavelength band were derived from the pyr heliometric data using the spectral one-layer radiative transfer model of *Bird and Riordan* [1986]. This wide-band method has proven sufficiently stable to provide an excellent τ record beginning in 1976. The BRW instrument has been calibrated by a comparison with a traveling standard at about 2-year intervals. The calibration of the traveling standard has been maintained by comparison with an absolute cavity laboratory standard in Boulder, Colorado. The measurement accuracy for computed σ is about ± 0.04 with an overall precision of better than ± 0.02 .

Data Analysis

Monthly means of σ_{sp} (550 nm) and τ are presented in Figure 3.18. Both data sets clearly show an annual cycle with a maximum in March-April, known as the "Arctic haze" phenomenon, which is caused by long-range transport from industrial regions in the springtime. σ_{sp} and τ reached monthly mean values as high as about $2 \times 10^{-5} \text{ m}^{-1}$ and 0.3 respectively in March-April, and as low as 10^{-6} m^{-1} and 0.05 in the summertime. The τ data set shown here was cut off just prior to the stratospheric aerosol influx from the Pinatubo eruption in 1991. The τ data in Figure 3.18 have not been corrected for the effects of volcanic eruptions. However, volcanic corrections were included in further analyses presented here.

Because τ is measured over the entire vertical column, the data can be significantly influenced by volcanic eruptions that inject aerosol into the stratosphere. During the time period under study, four eruptions may have affected the BRW τ data: (1) Nyamuragira (December 20, 1981); (2) El Chichon (April 4, 1982); (3) Nevada del Ruiz (November 13, 1985); and (4) Pinatubo (June 14, 1991).

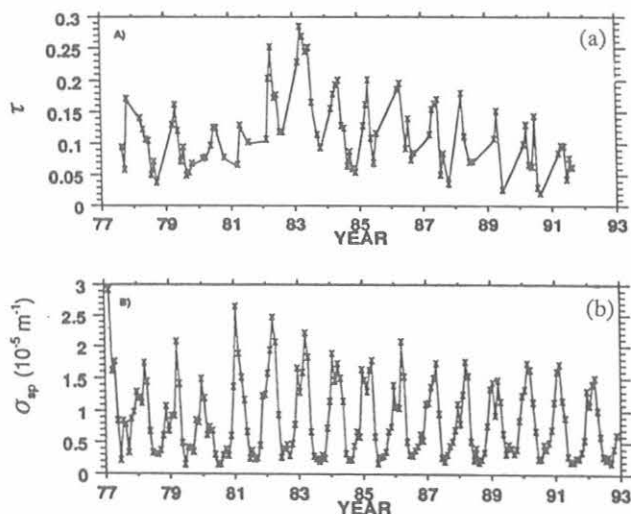


Fig. 3.18. Monthly means of τ (a) and σ_{sp} (b) for 1977-1992 at Barrow, Alaska. The effects of El Chichon have not been removed, and the τ data have been terminated in 1991 to avoid the effects of Pinatubo.

Corrections for the effects of Nyamuragira and Nevada del Ruiz were made on the basis of balloon measurements near Laramie, Wyoming [D. Hofmann, personal communication], and El Chichon on the basis of *Dutton et al.* [1984]. The Pinatubo contribution was removed by assuming that the 1992 data would have been the same as in 1991. However, the 1992 τ data point was omitted from the trend analysis described below because of the uncertainty of the Pinatubo contribution. A 1-year e-folding decay time was assumed for each volcanic pulse. It should be noted that in April 1986, aircraft measurements gave stratospheric τ values near 0.00 and never larger than 0.03 [*Dutton et al.*, 1989].

To investigate the time of year that shows the largest long-term decrease, a trend line for σ_{sp} during 1982-1992 was calculated for each 2-day period of the year. The March 7-May 5 time period showed downward trends significantly larger than the rest of the year. Next, the 2-day mean data sets were used to calculate a March 7-May 5 mean and standard deviation for each year. These data are plotted in Figure 3.19 where the standard error (S.E.) for each data point is shown. A linear regression for 1982-1992 was calculated where each point was weighted inversely by $(3 \text{ S.E.})^2$ (99% confidence level) for that point. The slope of the trend line is $-9.34 \times 10^{-7} \pm 1.95 \times 10^{-7} \text{ m}^{-1} \text{ yr}^{-1}$, at the 99% confidence level, and with a correlation coefficient of $r = -0.934$, a significant downward trend for this data set.

A similar analysis was performed on the 1982-1991 τ data set. A linear regression gave a slope of $-0.0032 \pm 0.0029 \text{ yr}^{-1}$, at the 95% confidence level, with a correlation coefficient of $r = -0.640$. The τ data along with the S.E. for each data point are also shown in Figure 3.19. The correlation coefficient between the σ_{sp} and τ data sets for 1977-1991 is $r = 0.760$ at the 99% confidence level.

Discussion

According to Figure 3.19, the Arctic haze reached a peak in 1982 and then declined thereafter. A similar long-term trend in optical depth was shown by *Radionov and Marshunova* [1992]. It is well known that the primary contributors to Arctic haze were Europe and Asia, including the former Soviet Union [*Rahn and Lowenthal*, 1984; *Barrie et al.*, 1989]. Although the exact percentages of contributions may be open to question, Europe and Asia are considered to be the primary source regions for the BRW site.

A decrease by approximately a factor of two in the Arctic haze phenomenon during 1982-1992, as shown here in the σ_{sp} and τ data, implies a decrease in the output of pollution aerosol by Europe and the Soviet Union. Since it is known that during 1980-1989 the Soviet Union increased the use of natural gas and decreased the use of coal and oil, thus decreasing SO_2 and particulate emissions [*J. Pacyna*, personal communication], part of the long-term decrease of σ_{sp} and τ at BRW may be attributed to this decline.

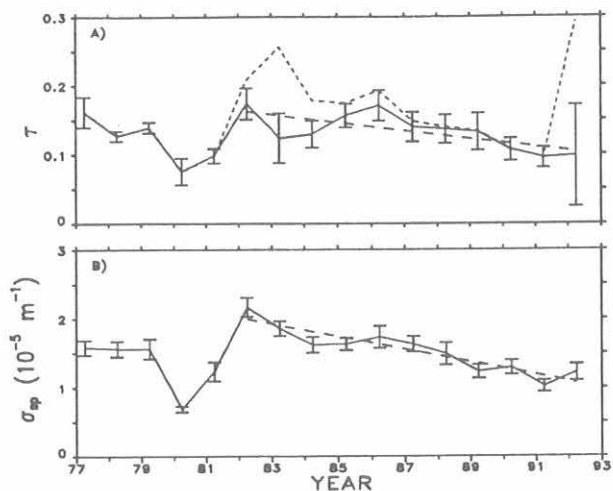


Fig. 3.19. Means and standard errors of τ (A), and σ_{sp} (550 nm) (B), calculated from 2-d means for March 7-May 5 for each year, and plotted as a time series for 1977-1992. The straight dashed lines show linear regressions for 1982-1992 calculated by weighting each data point inversely by $(3 \text{ S.E.})^2$ (99% confidence level). The short-dashed line shows τ before volcanic corrections were applied. Details of the regression lines are given in the text.

Stricter pollution controls in western Europe over this time period may have contributed to our long-term decrease in σ_{sp} and τ .

It is not entirely clear what effect this decrease of Arctic haze might have on climate. However, Valero and Ackerman [1986] suggested heating rates of 0.15-0.25 K d⁻¹ on the basis of measurements made in the spring of 1983. This is almost entirely due to absorption because the effect of a scattering aerosol above a bright surface is small. Therefore, in the absence of detailed aerosol size and chemistry information, and assuming that the single scatter albedo remained constant, it is suggested that the decrease of the Arctic haze phenomenon shown here would result in a 1992 warming of only about half the 1983 warming suggested by Valero and Ackerman [1986].

Conclusions

On the basis of the BRW record of σ_{sp} and τ obtained over the time period 1976-1992, the following conclusions may be drawn: (1) The phenomenon known as the Arctic haze, as observed at BRW, reached a maximum in 1982 and then decreased over the remainder of the time period through 1992. (2) This decrease was most likely due to a decrease of pollution aerosols that originated in Europe and the Soviet Union. (3) The effect of this decrease on climate is uncertain, but would most likely lead to a warming effect about half that estimated for Arctic haze for 1983 by Valero and Ackerman [1986].

3.3. REFERENCES

- Ahlquist, N.C., and R.J. Charlson, Measurement of the wavelength dependence of atmospheric extinction due to scatter, *Atmos. Environ.*, **3**, 551-564, 1969.
- Barrie, L.A., Arctic air pollution: An overview of current knowledge, *Atmos. Environ.*, **20**, 643-663, 1986.
- Barrie, L.A., M.P. Olson, and K.K. Oikawa, The flux of anthropogenic sulphur into the Arctic from midlatitudes in 1979/80, *Atmos. Environ.*, **23**, 2505-2512, 1989.
- Bass, A.M., and R.J. Paur, The ultraviolet cross-sections of ozone: I. The measurements, in *Atmospheric Ozone*, edited by C.S. Zerefos and A. Ghazi, pp. 606-610, D. Reidel, Hingham, MA, 1985.
- Bird, R.E., and C. Riordan, Simple solar spectral model for direct and diffuse irradiance on horizontal and tilted planes at the earth's surface for cloudless atmospheres, *J. Clim. Appl. Meteorol.*, **25**, 87-97, 1986.
- Bodhaine, B.A., Barrow surface aerosol: 1976-1986, *Atmos. Environ.*, **11**, 2357-2369, 1989.
- Bodhaine, B.A., and J. J. DeLuisi, An aerosol climatology of Samoa, *J. Atmos. Chem.*, **3**, 107-122, 1985.
- Bodhaine, B.A., and E.G. Dutton, A long-term decrease in Arctic Haze at Barrow, Alaska, *Geophys. Res. Lett.*, **20**, 947-950, 1993.
- Bodhaine, B.A., and M.K. Shanahan, Condensation nucleus and aerosol scattering extinction measurements at the South Pole Observatory: 1979-1988, *NOAA Data Rep. ERL CMDL-1*, Climate Monitoring and Diagnostics Laboratory, Boulder, CO, 1990.
- Bodhaine, B.A., E.G. Dutton, and J.J. DeLuisi, Surface aerosol measurements at Barrow during AGASP, *Geophys. Res. Lett.*, **11**, 377-380, 1984.
- Bodhaine, B.A., J.J. DeLuisi, J.M. Harris, P. Houmère, and S. Bauman, Aerosol measurements at the South Pole, *Tellus*, **38B**, 223-235, 1986.
- Bodhaine, B.A., J.J. DeLuisi, J.M. Harris, P. Houmère, and S. Bauman, PIXE analysis of South Pole aerosol, *Nuclear Instr. Meth.*, **B22**, 241-247, 1987.
- Bodhaine, B.A., E.G. Dutton, J.J. DeLuisi, G.A. Herbert, G.E. Shaw, and A.D.A. Hansen, Surface aerosol measurements at Barrow during AGASP-II, *J. Atmos. Chem.*, **9**, 213-224, 1989.
- Brasseur, G., and C. Granier, Mount Pinatubo aerosols, chlorofluorocarbons, and ozone depletion, *Science*, **257**, 1239-1242, 1992.
- Cacciani, M., P. DiGinolamo, A. diSarra, G. Fiocco, and D. Fua, Volcanic aerosol layers observed by lidar at South Pole, September 1991-June 1992, *Geophys. Res. Lett.*, **20**, 807-810, 1993.
- Cess, R.D., S. Nemesure, E.G. Dutton, J.J. DeLuisi, G.L. Potter, and J.-J. Morcrette, The impact of clouds on the shortwave radiation budget of the surface-atmosphere system: interfacing measurements and models, *J. Climate*, **6**, 308-316, 1993.
- Cess, R.D., E.G. Dutton, J.J. DeLuisi, and F. Jiang, Determining surface solar absorption from broadband satellite measurements for clear skies: Comparison with surface measurements, *J. Clim.*, **4**, 236-247, 1991.
- Charlson, R.J., S.E. Schwartz, J.M. Hales, R.D. Cess, J.A. Coakley, Jr., J.E. Hansen, and D.J. Hofmann, Climate forcing by anthropogenic aerosols, *Science*, **255**, 423-430, 1992.
- Dutton, E.G., A coherence between the QBO and the amplitude of the Mauna Loa atmospheric transmission annual cycle. *Int. J. Clim.*, **12**, 383-396, 1992a.
- Dutton, E.G., An extended comparison between LOWTRAN7-computed and observed broadband thermal irradiance: Global

- Dutton, E.G., and J.R. Christy, Solar radiative forcing a selected locations and evidence for global lower tropospheric cooling following the eruptions of El Chichon and Pinatubo, *Geophys. Res. Lett.*, 19, 2313-2316, 1992.
- Dutton, E.G., and D.J. Endres, Date of snowmelt at Barrow, Alaska, U.S.A., *Arctic Alpine Res.*, 23, 115-119, 1991.
- Dutton, E.G., J.J. DeLuisi, and B.A. Bodhaine, Features of aerosol optical depth observed at Barrow, March 10-20, 1983, *Geophys. Res. Lett.*, 11, 385-388, 1984.
- Dutton, E.G., J.J. DeLuisi, and G.A. Herbert, Shortwave optical depth of Arctic haze measured on board the NOAA WP-3D during AGASP-II, April 1986, *J. Atmos. Chem.*, 9, 71-79, 1989.
- Dutton, E.G., R.S. Stone, D.W. Nelson, and B.G. Mendonca, Recent interannual variations in solar radiation, cloudiness, and surface temperature at the South Pole, *J. Climate*, 4(8), 848-858, 1991.
- Dutton, E.G., P. Reddy, S. Ryan, and J. DeLuisi, Features and effects of aerosol optical depth at Mauna Loa, 1982-1992, *J. Geophys. Res.*, in press, 1993.
- Elkins, J.W., and R.M. Rosson (Eds.), *Geophysical Monitoring for Climatic Change, No. 17: Summary Report 1988*, NOAA ERL Air Resources Laboratory, Boulder, CO, 1989.
- Ferguson, E.E., and R.M. Rosson (Eds.), *Climate Monitoring and Diagnostics Laboratory, No. 20: Summary Report 1991*, pp 33-35, NOAA Environmental Research Laboratories, Boulder, CO, 1992.
- Foster, J.L., J.W. Winchester, and E.G. Dutton, The date of snow disappearance on the Arctic tundra as determined from satellite, meteorological station and radiometric in-situ observations, *IEEE Trans. Geosci. Remot. Sens.*, 30, 793-798, 1992.
- Gleason, J.F., P.K. Bhartia, J.R. Herman, R. McPeters, P. Newman, R.S. Stolarski, L. Flynn, G. Labow, D. Larko, C. Seftor, C. Wellemeyer, W.D. Komhyr, A.J. Miller, and W. Planet, Record low global ozone in 1992, *Science*, 260, 523-526, 1993.
- Herman, J.R., R. Hudson, R. McPeters, R.S. Stolarski, Z. Ahmad, X.-Y. Gu, S. Taylor, and C. Wellemeyer, A new self-calibration method applied to TOMS and SBUV backscattered ultraviolet data to determine long-term global ozone change, *J. Geophys. Res.*, 96(D4), 7531-7545, 1991.
- Hickey, J.R., D.B. Daniels, and D.W. Nelson, Automation of cavity pyrheliometer operation routine direct solar irradiance measurements, *Proceedings, 1992 Annual Conference of the American Solar Energy Society*, Coco Beach, FL, pp 340-344, 1992, American Solar Energy Society, Boulder, CO, 1992.
- Hickey, J., D.B. Daniel, and D.W. Nelson, Automated (HF) cavity pyrheliometer systems: Operational experience, test results and modification, *Proceedings, 1993 Annual Conference of the American Solar Energy Society*, Washington, DC, April 22-28, 1993, pp. 427-432, American Solar Energy Society, Boulder, CO, 1993.
- Hofmann, D.J., and S.J. Oltmans, Anomalous Antarctic ozone during 1992: Evidence for Pinatubo volcanic aerosol effects, *J. Geophys. Res.*, in press, 1993.
- Hofmann, D.J., S.J. Oltmans, J.M. Harris, W.D. Komhyr, J.A. Lathrop, T. DeFoor, and D. Kuniyuki, Ozone measurements at Hilo, Hawaii, following the eruption of Mt. Pinatubo, *Geophys. Res. Lett.*, 20(15), 1555-1558, 1993.
- Hofmann, D.J., S.J. Oltmans, J.M. Harris, S. Solomon, T. Deshler, and B.J. Johnson, Observations and possible causes of new ozone depletion in Antarctica in 1991, *Nature*, 359, 283-287, 1992.
- Komhyr, W.D., C.L. Mateer, and R.D. Hudson, Effective Bass-Paur 1985 ozone absorption coefficients for use with Dobson ozone spectrophotometers, *J. Geophys. Res.*, in press, 1993a.
- Komhyr, W.D., A. Lapworth, and K. Vanicek, *Dobson Data Re-evaluation Handbook*, edited by W.G. Planet and R.D. Bojkov, NOAA Tech. Report NESDIS 66, 141 pp., NOAA National Environmental Satellite, Data, and Information Service, Washington, DC, 1993b.
- LeTexier, H., S. Solomon, and R.R. Garcia, The role of molecular hydrogen and methane oxidation in the water vapour budget of the stratosphere, *Quart. J. R. Met. Soc.*, 114, 281-195, 1988.
- Massey, D.M., T.K. Quakenbush, and B. A. Bodhaine, Condensation nuclei and aerosol scattering extinction measurements at Mauna Loa Observatory: 1974-1985, *NOAA Data Rep. ERL ARL-14*, Air Resources Laboratory, Silver Spring, MD, 1987.
- Mitchell, J.M., Visual range in the polar regions with particular reference to the Alaskan Arctic, *J. Atmos. Terr. Phys., Special Supplement*, 195-211, 1957.
- Oltmans, S.J., D.J. Hofmann, W.D. Komhyr, and J.A. Lathrop, Ozone vertical profile changes over South Pole, *Proceedings, Quad. Ozone Symposium, 1992*, Charlottesville, VA, June 4-13, edited by R.D. Hudson, in press, 1993.
- Oltmans, S.J., and H. Levy II, Surface ozone measurements from a global network, *Atmos. Environ.*, in press, 1993.
- Penner, J.E., R.J. Charlson, J.M. Hales, N. Laulainen, R. Leifer, T. Novakov, J. Ogren, L.F. Radke, S.E. Schwartz, and L. Travis, Quantifying and minimizing uncertainty of climate forcing by anthropogenic aerosols, U.S. Department of Energy Report DOE/NBB-0092T, 53 pp., March 1993.
- Quakenbush, T.K., and B.A. Bodhaine, Surface aerosols at the Barrow GMCC Observatory: Data from 1976 through 1985, *NOAA Data Rep. ERL ARL-10*, Air Resources Laboratory, Silver Spring, MD, 1986.
- Radionov, V.F., and M.S. Marshunova, Long-term variations in the turbidity of the Arctic atmosphere in Russia, *Atmos. Ocean*, 30, 531-549, 1992.
- Rahn, K.A., and D.H. Lowenthal, Elemental tracers of distant regional pollution aerosols, *Science*, 223, 132-139, 1984.
- Rahn, K.A., R.D. Borys, and G.E. Shaw, The Asian source of Arctic haze bands, *Nature*, 268, 713-715, 1977.
- Russell, P.B., E.G. Dutton, R.F. Pueschel, J.M. Livingston, T. DeFoor, D. Allen, P. Pilewskie, M.A. Box, J.A. Reagan, B.M. Herman, S.A. Kinne, and D.J. Hofmann, Pinatubo and pre-Pinatubo optical depth spectra: Mauna Loa measurements, comparison, inferred particle size distributions, radiative effects, and relationship to lidar, *J. Geophys. Res.*, in press, 1993.
- Schnell, R.C., S.C. Liu, S.J. Oltmans, R.S. Stone, D.J. Hofmann, E.G. Dutton, T. Deshler, W.T. Sturges, J.W. Harder, S.D. Sewell, M. Trainer, and J.M. Harris, Decrease of summer tropospheric ozone concentrations in Antarctica, *Science*, 351, 726-729, 1991.
- Shaw, G.E., and M.A.K. Khalil, Arctic haze, in *The Handbook of Environmental Chemistry, Vol. 4(B)*, edited by O. Hutzinger, pp. 69-111, Springer-Verlag, New York, 1989.
- Steele, L.P., E.J. Dlugokencky, P.M. Lang, P.P. Tans, R.C. Martin, and K.A. Masarie, Slowing down of the global accumulation of atmospheric methane during the 1980s, *Nature*, 358, 313-316, 1992.
- Valero, F.P.J., and T.P. Ackerman, Arctic haze and radiation balance, in *Arctic Air Pollut.*, edited by B. Stonehouse, pp. 121-133, Cambridge, 1986.
- Vigroux, E., Détermination des coefficients moyens d'absorption des l'ozone en vue des observations concernant l'ozone atmosphérique a l'aide du spectromètre Dobson, *Ann. Phys.*, 2, 209-215, 1957.

4. Acquisition and Data Management Division

G. HERBERT (EDITOR), M. BIENIULIS, T. MEFFORD, AND K. THAUT

4.1. CONTINUING PROGRAMS

4.1.1. STATION CLIMATOLOGY

The climatology of surface weather observations at the CMDL observatories is based on hourly-average measurements of the wind direction, wind speed, station pressure, air and dewpoint temperature, and precipitation amount. The 16-year station climatologies are an important record for the interpretation of measured values of aerosols, trace gases, and climatic change. The sensors currently in use were selected not only for high accuracy, but also for ruggedness, to minimize failures in the extreme conditions of the polar region (Table 4.1). To the extent that is practical, WMO siting standards were followed.

On DOY 336, air temperature sensor 291 was moved to a height of 20.7 m from a height of 21. m. On DOY 350, the primary anemometer 826, was moved to a height of 10.9 m from a height of 11.8 m. There were no changes in the instruments at BRW, MLO, or SMO in 1992. At SPO on DOY 70, thermometer 703 was replaced with 293 and 704 was replaced with 291. Table 4.1 describes the disposition of the sensors as of December 31, 1992.

Barrow

Descriptions of the BRW station and its climate are given in previous *CMDL Summary Reports* [e.g., *DeLuisi*, 1981]. Wind roses of hourly averages resultant wind direction and speed are presented in 16 direction classes and 4 speed classes (Figure 4.1). Winds from the "clean-air" sector, north-northeast-

southeast directions occurred 55.7% of the time as compared to 62.6% for the 15-year climatology. Wind speeds greater than 10 m s⁻¹ occurred 14.3% of the time as compared to 11.5% for the 15-year climatology. The year's maximum hourly average wind speed of 24 m s⁻¹ occurred on December 4, which ties the all time record for December. New maximum wind speeds were measured during the months of April and June as well.

The average temperature for 1992 tied the climatological average of -12.7°C (Table 4.2). Like 1991, the monthly mean pressure was not significantly different from normal.

Mauna Loa

In this report, the climatology of MLO is regarded as consisting of two distinct regimes because the bimodal distribution of the wind direction changes with the time of day. The night (downslope) period (1800-0600 LST) and the day (upslope) period (0600-1800 LST) define the two regimes. The 15-year night and day wind roses illustrate the two distinct wind patterns (Figure 4.2).

Night Regime. The 15-year wind rose (Figure 4.2), shows that 92.6% of all the winds observed had a southerly component with south-southeast dominating. Storm related winds (WS ≥ 10 m s⁻¹) with westerly and easterly components are evident in both the 1992 and 15-year wind rose. The 1992 wind rose (Figure 4.3) shows these winds occurred 5.5% of the time as compared to 7.1% for the 15-year climatology. The upslope or northerly component winds (north-northwest through east-northeast) about 5% of the time, are primarily the results of the daytime, upslope flow extending into the evening hours. A new maximum

TABLE 4.1. CMDL Meteorological Sensor Deployment December 31, 1992

Sensor	BRW		MLO		SMO		SPO	
	Serial No.	Elevation, m						
Primary anemometer*	576	16.7	[1829]	8.5	[883]	14.3	[826]	10.9
Secondary anemometer*			[782]	38.5				
Pressure transducer†	2366	9	225	3403	752	30	28	2840
Mercurial barometer	641	9	278	3403	961	30	1215	2840
Air temperature A‡	8801	2.5	8805	1.7	8803	9.8	{293+}	2.0
Air temperature B§¶	8802	15.3	8809	37.8	8806	2.3	{[291+]}	20.7
Air temperature C‡	8	3.1	46	2.0	50	9.8	835+	2.0
Dewpoint temperature hygrometer**	8	3.1	46	2.0	50	9.8	3720	2.0

*Aerovane, Bendix, Inc., model no. 141, Baltimore, Maryland

†Pressure transducer, Rosemount, Inc., model no. 1201F1b, Minneapolis, Minnesota. Heights of all pressure sensors are given with respect to MSL.

‡Linearized thermistors, Yellow Springs Inst. Co., model no. 44212, Yellow Springs, Ohio, except at SPO

+Platinum resistance thermometer, Yellow Springs Inst. Co., model no. RTD-385, Yellow Springs, Ohio

§Thermometer, positioned at the top of the local sampling tower to facilitate an estimation of boundary layer stability

**Hygrothermometer, Technical Services Laboratory model no. 1063, Fort Walton Beach, Florida

[] Instrument put in service in 1991

{ } Instrument put in service in 1992

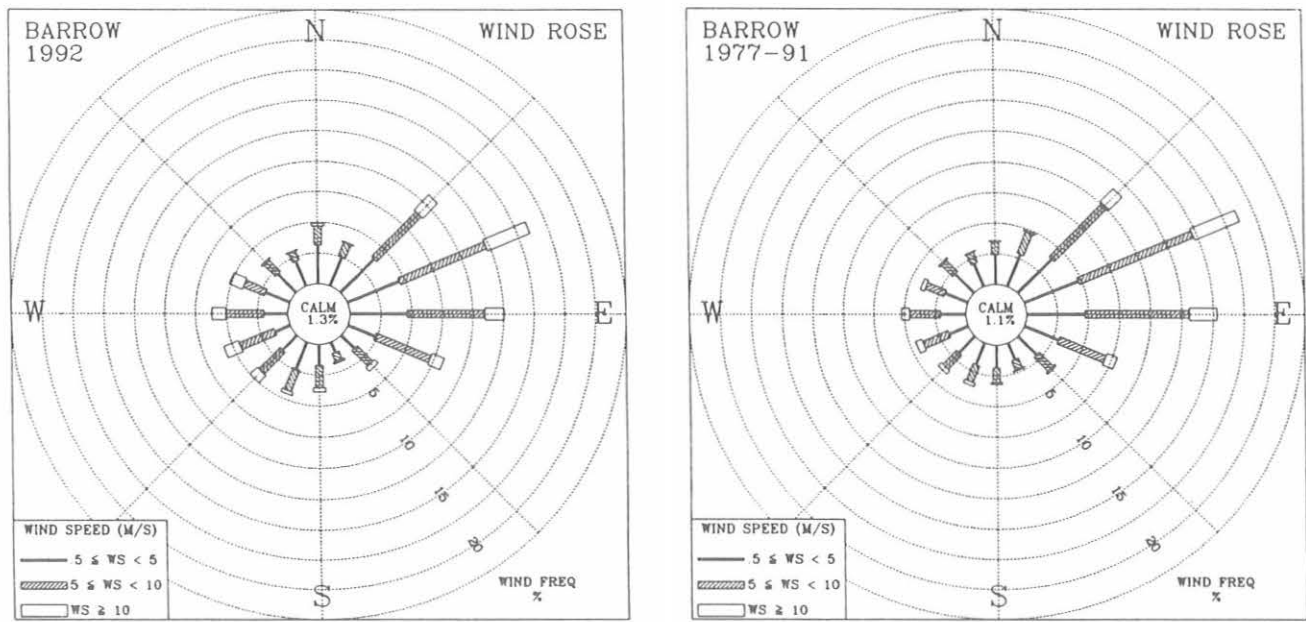


Fig. 4.1. Wind rose of surface winds for BRW for 1992 (left) and 1977-1990 (right).

TABLE 4.2. BRW 1992 Monthly Climate Summary

	Jan.	Feb.	March	April	May	June	July	Aug.	Sept.	Oct.	Nov.	Dec.	1992
Prevailing wind direction	ENE	NE	ENE	ENE	WSW	ENE	E	E	ENE	ENE	ENE	NE	ENE
Average wind speed ($m s^{-1}$)	7.5	5.5	5.0	6.5	6.8	5.9	5.8	6.6	6.1	6.9	7.2	8.1	6.5
Maximum wind speed* ($m s^{-1}$)	17	15	13	19	13	17	13	13	17	17	20	24	24
Direction of max. wind* (deg.)	60	107	80	58	187	238	86	289	254	156	57	238	238
Average station pressure (hPa)	1015.5	1021.5	1013.5	1021.0	1011.1	1014.1	1015.1	1008.7	1014.7	1008.7	1010.4	1015.0	1014.1
Maximum pressure* (hPa)	1033	1045	1033	1040	1022	1026	1026	1024	1027	1030	1038	1044	1045
Minimum pressure* (hPa)	1002	993	988	1002	997	997	1005	990	995	980	980	982	980
Average air temperature ($^{\circ}C$)	-28.4	-29.2	-23.3	-17.5	-6.7	1.1	2.6	2.9	-3.6	-10.4	-18.8	-23.2	-12.7
Maximum temperature* ($^{\circ}C$)	-18	-8	-11	-6	3	11	12	16	4	3	-5	-5	16
Minimum temperature* ($^{\circ}C$)	-42	-38	-41	-29	-25	-6	-4	-3	-14	-21	-37	-37	-42
Average dewpoint temperature ($^{\circ}C$)	-31.3	-32.0	-25.8	-19.7	-8.6	-0.6	0.9	1.3	-5.5	-12.1	-20.9	-25.5	-14.8
Maximum dewpoint temperature ($^{\circ}C$)	-21	-9	-12	-8	1	7	9	10	3	0	-6	-7	10
Minimum dewpoint temperature ($^{\circ}C$)	-45	-41	-45	-31	-27	-8	-5	-4	-15	-24	-40	-41	-45
Precipitation (mm)	0	0	0	0	0	1	0	0	1	1	0	0	3

Instrument heights: wind, 16.7 m; pressure, 9 m (MSL); air temperature, 2.5 m; dewpoint temperature, 3.1 m. Wind and temperature instruments are on tower 25 m northeast of the main building.

*Maximum and minimum values are hourly averages.

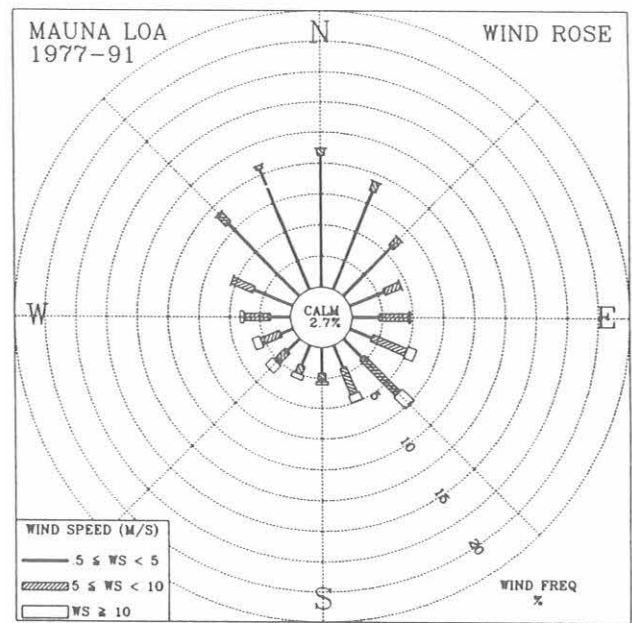
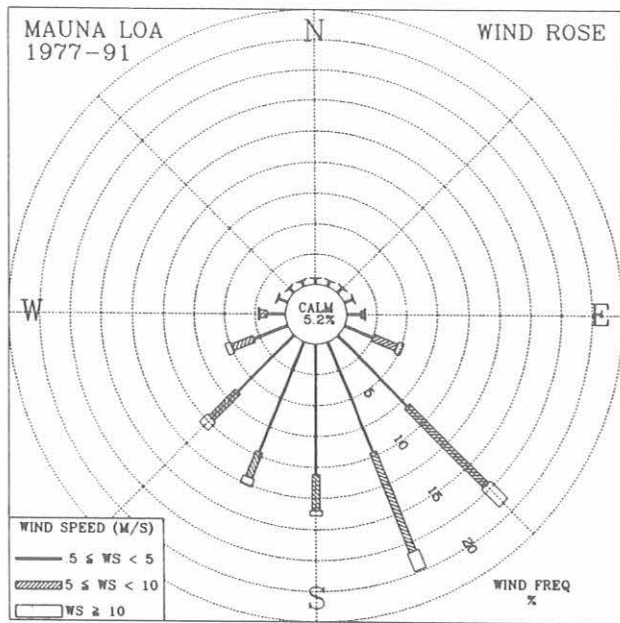


Fig. 4.2. Wind roses of the surface winds for MLO for 1977-1991 night (left) and day (right). The distribution of resultant wind direction and speed are given in units of percent occurrence for the 15-year period. Wind speed is displayed as a function of direction in three speed classes.

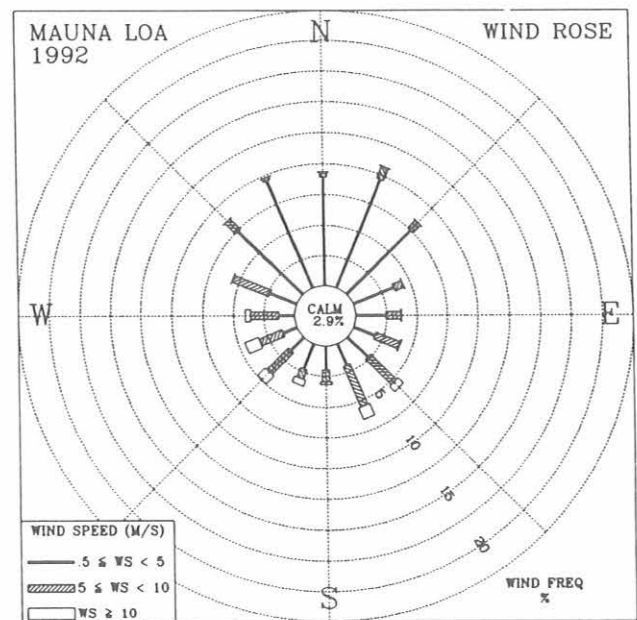
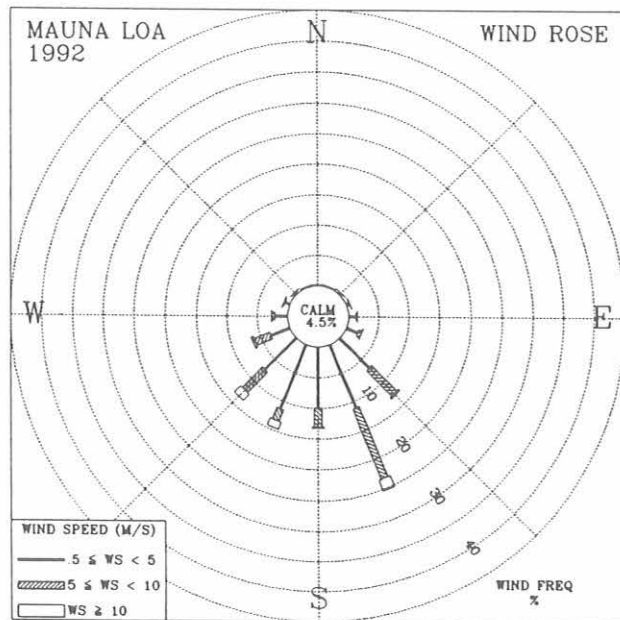


Fig. 4.3. Wind roses of the surface winds for MLO for 1992 night (left) and day (right). The distribution of resultant wind direction and speed are given in units of percent occurrence for the year. Wind speed is displayed as a function of direction in three speed classes.

TABLE 4.3. MLO 1992 Monthly Climate Summary

	Jan.	Feb.	March	April	May	June	July	Aug.	Sept.	Oct.	Nov.	Dec.	1992
	<i>Night</i>												
Prevailing wind direction	SSW	SW	SSE	SW	SW	SSE	SSE	SSE	SSE	SSE	SSE	SE	SSE
Average wind speed (m s ⁻¹)	4.6	5.4	3.3	4.4	5.4	5.2	4.2	4.1	3.3	4.7	5.1	5.6	4.6
Maximum wind speed* (m s ⁻¹)	15	13	9	13	14	11	13	11	10	16	14	13	16
Direction of max. wind* (deg.)	159	204	150	222	207	160	159	163	163	149	153	150	149
Average station pressure (hPa)	679.4	678.4	680.0	679.1	679.6	680.9	680.7	681.7	680.1	680.6	679.8	679.1	680.0
Maximum pressure* (hPa)	683	683	683	684	684	684	685	684	685	684	683	684	685
Minimum pressure* (hPa)	673	675	677	675	676	678	678	680	677	677	677	674	673
Average air temperature (°C)	4.2	3.5	4.0	5.9	6.0	7.5	6.5	6.2	6.1	6.0	5.2	4.0	5.4
Maximum temperature* (°C)	10	12	12	13	12	13	13	13	11	10	9	9	13
Minimum temperature* (°C)	-3	-2	-1	1	3	2	2	2	2	3	1	0	-3
Average dewpoint temperature (°C)	-13.2	-15.5	-17.2	-14.4	-10.5	-13.5	-7.4	-3.4	-0.8	-7.1	-8.0	-8.4	-10.0
Maximum dewpoint temperature (°C)	4	4	4	10	7	7	8	9	9	7	7	4	10
Minimum dewpoint temperature (°C)	-28	-29	-33	-29	-34	-23	-24	-19	-21	-31	-30	-26	-34
Precipitation (mm)	11	0	0	0	0	0	9	27	14	4	51	7	124
	<i>Day</i>												
Prevailing wind direction	NW	SW	NNE	NNW	WNW	NE	NNE	NNW	NW	N	SE	SSE	NNE
Average wind speed (m s ⁻¹)	4.1	5.6	3.5	5.1	6.0	4.4	4.0	3.6	3.4	4.3	4.6	5.2	4.5
Maximum wind speed* (m s ⁻¹)	13	14	9	15	13	11	11	10	17	12	14	13	17
Direction of max. wind* (deg.)	157	235	152	234	243	153	98	169	168	137	155	139	168
Average station pressure (hPa)	679.4	678.4	680.1	679.2	679.8	681.1	680.9	681.8	680.2	680.8	679.8	679.1	680.0
Maximum pressure* (hPa)	684	683	682	684	684	684	685	684	684	684	683	685	685
Minimum pressure* (hPa)	673	675	678	675	676	678	678	680	678	677	676	674	673
Average air temperature (°C)	8.5	7.6	9.1	10.7	11.1	12.7	11.0	10.6	10.0	10.3	9.0	7.3	9.8
Maximum temperature* (°C)	17	16	15	18	17	18	18	17	18	16	15	14	18
Minimum temperature* (°C)	-3	-1	-1	2	3	4	4	3	3	3	1	1	-3
Average dewpoint temperature (°C)	-7.0	-10.0	-7.9	-4.9	-3.9	-4.3	0.1	1.2	3.0	-3.2	-5.7	-5.3	-4.0
Maximum dewpoint temperature (°C)	8	5	7	13	11	8	9	9	10	8	9	8	13
Minimum dewpoint temperature (°C)	-29	-29	-29	-26	-33	-21	-20	-19	-21	-29	-30	-26	-33
Precipitation (mm)	25	5	0	0	0	0	60	61	116	6	58	32	364

Instrument heights: wind, 8.5 m; pressure, 3403 m (MSL); air temperature, 1.7 m; dewpoint temperature, 2.0 m. Wind and temperature instruments are on a tower 15 m southwest of the main building.

*Maximum and minimum values are hourly averages.

TABLE 4.4. SMO 1992 Monthly Climate Summary

	Jan.	Feb.	March	April	May	June	July	Aug.	Sept.	Oct.	Nov.	Dec.	1992
Prevailing wind direction	SSE	SE	SE	SE	SE	SE	SE	ESE	ESE	E	SE	E	SE
Average wind speed (m s ⁻¹)	3.7	4.7	3.9	4.5	4.2	5.0	4.0	3.0	3.2	2.2	2.6	1.7	3.6
Maximum wind speed* (m s ⁻¹)	10	11	10	11	8	9	8	9	7	8	6	4	11
Direction of max. wind* (deg.)	149	147	105	142	150	128	109	125	132	128	139	100	142
Average station pressure (hPa)	998.1	999.0	997.3	999.7	1001.1	1001.4	1002.3	1002.3	1001.5	999.8	1000.1	997.7	1000.0
Maximum pressure* (hPa)	1003	1004	1005	1004	1005	1005	1006	1006	1005	1004	1004	1003	1006
Minimum pressure* (hPa)	991	996	987	992	996	998	998	998	998	995	995	990	987
Average air temperature (°C)	27.6	27.7	27.6	27.6	27.4	27.3	27.3	27.4	27.8	28.2	27.5	28.8	27.7
Maximum temperature* (°C)	32	32	31	31	31	33	34	34	34	36	36	38	38
Minimum temperature* (°C)	22	21	24	23	24	25	23	23	23	23	21	23	21
Average dewpoint temperature (°C)	23.2	24.0	24.4	24.1	23.8	21.9	22.5	22.8	22.7	22.4	22.4	23.4	23.0
Maximum dewpoint temperature (°C)	25	26	26	25	25	25	24	25	24	25	25	25	26
Minimum dewpoint temperature (°C)	20	21	20	22	19	18	17	20	19	16	17	21	16
Precipitation (mm)	194	216	222	509	170	33	60	151	96	166	219	158	2194

Instrument heights: wind, 13.7 m; pressure, 30 m (MSL); air temperature, 9 m. Wind and temperature instruments are on Lauagae Ridge, 110m northeast of the main building. Pressure sensors are in the main building.

*Maximum and minimum values are hourly averages.

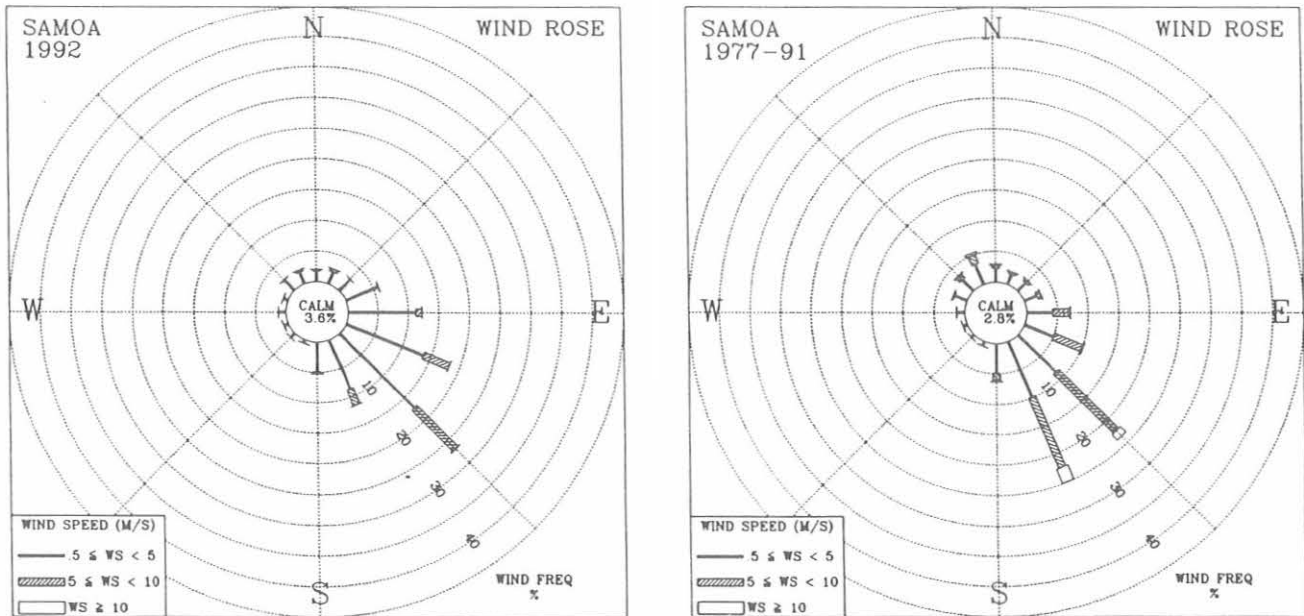


Fig. 4.4. Wind roses of the surface winds for SMO for 1992 (left) and 1977-1991 (right). The distribution of resultant wind direction and speed are given in units of percent occurrence for the year and 15-year period, respectively. Wind speed is displayed as a function of direction in three speed classes.

TABLE 4.5. SPO 1992 Monthly Climate Summary

	Jan.	Feb.	March	April	May	June	July	Aug.	Sept.	Oct.	Nov.	Dec.	1992
Prevailing wind direction	N	ENE	ENE	E	E	NNE	E	E	N	ENE	NNE	ENE	ENE
Average wind speed (m s ⁻¹)	3.7	5.2	5.9	5.8	4.8	7.3	4.7	6.3	7.0	5.3	5.9	3.2	5.4
Maximum wind speed* (m s ⁻¹)	8	11	11	14	13	15	11	13	14	12	11	7	15
Direction of max. wind* (deg.)	357	346	107	313	8	7	354	16	2	306	352	278	7
Average station pressure (hPa)	687.2	687.0	680.1	678.4	683.8	684.3	675.6	671.0	670.0	678.7	676.7	684.3	679.7
Maximum pressure* (hPa)	698	696	693	695	697	702	695	686	696	689	690	690	702
Minimum pressure* (hPa)	679	676	671	664	671	662	658	649	647	668	667	677	647
Average air temperature (°C)	-28.0	-41.7	-55.7	-52.8	-58.4	-54.9	-59.7	-60.1	-57.3	-46.5	-38.3	-28.4	-48.6
Maximum temperature* (°C)	-23	-31	-43	-31	-46	-38	-40	-42	-33	-30	-31	-22	-22
Minimum temperature* (°C)	-34	-54	-64	-68	-68	-71	-71	-74	-77	-62	-47	-34	-77
Average dewpoint temperature (°C)	-29.3	-42.5	-55.4	-52.1	-57.7	-54.0	-58.1	-59.2	-56.3	-45.5	-38.7	-30.1	-48.3
Maximum dewpoint temperature (°C)	-25	-30	-44	-30	-46	-38	-40	-42	-33	-30	-31	-25	-25
Minimum dewpoint temperature (°C)	-35	-54	-63	-66	-66	-66	-67	-69	-70	-60	-46	-36	-70
Precipitation (mm)	0	0	0	0	0	0	0	0	0	0	0	0	0

Instrument heights: wind, 12.2 m; pressure, 2841 (MSL); air temperature, 2.2 m. The anemometer and thermometer are on a tower 100 m grid east-southeast of CAF. Pressure measurements are made inside CAF.

*Maximum and minimum values are hourly averages.

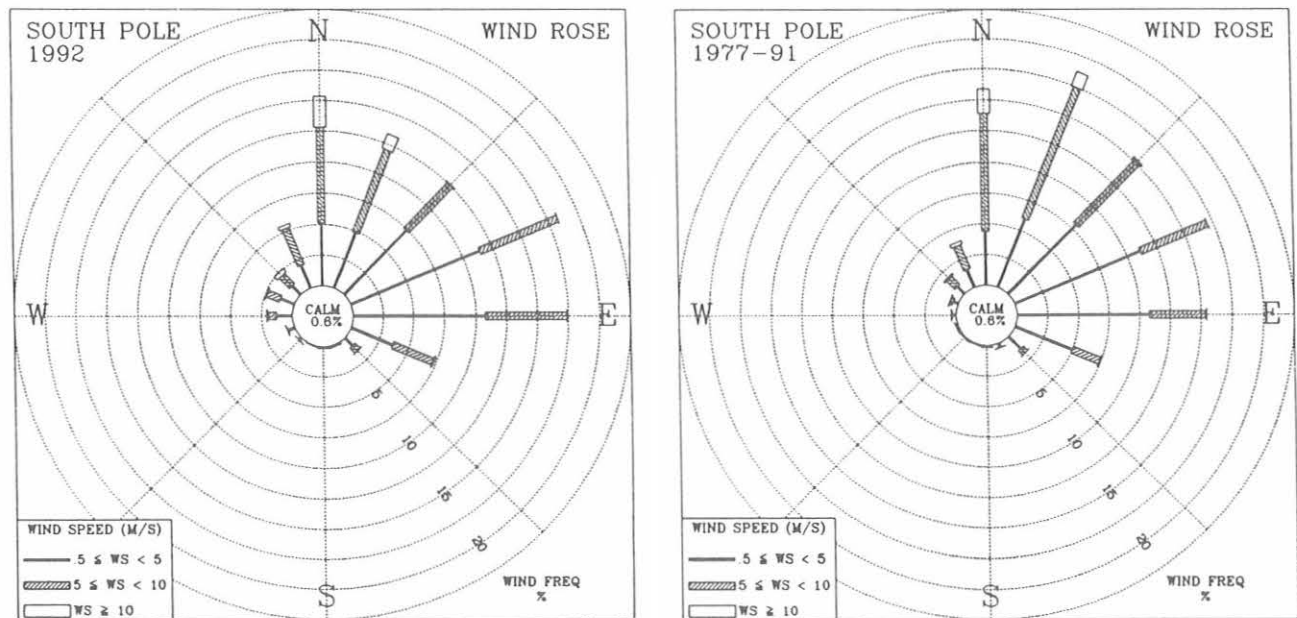


Fig. 4.5. Wind roses of the surface winds for SPO for 1992 (left) and 1977-1991 (right). The distribution of resultant wind direction and speed are given in units of percent occurrence for the year. Wind speed is displayed as a function of direction in three speed classes.

TABLE 4.6a. CMDL CAMS Operations Summary, 1992

Individual CAMS	Expected No. of Blocks 1992	Percent Data Capture			
		BRW	MLO	SMO	SPO
ASR	8784	98.51% [131]	99.10% [79]	99.09% [80]	94.18% [511]
CO2	8784	98.48% [133]	99.87% [11]	97.29% [238]	96.40% [316]
MO3	4392	99.16% [37]	99.79% [9]	96.95% [134]	99.95% [2]
Total	21960	98.72% [301]	99.59% [99]	97.78% [452]	96.84% [829]

TABLE 4.6b CMDL CAMS Operational Summary, 1992

Block Type	Description	Expected No. of Blocks 1992	Blocks Recorded and [Blocks Missing]			
			BRW	MLO	SMO	SPO
A	Hourly aerosol data	2196	2165 [31]	2176 [20]	2176 [20]	2069 [127]
B	Secondary aerosol data	Variable	272	824	1244	993
C	Hourly CO ₂ data	8732*	8290 [442]	8404 [328]	8207 [525]	8133 [599]
D	Daily CO ₂ data	366	366	367	363 [3]	354 [12]
E	Hourly CO ₂ calibration data	Variable†	361	369	339	335
F	CO ₂ calibration report	52	52	53	49 [3]	53
H	Daily aerosol data	366	366	373	366	343 [23]
I	Meteorological calibration	366	364 [2]	365 [1]	356 [10]	366
M	Hourly meteorological data	4392	4355 [37]	4383 [9]	4258 [134]	4390 [2]
N	Surface ozone calibration	52	51 [1]	56	28 [24]	0
O	Daily surface ozone data	366	367	366	364 [2]	366
S	Hourly solar radiation data	8784	8653 [131]	8705 [79]	8704 [80]	8273 [511]
T	Daily solar radiation data	366	359 [7]	361 [5]	362 [4]	342 [24]
W	Daily meteorological data	366	366	366	364 [2]	366

*Nominal block count equal to total hours in year less 52 7-hour calibration periods.

†Nominal block count equal to 52 7-hour calibration periods.

hourly average wind speed of 16 m s⁻¹ occurred during the month of October. The average air temperature for 1992 was 5.4°C, which is 0.7°C higher than the 15-year average while the station pressure was 0.6 mb below the 15-year average.

Day Regime. The 15-year wind rose (Figure 4.2) indicates that light wind speeds in the west-northwest through east-northeast sectors were observed 58.9% of the time. This represents the upslope flow attributed to the daytime heating of Mauna Loa. The 1992 wind rose (Figure 4.3) compares well with the 15-year rose in that northerly wind components prevail 58.6% of the time. The day wind rose was more uniformly distributed in the light wind classes than that of the night wind rose. This was due to the occurrence of variable wind directions during the transition periods of dawn and dusk, most of which were included in this regime. The percent frequency of occurrence of wind in the 10 m s⁻¹ or greater wind class for 1992 was only 0.3% less than the 15-year average.

The 1992 average day-night temperature difference was 4.4°C and the average dewpoint temperature for 1992 was -7.0°C (Table 4.3). The year's maximum temperature of 18°C occurred on April 20 and again on September 25. The minimum temperature of -3°C occurred on January 16. The average station pressure for 1992 was 680.0 mb, which was 0.6 mb below the 15-year average. Precipitation for 1992

was below normal with 488 mm as compared to 545 mm for the 15-year climatology. The months of March through June recorded no precipitation.

Samoa

A comparison of SMO's 1992 wind rose (Figure 4.4) with that of the 15-year period shows a much higher percentage (75.8%) of "clean air" sector winds (north-northwest through east-southeast) in 1992 than for the 1977-1991 period (58.3%). (If air passing over the offshore island of Aunu'u is to be avoided, the south-southeast wind sector (25.6%) cannot be considered in the "clean air" sector.) The average wind speed of 3.6 m s⁻¹ was 1.4 m s⁻¹ below the 15-year average.

Station pressure was slightly above normal with an average of 1000.0 mb as compared to the 15-year average of 999.3 mb (Table 4.4). The temperatures for June tied the record high for the month while the rest of the year set new monthly records. A temperature of 38°C, which occurred on December 24, set the all time record high temperature for the station. The precipitation total for the year measured 2194 mm, which is slightly higher than the average of 2080 mm.

South Pole

The distribution of the surface wind direction in 1992 (Figure 4.5) shows a lower percentage of winds (90.3%)

from the "clean air" sector (grid north-northwest through east-southeast) than the 15-year average (94.2%). A higher percentage of winds in the $\geq 10 \text{ m s}^{-1}$ range (4.8%) was observed in 1992 than the long term average of 4.0%. The average wind speed for 1992 very closely follows that of the 15-year average. The maximum hourly average wind speed was 15 m s^{-1} on June 19.

While the 1992 annual average temperature was slightly cooler than normal, the annual average station pressure was slightly higher than normal (Table 4.5). During 1992, the minimum pressure for August tied the record for the month. Also, the maximum temperature for October tied its record for the month. The maximum temperature was -22°C while the minimum was -77°C .

4.1.2. DATA MANAGEMENT

During 1992, the CAMS operated 98.2% of the time. CAMS gathers data from sensors that operate continuously at each of

the four CMDL observatories. The CAMS performance was monitored by comparing the number of data files recorded against those expected for the year. In CAMS, there are data files regularly recorded 12 or 24 times a day. In the summary table (Table 4.6a, b), the hourly solar radiation file was used to monitor the ASR CAMS. The hourly CO_2 data files were used for the CO_2 CAMS. The hourly average meteorological data file was used for the MO3 CAMS.

Due to the remoteness of the observatories, power outages are common and are the main reason for data loss. Hardware failure is another reason for data loss. During 1992, BRW had the line conditioner fail, MLO had two boards fail, SMO had five RS422 interface boards fail, and SPO had two clock boards and the solar radiation preamp board failed.

4.2. REFERENCE

DeLuisi, J.J. (Ed.), *Geophysical Monitoring for Climatic Change, No. 9: Summary Report 1980*, 163 pp., NOAA Environmental Research Laboratories, Boulder, CO, 1981.

5. Nitrous Oxide and Halocarbons Division

T.H. SWANSON (EDITOR), J.W. ELKINS, J.H. BUTLER, S.A. MONTZKA, R.C. MYERS, T.M. THOMPSON, T.J. BARING, S.O. CUMMINGS, G.S. DUTTON, A.H. HAYDEN, J.M. LOBERT, G.A. HOLCOMB, W.T. STURGES, AND T.M. GILPIN

5.1. CONTINUING PROGRAMS

5.1.1. FLASK SAMPLES

Air sample pairs were collected and analyzed for CFC-11 (CCl_3F), CFC-12 (CCl_2F_2), and nitrous oxide (N_2O) on the original HP 5710A GC. Both CFCs, particularly CFC-11, show a decrease in growth rate during the past few years that is apparent at all flask locations. In 1992 the growth rates of CFC-11 and CFC-12 were about 3 ppt yr^{-1} (Figure 5.1) and 11 ppt yr^{-1} (Figure 5.2). For a complete discussion of the slowdown of the growth rates, refer to *Elkins et al.*, [1993]. The global slowdowns of the growth rates observed after 1989 are also supported by estimates of reduced emissions [AFEAS, 1993; McFarland and Kaye, 1992] made by the CFC producers and are directly attributed to the international efforts of the Montreal Protocol [UNEP, 1987] and voluntary reductions from producers and users to reduce stratospheric ozone depletion. If the observed slowdowns in the growth rates continue at 1990-1992 levels, global atmospheric CFC-11 and -12 mixing ratios would reach a maximum well before the turn of the century, and thereafter begin to decline [Elkins et al., 1993].

The growth rate of N_2O in the northern hemisphere has dropped significantly in 1992 and the decline may have started as soon as June 1991 (Figure 5.3). From 1977

to 1985, the growth rate was about 0.5-0.6 ppb yr^{-1} . From 1986 through mid-1991, the growth rate reached near 1 ppb yr^{-1} , with the peak value in 1989. In 1992, the growth rate dropped to about 0.5 ppb yr^{-1} . Whether this drop is a long-term feature remains to be seen. The cause of this slowdown is unknown because the relative magnitudes of the sources of atmospheric N_2O are still uncertain. The gap in the N_2O and CFC-12 data are the result of a GC problem that did not affect CFC-11.

5.1.2. RITS CONTINUOUS GAS CHROMATOGRAPH SYSTEMS AT CMDL STATIONS AND NIWOT RIDGE

In situ measurements of tropospheric air were made at the CMDL baseline stations, BRW, MLO, SMO, SPO, and at a cooperative site on Niwot Ridge (NWR). CMDL GCs made 24 measurements per day at each site. Each in situ GC system has three channels to measure different species of halocarbons; (1) N_2O , (2) CFC-12, and (3) CFC-11, CFC-113, CH_3CCl_3 , and CCl_4 . Each channel is equipped with a chromatographic column and an electron capture detector (ECD).

During a scheduled maintenance trip to SPO, a new sampling inlet system was installed. This system draws air from the meteorological tower in the clean air sector of the South Pole station via two sections of 0.9 cm o.d. Dekabon

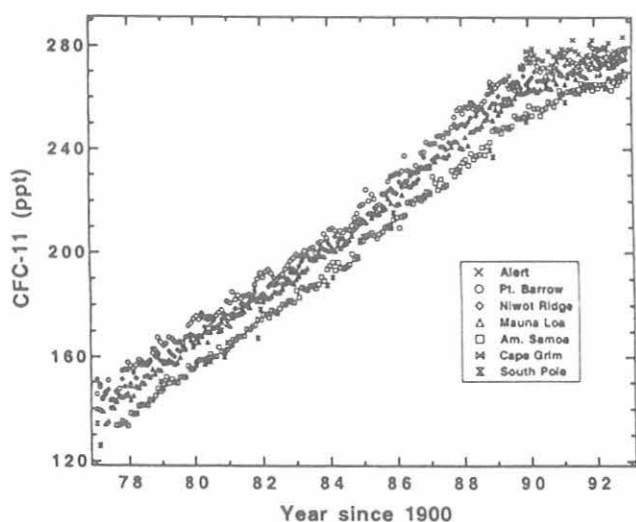


Fig. 5.1. Long-term trend of CFC-11 (dry, ppt by mole fraction) at the seven flask sites. A color plot of the figure is available from the NOAA division. Each tick mark on the x-axis is January 1st of every year.

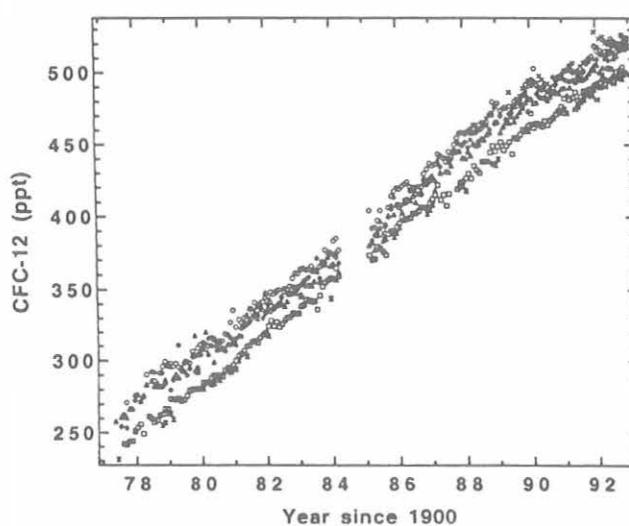


Fig. 5.2. Long-term trend of CFC-12 (dry, ppt by mole fraction) at the seven flask sites. A color plot of the figure is available from the NOAA division. Each tick mark on the x-axis is January 1st of every year.

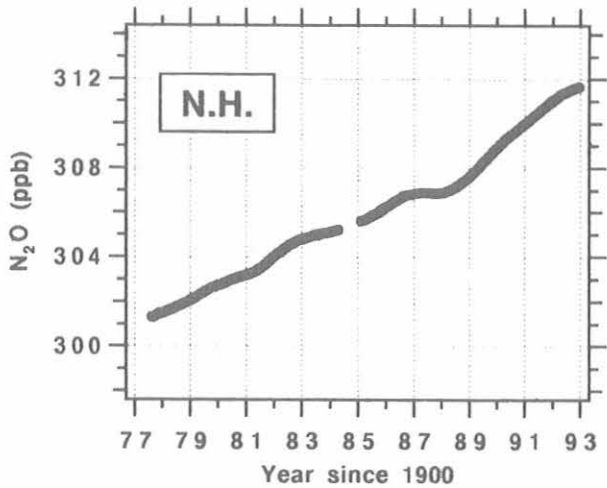


Fig. 5.3. Northern hemispheric mean mixing ratios of N_2O (dry, ppb by mole fraction) from 1977 through 1992. A loess fit ($f \sim 24$ months) was applied to the data.

tubing to a continuously operating pump mounted near the GC system. A stream select valve allows air to be sampled either from one of the two lines or from calibration cylinders. The installation of this air sampling system at SPO completes the upgrade for the RITS network. At this time, all of the RITS systems use this air sampling method.

During 1992, we found the mixing ratios of CFC-11 and CFC-12 indicate a change in trend from increasing or stable growth toward decreasing growth in data from SPO [Swanson *et al.*, 1992]. The daily means for N_2O , CFC-12, CFC-11, and CCl_4 from the in situ systems are shown in Figures 5.4-5.7, respectively. The long-term trend of increasing mixing ratios of the CFC's is apparent in the

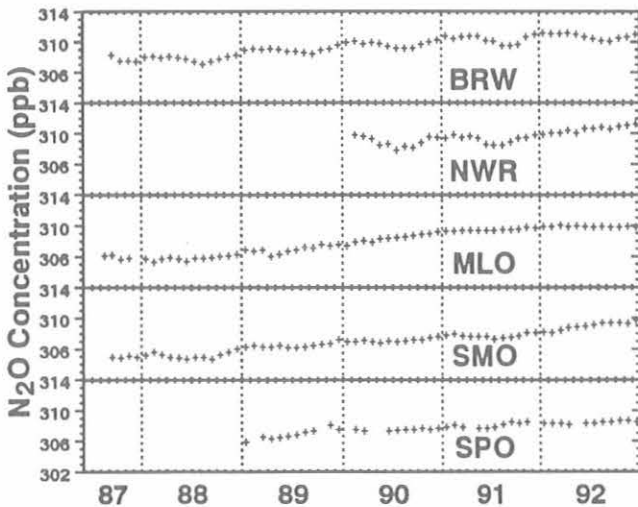


Fig. 5.4. Daily average N_2O mixing ratios in ppb from the in situ GCs.

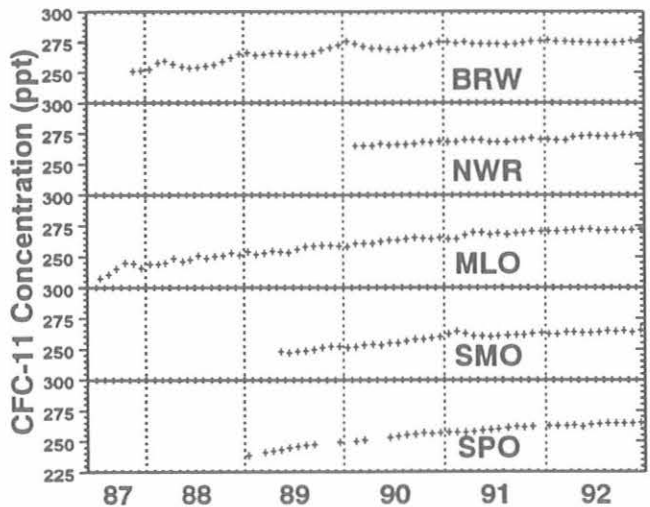


Fig. 5.5. Daily average CFC-11 mixing ratios in ppt from the in situ GCs.

graph of the data. Observations seem to indicate that the growth rate of CFC's has decreased since 1989. To illustrate the change in growth rates of the CFC's, an estimate of the growth rates for CFC-11 and CFC-12 was calculated by differentiating the mixing ratio data sets. Prior to 1989 the growth rate of the CFC's in the troposphere at SPO was approximately 11 ppt yr^{-1} for CFC 11 and 19 ppt yr^{-1} for CFC 12. After 1989 the growth rate of CFC's is calculated to be approximately 4 ppt yr^{-1} for CFC 11 and 14 ppt yr^{-1} for CFC 12.

These decreased overall growth rates are encouraging. Our laboratory plans to continue to monitor CFC molecules to further document their decline and to extend our

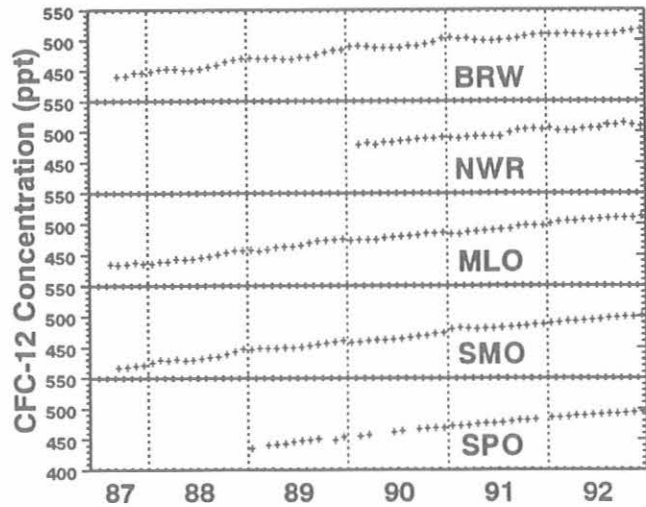


Fig. 5.6. Daily average CFC-12 mixing ratios in ppt from the in situ GCs.

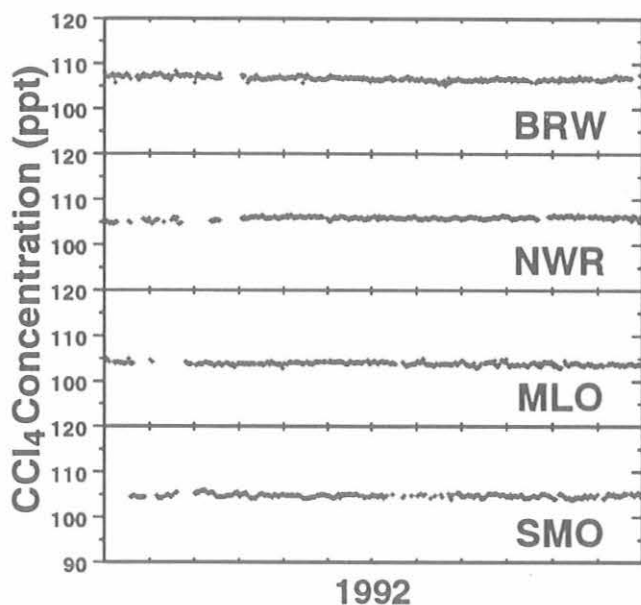


Fig. 5.7. Daily average CCl_4 mixing ratios in ppt from the in situ GCs.

understanding of the transport of these compounds to the atmosphere over Antarctica.

5.1.3. LOW ELECTRON ATTACHMENT POTENTIAL SPECIES (LEAPS)

The LEAPS program was marked by two significant developments in 1992. The old GC system was replaced with a new system that yields higher precision and better accuracy. Also, year-round samples from SPO were collected and analyzed for the first time.

Near the end of the year, the old LEAPS analysis system, consisting of a Shimadzu GC-9A and Chrompack cryotrap, was replaced with an HP5890 Series II GC and a modified Tekmar dual cryo-trapping unit (Figure 5.8). The new analysis system yields precisions (1 s.d.) of ± 0.02 ppt for a single measurement of halon H-1301 and ± 0.04 ppt for H-1211, which are almost an order of magnitude better than with the old system. On the new system, gases of interest are first trapped onto a porous adsorbent (Porapak Q) at -60°C , separating them from O_2 and N_2 . Sample volume is determined accurately by monitoring the temperature and pressure of an evacuated bulb downstream of the trap. (On the old system, sample volume was determined indirectly by ratio to CFC-12.) Trapped gases are then focused onto a megabore (0.53 mm i.d.), $\text{Al}_2\text{O}_3/\text{KCl}$ -lined, capillary trap (Chrompack) at -60°C at the head of the column. Gases are injected at 100°C onto a wide-bore (30 m \times 0.32 mm i.d.) DB-1 column (J and W) at 30°C . After 3 minutes, the column is heated at 8°C min^{-1} to 100°C , during which most gases are eluted to the ECD's. The column is then purged for 5 minutes at 150°C .

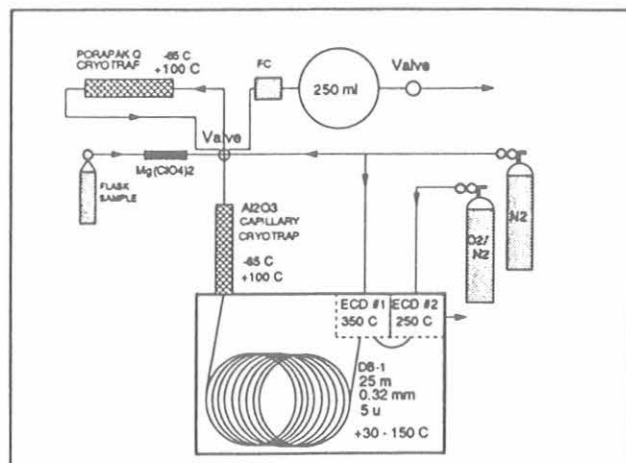


Fig. 5.8. New GC system for analysis of LEAPS gases.

Most flasks collected during 1992 were analyzed with the old system, but those from SPO, which were returned to Boulder at the end of the year, were all analyzed with the new GC and dual cryotrap. In previous years flask samples from SPO have been collected only during summer months. In November of 1991, however, flasks were shipped to SPO for sampling throughout the year. Most of these flasks were 0.85-L electropolished flasks suitable for analysis of low-concentration or poorly responding gases. Flasks were filled monthly throughout the year and shipped to Boulder in November 1992 after SPO opened for the next summer season.

These large flasks were analyzed for H-1301 and H-1211 on the newly configured LEAPS GC. There was no apparent serious degradation or enhancement of either of these compounds during storage, as the numerical values were similar to those for other sampling sites in the southern hemisphere. The growth rate of H-1301 during this sampling period was $7.3\% \text{ yr}^{-1}$. H-1211 appeared to increase at $3.9\% \text{ yr}^{-1}$, although the growth rate was not significantly different from 0 because of larger variability in the data (Figures 5.9 and 5.10). These trends are consistent with those reported for the other CMDL sampling sites during 1992 [Butler *et al.*, 1992].

The absolute values for H-1211 reported here differ from those in previous annual reports and from those in Butler *et al.*, [1992] because of a calculation error in the calibration scale of H-1211. The revised scale will be published in the next annual report, as additional re-calibrations are also necessary on the new instrument.

5.1.4. ALTERNATIVE HALOCARBON MEASUREMENTS

In response to warnings of stratospheric ozone depletion and global warming, the production of many industrial chlorine-containing compounds will be banned within the next few years [UNEP, 1987]. Although the ultimate goal of this legislation is to replace chlorinated compounds with

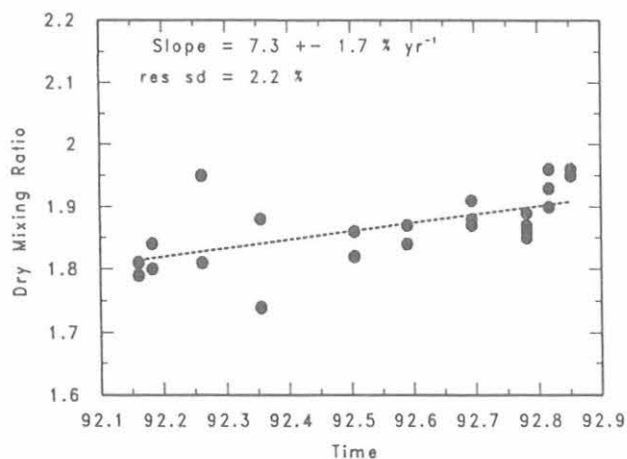


Fig. 5.9. 1992 H-1301 results from SPO.

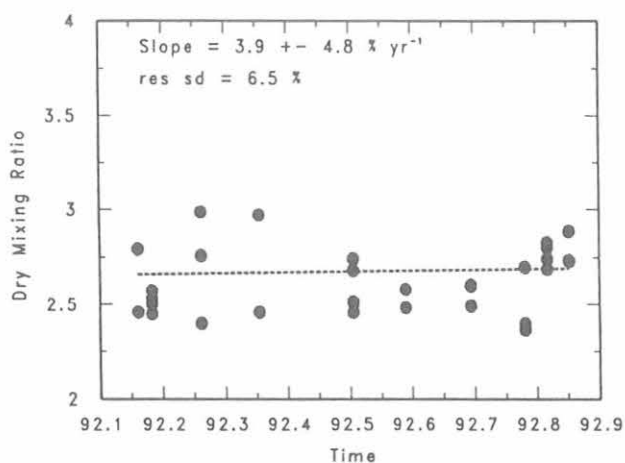


Fig. 5.10. 1992 H-1211 results from SPO.

non-chlorinated substitutes, such as hydrofluorocarbons (HFCs), hydrochlorofluorocarbons (HCFCs) are currently being used until suitable non-chlorinated materials are developed. HCFCs are viewed as suitable temporary replacements for CFCs because current technology for their production and use in air-conditioners and refrigeration devices is already in place, and because model calculations suggest that the adverse effects of HCFCs on the atmosphere will be substantially less than those of CFCs. Accurate and precise measurements of these compounds in the atmosphere are essential in order to validate these predictions. These measurements also allow for accurate predictions of atmospheric impacts of other proposed substitute compounds, such as HFCs, because both HFCs and HCFCs are destroyed mostly in the troposphere by reaction with hydroxyl radical (OH). This is in contrast to CFCs, which are decomposed primarily by photolysis in the stratosphere. Presently, estimates of global OH are based on the atmospheric budget of a single industrial compound, 1,1,1-trichloroethane. Because there is considerable error

in such a limited estimate there is a need for other trace species to test model-generated distributions of OH [Prather and Spivakovsky, 1990].

It is within this framework that a program for measuring alternative halocarbons was begun at CMDL. Measurements of chlorodifluoromethane (HCFC-22) from flasks collected in the NOAA flask network were initiated in 1991 and continued in 1992. In addition, 1-chloro-1,1-difluoroethane (HCFC-142b) and 1,1-dichloro-1-fluoroethane (HCFC-141b) were detected and first measured in ambient air samples during 1992.

The measurements were conducted as described by Montzka et al. [1992, 1993a,b] from paired air samples that were collected on a monthly basis (on average) at BRW, MLO, SMO, SPO, and at the three cooperative flask sampling locations of ALT, NWR, and CGO.

Chlorodifluoromethane (HCFC-22)

Chlorodifluoromethane is the major HCFC in use today and represents a second trace species available for testing models that estimate the global tropospheric abundance of OH [Midgley and Fisher, 1993; Fraser et al., 1991]. Unfortunately, significant discrepancies among measurements of HCFC-22 by different techniques have been reported in the past. Mixing ratios determined from ground-based chromatographic measurements of northern hemispheric air [Khalil and Rasmussen, 1988, 1990, 1991] are 10-30% higher than those determined from long-path absorption measurements within the troposphere and lower stratosphere [Rinsland et al., 1989, 1990; Zander et al., 1992], and a small set of grab samples obtained in the lower troposphere [Pollock et al., 1992]. Furthermore, the lifetime of HCFC-22 suggested by a comparison of emission estimates and ambient measurements varies from 13 to 40 years [Midgley and Fisher, 1993]. Lifetime estimates that are based on 3-D models and the reaction rate constant between HCFC-22 and hydroxyl radical, suggest a lifetime for HCFC-22 of 14-16 years [Prather and Spivakovsky, 1990; Golombek and Prinn, 1989].

Our analysis of air collected in flasks during 1992 at the four CMDL stations and three cooperative flask sampling sites indicates that the latitudinally-weighted, global mean mixing ratio of HCFC-22 in 1992 was 102 ppt (Tables 5.1 and 5.2). These results are plotted as bi-monthly averages together with measurements of air from archived samples [Montzka et al., 1992, 1993a] and data from previous

TABLE 5.1. Mean Mixing ratios of HCFC-22 in 1992 (ppt)*

	Mixing Ratio
Global mean	101.9
Northern hemisphere	108.4
Southern hemisphere	95.4

*All values were weighted by cosine of latitude. Numbers believed accurate within $\pm 2.5\%$.

TABLE 5.2. Atmospheric Measurements of HCFC-22 From Flasks in 1992

Station	Date	ppt	Station	Date	ppt
ALT	1992.052	110.0	MLO	1992.893	108.4
ALT	1992.128	109.5	MLO	1992.913	105.0
ALT	1992.328	110.5	MLO	1992.970	111.6
ALT	1992.385	113.4	MLO	1992.989	111.0
ALT	1992.620	111.5			
ALT	1992.713	112.1	SMO	1992.046	93.6
ALT	1992.907	115.0	SMO	1992.112	90.4
			SMO	1992.262	95.2
BRW	1992.022	112.2	SMO	1992.301	95.7
BRW	1992.120	109.1	SMO	1992.456	95.5
BRW	1992.268	110.7	SMO	1992.530	95.0
BRW	1992.372	111.2	SMO	1992.607	96.3
BRW	1992.459	110.0	SMO	1992.686	98.2
BRW	1992.538	110.4	SMO	1992.784	98.3
BRW	1992.618	111.4	SMO	1992.921	97.5
BRW	1992.866	114.5			
BRW	1992.940	116.3	CGO	1992.036	90.3
BRW	1992.959	115.7	CGO	1992.115	92.4
			CGO	1992.153	92.4
NWR	1992.131	107.3	CGO	1992.306	94.2
NWR	1992.265	108.4	CGO	1992.363	95.1
NWR	1992.322	112.7	CGO	1992.402	94.8
NWR	1992.552	111.5	CGO	1992.555	94.5
NWR	1992.571	109.7	CGO	1992.587	96.2
NWR	1992.609	111.7	CGO	1992.669	96.3
NWR	1992.727	111.8	CGO	1992.705	96.6
NWR	1992.877	108.7	CGO	1992.746	96.2
NWR	1992.954	115.1	CGO	1992.798	96.0
			CGO	1992.951	97.6
			CGO	1992.970	98.6
MLO	1992.033	104.4			
MLO	1992.109	101.8			
MLO	1992.262	103.7	SPO	1992.063	92.1
MLO	1992.281	103.6	SPO	1992.079	90.3
MLO	1992.473	105.7	SPO	1992.434	93.8
MLO	1992.530	106.1	SPO	1992.506	96.9
MLO	1992.596	108.5	SPO	1992.590	96.2
MLO	1992.607	104.3	SPO	1992.694	96.4
MLO	1992.691	103.0	SPO	1992.781	96.8
MLO	1992.740	109.1	SPO	1992.817	96.2
MLO	1992.779	106.3	SPO	1992.853	97.1

investigators over a broad time-scale in Figure 5.11. In the northern hemisphere, measurements based on the CMDL calibration standards agree with long-path absorption measurements of HCFC-22 in the troposphere near 30°N [Rinsland et al., 1989]. They also agree with the results obtained at 30°N and above 12.5 km with the Atmospheric Trace Molecule Spectroscopy (ATMOS)-Fourier transform spectrometer on board Spacelab 3 [Zander et al., 1992]. Although it is difficult to accurately compare ground-based measurements directly with measurements at altitudes above 12.5 km, a limited number of studies suggest that the mixing ratio of HCFC-22 within the troposphere is fairly constant, making these comparisons valid [Leifer et al., 1981; Rasmussen et al., 1982].

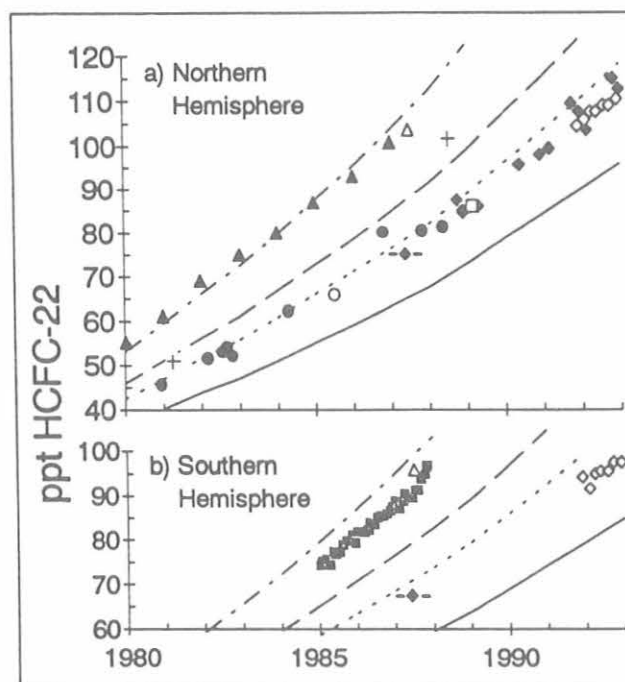


Fig. 5.11. Measurements of HCFC-22 and results of a 2-box model as described in the text for the northern (a) and southern (b) hemisphere. Results from flasks collected at the four CMDL stations and three cooperative flask sampling sites are bimonthly, latitudinally-weighted hemispheric means (\diamond , Montzka et al., [1993]). Flasks collected during the SAGA II Cruise (\diamond , Montzka et al., [1992]; Δ , Khalil and Rasmussen [1988]) are presented as latitudinally-weighted hemispheric means. Archived samples were collected at Niwot Ridge (\diamond , Montzka et al. [1992]). Other measurements from flasks are from northern mid-latitudes in the upper troposphere (\square , Pollock et al., [1992]), Mauna Loa, USA (Δ , Khalil and Rasmussen [1991], and C. Grim, Australia (\blacksquare , Fraser et al., [1988, 1989]). Long path absorption measurements were made, at 12.5 km (\circ , Zander et al., [1992]), throughout the troposphere (\bullet , Rinsland et al., [1989]), and below 15 km ($+$, Rinsland et al., [1990]). Measurements of Rinsland et al. [1989] were increased by a factor of 1.28 to account for an updated cross-section estimate [Rinsland et al., 1990]. Model calculations were performed for different lifetimes of HCFC-22, 10 years (—), 15 years (- - -), 20 years (- · - ·), and 50 years (- · · - ·). Abscissa tic marks correspond to the beginning of the year indicated.

The results of Pollock et al. [1992] were obtained from a small set of samples collected in the upper troposphere in the northern mid-latitudes and are also in close agreement with the results based on the CMDL standards. Their results were obtained from GC-MS analysis of air collected in flasks. The similarity between the results of Pollock et al. [1992] and those reported by Montzka et al. [1992, 1993a] suggest that these two independent calibration scales agree to within 5%.

The measurements of *Khalil and Rasmussen* [1988, 1990, 1991] and *Fraser et al.* [1989] are ~28% higher than measurements based on the CMDL calibration standards (Figure 5.11). Their measurements were based on a calibration scale that was developed in the late 1970s and believed accurate to within $\pm 10\%$ on the basis of comparisons with another laboratory at that time [*Rasmussen et al.*, 1980]. The differences between these results and those based on the CMDL standards are likely the result of different calibration scales for HCFC-22. Given that measurements by different techniques are converging towards a lower atmospheric burden of HCFC-22 than suggested by *Khalil and Rasmussen* [1988, 1990, 1991] and *Fraser et al.* [1989], it is possible that calibration standards used for their measurements were inaccurate. Overestimation of HCFC-22 by these investigators could explain the large discrepancies reported in the past between measured atmospheric mixing ratios and emission estimates [*Khalil and Rasmussen*, 1981] and between surface-based flask samples and long-path absorption measurements [*Rinsland et al.*, 1990].

Using the emission estimates of *Midgley and Fisher* [1993], atmospheric mixing ratios of HCFC-22 were calculated with a 2-box, finite increment model [*Elkins et al.*, 1993]. The factor "f" [*Butler et al.*, 1992] was used to account for the vertical distribution of HCFC-22 throughout the atmosphere, and was estimated at $1.07 (\pm 0.2)$ [*Zander et al.*, 1992; *Leifer et al.*, 1981; *Fabian et al.*, 1985]. The model was initialized with 10 ppt of HCFC-22 in 1970 to account for emissions in years before 1970. Emissions after the end of 1991 were estimated by a linear extrapolation of emissions from 1985 to 1991.

When compared to mixing ratios calculated with the model and data in *Midgley and Fisher* [1993], measurements based on CMDL standards, suggest an atmospheric lifetime for HCFC-22 of 13.6 (+1.9, -1.5) years (Figure 5.11). A similar lifetime can be estimated from the results of *Zander et al.* [1992], *Rinsland et al.* [1989], and *Pollock et al.* [1992]. Recent estimates of the atmospheric lifetime of HCFC-22 from global 3-D models yield values of 14.2-15.5 years, and are based on an atmospheric lifetime for CH_3CCl_3 of 5.7 or 6.3 years [*Prather and Spivakovsky*, 1990, *Golombek and Prinn*, 1989]. However, revised estimates of the reaction rate constant between OH and CH_3CCl_3 suggest that HCFC lifetimes should be shortened by 15% [*Talukdar et al.*, 1992]. Given a lifetime for CH_3CCl_3 of 5.7 yr^{-1} [*Prinn et al.*, 1992], and rate constant for CH_3CCl_3 loss to the oceans of between $1/59$ and $1/129 \text{ yr}^{-1}$ [*Butler et al.*, 1991], the lifetime of HCFC-22 is estimated at 12-14 years. Although error estimates for the lifetime of CH_3CCl_3 and emission of HCFC-22 are $\pm 10\%$ and $\pm 12\%$, respectively, it is clear that our measurements agree well with this revised lifetime estimate.

Until measurements of HCFC-22 are extensive enough to allow for calculation of lifetime directly (as done by *Prinn et al.*, [1992] for CH_3CCl_3), estimates of HCFC-22

lifetime, and most other HCFCs and HFCs, are dependent on the accuracy of rate constants and calibration of CH_3CCl_3 and are subject to change as these latter parameters are refined.

Measurements of archived air and air obtained from flasks allow for an estimate of the growth rate of HCFC-22 from 1987 to the present. From the data based on CMDL calibration standards shown in Figure 5.11, a linear growth rate of $6.3 (\pm 0.3) \text{ ppt yr}^{-1}$ or compounding growth of $7.3 (\pm 0.3)\% \text{ yr}^{-1}$ (in which the mixing ratio (X) since an initial time is defined as $X = X_0 \cdot (1 + \text{GR})^{\Delta t}$, and X_0 is the initial mixing ratio, GR is the fractional increase per year, and Δt is the time elapsed since time t_0) is obtained for HCFC-22 between 1987 and December 1992.

The global distribution of HCFC-22 as defined by flasks collected in 1992 (Figure 5.12) can also be used to estimate an instantaneous growth rate in the southern hemisphere (SH) during this year [*Butler et al.* 1992]. Given an interhemispheric difference of $13 (\pm 1) \text{ ppt}$, an interhemispheric exchange time of $1.1 (\pm 0.1) \text{ yr}^{-1}$, and a 1992 mean SH mixing ratio of $95.4 (\pm 2) \text{ ppt}$, we estimate a 1992 SH growth rate for HCFC-22 of $5.0 (\pm 1.6) \text{ ppt yr}^{-1}$ or $5.2 (\pm 1.7)\% \text{ yr}^{-1}$.

These estimates of growth for HCFC-22 between 1987 and 1992 agree with predictions from our model calculation and that reported by *Midgley and Fisher* [1993]. Previous estimates of HCFC-22 growth from ambient air measurements suggest that between 1984 and 1989 HCFC-22 was increasing at 6 to $8\% \text{ yr}^{-1}$ [*Fraser et al.*, 1991]. Our measurements, when combined with these earlier estimates, suggest that the relative growth rate of HCFC-22 has remained fairly constant ($\pm 2\%$) since 1984 through 1992.

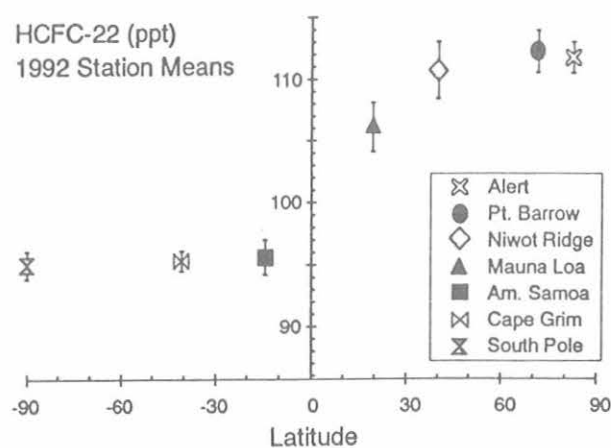


Fig. 5.12. Mean mixing ratios of HCFC-22 in 1992 as determined from air samples collected in flasks at the seven sampling stations. Vertical bars represent ± 1 standard deviation of residuals from a linear fit to the data obtained at each station.

1,1-Dichloro-1-Fluoroethane (HCFC-142b)

HCFC-142b was recently incorporated in air conditioners and refrigeration devices where mixtures of CFC-11 and CFC-12 were formerly used. This compound was identified in ambient air collected at all seven stations around the globe in 1992. The only other reported measurement of this compound from air samples in the remote atmosphere was by *Pollock et al.* [1992]. These investigators reported an ambient mixing ratio for HCFC-142b of 1.1 ppt in air collected in 1989 from the upper troposphere in the northern hemisphere. These investigators reported that the mixing ratio of HCFC-142b was increasing over time at a rate of approximately 7% yr⁻¹.

Measurements of HCFC-142b from air collected as part of the NOAA flask sampling network are summarized in Figure 5.13. The mean global growth rate of this compound was estimated using linear regression at approximately 1 ppt yr⁻¹ in 1992. Using the methods of *Butler et al.* [1992] the growth rate in the southern hemisphere is estimated at 0.9 ppt yr⁻¹ over this period. This corresponds to an atmospheric growth of ~30% yr⁻¹ for HCFC-142b in 1992. These numbers are preliminary and will be finalized in 1993 after standards are made at CMDL. While the scale reported in Figure 5.13 is preliminary at this time, the relative rate of growth of HCFC-142b indicated by the results in this figure are independent of calibration and are robust, assuming that no drifts have occurred in reference gases. A growth of 30% yr⁻¹ for HCFC-142b is large compared to atmospheric growth rates of other CFCs and HCFCs currently being used by industry. However, the yearly increase in the atmospheric chlorine burden due to HCFC-142b is small at this point in time as the mixing ratio of this compound is less than 10 ppt.

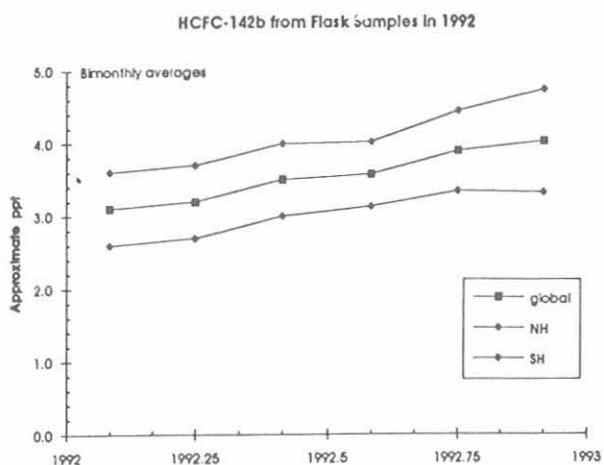


Fig. 5.13. Bimonthly mean mixing ratios of HCFC-142b for both hemispheres and the globe in 1992. Stated mixing ratios are preliminary and based on a NOAA scale (see text).

1-dichloro-1,1-difluoroethane (HCFC-141b)

HCFC-141b is a compound currently in use as a substitute for CFCs and is also present as an impurity in samples of HCFC-142b. This compound was identified in air samples in the northern hemisphere during 1992. Levels in the southern hemisphere were at or below the detection limit of the instrument so as to preclude precise quantitation. Work in 1993 will focus on developing calibration standards and increasing the sensitivity of the GC-MS instrument.

5.1.5. GRAVIMETRIC STANDARDS

Chlorodifluoromethane (HCFC-22)

The focus of the standards laboratory was on completing the work started in 1991 for developing a primary calibration scale for HCFC-22 (chlorodifluoromethane). Research was conducted into the stability of the gas contained in specially treated aluminum cylinders both as single-component and multi-component mixtures ranging from 50 parts per trillion to 1 part per thousand using gas chromatography/mass spectrometry (GC/MS) techniques [*Montzka et al.*, 1993b] and by GC using an oxygen-doped electron capture detector. The comparison of standards prepared in May 1989 to standards prepared recently, indicate that stability in Aculife-treated aluminum cylinders is maintained. The response curve for gravimetric standards containing HCFC-22 by GC using an oxygen-doped ECD is shown in Figure 5.14.

To investigate the containers and techniques used to generate calibration standards for HCFC-22, standards from levels as low as 50 ppt to as high as 1 part per thousand (Figure 5.15) were analyzed with GC/MS techniques [*Montzka et al.* 1992, 1993a,b]. Standards at levels below 15 ppb were analyzed in the same manner as flask air

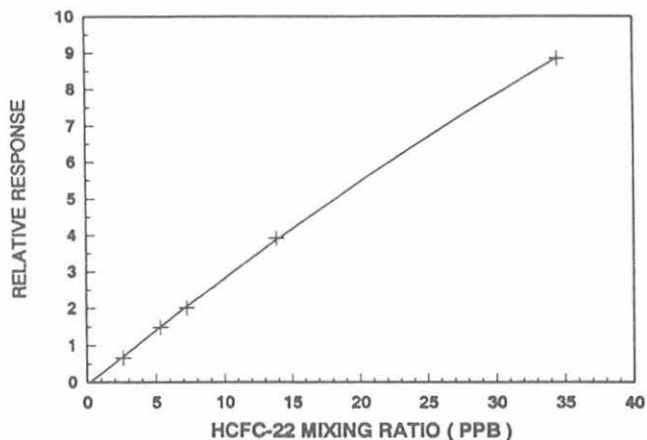


Fig. 5.14. Response curve of HCFC-22 gravimetric standards with an oxygen-doped electron capture detector.

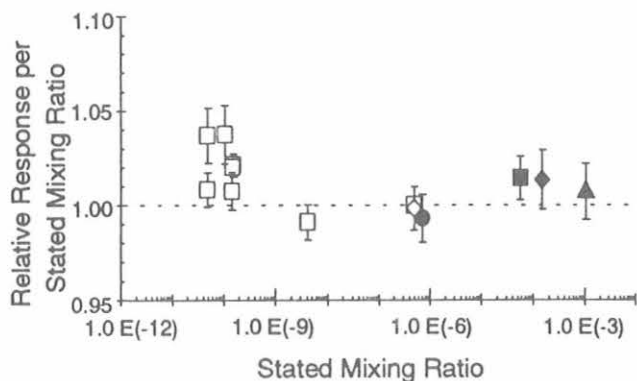


Fig. 5.15. The response per stated mixing ratio of HCFC-22 in different gravimetric standards from 50 parts per trillion to 1 part per thousand. Vertical bars correspond to one standard deviation of the results. All standards are plotted relative to the standard at 489.9 ppb, to which a response per ppt of 1.00 was assigned. Standards made from "pure" HCFC-22 are indicated with shaded symbols. The parent cylinder of lower level standards is indicated by the symbol shape. Standards below 10 ppb were multi-component mixtures containing carbon dioxide, methane, nitrous oxide, and numerous chlorofluorocarbons.

samples, but without the presence of a drying agent. For standards above 10 ppb, sample loops of 81.8 and 13.1 μL were filled to atmospheric pressure and injected directly onto the column. Loop volumes were determined gravimetrically to within 1% with multiple injections of de-ionized distilled water onto a desiccant. The volume of the evacuated chamber (used for cryo-collection of low level samples) was determined barometrically by reference to a known volume. When two standards of widely varying mixing ratios were compared, different loop sizes and cryo-collection volumes were used to minimize the difference in the amount of HCFC-22 reaching the detector, thereby minimizing non-linearity effects. For standards below 1 ppm this difference was always less than a factor of 6 and was typically a factor of 2. For standards above 1 ppm, the amount of HCFC-22 in standards being compared never differed by more than a factor of 20. Linearity has been confirmed (within 1%) over a range of 6.5x for HCFC-22 by injections of different loop volumes of the same standard directly onto the column. For standards containing CFC-12 and CFC-11, we have found that the detector responds linearly (within 2%) over a range of greater than 100x in the region of interest. With the exception of two standards above 100 ppm (Figure 5.15), the HCFC-22 standards were referenced to loop injections of the standard at 489.9 ppb. The two standards above 100 ppm were directly compared only to the standard at 56 ppm shown in Figure 5.15.

The response per ppt of our standards is consistent within $\pm 2\%$ (± 1 s.d.) and these data suggest that the integrity of HCFC-22 is maintained in Aculife-treated

aluminum cylinders even at the 50 ppt level (Figure 5.15). In addition, the data demonstrate that ambient levels of CO_2 , N_2O , CH_4 , or other halocarbons in a sample do not affect our analysis for HCFC-22. We feel that the different conditions under which these standards were made and the lack of impurities found in our starting reagents (none above 1 part per thousand) allow us to estimate the accuracy of our HCFC-22 scale by the variance among these standards. At the 95% confidence level, we believe our standards accurate to within $\pm 2.5\%$.

Blended Multi-Component Standards

Research started this year into preparing synthetically blended multi-component standards for use as calibration standards for our GCs located at our observatory stations and in the standards laboratory. Our division was also contracted by the Aeronomy Laboratory to provide a suite of round-robin standards for worldwide inter-laboratory analysis comparisons. Nine single-component gravimetric mixtures were prepared from pure reagents in specially treated aluminum cylinders using various dilution techniques. These parent mixtures were then used to prepare single-component gravimetric standards at lower concentrations. The standards were then blended together into three nine-component mixtures containing CFC-11, CFC-12, CFC-113, methyl chloroform (CH_3CCl_3), carbon tetrachloride (CCl_4), HCFC-22, N_2O , CH_4 , and CO_2 in blended air. These were then used to prepare two cylinders each of gases containing concentrations matching real air. Each of the three cylinders contained the gases at various mixing ratios found in atmospheric air ranging from the mid-latitude to the arctic stratosphere. The gases contained in all of the cylinders were analyzed over time to insure stability. Unfortunately, the six cylinders used for preparing the low concentration standards were found to readily absorb CH_3CCl_3 and CCl_4 from the gas mixtures. Losses ranging from approximately 10 to 100% were observed for CH_3CCl_3 and from approximately 5 to 90% for CCl_4 within 1 week after preparing the standards. The cylinders were returned to the vendor and were retreated using their proprietary treatment process. The same cylinders were then used to remake the standards. The new suite of standards were analyzed and were found to be acceptable except for one that exhibited CFC-113 contamination due to a dirty cylinder valve. A standard similar to one of the six has been placed online at the NWR station for calibrating the GCs.

Two gravimetric standards containing approximately 100 ppm of CO in air and two containing ambient concentrations of CH_4 in air were prepared for NCAR. The standards were used to calibrate a tunable diode laser system.

Three CO in air gravimetric standards were prepared for use as supplemental primary standards to the CO reference scale maintained by the Carbon Cycle Division. The three standards were prepared at nominal concentrations of 50, 100, and 150 ppb. The intercomparison of these standards to the current scale showed no significant bias.

Several cylinders containing dilute mixtures of N_2O in N_2 and N_2O in air were analyzed for the NASA Ames Research Center. The analyses of these cylinders required the preparation of six gravimetric standards. Four of the primary calibration standards were prepared containing N_2O in blended air and two were prepared containing N_2O in N_2 . The mixing ratios of the primary standards were targeted in order to closely bracket the mixtures to be analyzed. This analysis proved interesting in that it allowed us to intercompare NOAA N_2O in N_2 standards to N_2O in air standards to determine if mixtures containing different diluents (e.g., N_2 , air) had any effect on ECDs and/or presented a problem involving chromatographic peak integration. The results of this experiment indicated there was a small bias between analyzing N_2O -in- N_2 mixtures using N_2O -in-air and N_2O -in- N_2 standards. The calculated value for a N_2O in air mixture using N_2O in N_2 standards was approximately 0.8% higher than what was calculated using N_2O in air standards (Figure 5.16).

Instrumentation

Two GCs with ECDs were added to the standards laboratory this year. The two were combined with a third on hand to create an automated analytical system similar to the systems used by the RITS program at the observatory stations. Previously, analysis of standards was conducted on the flask analysis system. More time can now be devoted to both flask analysis and standards analysis with the use of two separate systems. The system for standards analysis is capable of measuring CFC-11, CFC-12, CFC-113, CH_3CCl_3 , CCl_4 , and N_2O . It is also capable of measuring HCFC-22 concentrations as low as 1 ppb without injecting cryogenically collected samples. This is made possible with the use of a Carbo-pack B column operated at $\sim 70^\circ C$ which gives good separation of the HCFC-22 and CFC-12 peaks from the air peak and by doping the electron capture detector with a 5% mixture of oxygen in N_2 .

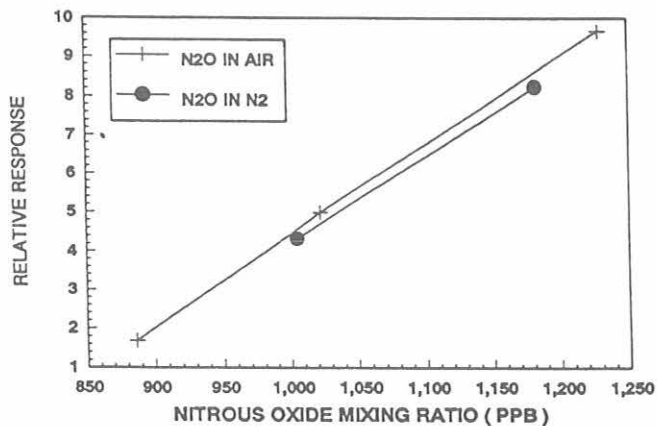


Fig. 5.16. Response curve of N_2O in air and N_2O in N_2 with an electron capture detector and 5% CH_4 in Ar carrier gas.

Standards with concentrations lower than 1 ppb are measured on the GC/MS by cryogenic collection.

There were 56 gravimetric standards prepared in the standards laboratory for the year of 1992 (Table 5.3). In addition, there were seven calibration standards replaced at our various observatory stations for the RITS program. To reduce vibrations, our gas standard laboratory was relocated from the third floor of building RL-3 to the ground floor of building RL-6.

5.2. SPECIAL PROJECTS

5.2.1. AIRCRAFT MEASUREMENTS OF THE CFCs

The Airborne Chromatograph for Atmospheric Trace Species (ACATS) instrument has had considerable success over the past 2 years in measuring CFC-11 and CFC-113 in the troposphere and lower stratosphere. ACATS was built inside the reactive nitrogen instrument [Fahey et al., 1989] and was described in last year's Summary Report [Montzka et al., 1992]. Since its construction in 1991, ACATS has participated in two major projects, NASA's stratospheric ozone program and High Speed Research Program (HSRP). These projects use CFC measurements as anthropogenic tracers to indicate stratospheric ozone loss. Using an airborne platform, in this case the ER-2 (a civilian version of the U-2), allows ACATS to measure vertical profiles extending into the lower stratosphere. Vertical profiles of trace species, including CFCs, have become an integral component of the NOAA division's research and is NOAA's

TABLE 5.3. Summary of Gravimetric Standards

Compounds	Quantity	Concentration Range	Prepared For
HCFC-22	12	ppt, ppm	NOAH/AL
CFC-11, CFC-12, CFC-113, CCl_4 , CH_3CCl_3 , N_2O , HCFC-22	3	ppt, ppb	ACATS/NOAH
CFC-11	1	ppb	NOAH/AL
CFC-12	2	ppm	NOAH/AL
CFC-113	1	ppb	NOAH/AL
CH_3CCl_3	1	ppb	NOAH/AL
CCl_4	1	ppb	NOAH/AL
CH_4	5	ppm, percent	NOAH/AL/ CC/NCAR
CO	5	ppb, ppm	CC/NCAR
N_2O	8	ppb, ppm	NOAH/U. of N.H./CANMET
CFC-11, CFC-12, CFC-113, CCl_4 , CH_3CCl_3 , N_2O , HCFC-22, CO, CH_4	17	ppt, ppm	NOAH/AL

key responsibility to the Global Climate Change Program [GCRP, 1993]. The Airborne Arctic Stratospheric Expedition II (AASE II) and the forthcoming Stratospheric Photochemistry, Aerosols, and Dynamics Expedition in 1993 (SPADE, a component of HSRP) missions have used and will continue to utilize ACATS CFC measurements. In November test flights for SPADE were conducted at NASA Ames, Moffitt Field, California. Although the primary goal of the November flights was to integrate new and modified instruments into the ER-2 payload, ACATS made measurements on two 2-hour flights. For the future 1993 SPADE project, ACATS will have an additional N₂O-doped ECD channel to measure CH₄ and CO in collaboration with Carbon Cycle Division [Goldan, et al., 1982].

AASE-II mission

The AASE-II mission was designed to primarily focus on photochemistry of the lower stratosphere and ozone destruction or production due to chemical perturbations. Addition of these two CFC molecules to the complement of species already measured on the ER-2 platform offers new science opportunities. Atmospheric CFC-11 and -113 are

important ozone depleting chemicals, which together represent about 30% of the total organic chlorine in the atmosphere. The use of high resolution CFC measurements along with correlations between different tracers generated by dynamic models [Solomon et al., 1992] permits calculation of the total organic chlorine over the complete flight. Since 1989, the growth rates of both chemicals, particularly CFC-11 [Elkins et al., 1993], have been slowing down in the troposphere. Monitoring the slowdown of the growth rates in the troposphere and stratosphere, together with accurate tracking of emissions, will further aid in the refinement of chemical lifetimes of these species and may provide for a more complete understanding of the transport properties of the atmosphere.

These CFC molecules are excellent tracers of stratospheric dynamics. High levels of chlorine monoxide (ClO) indicate that O₃ has been destroyed. The decrease in CFC mixing ratios that were observed on the ER-2 aircraft flight of January 16, 1992, in a region where ClO mixing ratios increased delineates the extent of the polar vortex (Figure 5.17). The slow, steady photochemical destruction of the CFCs is the source of the chlorine atom for the more

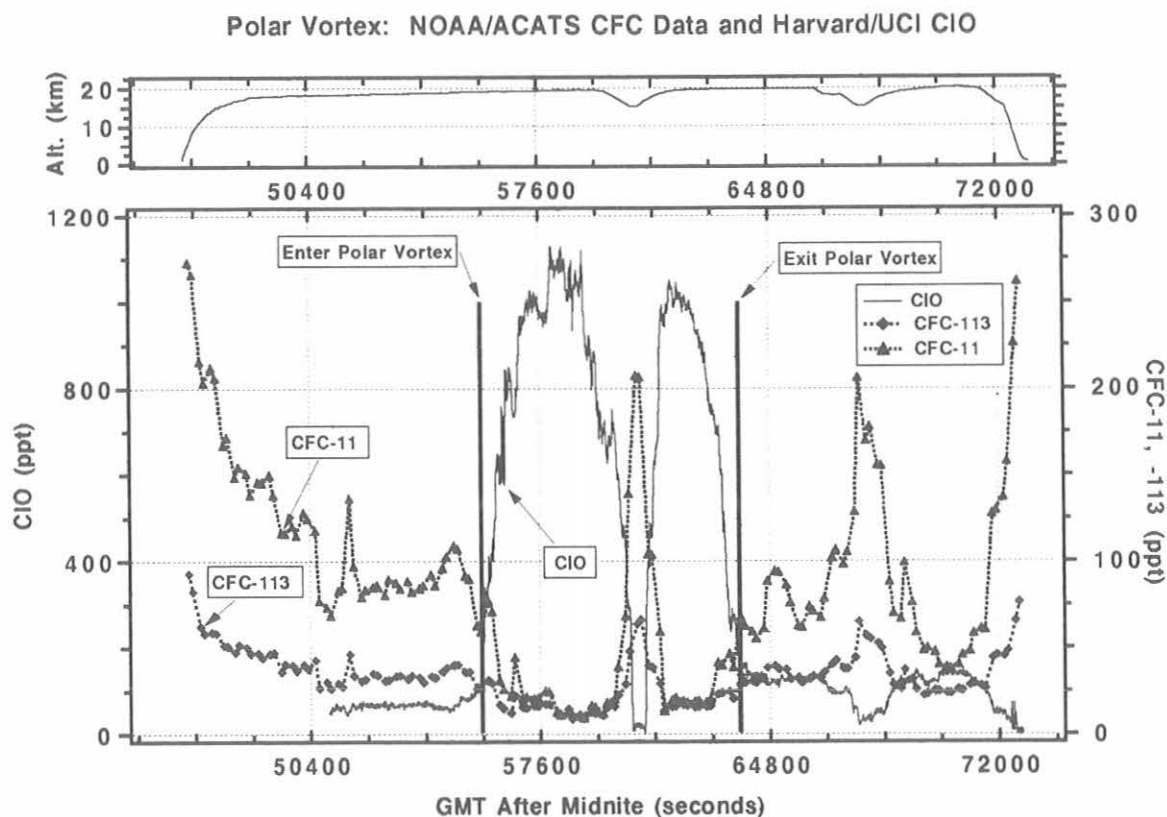


Fig. 5.17. Altitude in km (top) and mixing ratios of CFC-11 (▲) and CFC-113 (◆) from ACATS and of ClO (—) in parts-per-trillion (ppt) on the ER-2 flight (bottom) of January 16, 1992. The boundaries of the polar vortex are clearly defined by the increase in mixing ratios of ClO and by the decrease in CFC levels. Mixing ratios of ClO were measured by methods described by Brune et al., [1989] and preliminary values from AASE-2 were made available by Toohey et al. [1993].

reactive and destructive ClO molecule. It was this flight and one on January 20 showing high levels of ClO over the United States that convinced President Bush to move up the timetable for the complete phaseout of the CFCs from the year 2000 to 1996, 4 years ahead of the schedule mandated by the Montreal Protocol. All signatory nations agreed to this new schedule in the Copenhagen Amendment of 1992 for the Montreal Protocol. The concern over the timetable was the long atmospheric lifetimes of the CFC molecules. The lifetime for CFC-11 is about 55 years [Elkins *et al.*, 1993] and for CFC-113 is 110 years [WMO, 1992], whereas the chemical lifetimes of ClO plus its dimer are about 1 month [Salawitch *et al.*, 1993]. This diversity in the lifetimes of tracers will allow modelers to check theories on transport inside the stratosphere. Linear correlations are found for molecules with similar lifetimes or at altitudes where the local lifetimes are greater than the time scales of vertical transport [Plumb and Ko, 1992]. Correlation of mixing ratios of CFC-113 versus CFC-11 (Figure 5.18) shows a strictly linear relationship for mixing ratios of ~50 ppt for CFC-11 and considerable curvature at lower values where CFC-11 is more rapidly destroyed than CFC-113. During previous missions, ozone depletion at a particular altitude was calculated relative to the long-lived tracer, N₂O. Additional measurements of the CFCs and their correlations with N₂O allow other tracers to be used to evaluate the effects of ozone depletion.

SPADE Mission

ACATS is a versatile instrument that will be utilized in the Stratospheric Photochemistry, Aerosols, and Dynamics Expedition (SPADE) and future polar missions like Airborne Southern Hemispheric Ozone Expedition (ASHOE) in 1994. The SPADE mission will provide

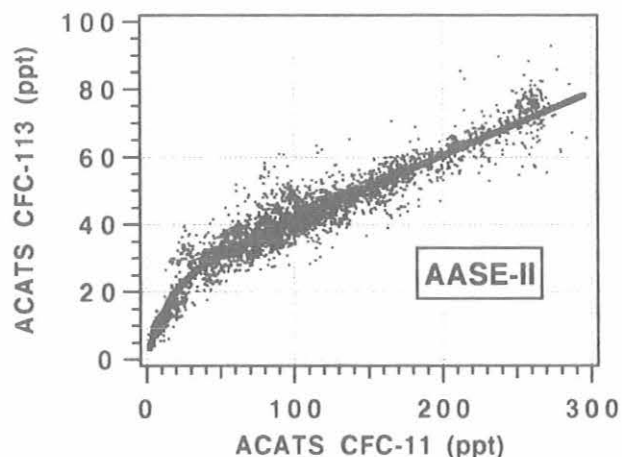


Fig. 5.18. Mixing ratios of CFC-113 versus CFC-11 in ppt for all flights during AASE-2. All data were fit to following equation: $CFC-113 = 21.8 + 0.186 CFC-11 - 22.8 e^{-(0.059 CFC-11)}$ using least squares techniques. The linear range covers mixing ratios for CFC-11 between 50 and 300 ppt, and CFC-11 is destroyed more rapidly than CFC-113 below mixing ratios of 50 ppt.

additional measurements for key components of the prior AASE I and II missions. This year's SPADE test flights and the 1993 SPADE project are components of NASA's HSRP that is in charge of assessing the environmental impact of a projected fleet of supersonic high-speed civil transports. SPADE has two primary scientific objectives: (1) To determine the key chemical processes that affect ozone levels in the parts of the stratosphere that would be most influenced by future stratospheric aircraft. This includes free-radical and heterogeneous chemistry. (2) To estimate the distribution of exhaust effluent in the stratosphere. This involves measurements of a wide range of tracers in the lower stratosphere.

ACATS measured CFC-11 and CFC-113 on two of the test flights this November (Figure 5.19). Both of these flights were during the day, lasted about 2 hours, and reached a maximum altitude of 20 km. The flight path on November 9 stayed completely over land, south of the San Francisco Bay area, while the flight on the 12th was mainly over the Pacific coast. The CFC-11 stratospheric mixing ratios for these flights are in good agreement with the previous AASE II data. Similarly, the tropospheric mixing ratios for these flights agree with northern hemispheric station measurements. Unfortunately, the CFC-113 measurements for the flight on November 9 were lost due to contamination, but the data on the 12th also agrees with AASE II and station measurements.

5.2.2. OCEAN/ATMOSPHERE EXCHANGE OF TRACE COMPOUNDS

The Ocean Atmosphere Exchange of Trace Compounds (OAXTC) mission was conducted aboard the University of Southern California research vessel *John V. Vickers* between August and October 1992. (Figure 5.20). The main goal of this study was to determine the atmospheric mixing ratio of HCFC-22 and its partial pressure in surface waters of the West Pacific Ocean to assess the possible existence of an oceanic sink for this compound. HCFC-22 is one of the major halocarbons in use today with a growth rate of 7.3% per year and a global mean of around 101.8 ppt [Montzka *et al.*, 1993a]. Water column measurements of HCFC-22 were carried out to complement air and surface water determinations to better illustrate its behavior in the ocean. CFC-11, CFC-12, methyl chloroform (CH₃CCl₃), and carbon tetrachloride (CCl₄) were added to these measurements for comparison to similar data that were obtained during previous cruises [Butler *et al.*, 1991] and to data from our network sites. CFC-113 and N₂O were also measured but are not reported here.

Sampling and Analysis

Surface water gases were partitioned with an acrylic seawater equilibrators as done on previous cruises [Butler *et al.*, 1988]. Ambient air and equilibrators headspace were sampled with a two-channel pumpboard. In addition, 27 pairs of flask samples, one each for air and equilibrators headspace, were collected along meridian 165°E for the

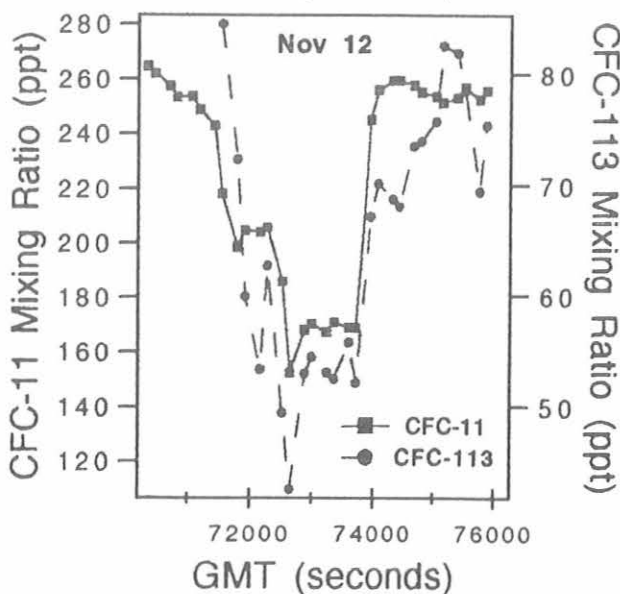
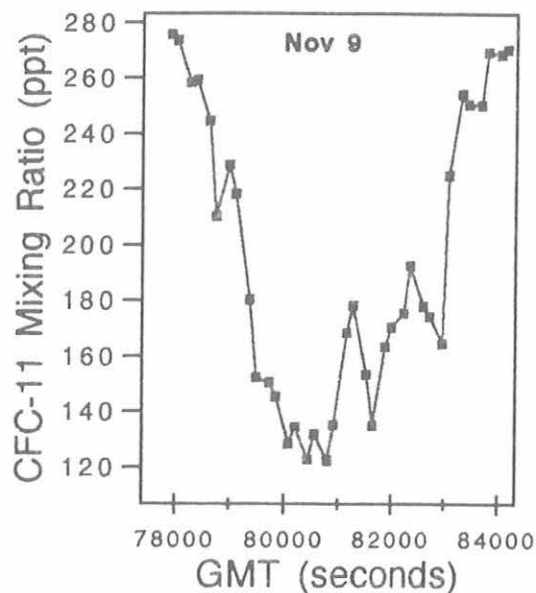


Fig. 5.19. CFC-11 and CFC-113 mixing ratios in ppt by mole fraction for the SPADE test flights on November 9 and November 12, 1992.

determination of gases other than the compounds included in this report and to compare flask data with those from in situ analyses. CFC-12, CFC-11, CH_3CCl_3 , and CCl_4 were measured with a custom-designed, three-channel GC. New technology was adapted from our ACATS aircraft projects for the design of this GC to minimize space requirements [Montzka et al., 1992]. In addition to this three-channel GC, we built a fourth gas chromatographic channel for the determination of HCFC-22, using a 35 cm^3 sample loop and a preconcentration step before analysis with an oxygen doped ECD. Most of the data were analyzed with custom

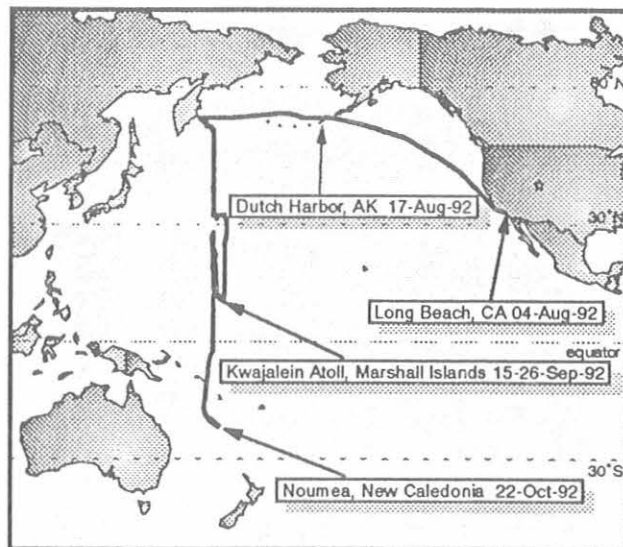


Fig. 5.20. Map with OAXTC cruise track and locations of port stops. A total distance of about 19000 km was covered during this 12-week expedition and about 26000 chromatograms were taken with one datapoint each for air and surface water at 40- to 48-minute intervals.

software *NOAHchrom*, developed in our division, for both integration of chromatograms and advanced database analysis.

CFC-11 and CFC-12

CFC-11 and CFC-12 are anthropogenic halocarbons that have long atmospheric lifetimes and are inert in seawater. Hence, they are very useful as tracers of physical processes. These two halocarbons are also useful in evaluating atmospheric circulation and in determining the effects of physical processes, such as mixing, heating, cooling, and bubble injection, upon air-sea exchange.

CFC-11 behaved predictively in both the atmosphere and the surface water. Apparent large scatter in the latitudinal profile between 55°N and 44°N as well as 28°N and 8°N can be explained in part by air mass movement and temporal variations during the several crossings of these latitudes and must be taken as the expected variability in the mixing ratios of such compounds. CFC-11 mixing ratios did not drop significantly until 30°N and leveled out below 10°S (Figure 5.21). Saturation anomalies were highest in the northern hemisphere where the waters had been subjected to warming throughout the summer. Below 10°S , the saturation anomaly was negative for CFC-11. From cooling alone, one might expect negative anomalies below the equator, but effects of cooling are offset to some degree by air-injection (air bubble dissolution), which tends to supersaturate all gases [Kester et al., 1975].

CFC-12 data show basically the same effects as explained for CFC-11 (Figure 5.22). CFC-12 in seawater is affected only by physical processes, as is CFC-11, so its

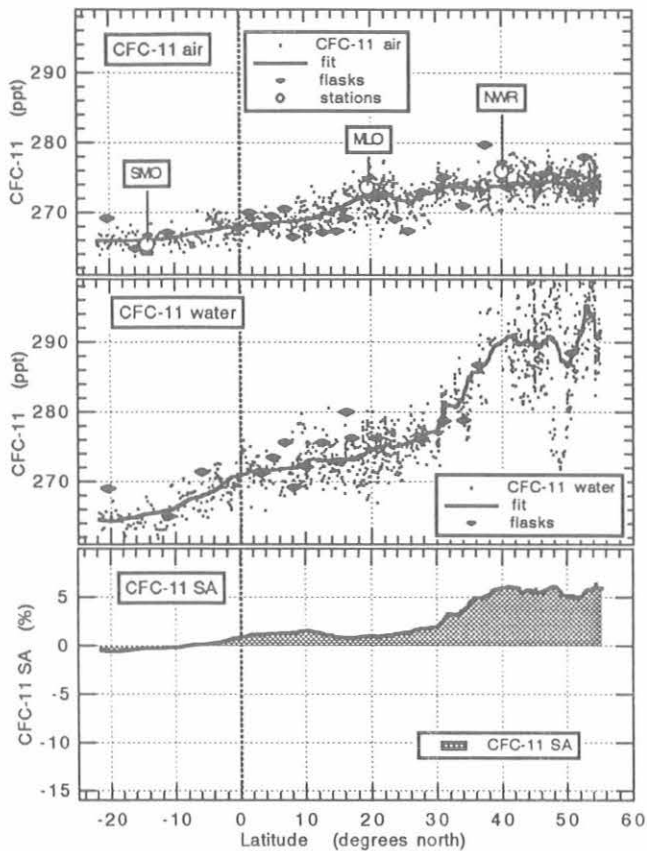


Fig. 5.21. Dry mixing ratios of CFC-11 in the air and the headspace of the sea water equilibrator. The saturation anomaly (SA) is defined as $(MR_{\text{water}} - MR_{\text{air}}) / MR_{\text{air}} * 100$, with MR=mixing ratio. Solid lines through the data sets (fit) are running means of 51 to 81 data points, as are all saturation anomalies shown here.

saturation anomaly should not differ substantially from that of CFC-11, and its net saturation anomaly should be near zero. The observed values between 0 and -2% represent the effects of slightly different behaviors of physically controlled gases.

Atmospheric mixing ratios from the in situ measurements of all compounds agreed well with those from flask samples collected on the ship and agreed within one s.d. with data from NWR, MLO, and SMO. Most flask data between 8°N and 30°N were taken on our first of several passes across this region where we observed much lower mixing ratios in both air and surface water because of an influence of southern hemispheric air.

HCFC-22

As with CFC-11 and CFC-12, the mixing ratio of HCFC-22 in the atmosphere decreased with latitude from 30°N (108 ppt) to the equator, where it tended to level off at a value of 98 ppt with latitude (Figure 5.23). This is consistent with recently published results from the CMDL flask sampling network [Montzka *et al.*, 1993a]. Data from

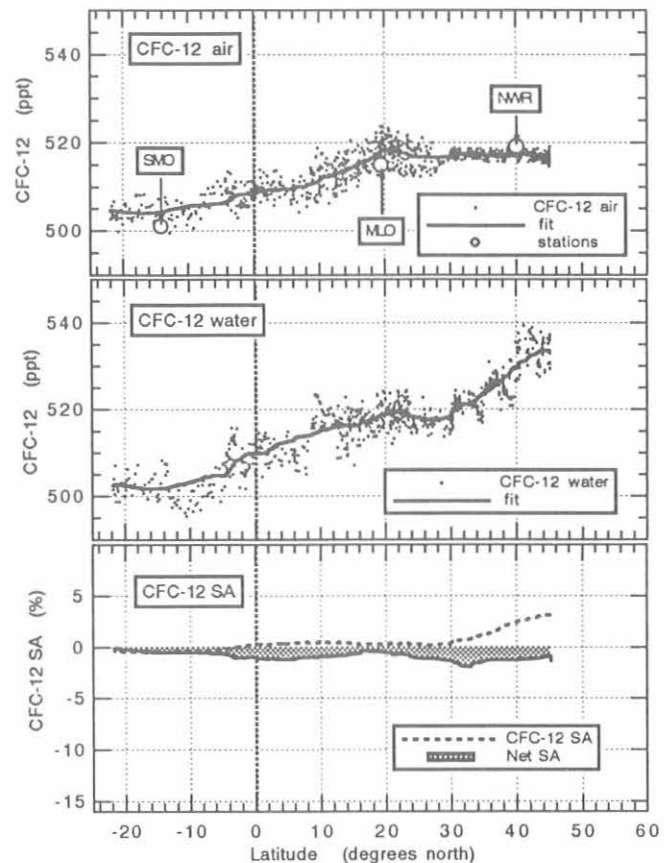


Fig 5.22. Dry mixing ratios of CFC-12 in the air and the headspace of the sea water equilibrator. The net saturation anomaly NSA is the saturation anomaly SA according to Figure 5.21, minus the saturation anomaly of CFC-11.

flasks taken during the cruise extend the dataset of in situ measurements to about 40°N and show an HCFC-22 latitudinal profile that is similar to those of the CFCs. The observed latitudinal gradient for HCFC-22 was on the order of 12 ppt between 40°N and 22°S, and is consistent with a growth rate of about 7% yr⁻¹ as reported by Montzka *et al.* [1993a].

Although differences in physical properties can explain the observed CFC-11 and CFC-12 anomalies, they cannot explain the differences between HCFC-22 and CFC-11 anomalies. Both the HCFC-22 and CFC-11 anomalies were negative through much of the tropics. Warming and cooling was minimal in these areas at this time and cannot quantitatively explain the observed departures. Dissolution of air bubbles only creates positive saturation anomalies, and the anomaly for HCFC-22 was negative over a wide latitudinal range even before being corrected with CFC-11. Finally, there is some latitudinal dependence of the HCFC-22 net saturation anomaly, which implies a possible temperature-dependent effect. By contrast, the net anomaly for CFC-12 is reasonably constant. Thus, it is also likely

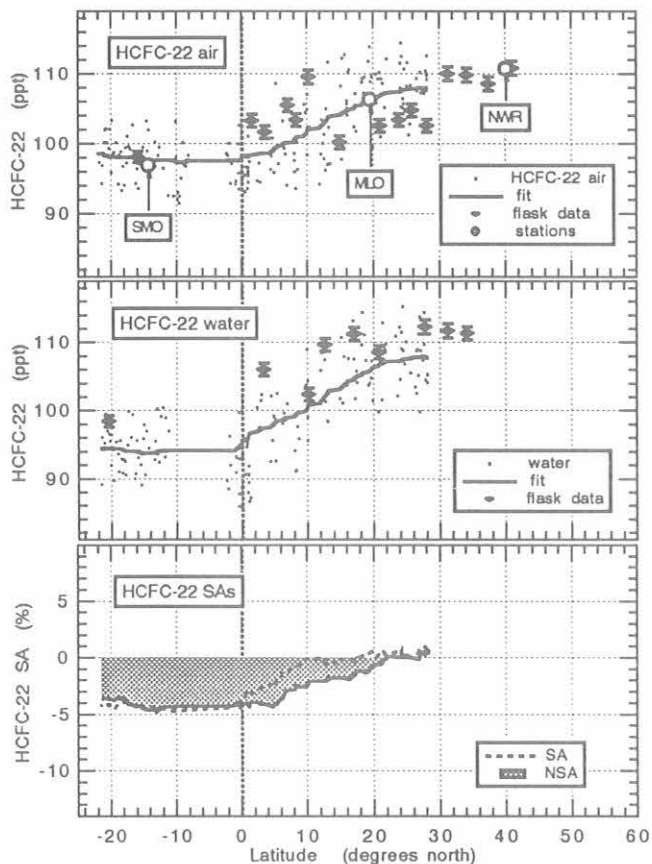


Fig. 5.23. Dry mixing ratios of HCFC-22 in the air and the headspace of the sea water equilibrator, and its saturation anomalies.

hydrolysis, reactions with solvated ions, or even microbial metabolism. The removal rate could be as much as 10 times the published hydrolysis rates, but those rates must be considered only tentative at this time. The removal rate, whatever its cause, corresponds to a partial atmospheric lifetime of 700 years. With an atmospheric lifetime of 13.6 years, this accounts for 2% of all atmospheric losses.

HCFC-22 depth profiles, although somewhat noisy, were similar to those for CFC-11 and CFC-12 (Figure 5.24). At this point, differences in the profiles must be considered insignificant and do not reveal any hard evidence of subsurface breakdown of HCFC-22. Ratios of surface-water concentrations of the CFCs relative to HCFC-22 were very close to the predicted values, calculated from Henry's solubility law.

Methyl Chloroform

The net saturation anomaly for methyl chloroform is negative almost everywhere except for the region around 30°N where we observed slightly positive values (Figure 5.25). Our data show a significant tropical sink centered that some in situ process is removing HCFC-22 in tropical

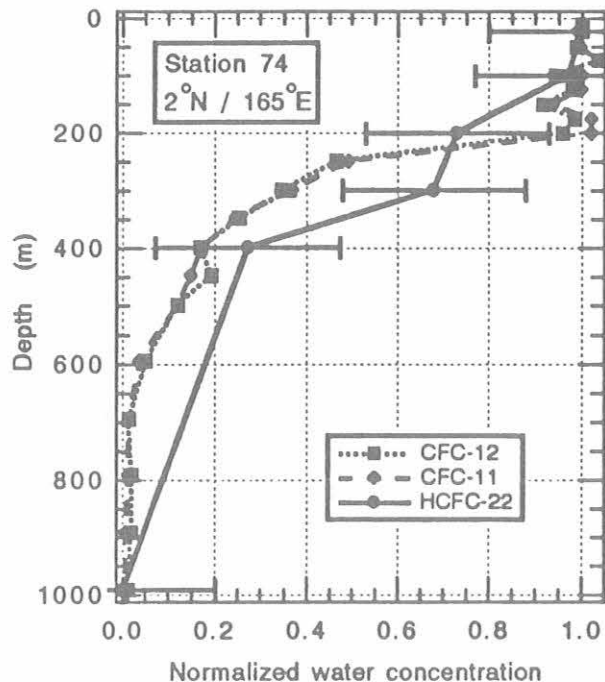


Fig. 5.24. Deep water profiles of HCFC-22, CFC-11, and CFC-12 for a station in the tropics. Water concentrations are normalized to their surface value. Error bars indicate an uncertainty of 15% for the HCFC-22 measurements. Deep water profiles of CFC-11 and CFC-12 were provided by Bullister et al., NOAA/PMEL (private communication, 1993).

and subtropical surface waters. This process may involve the equator where upwelling and oceanic breakdown by hydrolysis, and maybe by biological activity, is most intense [Butler et al., 1991].

Our results show a latitudinal dependence of the saturation anomaly for CH_2Cl_2 , but no obvious temperature dependence of the calculated flux. The temperature/flux-relationship was confounded by a positive net saturation anomaly between 30°N and 40°N and a negative net anomaly in the higher latitudes. Although these variations are not outside the realm of physical effects, they represent fairly strong fluxes, especially in the higher latitudes, because of the higher wind speeds and higher gas solubilities in those regions. The possible existence of a biological sink might explain negative fluxes at the higher latitudes, but despite their large magnitude, they would not be as great a global contribution as the sink in the tropics, because the coverage of the ocean at higher latitudes is less compared to the ocean in tropical regions.

Carbon Tetrachloride

Although CCl_4 appears slightly supersaturated at the higher north latitudes, its net saturation anomaly is strongly negative at all latitudes (Figure 5.26), which is also consistent with earlier findings by CMDL [Butler et al., 1993]. Laboratory hydrolysis data do not support the loss rate required to sustain the observed saturation anomaly for

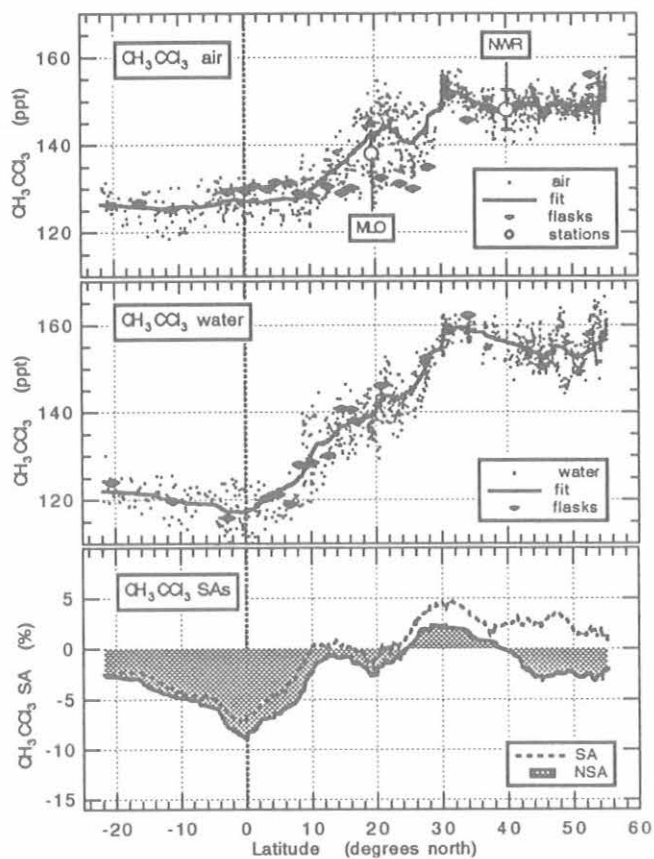


Fig. 5.25. Dry mixing ratios of CH_3CCl_3 in the air and the headspace of the sea water equilibrator, and its saturation anomalies.

CCl_4 . The highest expected rate of hydrolysis could only give rise to a net saturation anomaly of -0.1% . However, some deep water profiles obtained by investigators on this and other expeditions indicate that CCl_4 is consumed at a depth below the thermocline but near the oxygen minimum.

The flux of CCl_4 from the atmosphere required to sustain the observed saturation anomalies under steady-state conditions represents a partial atmospheric lifetime of around 250 years for loss to the ocean. The best estimate of the global CCl_4 atmospheric lifetime is 40 years, meaning that 16% of the atmospheric CCl_4 is lost to the ocean. This number is a little smaller than the range of values calculated from our other cruises (15-35%), but not outside an expected range of variability. The loss of CCl_4 to the ocean is a significant sink, as it means substantially less chlorine will be delivered to the stratosphere.

5.2.3. SOFTWARE DEVELOPMENT

The NOAA Division has developed a chromatographic interpretation and management system, NOAHchrom, and proved it in 1992 on three separate field missions (AASE

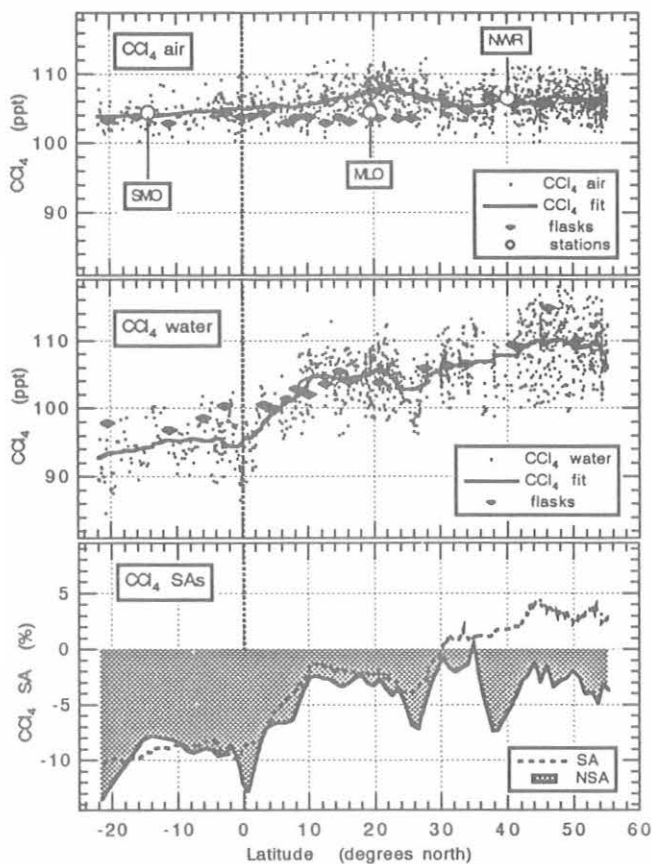


Fig. 5.26. Dry mixing ratios of CCl_4 in the air and the headspace of the sea water equilibrator, and its saturation anomalies.

II, OAXTC, and SPADE). NOAHchrom runs on Apple Macintosh computers within a commercially available data analysis and presentation application, Igor, by Wavemetrics Corporation. Igor is highly extensible (by virtue of "external operations and functions" written in the "C" programming language, and its own internal programming language), and thus proved to be an excellent platform for the development of a unique system for the interpretation of chromatographic data.

The NOAHchrom package provides a variety of tools for accurate peak integration and subsequent analysis of large data sets. NOAHchrom is essentially a simple database management system designed specifically for chromatographic data: all peak locations, integration results, concentrations, and standard sampling attributes (e.g., chromatogram name and injection time), as well as user-defined (binary) flags and user-defined, quantifiable, sampling attributes (e.g., wind direction, equilibrator temperature) are accessible through the manager. Database searches based on multiple criteria allow the user to define an interesting subset of the entire data set for scrutiny or reprocessing (e.g., find all chromatograms with CFC-11

concentrations greater than 320 ppt and with wind direction between 170-190 degrees, and then reintegrate those peaks using an exponential fit to the baseline). NOAAchrom supports both automatic and manual peak identification and detection. After peaks are located, the user has a variety of integration options: linear or non-linear curve fit to the baseline and an optional curve fit (e.g., Gaussian) to the peak itself. Quality data presentation is accomplished within the Igor application, and thus within NOAAchrom itself, at any stage of data processing.

5.3. REFERENCES

- AFEAS (Alternative Fluorocarbons Environmental Acceptability Study), Production and atmospheric release data for CFC-11 and CFC-12 (through 1992), in *Production, Sales and Atmospheric Release of Fluorocarbons Through 1992*, Washington, DC, 1993.
- Brune, W. H., J. G. Anderson, and K. R. Chan, In situ observations of ClO in the Antarctic: ER-2 aircraft results from 54°S to 72°S latitude, *J. Geophys. Res.*, *94(D14)*, 16,649-16,663, 1989.
- Butler, J.H., J.W. Elkins, B.D. Hall, S.O. Cummings, and S.A. Montzka, A decrease in the growth rates of atmospheric halon concentrations, *Nature*, *359*, 403-405, 1992.
- Butler, J.H., J.W. Elkins, T.M. Thompson, B.D. Hall, J.M. Lobert, and T.S. Swanson., A significant oceanic sink for atmospheric CCl₄, (abstract), *Third Scientific Meeting of the Oceanography Society*, 55 pp., Seattle, April 13-16, 1993.
- Butler, J.H., J.W. Elkins, T.M. Thompson, B.D. Hall, T.H. Swanson and V. Koropalov, Oceanic consumption of CH₃CCl₃: implications for tropospheric OH, *J. Geophys. Res.*, *96*, 22,347-22,355, 1991.
- Butler, J.H., J.W. Elkins, C.M. Brunson, K.B. Egan, T.M. Thompson, T.J. Conway, and B.D. Hall, Trace gases in and over the West Pacific and the East Indian Oceans during the El Nino Southern Oscillation event of 1987, NOAA Data Report ERL ARL-16, 1988.
- Elkins, J. W., T. M. Thompson, T. H. Swanson, J. H. Butler, B. D. Hall, S. O. Cummings, D. A. Fisher, A. G. Raffo, Decrease in the growth rates of atmospheric chlorofluorocarbons 11 and 12, *Nature*, *364*, 780-783, 1993.
- Fabian, P., R. Borchers, B.C. Kruger, S. Lal, and S.A. Penkett, The vertical distribution of CHClF₂ (CFC-22) in the stratosphere, *Geophys. Res. Lett.*, *12*, 1-3, 1985.
- Fahey, D.W., D.M. Murphy, K.K. Kelly, M.K.W. Ko, M.H. Proffitt, C.S. Eubank, G.V. Ferry, M. Loewenstein, and K.R. Chan, Measurements of nitric oxide and total reactive nitrogen in the Antarctic stratosphere: Observations and chemical implications, *J. Geophys. Res.*, *94(D14)*, 16,655-16,681, 1989.
- Fraser, P.J., R.A. Rasmussen, and M.A.K Khalil, Atmospheric observations of chlorocarbons, nitrous oxide, methane, carbon monoxide, and hydrogen from the Oregon Graduate Center flask sampling program, in *Baseline Atmospheric Program (Australia) 1987*, edited by B.W. Forgan and G.P. Ayers, pp. 40-43, Bureau of Meteorology CSIRO, 1989.
- Fraser, P.J., R. Harriss, S. Penkett, Y. Makide and E. Sanhueza, Source gases: concentrations, emissions, and trends, in *Scientific Assessment of Ozone Depletion: 1991, Chapter 1*, World Meteorological Organization Global Ozone Research and Monitoring Project--Rpt. No. 25, Geneva, 1991.
- GCRP (Global Change Research Program), *Our Changing Planet: The FY 1993 Research Plan, The U.S. Global Change Research Program*, A Report by the Committee on Earth Sciences, pp. 120, U.S. Geological Survey, Reston, VA, 1993.
- Goldan, P.D., F.C. Fehsenfeld, and MP. Phillips, Detection of carbon monoxide at ambient levels with an N₂O-sensitized electron-capture detector, *J. Chromatog. Sci.*, *239*, 15-126, 1982.
- Golombek, A., and R.G. Prinn, Global three-dimensional model calculations of the budgets and present-day atmospheric lifetimes of CF₂ClCFCl₂ (CFC-113) and CHClF₂ (CFC-22), *Geophys. Res. Lett.*, *16*, 1153-1156, 1989.
- Kester, D.R., Dissolved gases other than CO₂, in *Chemical Oceanography I*, 497-556, J.P. Riley and G. Skirrow (Eds), Academic Press, New York, 1975.
- Khalil, M.A.K. and R. A. Rasmussen, Increase of CHClF₂ in the Earth's atmosphere, *Nature*, *292*, 823-824, 1981.
- Khalil, M.A.K., and R.A. Rasmussen, Global distributions of anthropogenic chlorocarbons: A comparison of CFC-11, CFC-12, CFC-22, CFC-113, CCl₄, and CH₃CCl₃ from an ocean cruise and from land-based sampling sites, *Geophysical Monitoring for Climatic Change No. 16: Summary Report 1987*, 85-86, B. Bodaine and R.M. Rosson (Eds.), Boulder, CO, 1988.
- Khalil, M.A.K., and R.A. Rasmussen, Trace gas data reported in atmosphere and climate, Section 24, in *World Resources 1990-1991*, World Resources Institute, UNEP-UNDP, Oxford University Press, 345-356, 1990.
- Khalil, M.A.K., and R.A. Rasmussen, Trace gases over Hawaii; concentrations, trends, and vertical gradients, in *Climate Monitoring and Diagnostics Laboratory No. 19: Summary Report 1990*, 102-104, E.E. Ferguson and R.M. Rosson (Eds.), NOAA Environmental Research Laboratories, Boulder, CO, 1991.
- Leifer, R., K. Sommers, and S.F. Guggenheim, Atmospheric trace gas measurements with a new clean air sampling system, *Geophys. Res. Lett.*, *8*, 1079-1081, 1981.
- McFarland, M. and J. Kaye, Chlorofluorocarbons and ozone, Annual reviews, *J. Photochem. Photobiol.*, *55*, 911-929, 1992.
- Midgley, P.M., and D.A. Fisher, The production and release to the atmosphere of chlorodifluoromethane (HCFC-22), *Atmos. Environ.*, *27A*, 2215-2223, 1993.
- Montzka, S.A., R.C. Myers, J.H. Butler, J.W. Elkins, and S.O. Cummings, Global tropospheric distribution and calibration scale of HCFC-22, *Geophys. Res. Lett.*, *20*, 703-706, 1993a.
- Montzka, S.A., M.R. Nowick, R.C. Myers, J.W. Elkins, J.H. Butler, S. O. Cummings, P.J. Fraser, and L.W. Porter, NOAA/CMDL Chlorodifluoromethane (HCFC-22) observations at Cape Grim, *Baseline Atmospheric Program (Australia) 1991*, submitted 1993b.
- Montzka, S.A., J.W. Elkins, J.H. Butler, T.M. Thompson, W.T. Sturges, T.H. Swanson, R.C. Myers, T.M. Gilpin, T.J. Baring, S.O. Cummings, G.A. Holcomb, J.M. Lobert, and B.D. Hall, *Climate Monitoring and Diagnostics Laboratory No. 20: Summary Report 1991*, 60-81, E.E. Ferguson and R.M. Rosson (Eds.), NOAA Environmental Research Laboratories, Boulder, CO, 1992.
- Plumb, R.A., and M.K.W. Ko, Interrelationships between mixing ratios of long-lived stratospheric constituents, *J. Geophys. Res.*, *97(D9)*, 10,145-10,156, 1992.
- Pollock, W.H., L.E. Heidt, R.A. Lueb, J.F. Vedder, M.J. Mills, and S. Solomon, On the age of stratospheric air and ozone depletion potentials in polar regions, *J. Geophys. Res.*, *97*, 12,993-12,999, 1992.
- Prather M., and C.M. Spivakovsky, Tropospheric OH and the lifetimes of hydrochlorofluorocarbons, *J. Geophys. Res.*, *95*, 18,723-18,729, 1990.
- Prinn, R., D. Cunnold, P. Simmonds, F. Alea, R. Boldi, A. Crawford, P. Fraser, D. Gutzler, D. Hartley, R. Rosen, and R. Rasmussen, Global average concentration and trend for hydroxyl radicals

- deduced from ALE/GAGE trichloroethane (methyl chloroform) data for 1978-1990, *J. Geophys. Res.*, *97*, 2445-2461, 1992.
- Rasmussen R.A., M.A.K Khalil, S.A. Penkett, and J.D. Prosser, CHClF₂ (F-22) in the earth's atmosphere, *Geophys. Res. Lett.*, *7*, 809-812, 1980.
- Rasmussen R.A., M.A.K Khalil, A. J. Crawford, and P. J. Fraser, Natural and anthropogenic trace gases in the southern hemisphere, *Geophys. Res. Lett.*, *9*, 704-707, 1982.
- Rinsland, C.P., D.W. Johnson, A. Goldman, J.S. Levine, Evidence for a decline in the atmospheric accumulation rate of CHClF₂ (CFC-22), *Nature*, *337*, 535-537, 1989.
- Rinsland, C.P., A. Goldman, F.J. Murcray, R.D. Blatherwick, J.J. Kusters, D.G. Murcray, N.D. Sze, and S.T. Massie, Long-term trends in the concentrations of SF₆, CHClF₂, and COF₂ in the lower stratosphere from analysis of high-resolution infrared solar occultation spectra, *J. Geophys. Res.*, *95*, 16,477-16,490, 1990.
- Salawitch, R.J., S. C. Wofsy, E. W. Gottlieb, L. R. Lait, P. A. Newman, M. R. Schoberl, M. Loewenstein, J.R. Podolske, S.E. Strahan, M.H. Proffitt, C.R. Webster, R.D. May, D.W. Fahey, D. Baumgardner, J.E. Dye, J.C. Wilson, K.K. Kelly, J.W. Elkins, K.R. Chan, and J.G. Anderson, Chemical loss of ozone in the Arctic polar vortex in the winter of 1991-1992, *Science*, *261*, 1146-1149, 1993.
- Solomon, S., M. Mills, L.E. Heidt, W.H. Pollack, and A.F. Tuck, On the evaluation of ozone depletion potentials, *J. Geophys. Res.*, *97(D1)*, 825-842, 1992.
- Swanson, T.H., J.W. Elkins, T.M. Thompson, S.O. Cummings, J.H. Butler, and B.D. Hall, Decline in the accumulation rates of atmospheric chlorofluorocarbons 11 and 12 at the South Pole, *Ant. J. U. S.*, *27*, 1992.
- Talukdar, R.K., A. Mellouki, A. Schmolner, T. Watson, S.A. Montzka, and A.R. Ravishankara, Kinetics of the OH reaction with methyl chloroform and its atmospheric implications, *Science*, *257*, 227-230, 1992.
- Toohey, D.W., L.M. Avallone, L.R. Lait, P.A. Newman, M.R. Schoeberl, D.W. Fahey, E.L. Woodbridge, and J.G. Anderson, The seasonal evolution of reactive chlorine in the northern hemisphere stratosphere, *Science*, *261*, 1134-1136, 1993.
- UNEP (United Nations Environmental Programme), Montreal Protocol to reduce substances that deplete the ozone layer report, Final Report, UNEP, 15 pp., New York, 1987.
- WMO (World Meteorological Organization), *Scientific Assessment of Ozone Depletion, 1991*, 25 pp., Geneva, 1992.
- Zander, R., M.R. Gunson, C.B. Farmer, C.P. Rinsland, F.W. Irion, and E. Mahieu, The 1985 chlorine and fluorine inventories in the stratosphere based on ATMOS observations at 30°N latitude, *J. Atmos. Chem.*, *15*, 171-186, 1992.

6. Director's Office

STRATOSPHERIC AEROSOL AND RADIATION MEASUREMENTS IN THE ALASKAN ARCTIC DURING AGASP-IV/LEADEX, APRIL 1992

P.J. SHERIDAN AND R.S. STONE

Cooperative Institute for Research in Environmental Sciences, University of Colorado, Boulder, Colorado

6.1. INTRODUCTION

The Fourth Arctic Gas and Aerosol Sampling Program (AGASP-IV), a component of the Arctic Leads Experiment (LEADEX), was conducted over the Beaufort Sea during late March and April 1992. The NOAA WP-3D (P-3) Orion research aircraft was the primary measurement platform for AGASP-IV and was one of several airborne laboratories used for atmospheric measurements in LEADEX. The NOAA P-3 was instrumented to measure atmospheric gas and aerosol species, radiation parameters at multiple wavelengths, and meteorological state variables. The purpose of these airborne measurements in LEADEX was to complement and compare with concurrent baseline station, ice camp, ice buoy, and submarine measurement programs.

The NOAA P-3 flew a total of nine research missions in the Beaufort Sea area (~90 research hours), operating at altitudes between ~10 and 10,500 m above the surface [Herbert *et al.*, 1993]. The major objectives of AGASP-IV were to (1) measure the concentration and composition of gaseous and particulate constituents of springtime Arctic haze in the Alaskan Arctic, (2) determine components of the atmospheric (especially the marine) sulfur cycle, through measurements of DMS, MSA, SO₂, OCS, and SO₄⁻ in the inversion layer over lead-filled pack ice, and (3) determine whether significant amounts of volcanic aerosols from Mount Pinatubo were present in the atmosphere over Alaska and the Beaufort Sea. In this report, we focus on the analysis of stratospheric aerosol and radiation measurements that show severe perturbations from "normal" or background values.

In the polar regions it is especially difficult to observe and quantify the effects of volcanic forcing because natural climate fluctuations are anomalously large there. In particular, efforts to estimate the radiation balance for the polar regions using satellite data are hampered by problems associated with the remote sensing of atmospheric properties over bright, cold surfaces [Key and Barry, 1989]. Thus, there is a critical need for "ground truth" measurements to validate and improve operational algorithms that use satellite data to monitor polar climate variables. Our aircraft data include nearly 1300 discrete spectral measurements of solar irradiance using handheld sunphotometers, and in situ measurements of aerosol light scattering, number concentration, and particle size distribution. Our

measurements reveal elevated aerosol concentrations and significant numbers of large (supermicrometer) particles in the lower Arctic stratosphere and upper troposphere, indicating the presence of considerable amounts of Mount Pinatubo volcanic debris. These data corroborate and should be useful for quantifying polar-orbiting satellite observations of greatly enhanced aerosol optical depths at high northern latitudes in the spring of 1992 [Long and Stowe, 1993].

6.2. METHODS

The primary optical depth data are derived from spectral measurements made during AGASP-IV flight segments flown above the Arctic tropopause. These observations were made using handheld, dual-channel sunphotometers that sense directly-transmitted solar irradiance at 380 and 500 nm, and at 778 and 862 nm, respectively. Each channel has a nominal half-band width of 5 nm and a field-of-view of 2.4° [Reddy *et al.*, 1990]. Only data collected during cloud-free periods were analyzed. Ancillary surface-based measurements of optical depth used in support of aircraft analyses and to evaluate the decay rate of Mount Pinatubo aerosols in the Arctic are discussed in Stone *et al.* [1993].

Airborne measurements were made whenever viewing was possible within ±30° of the solar azimuth angle through optical glass windows fitted on either side of the aircraft [Dutton *et al.*, 1989]. The sunphotometers were carefully calibrated at high altitude sites before and after AGASP-IV in accordance with recommended procedures using the Langley plot method [Shaw, 1983]. Each instrument was determined to be stable with precision of ~0.002. All optical depth values reported in this paper account for Rayleigh scattering, ozone absorption at 500 nm, and changes in relative airmass as a function of time and location. A correction due to attenuation by the optical glass was also performed. Thus, from total slant path irradiance measurements, columnar aerosol optical depths were computed. Estimated uncertainties due to all sources are <10% of typical values reported here.

The optical depth data are supported by several other types of aerosol measurements. An automated three-wavelength integrating nephelometer [Bodhaine *et al.*, 1991] made continuous aerosol light scattering (B_{sp}) measurements. This instrument performs continuous checks of operating parameters and corrects for Rayleigh

scatter and instrument background in real time. A condensation nucleus (CN) counter [Schnell *et al.*, 1989] monitored stratospheric particle number concentrations. Two aerosol spectrometer probes permitted optical particle sizing measurements for calculation of particle number- and volume-size distributions [Sievering *et al.*, 1989]. Cascade impactor samples of stratospheric particulate material were also collected and later analyzed using standard analytical electron microscopy techniques [Sheridan, 1989].

6.3. RESULTS

6.3.1. STRATOSPHERIC AEROSOL OPTICAL DEPTH

The locations and dates corresponding to the various sunphotometer measurement periods are shown in Figure 6.1. The curved arrows are isentropic 36-hour back-trajectories representing stratospheric winds prior to each flight. Only direct measurements made above the tropopause were selected for analysis. Bridgman *et al.* [1993] give case-by-case analyses of eight AGASP-IV flights including discussions of a variety of tropospheric measurements. Tropopause heights for each flight were determined on the basis of analyses performed by Herbert *et al.* [1993]; these range from approximately 7 km to 10 km depending on geographic location and synoptic conditions.

Figure 6.2 shows the mean spectral optical depths derived for the corresponding times and locations shown in Figure 6.1. Several features of Figure 6.2 are notable. First and most important, the values derived for all times and locations are one to two orders of magnitude greater than stratospheric background levels which range between 0.002 and 0.006 for visible wavelengths [Toon and Pollack, 1976]. These

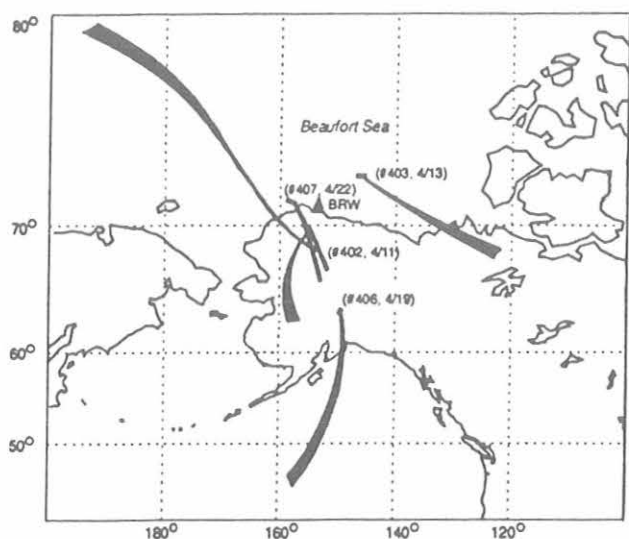


Fig. 6.1. Distribution of sunphotometer measurements made during AGASP-IV/LEADEX stratospheric flight segments. Curved vectors represent stratospheric winds as described in the text.

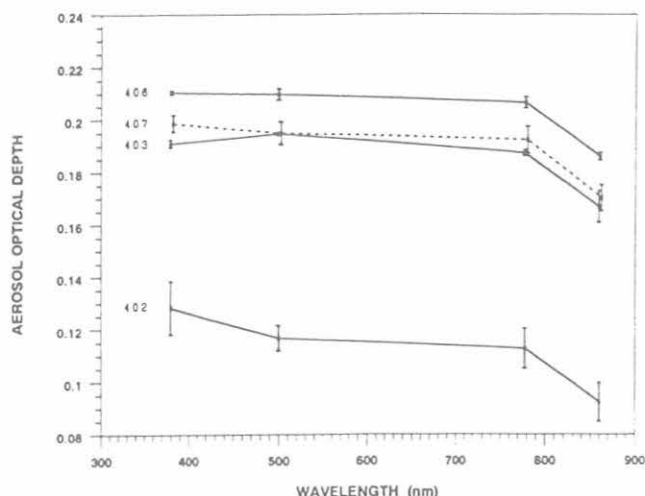


Fig. 6.2. Stratospheric spectral optical depths derived for the flight segments shown in Figure 6.1. Slight offsets are used to clearly indicate values at plus and minus one standard deviation (vertical bars) of the means.

values also exceed similar measurements made in the Arctic approximately a year after El Chichon erupted [Dutton *et al.*, 1984; Spinhirne and King, 1985]. Second, the optical depths are rather flat spectrally in the visible range but show a marked decrease in the near infrared. Third, three of the flights (nos. 403, 406, and 407) show a high degree of homogeneity in time and space as evidenced by their small standard deviations, similar magnitudes, and spectral dependencies. Finally, the values for flight no. 402 are about 60% lower than those measured during flight no. 407 despite their having similar flight tracks and altitudes relative to the tropopause. These similarities and differences are discussed below.

Based on the data presented in Figure 6.2, effective aerosol size distributions were inferred using the constrained linear inversion algorithm of King *et al.* [1978]. The maximum radius sensitivity ($r_{\min} \leq r \leq r_{\max}$) [Spinhirne and King, 1985] determined for our particular set of measurements was within the range $r_{\min} = 0.10 \pm 0.02 \mu\text{m}$ and $r_{\max} = 1.10 \pm 0.10 \mu\text{m}$. We assumed an index of refraction of 1.45-0.0i based on earlier in situ observations of the Mount Pinatubo aerosol layers [Deshler *et al.*, 1992]. The inversion results are presented in Figure 6.3. Each curve shows the total number concentration $dN \text{ (cm}^{-2} \mu\text{m}^{-1}\text{)}$ for seven radius increments ($d \log(r)$). The vertical bars indicate the range of number density determined by inverting the mean spectral optical depth data $\pm 1\sigma$ presented in Figure 6.2. The inferred size distributions are bimodal having a large particle mode centered at $\sim 0.5 \mu\text{m}$ and a small mode of higher concentration peaking below $0.18 \mu\text{m}$ radius.

6.3.2. STRATOSPHERIC AEROSOL MEASUREMENTS

Several sets of aerosol measurements taken during the AGASP-IV flights strongly support the optical depth

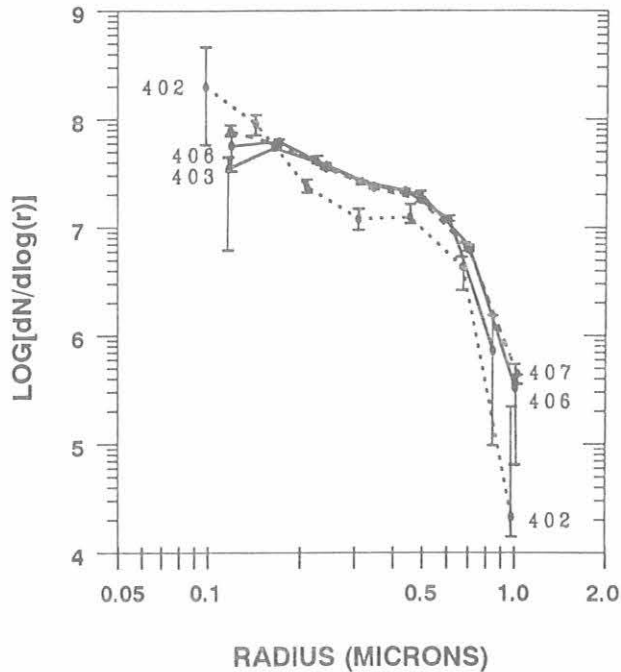


Fig. 6.3. Effective aerosol size distributions showing the range of number concentrations dN at each radius interval ($d\log(r)$) inferred from the optical depth data shown in Figure 6.2.

observations discussed previously. This corroboration is particularly evident in data collected during flight nos. 406 and 407. On both of these flights, and on flight nos. 402, 404, and 405, the tropopause was penetrated over Alaska during the inbound ferry to Anchorage, and substantial time was spent in stratospheric air [Herbert *et al.*, 1993]. In contrast to this scenario, the aircraft experienced an engine failure on flight no. 401 that prevented it from climbing into the stratosphere, and during flight no. 403, stratospheric air was only briefly encountered [Herbert *et al.*, 1993]. No sunphotometer measurements were taken on flight no. 408.

Stratospheric aerosol data from flight nos. 404 through 407 exhibit consistently high aerosol light scattering coefficients and particle number concentrations. As an example, Figure 6.4 (from Bridgman *et al.* [1993]) clearly shows the flight no. 406 stratospheric sampling period with enhanced CN and B_{sp} levels. During this flight segment, some of the highest optical depth measurements of the entire AGASP-IV program were observed (see Figure 6.2).

The aerosol spectrometer probes typically showed bimodal particle size distributions that display a large-particle number peak in the 1-2 μm diameter range, with the volume distribution secondary peak at slightly larger particle sizes than the number peak [Bridgman *et al.*, 1993]. Figure 6.5 (also from Bridgman *et al.* [1993]) shows the number-size and volume-size distributions for flight no. 405, which was chosen as a typical example and closely resembles those from other flights in the 404-407

sequence. These data confirm the size distributions inferred from the sunphotometer measurements (Figure 6.3), which display a large number peak at $<0.18 \mu\text{m}$ radius and a secondary large-particle peak centered at $\sim 0.5 \mu\text{m}$ radius.

Cascade impactor samples were also collected during AGASP-IV flights 402-407. Electron microscope analyses of these aerosol samples revealed heavy particulate loadings for stratospheric samples collected during flight nos. 404, 405, 406, and 407. Figure 6.6 is a photomicrograph of stratospheric aerosol particles collected during flight no. 406. The smaller (mostly $< 0.5 \mu\text{m}$ diameter) particles are nearly all composed of sulfate. The larger particles are one to several micrometers in size and are usually either sulfates or solid particles rich in Si or Na and Cl (suggesting terrestrial or marine origin, respectively). The types, sizes, and relative loadings of particles were similar for all stratospheric samples collected

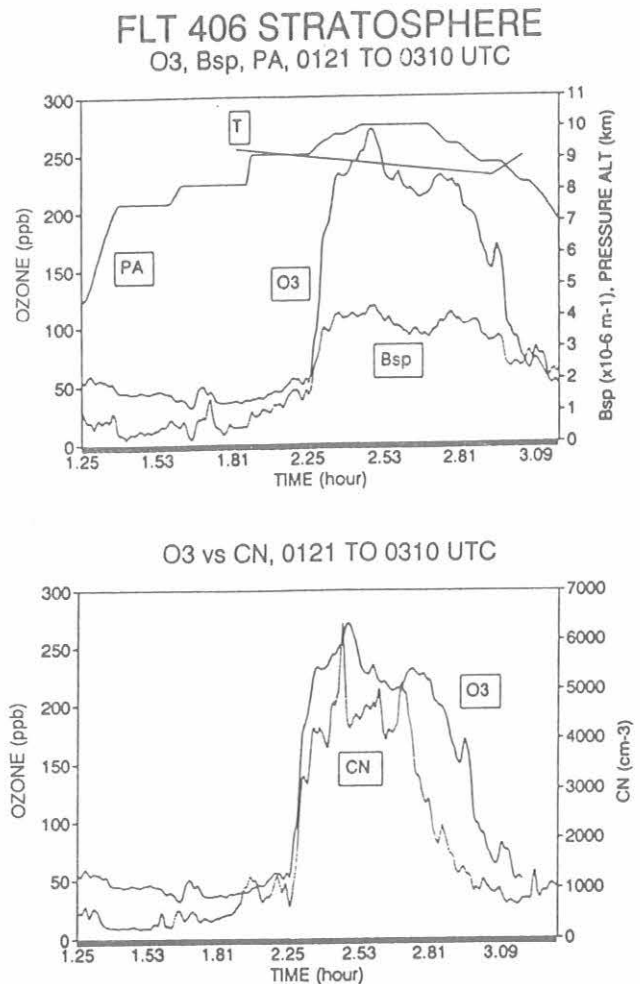


Fig. 6.4. Plots of atmospheric parameters measured by aircraft instruments during a portion of flight no. 406. The stratospheric flight segment is denoted by the period of high O_3 , decreasing temperature and the highest pressure altitudes. During this time, CN counts and B_{sp} were significantly elevated over upper tropospheric levels.

ASASP 405 PMS dN/dLOGd
0137-0316, 0455-0513 UTC

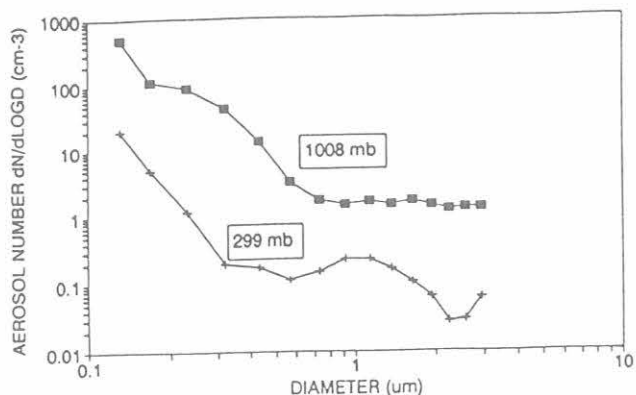


Fig. 6.5. Particle size distributions derived from the ASASP aerosol spectrometer probe data. This bimodal distribution was typical of stratospheric aerosols sampled during flight nos. 404-407.

during flights 404-407. High altitude impactor samples from flights 402 and 403 showed very light particulate loadings. For flight 403, this is probably because little time was spent in stratospheric air. The aerosol data from flight no. 402 suggest that the aircraft flew well into the stratosphere, but showed no significant elevation in aerosol concentrations (as was observed on the later flights). Possible explanations for these observations are discussed in section 6.4.

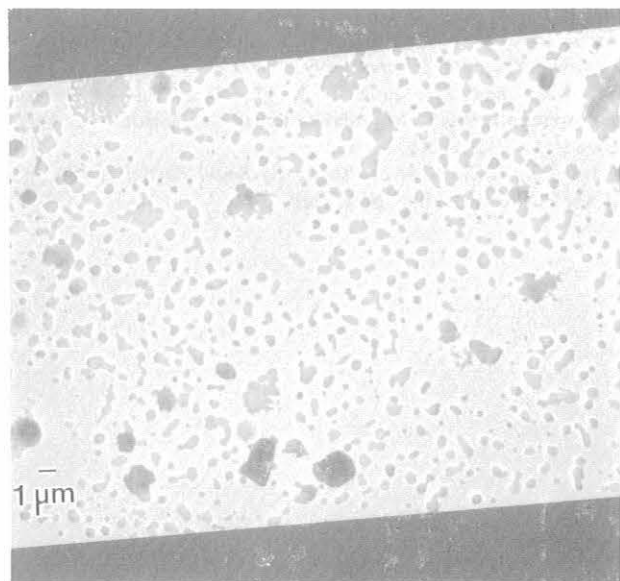


Fig. 6.6. Analytical electron micrograph of particles collected during the stratospheric flight segment of AGASP-IV flight 406. Aerosol optical depths and concentrations measured during this period were consistently among the highest observed in this study. Particles exhibited a roughly bimodal size distribution peaking at < 0.5 µm and several micrometers in diameter.

6.4. DISCUSSION

It appears from Figure 6.2 that some temporal and/or spatial variations in stratospheric aerosols occurred over the period and region represented by our data. The relatively lower stratospheric aerosol concentrations and opacity noted for flight no. 402 can be explained by differences in synoptic conditions during the respective flight periods [Herbert *et al.*, 1993]. During flight no. 402 strong northerly winds transported polar air into the region whereas weaker southerly flow generally characterized the later flights. An analysis of isentropic back-trajectories [Harris and Bodhaine, 1983] based on the ECMWF 2.5° gridded data supports the synoptic analyses. Figure 6.1 shows 36-hour backward air mass trajectories representing the flow at altitudes ranging from ~14.5 km to 15.8 km referenced to the respective mid-flight segments. This analysis suggests that relatively clean Arctic air displaced or mixed with lower latitude air effectively reducing the stratosphere's opacity prior to flight no. 402. The formation of the polar vortex during the previous autumn/winter probably prevented high concentrations of Mount Pinatubo aerosols from penetrating the central Arctic. Similar gradients related to the position, size and shape of the polar vortex were observed several months after El Chichon erupted [McCormick *et al.*, 1983].

The relatively large 380 nm optical depths measured during flight no. 402 (Figure 6.2) suggest fundamental differences in the aerosols' microphysical properties compared with the results of the other flights. Increased attenuation at shorter wavelengths can be explained by the presence of higher concentrations of small particles (Figure 6.3) that have greater extinction efficiencies as the ratio of size-to-wavelength (τ/λ) increases [van de Hulst, 1981]. The sharp decreases evident at the large particle end of the inferred size spectra are probably due to diminishing opacity as wavelength increases [Spinhirne and King, 1985].

In situ aerosol measurements (CN counts and B_{sp}) made during flight no. 402 [Bridgman *et al.*, 1993] indicate no enhanced small particle mode similar to those observed on flight nos. 404-407. This is the only case in which the aircraft aerosol measurements do not directly support the results derived from sunphotometer measurements. Figure 6.3 suggests a small-particle enhancement and large-particle depletion in the inferred size distribution relative to the other flights. It is conceivable that Mount Pinatubo sulfate aerosols were in the optical path above the aircraft flight level, but were not present in high concentrations at the altitude the aircraft reached on flight no. 402. This is consistent with the notion of low settling velocities for very small (i.e., few-tenth micrometer) particles.

The high degree of consistency between our optical depth measurements (including their inferred size distributions) and the in situ aerosol data lends confidence to our measurements that strongly support recent ground-based [Stone *et al.*, 1993] and satellite [Long and Stowe, 1993] observations of large aerosol optical depths in the Arctic in

spring 1992. Further, these data are being used in multiple-year studies that begin to address potential climate impacts of the volcanic aerosols by documenting their longevity (i.e., decay rate) in the atmosphere [Stone *et al.*, 1993]. Preliminary data from these studies suggest a significantly longer aerosol residence (e-folding) time in the arctic atmosphere compared with that observed for past volcanic episodes (e.g., El Chichon).

Acknowledgments. Thanks are due to G. Herbert, H. Bridgman, and E. Dutton for access to ancillary data; to J. Harris for kindly providing the isentropic trajectories; to J. Key for making sunphotometer measurements during several of the AGASP flights; and to the NOAA P-3 crew.

6.5. REFERENCES

- Bodhaine, B.A., N.C. Ahlquist, and R.C. Schnell, Three-wavelength nephelometer suitable for aircraft measurement of background aerosol scattering coefficient, *Atmos. Environ.* 25A, 2267-2276, 1991.
- Bridgman, H.A., P.J. Sheridan, R.S. Stone, P. McCaslin, B.A. Bodhaine, and R.C. Schnell, The analysis of haze distribution, aerosol chemistry, and optical depths for the Fourth Arctic Gas and Aerosol Sampling Program (AGASP IV), March-April 1992, *NOAA CMDL Technical Memorandum*, NOAA Environmental Research Laboratories, Boulder, CO, (in preparation) 1993.
- Deshler, T., D.J. Hofmann, B.J. Johnson, and W.R. Rozier, Balloonborne measurements of the Pinatubo aerosol size distribution and volatility at Laramie, Wyoming during the summer of 1991. *Geophys. Res. Lett.*, 19, 199-202, 1992.
- Dutton, E.G., J.J. DeLuisi, and B.A. Bodhaine, Features of aerosol optical depth observed at Barrow, March 10-20, 1983, *Geophys. Res. Lett.*, 11, 385-388, 1984.
- Dutton, E.G., J.J. DeLuisi, and G. Herbert, Shortwave aerosol optical depth of Arctic haze measured on board the NOAA WP-3D during AGASP-II, April 1986, *J. Atmos. Chem.*, 9, 71-79, 1989.
- Harris, J.M., and B.A. Bodhaine (Eds.), *Geophysical Monitoring for Climatic Change No. 11: Summary Report 1982*, 160 pp., NOAA Air Resources Laboratory, Boulder, CO, 1983.
- Herbert, G.A., P.J. Sheridan, R.C. Schnell, M.Z. Bieniulis, B.A. Bodhaine, and S.J. Oltmans, Analysis of meteorological conditions during AGASP-IV: March 30-April 23, 1992, *NOAA Technical Memorandum ERL CMDL-5*, NOAA Environmental Research Laboratories, Boulder, CO, April 1993.
- Key, J.R., and R.G. Barry, Cloud cover analysis with Arctic AVHRR, part 1: Cloud detection, *J. Geophys. Res.*, 94(D15), 18,521-18,535, 1989.
- King, M.D., D.M. Byrne, B.M. Herman, and J.A. Reagan, Aerosol size distributions obtained by inversion of spectral optical depth measurements, *J. Atmos. Sci.*, 35, 2153-2167, 1978.
- Long, C., and L. Stowe, Using the NOAA AVHRR to study stratospheric aerosol optical thickness following the Mount Pinatubo eruption, *Geophys. Res. Lett.* (in review) 1993.
- McCormick, M.P., C.R. Trepte, and G.S. Kent, Spatial changes in the stratospheric aerosol associated with the north polar vortex, *Geophys. Res. Lett.*, 10, 941-944, 1983.
- Reddy, P.J., F.W. Kreiner, J.J. DeLuisi, and Y. Kim, Aerosol optical depths over the Atlantic derived from shipboard sunphotometer observations during the 1988 global change expedition, *Glob. Biogeochem. Cycl.*, 4, (3), 225-240, 1990.
- Schnell, R.C., T.B. Watson, and B.A. Bodhaine, NOAA WP-3D instrumentation and flight operations on AGASP-II, *J. Atmos. Chem.*, 9, 3-16, 1989.
- Shaw, G.E., Sunphotometry, *Bull. Amer. Meteorol. Soc.*, 64, 4-10, 1983.
- Sheridan, P.J., Characterization of size segregated particles collected over Alaska and the Canadian high Arctic, AGASP-II flights 204-206, *Atmos. Environ.*, 23, 2371-2386, 1989.
- Sievering, H., P.J. Sheridan, and R.C. Schnell, Size distribution of large aerosol particles during AGASP-II: Absence of St. Augustine eruptive particles in the Alaskan Arctic. *Atmos. Environ.*, 23, 2495-2499, 1989.
- Spinhirne, J.D., and M.D. King, Latitudinal variation of spectral optical thickness and columnar size distribution of the El Chichon stratospheric aerosol layer, *J. Geophys. Res.*, 90(D6), 10,607-10,619, 1985.
- Stone, R.S., J.R. Key, and E.G. Dutton, Enhanced opacity of the Arctic stratosphere after the 1991 eruptions of Mount Pinatubo, *Geophys. Res. Lett.*, (in press) 1993.
- Toon, O.B., and J.B. Pollack, A global average model of atmospheric aerosols for radiative transfer calculations, *J. Appl. Meteorol.*, 15, 225-246, 1976.
- van de Hulst, H.C., *Light Scattering By Small Particles*, 470 pp., Dover Publications, Inc., New York, 1981.

7. Cooperative Programs

Antarctic Ultraviolet Spectroradiometer Monitoring Program: South Pole and Barrow Contrasts in UV Irradiance

C. R. BOOTH, T.B. LUCAS, J.R. TUSSON IV, J.H. MORROW, AND T. MESTECHKINA
Biospherical Instruments Inc., San Diego, California 92110-2621

1. INTRODUCTION

The Antarctic Ultraviolet spectroradiometer monitoring network was established by the United States National Science Foundation (NSF) in 1988 in response to predictions of increased UV radiation in the polar regions. The network consists of several automated, high resolution spectroradiometers placed in strategic locations in Antarctica and the Arctic (Table 1), and a new operational site in San Diego that is also used for training and testing. The network makes essential measurements of UV spectral irradiance and provides a variety of biological dosage calculations of UV exposure. Under contract to Antarctica Support Associates (ASA), directed by NSF, Biospherical Instruments Inc., is responsible for operating and maintaining the network and distributing data to the scientific community.

The spectroradiometer system contains an irradiance diffuser, double holographic grating monochromator, photomultiplier tube (PMT), and calibration lamps. Tungsten-halogen and mercury vapor lamps are used for automatic internal calibration of the optical pathway. The monochromator and PMT are located in individual temperature controlled subassemblies. The entire instrument is operated under computer control, including regular calibration cycles, several times each day. Details may be found in *Booth et al.*, [1992].

2. UV RADIATION CLIMATE AT THE AMUNDSEN-SCOTT SOUTH POLE STATION AND BARROW, ALASKA

The South Pole and Barrow, Alaska, installations are in locations that also have CMDL installations, and the balance

of this report will focus on these two sites. The South Pole site is uniquely suited to examinations of radiative transfer including the effects of ozone on UV radiation. This site is located away from the influence of mountains in a region of almost constant albedo. Cloud cover is relatively infrequent and generally thin when it does occur. The very small hourly change in the solar-zenith angle supports examination of changes in total column ozone (as estimated by UV irradiance) at hourly resolution.

Barrow can be contrasted with the South Pole in that it is located where a significant change in surface albedo occurs both due to the springtime snowmelt [*Dutton and Endres*, 1991] and changes in sea ice coverage. Significant changes in incident irradiance also occur due to Arctic storms. The contrast between Barrow and the South Pole can be seen in Figure 1b, where the integrated noontime irradiance over the UV-A (320-400 nm) for 1992 is plotted.

The large changes in total column ozone encountered at the South Pole make it an ideal site to examine the relationship between ozone depletion and enhanced UV irradiance. For example, in Figure 1a, a substantial drop is seen in the 300 nm irradiance around December 6. Data from Total Ozone Mapping Spectrometer (TOMS) report that the ozone column over the South Pole rose from 193 DU on December 5 to 292 DU on December 7, 1992. TOMS update on CD-ROM is available from the National Space Science Data Center, Goddard Space Flight Center.

Strong springtime depletion in ozone over the Pole, both in the spring and approaching mid-summer, compared with higher ozone levels in the fall, allow careful estimates of the impact of changes in ozone on UV irradiance with most other conditions (cloud cover, albedo, and solar zenith angle) being equal. Figure 2 shows the DNA dose weighted

TABLE 1. Installation Sites

Site	Latitude	Longitude	Established	Location
McMurdo	77°51'S	166°40'E	March 1988	Arrival heights
Palmer	64°46'S	64°03'W	May 1988	Clean air building
South Pole	90°00'S	0°	February 1988	Clear air building
Ushuaia, Argentina	54°59'S	68°W	November 1988	CADIC*
Barrow, Alaska	71°18'N	156°47'W	December 1990	UIC-NARL†
San Diego, California	32°47'N	117°14'W	October 1992	Biospherical Instruments Inc.

*CADIC: Centro Austral de Investigaciones Cientificas, Argentina

†Ukpeagvik Inupiat Corporation-National Arctic Research Laboratory

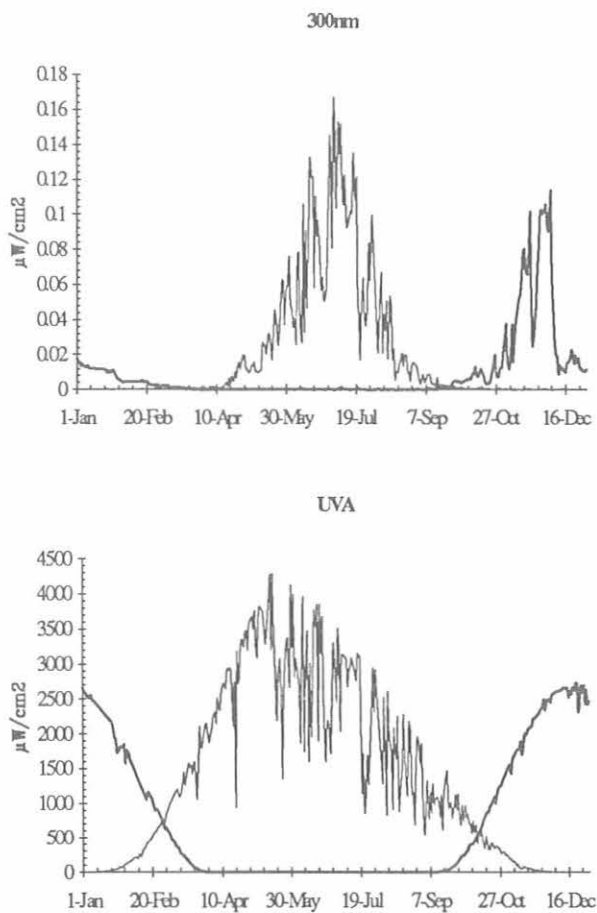


Fig. 1. The noontime irradiance is shown at Barrow (fine line) and the South Pole (heavy line) during 1992. Panel (a) shows the irradiance at 300 nm and is contrasted with panel (b) which shows the integrated UV-A (320-400 nm) irradiance. The higher values at Barrow are due to the higher sun elevation. The irradiances at Barrow peak in June, while the irradiances at the South Pole normally peak in December.

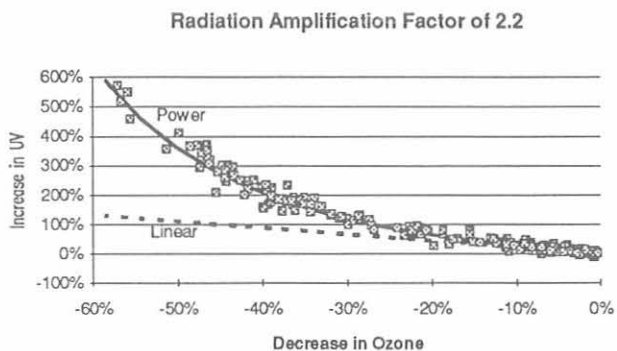


Fig. 2. Radiation amplification factor computed for South Pole data set covering 1991-1992. Points refer to equal solar zenith angles ($\pm 0.3^\circ$).

irradiance (after Setlow, 1974; see Booth *et al.*, 1992 for details) change measured for a series of day pairs when different amounts of ozone depletion were encountered. One scan per day was selected closest in time to the overpass of the TOMS satellite. A random mixture of 1 year against another, or spring against fall observations, was used covering ozone concentrations ranging from 111 DU to 408 DU. Figure 2 shows the observed relationship between ozone depletion expressed in percentage, versus dose-weighted irradiance enhancement, also in percentage. No scans were included when a time mismatch of greater than 5 hours occurred. Only data where the sun was higher than 80° (zenith angle) were considered. In all, 277 spectra were included in the analysis.

Two lines are shown in Figure 2: the straight line expresses a simple formulation of the effect of ozone depletion to amplify UV irradiance and is a linear extrapolation of a rule of "1% decrease in ozone will bring a 2.2% increase in UV," while the curved line expresses a power-based formulation of this rule as suggested by Madronich [1993]. This allows us to determine the "amplification" of UV irradiance caused by ozone depletion.

3. SUMMARY

High spectral resolution scanning UV spectroradiometers have been established at several high latitude sites and are successfully providing multiyear data sets. Resulting data have been used to test radiative transfer models (Lubin and Frederick, 1990, 1991, 1992); Lubin *et al.*, (1989); Smith *et al.*, (1991, 1992a), derive ozone concentrations (Stamnes *et al.*, 1990, 1991, 1992), and examine the biological impact of enhanced UV [Lubin *et al.*, 1993; Cullen *et al.*, 1992; Smith *et al.*, 1991, 1992b). The data are available on CD-ROM to a broad segment of the scientific community. Please contact the authors for more information.

The data from the NSF UV Spectroradiometer Network is available to all qualified researchers. The data shown in this report is available on CD-ROM, ISO 9660 format. NSF grantees have priority access to these data. For more information, please contact: C. R. Booth at Biospherical Instruments Inc., 5340 Riley St., San Diego, CA 92110 (Fax 619 686-1887, or BOOTH@SSURF.UCSD.EDU).

Acknowledgments. This research and monitoring activity was funded by contract A1T-M1743 from Antarctic Support Associates under direction of Polly Penhale at NSF, Office of Polar Programs. B. Mendonca of CMDL assisted in providing operators and support for the installations at the South Pole and Barrow. R. McPeters of NASA/GSFC provided TOMS total ozone data for comparison purposes. Barrow operators include D. Norton (Arctic Sivumun Ilisagvik College); D. Endres and Brad Halter (CMDL). The Ukpeagvik Inupiat Corporation of Barrow provided assistance in the installation. Operators at Palmer and McMurdo have been provided by ASA. Special thanks go to John Gress of ASA who has been invaluable in the operation of the network.

4. REFERENCES

- Booth, C.R., T. Lucas, T. Mestechkina, J. Tusson, D. Neuschuler, and J. Morrow, NSF polar programs UV spectroradiometer network 1991-1992 operations report, *Bio. Instr. Tech. Rep. 92-1*, 145 pp., Biospherical Instruments Inc., San Diego, CA, 1992.
- Cullen, J.C., P.J. Neale, and M.P. Lesser, Biological weighting function for the inhibition of phytoplankton photosynthesis by ultraviolet radiation, *Science*, 258, 646-650, 1992.
- Dutton, E.G., and D.J. Endres, Date of snowmelt at Barrow, Alaska, U.S.A., *Arctic Alpine Res.*, 23(1), 115-119, 1991.
- Lubin, D., and J.E. Frederick, Column ozone measurements at Palmer Station, Antarctica: variations during the austral springs of 1988 and 1989, *J. Geophys. Res.*, 95, 13,883-13,889, 1990.
- Lubin, D., and J.E. Frederick, The ultraviolet radiation environment of the Antarctic Peninsula: the roles of ozone and cloud cover, *J. Appl. Meteorol.*, 30, 478-493, 1991.
- Lubin, D., and J.E. Frederick, Observations of ozone and cloud properties from NSF ultraviolet monitor measurements at Palmer Station, Antarctica, *Ant. J. U.S.*, 1989 Review, 25(5), 241-242, 1992.
- Lubin, D., J.E. Frederick, C.R. Booth, T.B. Lucas, and D.A. Neuschuler, Measurements of enhanced springtime ultraviolet radiation at Palmer Station, Antarctica, *Geophys. Res. Lett.*, 16(8), 783-785, 1989.
- Lubin, D., Mitchell, B.G., J.E. Frederick, A.D. Alberts, C.R. Booth, T. Lucas, D. Neuschuler, A contribution toward understanding the biospherical significance of Antarctic ozone depletion, *J. Geophys. Res.*, 97, 7817-7828, 1993.
- Madronich, S., UV Radiation in the Natural and Perturbed Atmosphere, in *UV-B Radiation and Ozone Depletion*, edited by M. Tevini, pp. 28-29, Lewis Publishers, Boca Raton, FL, 1993.
- Setlow, R. B. The wavelengths in sunlight effective in producing skin cancer: a theoretical analysis, *Proc., Nat. Acad. Sci.*, 71(9), 3363-3366, 1974.
- Smith, R., K. Baker, D. Menzies, and K. Waters, Biooptical measurements from the Ice Colors '90 cruise 5 October-21 November 1990, SIO Reference 91-13, 121 pp., Scripps Institution of Oceanography, San Diego, CA, 1991.
- Smith, R., B.B. Prezelin, R.R. Bidigare, D. Karentz, and S. Macintyre, Ice Colors '90: Ultraviolet radiation and phytoplankton biology in Antarctic waters, *Ant. J. U.S.*, in press, 1993.
- Smith, R. C., Z. Wan, and K. S. Baker, Ozone depletion in Antarctica: Satellite and ground measurements, and modeling under clear-sky conditions, *J. Geophys. Res.*, 97, 7383-7397, 1992a.
- Smith, R. C., B. B. Prezelin, K. S. Baker, R. R. Bidigare, N. P. Boucher, T. Coley, D. Karentz, S. MacIntyre, H. A. Matlick, D. Menzies, M. Ondrusek, Z. Wan, and K. J. Waters, Ozone depletion: Ultraviolet radiation and phytoplankton biology in Antarctic waters, *Science*, 256, 952-959, 1992b.
- Stamnes, K., J. Slusser, and M. Boden, Derivation of total ozone abundance and cloud effects from spectral irradiance measurements, *J. Appl. Optics*, 30, 4418-4426, 1991.
- Stamnes, K., J. Z. Jin, J. Slusser, C. Booth, and T. Lucas, Several-fold enhancement of biologically effective ultraviolet radiation levels at McMurdo Station, Antarctica, during the 1990 ozone hole, *Geophys. Res. Letters*, 19, 1013-1017, 1992.
- Stamnes, K., J. Slusser, M. Bowen, C. Booth, and T. Lucas, Biologically effective ultraviolet radiation, total ozone abundance, and cloud optical depth at McMurdo Station, Antarctica, September 15, 1988, through April 15, 1989, *Geophys. Res. Letters*, 17, 2181-2184, 1990.

Lidar Observations of Volcanic Aerosol Layers and Polar Stratospheric Clouds at South Pole, 1990, 1991, and 1992

M. CACCIANI, P. DI GIROLAMO, A. DI SARRA, G. FIOCCO, D. FUÀ, P. COLAGRANDE, AND G. PANEGROSSI
Universita "La Sapienza", Physics Department, 00185 Roma, Italy

INTRODUCTION

The Physics Department of the University of Rome "La Sapienza" has maintained a lidar at SPO since December 1987, mainly to study polar stratospheric clouds (PSCs) and aerosols in the antarctic stratosphere. The system is run by winterover personnel of NOAA and NSF.

During 1991 the eruptions of Mt. Pinatubo in the Philippines and of Mt. Hudson in Chile produced a substantial increase of the aerosol load in the polar stratosphere. Two well-separated layers could be identified in the lidar echoes: the lower layer, L, around 10 km and with a vertical extent of about 3 km; and the upper layer, U, characterized by a lower value of the backscattering coefficient between 17-26 km [Deshler *et al.*, 1992].

The height and time of appearance of layer L support its attribution to the eruptions of Mt. Hudson. Layer U can be attributed to the aerosol cloud generated by the eruptions of Mt. Pinatubo, although the identification of the arrival time of the layer is difficult because of the poor performance of the lidar during the critical period of the vortex break-up. Analyses of the integrated backscatter suggest that the Pinatubo cloud first reached the Antarctic stratosphere at altitudes higher than 17 km, and at lower altitudes only later. After that time, approaching winter, the total integrated backscatter, IB, remained approximately constant at all levels. An example of the vertical profiles of the aerosol-to-molecules backscattering ratio in 1991 is given in Figure 1 distinctly showing the two layers: the lower one centered around 10 km and the higher one extending between 16 and 28 km.

The change in the characteristic features of lidar echoes, particularly as a function of the atmospheric temperature, has been studied with the aim of identifying the formation

of PSCs, type I (NAT) and type II (ice) when, during winter, the conditions leading to the condensation of either HNO_3 or H_2O are reached.

MASS LOAD AND SEDIMENTATION OF PINATUBO AEROSOL

Under the assumption that the particles are homogeneous spheres, the backscattering efficiency, Q_{bs} , has been approximated by a linear function of the size parameter [Pinnick *et al.*, 1980] and used to relate the mass content per unit volume, M , to the backscattering coefficient regardless of its dependence on the particle-size distribution.

The aerosol mass load was computed combining the known values of the composition of sulfuric acid aerosol [Steele and Hamill, 1988], water vapor profiles measured in Antarctica [Rosen *et al.*, 1991], and the temperature profiles at South Pole. In a similar way the sulfuric acid content of the particles was estimated [Cacciani *et al.*, 1993].

The columnar aerosol mass evolution follows the total IB trend, increasing to a maximum value around 80 mg m^{-2} comparable to those reported by other authors at low- and mid-latitudes [Valero and Pilewski, 1992; Winker and Osborn, 1992; Gobbi *et al.*, 1992].

To establish if sedimentation of the particles takes place in the stratosphere, the height of the center of the mass of the sulfuric acid contained in the aerosol was compared to the height of the 100 mb and 50 mb surfaces during the period January-early June. An estimate of the height decrease of the air mass due to the diabatic cooling is given by the altitude of the 100 mb isobar; the descent is about 1 km between January and June. In fact, the center of mass is decreasing at a faster rate than the isobaric altitude during January and February, when changes in the aerosol vertical distribution occur that are attributable to the arrival of aerosol-rich air in the lowest layers.

POLAR STRATOSPHERIC CLOUDS

Analyses of PSC observations have been carried out for the winters of 1990 and 1992. The comparison shows differences attributable to the large amount of sulfuric acid aerosol of volcanic origin present in the polar stratosphere during 1992 and its effect on nucleation.

The evolution of the backscattering in the two cases shows a different character: larger echoes attributable to PSCs were recorded in 1992 compared to 1990. The differences in the intensity of the echoes is being

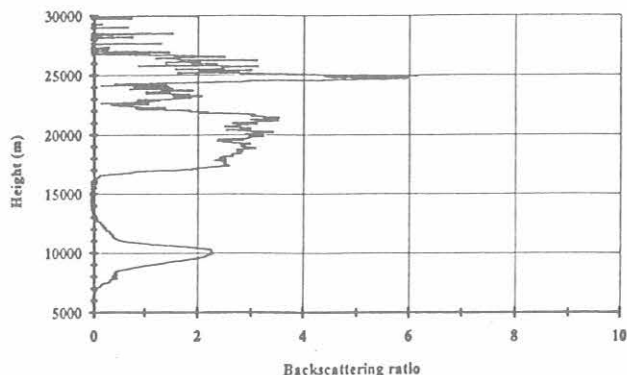


Fig. 1. The backscattering ratio profile for December 8, 1991.

interpreted as due to a large number of smaller particles present in PSCs in 1992 compared to those present in 1990.

An example of the vertical profile of the backscattering coefficient obtained in July is given in Figure 2 for 1990 and in Figure 3 for 1992.

Criteria to distinguish the echoes from PSCs from those due to the sulfuric acid aerosol and those due to type I PSCs from those due to type II, are being applied to the present set of data.

The sensitivity of the backscattering to temperature changes near the base of a PSC is amenable to a relatively

simple calculation [Fiocco *et al.*, 1991, 1992; Fuà *et al.*, 1992], in which this quantity can be related to the difference between the partial pressure of the condensing species. A more elaborate criterion is based on the use of a more complex model for aerosol formation.

REFERENCES

- Cacciani, M., P. Di Girolamo, A. di Sarra, G. Fiocco, and D. Fuà, Volcanic aerosol layers observed by lidar at South Pole, September 1991-June 1992, *Geophys. Res. Lett.*, *20*, 807-810, 1993.
- Deshler, T., A. Adriani, G.P. Gobbi, D.J. Hofman, G. Di Donfrancesco, and B.J. Johnson, Volcanic aerosol and ozone depletion within the antarctic polar vortex during the austral spring of 1991, *Geophys. Res. Lett.*, *19*, 1819-1822, 1992.
- Fiocco, G., D. Fuà, M. Cacciani, P. Di Girolamo, J. DeLuisi, On the temperature dependence of polar stratospheric clouds, *Geophys. Res. Lett.*, *97*, 5939-5946, 1991.
- Fiocco, G., M. Cacciani, P. Di Girolamo, D. Fuà, and J. DeLuisi, Stratospheric clouds at South Pole during 1988: I. Results of lidar observations and their relationship to temperature, *Geophys. Res. Lett.*, *97*, 5939-5946, 1992.
- Fuà, D., M. Cacciani, P. Di Girolamo, G. Fiocco, A. di Sarra, Stratospheric clouds at South Pole during 1988: II. Their evolution in relation to atmospheric structure and composition, *J. Geophys. Res.*, *97*, 5947-5952, 1992.
- Gobbi, G.P., F. Congeduti, and A. Adriani, Early stratospheric effects of the Pinatubo eruption, *Geophys. Res. Lett.*, *19*, 997-1000, 1992.
- Pinnick, R.G., S.G. Jennings, and P. Chylek, Relationship between extinction, absorption, backscattering, and mass content of sulfuric acid aerosols, *J. Geophys. Res.*, *85*, 4059-4066, 1980.
- Rosen, J.M., N.T. Kjome, and S.J. Oltmans, Balloon borne observations of backscatter, frost point, and ozone in polar stratospheric clouds at the South Pole, *Geophys. Res. Lett.*, *18*, 171-174, 1991.
- Steele, H.M., and P. Hamill, Effects of temperature and humidity on the growth and optical properties of sulfuric acid-water droplets in the stratosphere, *J. Aerosol Sci.*, *12*, 517-528, 1981.
- Valero, F.P., and P. Pilewskie, Latitudinal survey of spectral depths of the Pinatubo volcanic cloud-derived particle sizes, columnar mass loading, and effects on planetary albedo, *Geophys. Res. Lett.*, *19*, 163-166, 1992.
- Winker, D.M., and M.T. Osborn, Airborn lidar observation of the Pinatubo volcanic plume, *Geophys. Res. Lett.*, *19*, 167-170, 1992.

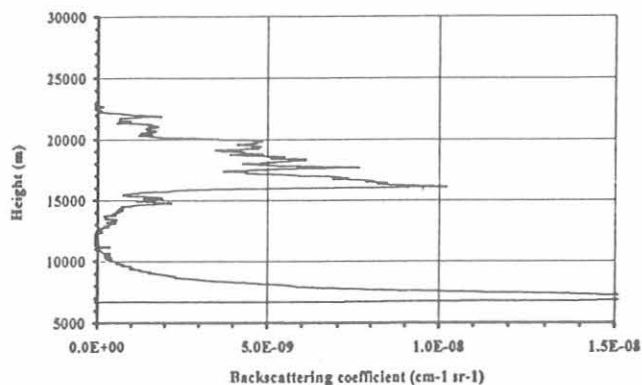


Fig. 2. The backscattering coefficient profile for July 3, 1990.

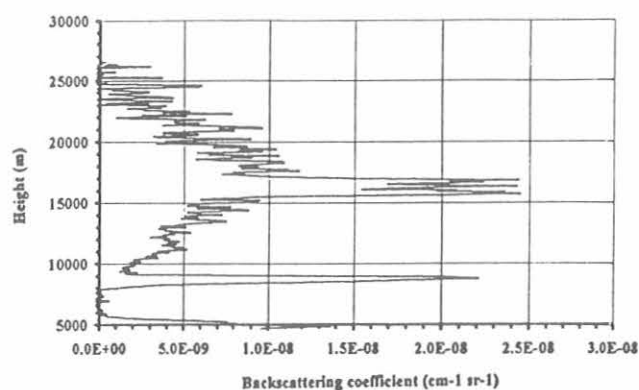


Fig. 3. The backscattering coefficient profile for July 17, 1992.

Fine Sulfur Concentrations at the Mauna Loa Observatory and Other Hawaiian Sites

THOMAS A. CAHILL

Air Quality Group, Crocker Nuclear Laboratory and Department of Land, Air, and Water Resources, University of California, Davis 95616

Fine aerosol mass and its components, including sulfur (= sulfate) aerosols, have been collected (Wednesday, Saturday) and analyzed at the Kilauea site of Hawaii Volcanoes National Park since fall 1986. This was a component of the National Park Service's fine aerosol network concerned with visibility degradation at national parks and monuments. In 1988 this formed the foundation of the Interagency Monitoring of Protected Visual Environments (IMPROVE) program, with the same mission but expanded scope, now operating at 57 sites in the United States. In 1990 sites were added at Haleakala National Park on Maui and at the Mauna Loa Observatory (MLO) on Hawaii, partly to better understand the effect of the continuously erupting volcano on the Hawaii Volcanoes data set. The data have also given a rare opportunity for a statistically significant fine aerosol data set in a mid ocean site as a function of elevation above sea level, with potential use in the aerosol forcing term of global climate models.

The aerosols are collected for a 24-hour period each Wednesday and Saturday at Hawaii Volcanoes and Haleakala parks at elevations of 1240 m and 1150 m above sea level, respectively. The samples from MLO (3380 m) are also collected twice a week, but the samplers operate on different time schedules. One operates continuously giving 3-day (Monday-Thursday) and 4-day (Thursday-Monday) samples (MALO1), while the other operates in the same manner but only for hours between 2200 and 0600, thus generally dominated by downslope winds (MALO2). Each sampler is the standard 22-L min⁻¹. IMPROVE 2.5 μm D(p) cyclone sampler with no pre-treatment of the air stream. Particles are collected on stretched Teflon filters with supporting plastic rings. In addition, at Hawaii Volcanoes and Haleakala National Park, the full IMPROVE array is present including a nylon filter following an acidic gas/vapor denuder [Eldred *et al.*, 1988]. The nylon filter is analyzed by ion chromatography for sulfates, nitrates, and chlorides, while the Teflon filters are analyzed for fine mass, hydrogen for organic, Na and heavier by PIXE and PESA [Cahill *et al.* 1990]. Sensitivity for transition metals is roughly 0.02 ng m⁻³, while for heavy metals it rises to roughly 0.06 ng m⁻³ [Cahill *et al.*, 1992].

While all collection and analysis protocols adhere to published quality control procedures, the IMPROVE network is designed to exploit ways to ensure knowledge of both precision and accuracy through our concept of "integral redundancy." In this concept, most major species are measured by two independent methods on two fully independent samplers operating side by side, with analysis on different substrates at different laboratories. For the

situation of sulfur, we can make measurements of sulfur by PIXE on Teflon in channel A which, when multiplied by 3.0, should equal the results of sulfate analyses by ion chromatography on nylon filters in channel B. Figure 1 shows this comparison for all western U.S. sites, excepting those in California but including all three Hawaiian sites, for summer 1992. The excellent agreement is not only proof that all samplers are operating properly, including flow rates, timing, etc., but that the sulfur present is consistent with sulfate. Similar redundancies are done for gravimetric fine mass versus the sum of all species, and organic matter by two very different techniques, from carbon analysis off quartz filters by combustion in channel C versus hydrogen by PESA from Teflon in channel A [Cahill *et al.*, 1990]. However, note that only channel A was operated at MLO so that quality assurance tests such as these at lower elevations must be extrapolated to this site.

An example of the type of data generated quarterly (and available to any user) is shown in Tables 1, 2, and 3 for the MLO downwind sampler. All values are in ng m⁻³ except mass which is in μg m⁻³. The term "KNON" means

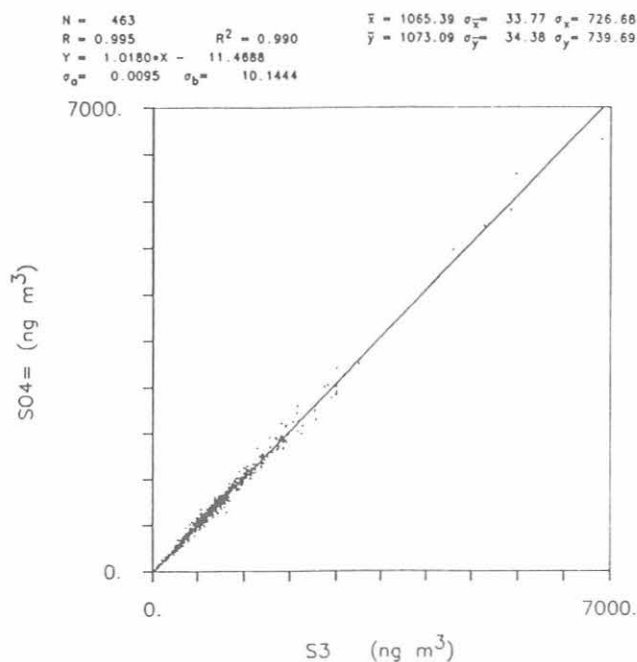


Fig. 1. Sulfur (from PIXE) versus sulfate (from ion chromatography) from IMPROVE western sites, summer 1992. IMPROVE sites in California have been deleted from this comparison, but all Hawaiian sites are included.

TABLE 1. 24-Hour Concentrations (ng m⁻³) of Major Elements, and Tracer Elements from the IMPROVE Particulate Network, June 1, 1993-August 31, 1992, at 0000 LST

Date	H	S	Mass†	Soil Elements						Smoke	Marine	Metallic Tracers							
				SI	K	CA	TI	MN	FE	KNON	NA	V	NI	CU	ZN	AS	SE	BR	PB
June 03	26.9	60.9	0.79	35.2	7.5	11.4	0.8	*0.2	10.0	1.5	*6.84	*0.26	*0.03	0.17	0.34	*0.02	0.03	0.23	0.12
June 06	33.0	76.7	0.73	61.9	12.5	20.6	1.8	0.6	16.8	2.4	*9.43	*0.35	*0.04	*0.04	0.32	*0.02	0.03	0.25	0.19
June 10	19.8	48.6	0.58	13.5	3.9	4.0	*0.3	*0.2	3.5	1.8	48.90	*0.27	*0.03	*0.03	0.11	*0.02	*0.02	0.09	0.06
June 13	32.6	70.0	0.68	39.4	7.1	11.2	1.0	0.9	10.4	0.9	74.90	0.37	*0.04	0.33	0.30	*0.02	0.05	0.13	0.25
June 17	19.4	61.0	0.75	27.4	5.8	9.3	0.5	0.2	8.2	0.9	*6.42	*0.24	*0.03	0.22	0.29	0.03	0.03	0.11	0.09
June 20	30.4	54.2	0.85	44.5	9.8	17.5	1.1	*0.2	14.3	1.3	34.50	*0.31	*0.04	0.06	0.25	*0.02	*0.02	0.14	0.14
June 24	25.0	59.6	0.82	41.5	8.5	14.9	1.0	0.3	12.4	1.0	22.60	*0.22	*0.03	*0.03	0.19	*0.02	0.03	0.17	0.12
June 27	17.2	47.5	0.44	13.8	2.8	3.1	0.6	0.5	2.9	1.1	45.20	0.52	*0.04	*0.04	0.20	*0.02	0.04	0.07	0.08
July 01	17.6	36.6	0.41	9.8	2.1	3.3	0.6	0.2	2.5	0.5	*5.47	*0.22	*0.03	*0.03	0.17	*0.02	*0.02	0.07	0.07
July 04	40.0	73.2	0.63	12.3	2.1	2.5	0.4	*0.2	2.6	0.6	58.00	*0.28	*0.04	*0.04	0.25	*0.02	0.04	0.13	0.11
July 08	28.7	73.1	0.78	11.8	3.0	3.3	0.3	*0.1	3.9	0.7	*4.67	0.28	*0.02	*0.03	0.18	*0.02	0.03	0.12	0.08
July 11	28.0	77.8	0.51	9.9	2.2	2.6	0.6	*0.2	2.5	0.7	31.70	*0.26	*0.04	0.13	0.51	*0.02	*0.02	0.11	0.10
July 15	40.0	105.0	0.95	35.5	9.6	9.1	0.6	0.5	11.2	2.9	61.50	*0.25	*0.03	0.39	0.56	*0.02	0.04	0.14	0.32
July 18	28.4	63.7	0.32	7.8	2.2	2.7	0.6	*0.2	1.6	1.2	87.10	*0.29	*0.04	0.22	0.26	*0.02	*0.02	0.11	0.09
July 22	29.4	103.0	0.72	4.6	1.9	0.7	0.3	0.2	0.9	1.3	53.20	0.53	*0.03	*0.03	0.12	*0.02	0.05	0.07	0.07
July 25	19.5	51.1	0.76	11.0	3.4	3.0	0.6	*0.2	3.2	1.5	54.50	*0.28	*0.04	0.06	0.24	*0.02	0.04	0.13	0.11
July 29	35.5	115.0	0.94	18.5	4.6	5.5	0.4	*0.2	5.3	1.4	48.20	*0.24	*0.03	0.19	0.15	0.07	0.06	0.09	*0.07
Aug. 01	16.6	68.2	1.12	17.1	4.9	6.6	1.0	0.4	5.0	1.9	88.80	0.51	*0.04	0.12	0.18	*0.02	*0.02	0.14	0.08
Aug. 05	25.8	76.7	0.72	6.6	1.6	1.1	0.2	0.2	1.2	0.9	29.90	*0.19	*0.03	0.08	0.25	0.05	0.03	0.10	*0.07
Aug. 08	56.3	219.0	1.13	6.0	1.4	1.1	0.4	*0.2	0.5	1.1	54.40	0.31	*0.04	0.31	0.29	*0.02	0.08	0.09	0.06
Aug. 12	15.4	43.1	0.44	2.6	2.5	0.4	0.5	*0.2	0.6	2.2	48.70	0.32	*0.03	*0.03	0.04	*0.02	0.02	0.03	0.09
Aug. 15	17.0	47.0	0.29	4.4	2.2	1.4	*0.4	*0.2	1.0	1.6	69.80	0.55	*0.04	*0.04	0.23	*0.02	0.04	0.06	0.05
Aug. 19	25.9	86.0	0.56	5.0	2.0	0.3	0.5	0.3	1.7	1.0	60.60	0.42	0.12	*0.03	0.12	*0.02	0.04	0.09	0.09
Aug. 22	29.2	80.1	0.51	4.6	1.5	1.0	*0.3	0.3	0.8	1.0	72.90	0.43	*0.04	0.06	0.16	*0.02	*0.02	0.13	0.06
Aug. 26	16.8	56.5	0.59	3.3	2.8	0.8	1.3	0.4	1.3	2.0	71.50	*0.23	*0.03	*0.03	0.18	*0.02	0.03	0.14	0.07
Aug. 29	51.1	152.0	1.16	9.3	2.9	2.1	0.4	0.2	2.7	1.3	66.90	*0.26	*0.04	*0.04	0.23	*0.02	*0.02	0.18	0.12

*Analytical minimum detectable limit (mdl).

†Mass in micrograms m⁻³

TABLE 2. Distribution of Concentrations (ng m⁻³) From the IMPROVE Particulate Network, June 1, 1992-August 31, 1992

	Cases	% of Cases Significant	Arithmetic Mean	Minimum	Median	Maximum	Maximum Occurs
H	26	100%	27.90	15.40	27.50	56.30	Aug. 08
S	26	100%	77.10	36.60	69.10	219.00	Aug. 08
SI	26	100%	17.60	2.57	11.40	61.90	June 06
K	26	100%	4.26	1.45	2.84	12.50	June 06
CA	26	100%	5.36	0.30	3.04	20.60	June 06
TI	26	88%	0.62	0.20	0.54	1.78	June 06
MN	26	53%	0.26?	0.13	0.24?	0.90	June 13
FE	26	100%	4.89	0.52	2.79	16.80	June 06
KNON	26	73%	1.32	0.54	1.25	2.91	July 15
NA	26	80%	46.20	4.67	51.10	88.80	Aug. 01
V	26	38%	0.24?	0.19	0.28?	0.55	Aug. 15
NI	26	3%	0.02?	0.02	0.04?	0.12	Aug. 19
CU	26	50%	0.10?	0.03	0.05?	0.39	July 15
ZN	26	100%	0.23	0.04	0.23	0.56	July 15
AS	26	11%	0.01?	0.02	0.02?	0.07	July 29
SE	26	69%	0.03	0.02	0.03	0.08	Aug. 08
BR	26	100%	0.12	0.03	0.11	0.25	June 06
PB	26	92%	0.10	0.05	0.09	0.32	July 15

A significant value is greater than 2 times the uncertainty of that value.

? = The percentage of significant values is less than 65%

KNON is nonsoil potassium, a qualitative smoke tracer, K - 0.6 Fe

TABLE 3. Distribution of Concentrations (µg m⁻³) and Percent of Fine Mass From the Improve Particulate Network, June 1, 1992 - August 31, 1992

	Cases	% of Cases Significant	Arithmetic Mean	Minimum	Median	Maximum	Maximum Occurs
MASS	26	100%	0.70	0.29	0.72	1.16	Aug. 29
RCMA	26	100%	0.66	0.33	0.61	1.16	Aug. 08
NHSO	26	100%	0.32	0.15	0.28	0.90	Aug. 08
NHSO%	26	100%	47%	25%	43%	83%	July 18
OMH	26	69%	0.12	-0.01	0.11	0.30	July 04
OMH%	26	61%	19%?	0%	17%?	54%	July 18
SOIL	26	100%	0.08	0.01	0.05	0.28	June 06
SOIL%	26	100%	11%	2%	8%	39%	June 06
BABS	26	73%	0.61	0.16	0.56	1.51	Aug. 08

A significant value is greater than 2 times the uncertainty of that value.

? = The percentage of significant values is less than 65%

NHSO	ammonium sulfate, (NH ₄) ₂ SO ₂	standard form of sulfate, sulfur times 4.125
SOIL	soil	sum of Al, Si, K, CA, Ti, Fe and oxides
OMH	organic mass by hydrogen	13.75 (H - S/4)
RCMA	reconstructed mass	sulfate+soil+OMH+BABS/2, but not nitrate

potassium not associated with soil, an excellent tracer of smoke from biomass. These values are very low, almost all within the uncertainty, showing essentially no smoke impact on the down-slope winds. The "all hours" sampler at the site, MALO1, occasionally shows heavy smoke impacts that could well reflect agricultural burning on the island. Formulas for the derived quantities (NHSO =

ammonium sulfate, OMH = organic matter from hydrogen, etc.) are explained on the bottom of Table 3. BABS is b(absorption) from the integrating plate method, in units of 10⁻⁶ m⁻¹. The most important of these is RCMA, reconstructed mass as the sum of all measured species. This should be close to, but somewhat less than, MASS, the gravimetric fine mass from weighing the Teflon filter. The

difference appears to be overwhelmingly water, since the filters are weighed in air but the analyses are done in hard vacuum, thus drying the filters.

In the analyses that follow, the median value was used as opposed to the mean, due to the extremely non-log normal distributions seen at Hawaii Volcanoes National Park. This is due to the occasional arrival of the plume of the ongoing eruption, which gives sharp spikes to the data not only for sulfur but selenium and other volcanic trace elements. At the Mauna Loa sites, this is not a problem and the median is close to the mean (0.70 versus $0.72 \mu\text{g m}^{-3}$, summer 1992).

Figures 2a, b, c, and d show the seasonal trends for sulfur (= sulfate) at all four sites for the period of record. No statistically significant trends can be seen in the annual values, but clear seasonal shifts are seen in the MALO2 (downwind) data. Since this is so, the last two years were

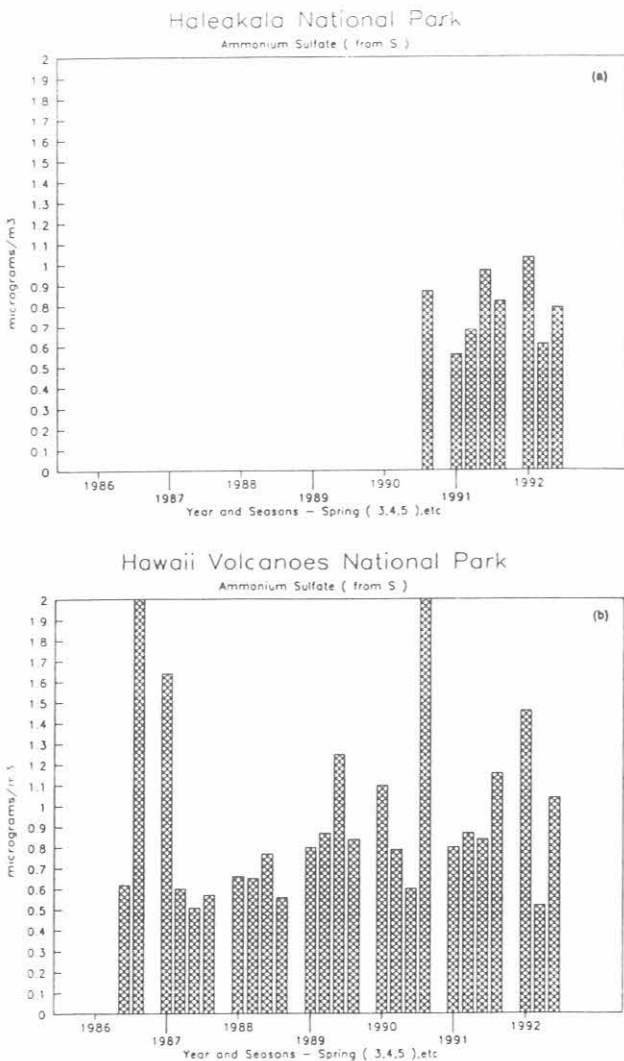


Fig. 2. Ammonium sulfate (from PIXE S times 4.125) at Haleakala National Park (a), and from Hawaii Volcanoes (b).

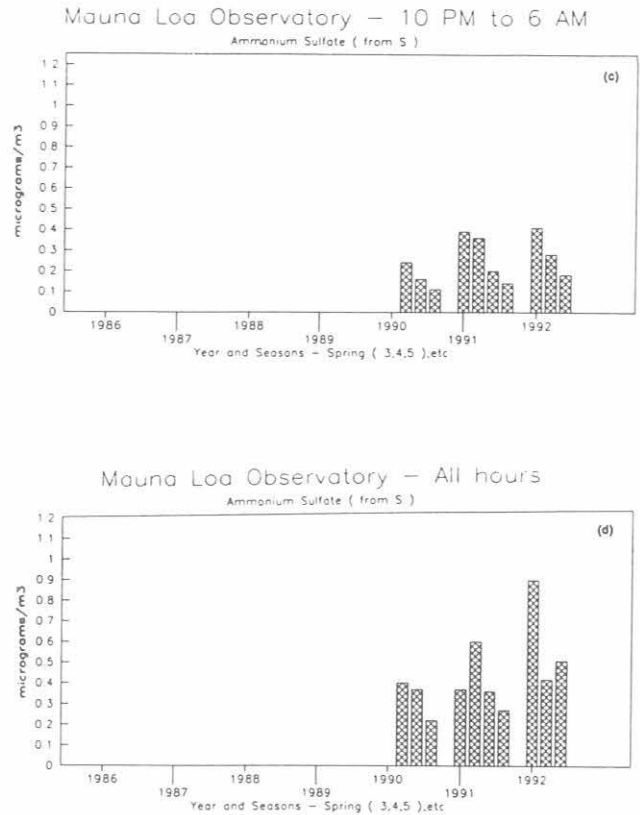


Fig. 2. Continued - Ammonium sulfate (from PIXE S times 4.125) at Mauna Loa Observatory - downwind (c), and all hours (d).

aggregated and provide the data for Table 4. There is a good deal of information in Table 4 that is going to require further analysis before it is fully understood. But the first point is the similarity between Hawaii Volcanoes and Haleakala National Parks. This was not expected due to the volcanic activity at Hawaii Volcanoes, but a closer inspection of the records show that there were few plume impacts on the site and thus did not influence the median for these two seasons. The situation was very different in winter when Hawaii volcanoes had numerous plume impacts and well elevated levels of sulfur, selenium, and other elements.

Thus we can use the summer and fall data to obtain a measurement of the vertical gradient of sulfur. This can be enhanced by deriving the "upslope" sulfur value at MALO1 by subtracting the data of MALO2 (Table 5). One can then assign an approximate "altitude" for the source of these aerosols almost all of which lie at elevations below that of MLO. The surprising consistency of the two NPS sites and the "upslope" MALO1 values gives us some confidence that an average value could represent the aerosol column from sea level to 3380 m. There then appears to be a sharp discontinuity to the MALO2 "downslope" aerosols with a ratio near 2.24 ± 0.02 spring and summer and 5.0 ± 0.6 fall and winter. Thus at this site, clear summer/winter

TABLE 4. Fine Ammonium Sulfate(S × 4.125) Winter 1990 to Fall 1992

	Hawaii Volcanoes National Park (elev. 1240 m)		Haleakala National Park (elev. 1150 m)		Mauna Loa All hours (elev. 3380 m)		Mauna Loa 2200 to 0600 (elev. 3380 m)	
	Conc. ($\mu\text{g m}^{-3}$)	% Mass	Conc. ($\mu\text{g m}^{-3}$)	% Mass	Conc. ($\mu\text{g m}^{-3}$)	% Mass	Conc. ($\mu\text{g m}^{-3}$)	% Mass
Spring	1.13 ± 0.33	43.5 ± 6.5	0.795 ± 0.23	26.0 ± 2.0	0.635 ± 0.27	38.5 ± 7.5	0.400 ± 0.01	23.5 ± 0.5
Summer	0.70 ± 0.17	35.0 ± 2.0	0.65 ± 0.03	24.5 ± 4.5	0.51 ± 0.09	52.5 ± 3.5	0.29 ± 0.05	30.0 ± 11.0
Fall	0.94 ± 0.10	46.5 ± 1.5	0.88 ± 0.09	32.5 ± 4.5	0.44 ± 0.07	51.5 ± 0.5	0.18 ± 0.02	34.3 ± 10.2
Winter	2.78 ± 1.61	50.5 ± 2.5	0.85 ± 0.02	28.5 ± 0.5	0.25 ± 0.02	40.5 ± 7.5	0.13 ± 0.02	22.0 ± 5.0
Spring	1.31 ± 0.38		0.91 ± 0.29		0.99 ± 0.52		0.77 ± 0.02	
Summer	0.81 ± 0.20		0.80 ± 0.03		0.80 ± 0.17		0.56 ± 0.09	
Fall	1.17 ± 0.12		1.08 ± 0.11		0.85 ± 0.14		0.34 ± 0.05	
Winter	3.22 ± 2.01		1.05 ± 0.02		0.49 ± 0.05		0.25 ± 0.05	

The top half of the table presents the data as $\mu\text{g m}^{-3}$ at altitude, the standard IMPROVE protocol for visibility correlations. The bottom half of the table presents the data corrected for the pressure differential to sea level (i.e., NTP).

Spring = March, April, and May

Summer = June, July, and August

Fall = September, October, and November

Winter = December, January, and February

TABLE 5. Vertical Profiles of Ammonium Sulfate Aerosols (Hawaiian Sites Winter 1990 to Fall 1992)

Season	Hawaii Volcanoes	Haleakala National Park	Mauna Loa (Up)	Average	Mauna Loa (Down)	Ratio
Spring	1.13	0.80	0.75	0.89 ± 0.17	0.40	2.23
Summer	0.70	0.65	0.62	0.66 ± 0.03	0.29	2.26
Fall	0.94	0.88	0.56	0.79 ± 0.17	0.18	4.41
Winter	2.78*	0.85	0.62	0.73 ± 0.12	0.13	5.60
Spring	1.31	0.91	1.17	1.13 ± 0.17	0.77	1.47
Summer	0.81	0.80	0.97	0.86 ± 0.08	0.56	1.54
Fall	1.17	1.08	1.08	1.11 ± 0.04	0.34	3.26
Winter	3.22*	1.05	1.24	1.14 ± 0.09	0.25	4.56

The top half of the table presents the data as $\mu\text{g m}^{-3}$ at altitude, the standard IMPROVE protocol for visibility correlations. The bottom half of the table presents the data corrected for the pressure differential to sea level (i.e., NTP).

* Note: Deleted winter, Hawaii Volcanoes, in averaging

Spring = March, April, and May

Summer = June, July, and August

Fall = September, October, and November

Winter = December, January, and February

differences appear due mainly to changes in the upper tropospheric aerosols, not the boundary layer aerosols.

In summary, we are beginning to obtain a statistically significant data set at MLO to match the data sets at unpolluted (at least, not anthropogenic pollution) sites at lower elevations. Based on the strong trade winds at the Hawaii Volcanoes and Haleakala

sites, these sites are sampling aerosols characteristic of the planetary boundary layer and, as such, represent all elevations from 0 to about 3380 m. Since the sites are well removed from the coast and since coarse particles are removed in sampling, these data then give an estimate of the sulfate column in the atmosphere on and over the Pacific Ocean.

Acknowledgments. I wish to thank the operators at the Mauna Loa and Park Service sites for excellent reliability and data quality that makes analysis and interpretation easy. I also wish to thank all members of the Air Quality Group for outstanding support in filter analysis and data handling.

REFERENCES

Cahill, T.A., R.A. Eldred, K. Wilkinson, W.C. Malm, M. Pitchford, and R. Fisher, Spatial and temporal trends of fine particles on a continental scale: First results of the U.S. IMPROVE network,

Aerosols, Proceedings of the third International Aerosol Conference, Kyoto, Japan, September 24-27, S. Masuda and K. Takahashi, (eds.), Vol. 2, 1105-1108, 1990.

Cahill, T.A., K. Wilkinson, and R. Schnell, Composition analyses of size-resolved aerosol samples taken from aircraft downwind of Kuwait, Spring, 1991, *J. Geophys. Res.*, 97(D13), 14,513-14,520, 1992.

Eldred, R.A., T.A. Cahill, M. Pitchford, and W.C. Malm, IMPROVE—a new remote area particulate monitoring system for visibility studies, *Proceedings of the Air Pollution Control Association 81st Annual Meeting*, Dallas, TX, June 19-24, 1988.

Artificial Windshielding of Precipitation Gauges in the Arctic

GEORGE P. CLAGETT

Soil Conservation Service, Anchorage, Alaska 99508

1. INTRODUCTION

Precipitation gauges can provide good measurements of the water equivalent of snow precipitation, provided the gauge is protected or shielded from wind effects. Unfortunately, there are no standards for collecting snow precipitation. Gauges located in exposed and windy areas may be totally unshielded, partially shielded by one or more buildings, or equipped with one of several types of artificial shields. The various shielding options in common use, therefore, produce a wide range of gauge catch efficiency. Also, the various studies of artificial shields in the United States and Canada have produced a wide range of results. This must be, in part, due to the wide range of weather conditions under which the various studies have been conducted. A lingering problem is applying the results to the local conditions of Alaska's tundra regions.

2. METHODS

A study of the windshield alternatives, under the unique conditions of Alaska's Arctic coastal region, was set up at the CMDL facility at BRW during September 1989. Snowfall catches from four newly installed precipitation storage gauges were compared with that from an existing storage gauge protected by a Wyoming shield [Hanson, 1988]. Two of the new gauges were shielded—one with a Nipher shield [Goodison *et al.*, 1983] and the other with an Alter shield [Alter, 1937]—and two were unshielded. One of the unshielded gauges was serviced on an event basis, the same as the three shielded gauges. The other unshielded gauge was treated as if it were a remote gauge, allowing rime to build up and dissipate naturally to see what effects rime had on the overall catch. The four newly installed gauges are 20.3 cm in diameter \times 100 cm tall, mounted with the orifice 2 m above the normal ground surface. The existing Wyoming-shielded gauge is 30.5 cm in diameter \times 2 m tall, and is equipped with a Leupold-Stevens water-level recorder.

3. RESULTS

Provisional results from the September 1, 1992, to June 2, 1993, winter season indicate that the Wyoming-shielded gauge provided 13.0 cm of snowfall water-equivalent catch. The Nipher-shielded gauge caught exactly the same amount over the same period. The Alter-shielded gauge caught 5.2 cm or 40% of the Wyoming-shielded gauge. The unshielded but serviced gauge caught only 1.8 cm of water-equivalent snowfall which was barely over 14% of that of the Wyoming-shielded gauge. The unshielded and non-serviced gauge did slightly better, catching 2.3 cm water-equivalent, or nearly 18% of the snowfall caught by the Wyoming-shielded gauge.

These results are right in the ballpark of expectations: the Wyoming and Nipher shields are expected to have very similar catches; the Alter-shielded catch drops off substantially; and a non-shielded gauge catch should drop off even substantially more at exposed and windy locations during snowfall events.

Acknowledgment. Appreciation is expressed to D. Endres, Station Chief, BRW, who serviced the precipitation gauges and collected the snow samples.

4. REFERENCES

- Alter, S.C., Shield storage precipitation gauges, *Mon. Weather Rev.*, 65, 262-265, 1937.
- Goodison, B.E., V.R. Turner, and J.E. Metcalfe, A nipher-type shield for recording precipitation gauges, *Proceedings, 5th Symposium on Meteorological Observations and Instrumentation*, Toronto, Ontario, Canada, pp. 2-126, American Meteorological Society, Boston, 1983.
- Hanson, C.L., Precipitation measured by gages protected by the Wyoming shield and the dual-gauge system, *Proceedings, 56th Western Snow Conference*, Kalispell, Montana, pp. 174-177, Colorado State University, Fort Collins, CO, 1988.

A Comparison of Aerosol Size Distributions and Nephelometer Measurements at Mauna Loa Observatory

ANTONY CLARKE

University of Hawaii, Department of Oceanography, Honolulu, Hawaii 96822

BARRY BODHAINE

NOAA CMDL, Boulder, Colorado 80303

1. INTRODUCTION

Mauna Loa Observatory (MLO) has maintained a long term and near continuous record of aerosol light scattering since 1974 [Bodhaine, 1983; Massey *et al.*, 1987]. The existing four-wavelength instrument allows for assessment of both the scattering coefficient, σ_{sp} , at four wavelengths and some inference of the aerosol size distribution through the parameter alpha [$\sigma_{sp}(\lambda) = K/\lambda^{-\alpha}$]. This data has been valuable in providing information on aerosol properties in the remote troposphere and their optical effects [Clarke and Charlson, 1985; Bodhaine *et al.*; 1992]. Because of this record and the accessibility of remote tropospheric air at MLO, this site was selected for aerosol measurements in support of the NASA Laser Atmospheric Wind Sounder program. One objective of this program was the assessment of the relationship of lidar backscatter to measured aerosol size distributions [Clarke and Porter, 1991]. A second objective was to examine the relationship of aerosol size distributions to the nephelometer record in order to see if the latter could be used as a surrogate measurement of the aerosol size distribution. If so, the long nephelometer record at MLO could be used to infer an aerosol climatology for the Pacific mid-troposphere. More recently, questions regarding the link of aerosol sulfate to scattering extinction in the atmosphere [Charlson *et al.*, 1991] prompted us to examine the relationship of the aerosol size distribution and σ_{sp} at MLO in order to assess the mass scattering efficiency for sulfate in the free troposphere.

Here, we report the results of these comparisons. One key observation is that changes in aerosol concentration of 1 to 2 orders of magnitude between upslope and downslope flow coupled with the long averaging time used for the nephelometer (about 1 hour) can prevent σ_{sp} from achieving the minimum representative downslope values. This often results in both hourly and mean nightly downslope σ_{sp} values that are several times greater than they should be and thereby posing a difficulty for direct comparison of σ_{sp} with other MLO data sets.

2. OBSERVATIONS

Aerosol heated to 40, 150, and 300°C and sized with a laser optical particle counter (OPC) was used to assess the size distribution (0.15-7.0 μm) of sulfuric acid, ammonium

sulfate and refractory (dust) components of the aerosol at MLO during January-March 1988 [Clarke and Porter, 1991]. During the downslope conditions of interest here the fine volume with diameters below 1 μm were primarily sulfate while the coarse volume tended to be refractory aerosol (remaining at 300°C) and probably dust. The few periods of high relative humidity were deleted in order to avoid σ_{sp} values that might reflect growth through water uptake rather than changes in aerosol sulfate. The refractory component remaining at 300°C was present at all sizes but was a small component of the total, and dust present in the submicrometer fraction appeared to be heavily coated with a sulfate shell.

Figure 1 shows the fine, coarse, and total volumes plotted against the corresponding nephelometer data during downslope conditions. These data usually represent the two cleanest 3-hour averages during each night and these generally occurred between 2200 and 0800 LST. The strongest relationship is evident between the fine aerosol

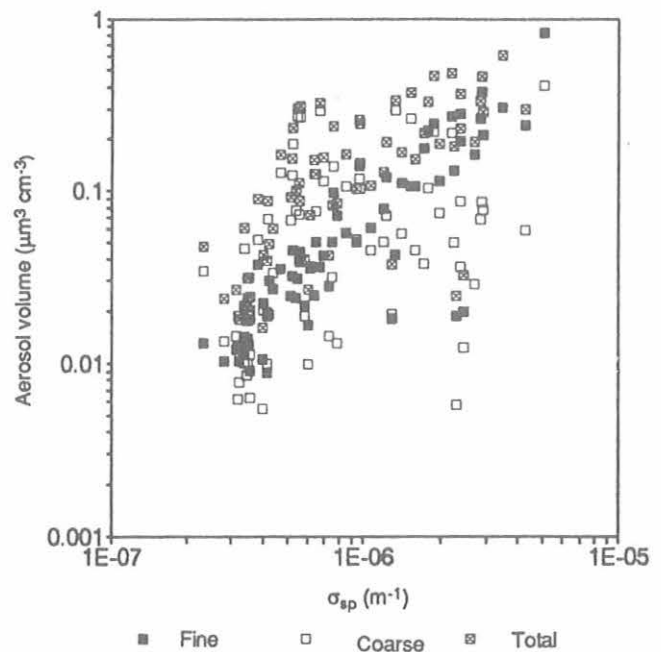


Fig. 1. A plot of fine (0.14 < D_p < 0.6 μm), coarse (0.6 < D_p < 7.0 μm) and total aerosol volume versus σ_{sp} for 3-hour nightly downslope minimum periods for DOY 16-86 1988.

volume and σ_{sp} as evidenced by the least scatter of the data points for this fraction. Similar behavior was also evident for upslope data (not shown). This measurement period includes times of episodic transport from Asia and it is common to observe three orders of magnitude change in both volume and scattering during this period. It is significant to note that during periods of highest σ_{sp} both fine particle sulfate and coarse particles are high. This is consistent with prior evidence for an anthropogenic source of pollutant aerosol that is coincident with periods of dust transport to MLO [Clarke and Charlson, 1985].

Examination of Figure 1 indicates that a measured fine (or total) particle volume may be associated with several values of σ_{sp} . Coincident 3-hour averages were plotted for σ_{sp} and the fine, coarse, and total volumes in order to make a direct comparison of these data. An example of several consecutive days are shown in Figure 2. A clear upslope/downslope signal is evident in both data but closer examination reveals that the transition to low aerosol volume occurs in the OPC data shortly after downslope flow has begun while the light scattering values decrease only gradually during the night to reach minimum values just before upslope recurs.

This delayed response is a consequence of the above mentioned long averaging time of the nephelometer and the large dynamic range often present between upslope and downslope flow. This is clearly evident for the case shown in Figure 3 where DOY 80 having moderate upslope aerosol is followed by DOY 81 with weak upslope aerosol. Here the optical particle counter (OPC) data reveals that downslope aerosol concentration for both nights are similar while the corresponding σ_{sp} values (see circled pairs) differ by a factor of about 5. In fact, the slope of the σ_{sp} data does not approach the slope in the aerosol volume data until about 1800 hr (GMT) on DOY 81, about 36 hours after the upslope peak on DOY 80. (The σ_{sp} value just before DOY 82 is a zero test.) This reveals that an

unbiased comparison of σ_{sp} with the aerosol mass from which the σ_{sp} signal is derived is only possible for about 3 hours out of the 48 shown. Moreover, this is only possible because the upslope aerosol on DOY 81 was little enhanced above free troposphere values.

The above observations have significant impact upon attempts to relate the optical scattering of the aerosol to aerosol properties at MLO. This is illustrated through our attempt to establish the specific scattering coefficient for sulfate (scattering coefficient divided by the mass concentration - σ_{sp}/M) in the clean free troposphere since this is a quantity of some significance to the assessment of sulfur emissions upon climate [Charlson et al., 1991]. Here we will examine data during the "clean" part of the year at MLO during the Mauna Loa Aerosol Backscatter Intercomparison Experiment (MABIE) carried out in November of 1988. As indicated in Figure 1, fine particle sulfate is the major contributor to σ_{sp} . However, because of the concerns mentioned above, we used only edited time periods when the nephelometer was stable and unperturbed by significant previous upslope aerosol. The result is shown in Figure 4a. In order to convert the predominantly sulfuric acid aerosol volume to mass, we have used our laboratory derived diameter correction (division by 1.1) due to the uptake of water at the typical downslope OPC relative humidity of 10% at MLO and employed a density of 1.8 g cm^{-3} to the resulting volume. A strong correlation ($r^2 = 0.9$) is evident between fine particle sulfate and σ_{sp} at 550 nm although the intercept does not go through zero. This is because some aerosol mass is present below the lower limit of detection of the OPC at $0.15 \mu\text{m}$ resulting in some scattering extinction due to fine particle mass not observed by the OPC. Because σ_{sp}/M decreases rapidly for decreasing size below $0.3 \mu\text{m}$ and because the mass mean diameter tends to increase with concentration, the relative contribution to σ_{sp} from these smaller aerosol decreases rapidly as concentrations increase. Moreover, the slope of

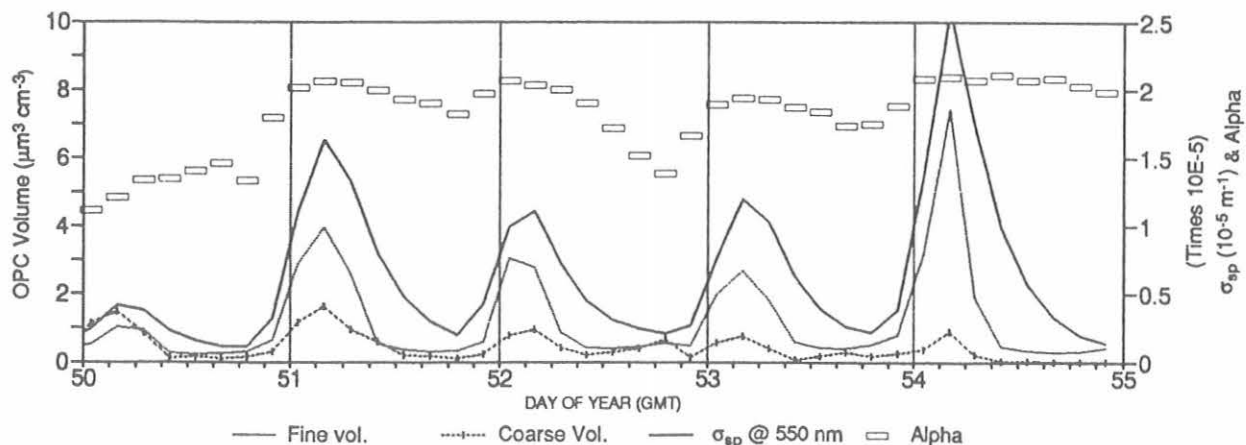


Fig. 2. Time series of 3-hour averaged values for fine and coarse aerosol volume, σ_{sp} at 550 nm and alpha for period with moderate daily upslope flow. Note slow decay of σ_{sp} signal and alpha compared to fine particle mass.

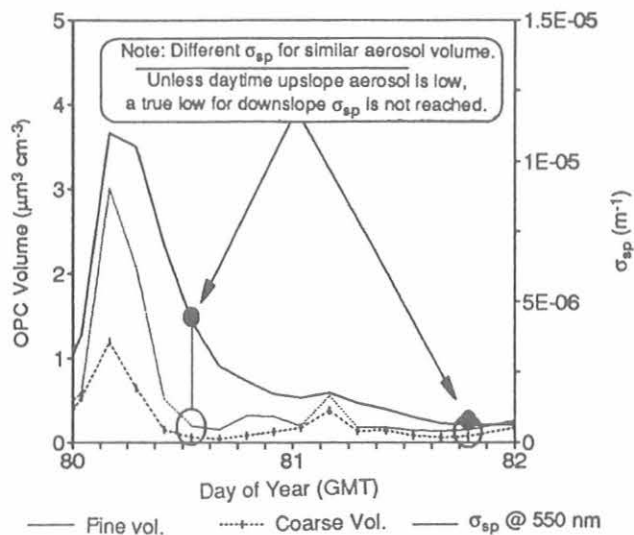


Fig. 3. Time series for DOY 81-82 as per Figure 2 showing the gradual decay of σ_{sp} values over a 2-day period when the intervening upslope perturbation is weak.

the regression line can be used to determine the σ_{sp}/M for the aerosol resulting in a value of about $5.6 \text{ m}^2/\text{g}$. Given the 20% estimated uncertainty in the OPC measurement, this tends to support the value of $5.0 \text{ m}^2/\text{g}$ recently suggested [Charlson *et al.*, 1991] for the remote troposphere.

In contrast to the above edited data, Figure 4b shows the data for downslope conditions between about 2200 and 0600 LST, similar to times often used for filter sampling for aerosol chemistry (e.g., sulfate). Note that the "best fit" regression line from Figure 4a falls along the upper boundary of this data set and that these downslope values show far greater scatter. The resulting σ_{sp}/M that might be derived from the 4b data would be both higher by about a factor of two and more uncertain than Figure 4a. The result of including both upslope and downslope data is shown in Figure 4c. In spite of increased scatter, this plot is more similar to the data in Fig 4b than 4a. This supports the point made earlier that "downslope" σ_{sp} values often retain the influence of prior "upslope" values due to the long averaging time.

3. CONCLUSION

These observations have important consequences for the use and interpretation of MLO σ_{sp} data. First, the common occurrence of significantly enhanced upslope aerosol means that for many nights a true minimum σ_{sp} value corresponding to the actual clean free tropospheric aerosol present at MLO will not be reached. Second, even for those nights when the prior upslope aerosol concentration was low, the decay to minimum σ_{sp} may not occur until the 3-hour period just before the onset of upslope flow. This may persist even though aerosol volume at MLO could

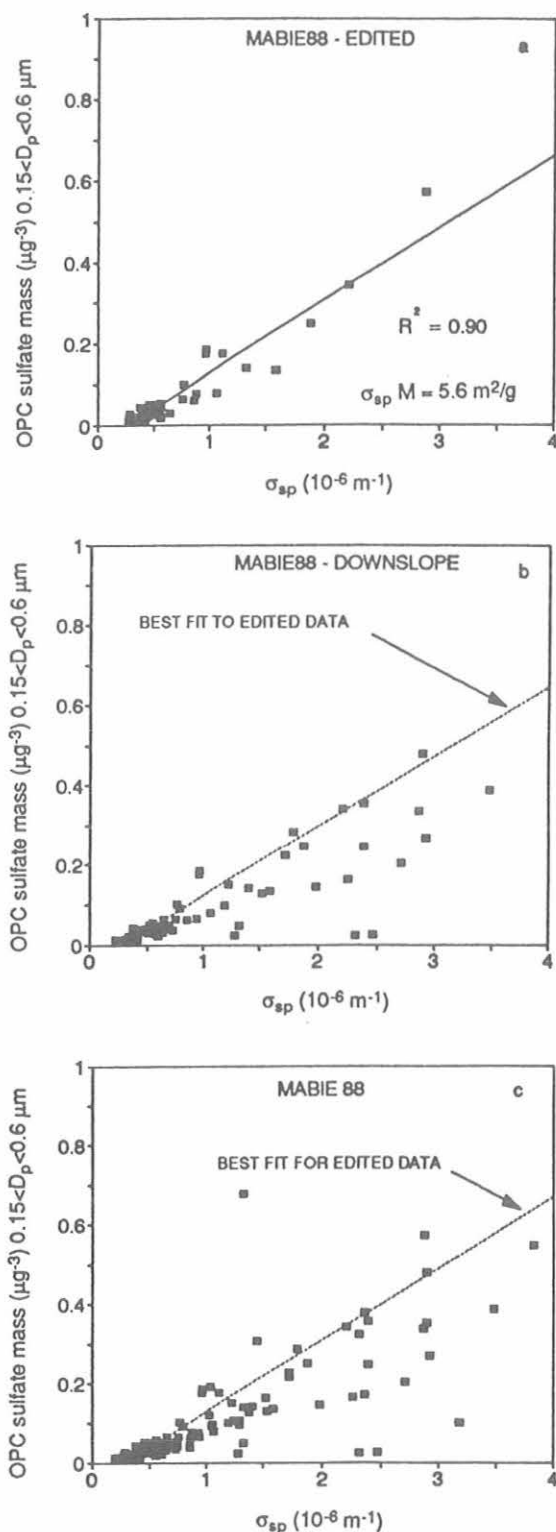


Fig. 4. (a) Fine sulfate mass versus σ_{sp} at 550nm for periods when both had a similar slope indicative of stabilized conditions and appropriate σ_{sp} values. (b) Fine sulfate mass versus σ_{sp} for all nightly periods characterized by downslope flow. (c) Fine sulfate mass versus σ_{sp} for all periods with σ_{sp} less than $4 \times 10^{-6} \text{ m}^{-1}$.

have been low for over 12 hours. Third, these effects will tend to make estimates of clean tropospheric scattering values based upon MLO data systematically higher than is warranted for the aerosol actually present. Fourth, averages of other nightly downslope measurements (e.g., filter samples) that are frequently compared to averaged downslope σ_{sp} will include a scatter in the relationship that may be appreciably influenced by the above effects.

This error in downslope values will be largest for periods when the previous day's upslope aerosol scattering is greatest. As a result, a careful evaluation of nephelometer data is required if it is to be used or compared reliably with other data representative of the clean free troposphere. Recognition of this bias and its nature can make it possible to stratify the σ_{sp} data in order to seek out times when the σ_{sp} values are most representative of the actual aerosol present. Comparing data with simply the minimum σ_{sp} on nights following a mild upslope aerosol influence is an obvious possibility. Even after stronger upslope, the evaluation of the slope of the σ_{sp} signal just before the downslope minimum might provide a means of extrapolating to the real σ_{sp} value.

Acknowledgments. We wish to thank Elmer Robinson and the CMDL staff at MLO for their help and assistance and David Bowdle of NASA MSFC for his encouragement. This work was supported by NASA Headquarters through Ramesh Kakar under NASA NAG8-634.

4. REFERENCES

- Bodhaine, B. A., Aerosol measurements at four background sites, *J. Geophys. Res.*, 88, 10,753-10,768, 1983
- Bodhaine, B.A., J.M. Harris, J.A. Ogren, and D.J. Hofmann, Aerosol optical properties at Mauna Loa Observatory: Long Range Transport from Kuwait?, *Geophys. Res. Lett.*, 19, 581-584, 1992.
- Charlson, R.J., J. Langner, H. Rhode, C.B. Leovy, and S.G. Warren, Perturbations to the northern hemisphere radiative balance by back-scattering from atmospheric aerosols, *Tellus*, 43AB, 152-163, 1991.
- Clarke, A.D., and R.J. Charlson, Radiative properties of the background aerosol: absorption component of extinction, *Science*, 229, 263-265, 1985.
- Clarke, A.D., and J. N. Porter, Aerosol size distribution, composition, and CO₂ backscatter at Mauna Loa Observatory, *J. Geophys. Res.*, 5237-5248, 1991.
- Massey, D.M., T.K. Quackenbush, and B.A. Bodhaine, Condensation nuclei and aerosol scattering extinction measurements at Mauna Loa Observatory: 1974-1985, *NOAA Data Rep., ERL ARL-14*, Air Resources Laboratory, Silver Spring, MD, 174 pp., 1987.

Improved MFOV Performance at Mauna Loa

PAUL F. HEIN, JOHN M. DAVIS, AND STEPHEN K. COX

Colorado State University, Department of Atmospheric Science, Fort Collins, Colorado 80523

1. INTRODUCTION AND BACKGROUND

The Multiple Field of View (MFOV) sunphotometer at Mauna Loa Observatory was replaced in November 1992 in order to improve the data quality. The instrument, which basically consists of five coaligned silicon photodiodes, each with a different field of view (fov), was originally designed to infer the optical depth of clouds by utilizing the information contained in the amount of scattering of solar radiation into the different fov's. The instrument was modified by using a different set of fovs and introducing a slope angle into the design of the collimating tubes. Additionally, the solar tracker was replaced. Results from the new configuration are encouraging. Data analysis algorithms are being improved with anticipation of adding the ability to infer some information concerning the cloud particle size.

The original approach is described in *Hein et al.*, [1990], wherein the transmittance from a particular fov $T(\text{fov})$ was described as resulting from attenuation of the incident solar radiation by an atmosphere of optical thickness τ , and enhancement of the measured signal by scattering from the same atmosphere into the fov, a process which is assigned an optical thickness for scattering τ_s . Or;

$$T(\text{fov}) = [\tau - \tau_s(\text{fov})],$$

Monte Carlo modeling results for a Rayleigh atmosphere indicate almost no enhancement by scattering into the larger fields of view as shown in Table 1, which is also being presented as a correction to a similar table presented in the 1991 summary CMDL report. The previous year's

TABLE 1. Modeled transmittances for solar zenith angles of 0°, 15°, 30°, 45°, and 60° and optical depths derived from the Langley method, for fields of view of 11.4°, 6.4°, 4.1°, 2.3°, and 2.0° and direct measurements

	11.4°	6.4°	4.1°	2.3°	2.0°	Direct
0°	0.9327	0.9325	0.9324	0.9324	0.9324	0.9324
15°	0.9304	0.9303	0.9302	0.9302	0.9302	0.9302
30°	0.9227	0.9225	0.9224	0.9224	0.9224	0.9224
45°	0.9066	0.9063	0.9062	0.9062	0.9062	0.9062
60°	0.8710	0.8707	0.8705	0.8705	0.8705	0.8704
τ_{lang}	0.0684	0.0686	0.0687	0.0687	0.0687	0.0688

discrepancy resulted from a coding error. The table shows modeled transmittances for a Rayleigh sky with a specified optical thickness of 0.07, for solar zenith angles of 0, 15, 30, 45 and 60 degrees. The last row shows optical thicknesses which are derived from the Langley method using the modeled data. By taking ratios of modeled (Monte Carlo) cloud transmittances, using the largest fov in the denominator, it was found that a parameter $a(\tau)$ could be established such that;

$$\frac{T(\text{fov})}{T(\text{max})} = \exp[-a(\tau)(\theta_{\text{max}} - \theta_{\text{fov}})],$$

and that $a(\tau)$ was nearly linear in τ up to an optical thickness of 10, at least for a stratocumulus base droplet distribution. In theory, this provided a method to find the optical depth from measured transmittances; however, in practice such determinations were uncertain due to poor solar tracking performance.

2. RECENT IMPROVEMENTS

The new instrument design appears to have improved its performance. For example, Figure 1 displays transmittances measured on a clear morning using the signal of each detector. The Langley method was used to determine "top of the atmosphere" values for the detector voltages $V_0(\text{fov})$, and the transmittances were calculated as the simple ratio $V(\text{fov})/V_0(\text{fov})$, where $V(\text{fov})$ is the instantaneous voltage from the detector. The divergence of the traces after 0900 LST may have resulted from thin clouds, slight tracking misalignment, or changing detector sensitivities; however, the spread in the transmittances reaches a maximum of about 0.02 at local noon, and scattering even by thin cloud cover is expected to produce differences in the transmittances exceeding that value.

The MFOV was not designed to measure clear sky scattering characteristics; however, typical clear sky optical depths derived by the Langley method for the Spring of 1992 were 0.18. The standard deviation of the optical thicknesses derived from the individual detectors on a typical clear sky morning was 0.006. This degree of stability is judged adequate for inference of thin cloud optical thicknesses.

3. DATA ANALYSIS

The current method of inferring cloud optical thickness differs somewhat from what is described above and consists of the following procedure. First, curves of the

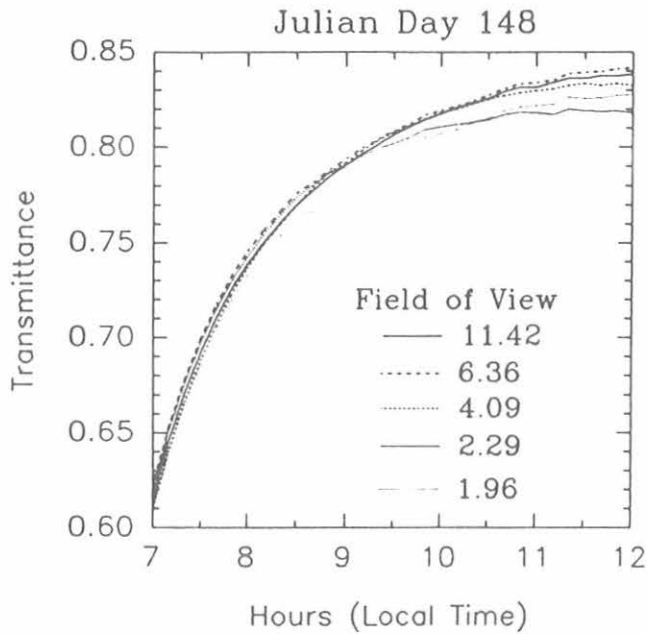


Fig. 1. Transmittances determined from each fov for the morning of Julian day 148.

natural log of the ratios of theoretically determined transmittances are plotted as a function of the difference in the detector fields of view for various optical thicknesses using an assumed microphysical distribution. Figure 2 shows such a plot for a C.6 ice sphere distribution characterized by a $20\ \mu\text{m}$ modal radius. The smallest optical depth corresponds to clear-sky conditions with a moderate volcanic aerosol in the stratosphere.

Next, the natural log of the transmittance ratios from the data are plotted in a similar manner, and an optical thickness is inferred for each microphysical distribution using the theoretical slopes associated each optical thickness. Finally, the derived optical thicknesses are plotted against the corresponding optical thicknesses determined from the transmittance as measured by the smallest fov. An example is shown in Figure 3 for three distributions using the data of Julian day 144, during a time for which the data indicated thin cloud conditions. Three droplet distributions have been used; the third distribution is a modified C.6 for which the modal radius has been adjusted from 20 to $30\ \mu\text{m}$.

From this plot one would conclude that the cloud's optical thickness varied between 0.2 and 2.0 and that it consists of particles with an equivalent sphere modal radius between 6 and $20\ \mu\text{m}$. Of course, as a rule it would be advisable to apply the information from additional distributions.

The advantage of this method of data analysis is that it appears to allow simultaneous determination of both the optical depth and some indication of an equivalent sphere modal radius for the cloud.

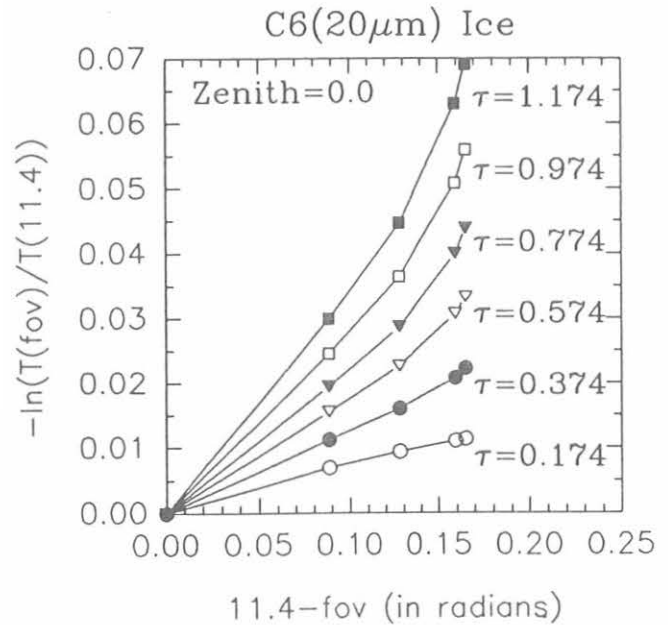


Fig. 2. Theoretically derived curves of the natural logarithm of transmittance ratios used in the MFOV data analysis.

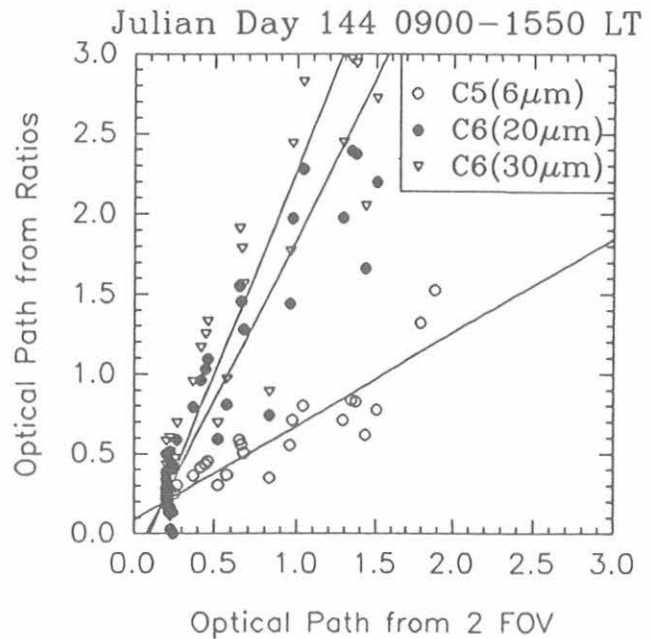


Fig. 3. Optical thicknesses derived from transmittance ratios versus those derived from extinction as measured by the smallest fov for three microphysical distributions.

4. FUTURE DEVELOPMENT

Perhaps the most interesting feature of the current data analysis is that the optical depth on the vertical axis is derived solely from scattering information (since the extinction optical depth subtracts out in the ratio), while the optical depth displayed on the horizontal axis is derived primarily from extinction information (this is the fov that is least affected by reentry from multiple scattering). This suggests that a more refined treatment may hold the promise of also utilizing the single particle scattering albedo as an upper limit constraint, which according to ongoing analysis, would be given directly by the slope of the line of best fit in a plot similar to Figure 3. Thus on such a plot, the C.6 and modified C.6 lines would be

eliminated since they would infer a single particle scattering albedo greater than unity.

Acknowledgments. We are sincerely grateful to the personnel at MLO who have monitored the tracking mechanism for the MFOV and forwarded data to Colorado State University. Funding for modification of the MFOV instrument was provided by the National Aeronautics and Space Administration Grant NAG 1-1146.

5. REFERENCE

Hein, P.F., J.M. Davis, and S.K. Cox, A new look at optical depth retrieval with the multiple field of view sunphotometer, in *Climate Monitoring and Diagnostics Laboratory, No. 18: Summary Report 1989*, edited W.D. Komhyr, 105-106., NOAA Environmental Research Laboratories, Boulder, CO, 1990.

Atmospheric Methane at Cape Meares, Oregon

M.A.K. KHALIL AND R.A. RASMUSSEN

Global Change Research Center, Department of Environmental Science and Engineering
Oregon Graduate Institute, Beaverton, Oregon 97006

1. INTRODUCTION

At Cape Meares, on the Oregon coast, we have taken measurements of CH_4 for nearly 15 years starting in the middle of 1978 and continuing at present. Numerous experiments have been conducted at this station because it is close to our laboratory and because it represents background air of the middle northern latitudes. In these latitudes, human activities have the greatest influence on atmospheric composition which eventually spreads to all parts of the world carried by the winds and atmospheric turbulence.

Three major experiments have been conducted on CH_4 at Cape Meares. The most elaborate is an automated high-frequency measurement of atmospheric CH_4 concentrations. This experiment has produced more than 120,000 individual measurements of CH_4 . The early portion of data first established the increasing concentration of CH_4 [Rasmussen and Khalil, 1981]. The other two experiments are to measure CH_4 in flask samples that are collected every week at the site. One set of flasks is for our research, which includes the analysis of more than 20 trace gases in which the Cape Meares site is one of six globally distributed locations. The other set of flask samples is collected for the NOAA/CMDL program for the analysis of CH_4 , CO_2 , and CO .

Here we describe briefly the continuous Cape Meares data and how readers may obtain them for their own research and, perhaps more important, to compare the broader features of the trend found in the available CMDL data with the results from the continuous measurements. The details of the nature, interpretation, and environmental implications of the continuous data set are discussed in our recent papers [Khalil *et al.*, 1993; Khalil and Rasmussen, 1993].

2. THE SALIENT RESULTS FROM CONTINUOUS MEASUREMENTS

(a) The data provide detailed observed concentration of CH_4 in the middle latitudes of the northern hemisphere as shown in Figure 1. Pronounced seasonal variations are apparent, as is the trend and decrease of the trend. (b) The cycle amplitude increased during the course of measurements (1979-1993). This finding is equivalent to the fact that CH_4 increased most rapidly in winter and least in late summer and fall. (c) The rate of increase of CH_4 declined in recent years. The rate during the most recent years is about half as large as in the early years of the measurements. See also Khalil and Rasmussen (1993 and

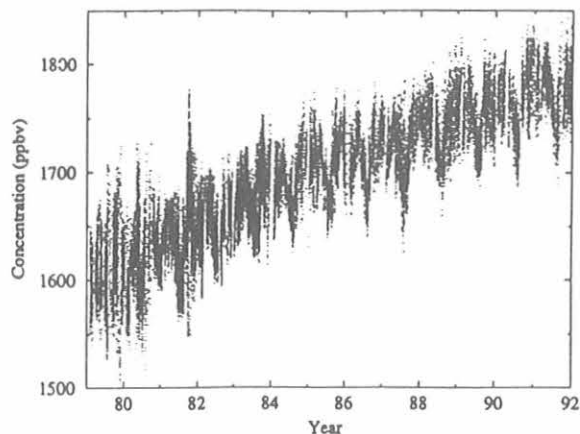


Fig. 1. High frequency measurements of CH_4 at Cape Meares, Oregon, between 1979 and 1993.

elsewhere) and for the CMDL data, see Steele *et al.* [1992]. (d) There are yet other variabilities that are not fully understood at present. These include diurnal cycles during fall and sub-monthly variabilities that may reflect seasonal long distance transport.

The data provide definitive information on the sources of CH_4 in this region. De-convolutions of the measurements to calculate emissions show that there are significant seasonal variations. The observed seasonal cycle of CH_4 is therefore caused not only by the cycles of OH that remove CH_4 from the atmosphere but also the seasonal cycles of emissions.

3. THE TRENDS AND DECLINE IN THE ACCUMULATION RATES

To verify the trends seen in the continuous data, we constructed an independent data set. It consists of two other primary data sets. The first is the flask sampling data of the CMDL from Cape Meares, Oregon, which is one of the 20 or so sites in their network. The other set is from the analysis of air stored in large 36-L stainless steel tanks. We recently analyzed 217 such air tanks over a 6-week period referenced against a single standard (NBS-982). It has been shown in numerous experiments that CH_4 concentrations remain stable in such tanks for decades [see Khalil *et al.*, 1993, for recent results]. The time series obtained from this instantaneous analyses we believe accurately represents the trends of the past.

There was a good distribution of air before 1984, and some air was also available for more recent times. But for

the crucial period of 1985-1989 when major changes of trends took place, there was almost no stored air. Fortunately the CMDL flask sample data were available for this period. Therefore, the two data sets that separately were not sufficient for comparisons with the long time-series of continuous measurements, together become most useful in verifying the trends in the continuous data. These comparisons are shown in Figures 2 (concentrations) and 3 (running slopes over 3-year periods). The continuous data

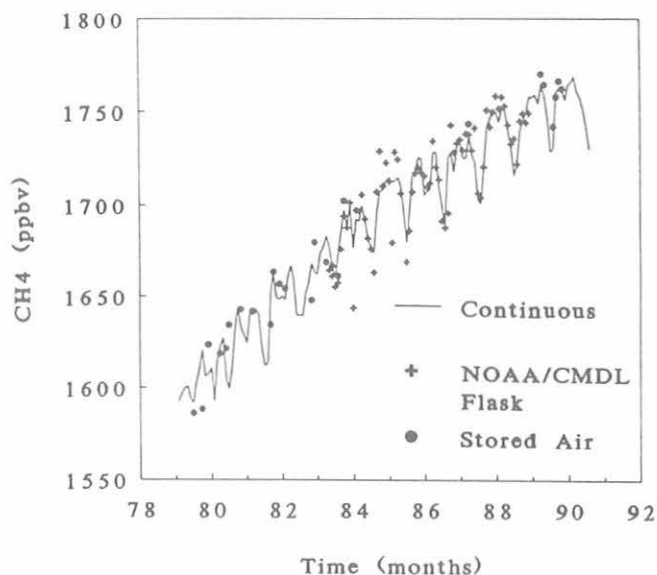


Fig. 2. Monthly average concentrations of the continuous measurements and the composite independent data described in the text. The composite data are taken at much lower frequency than the continuous data.

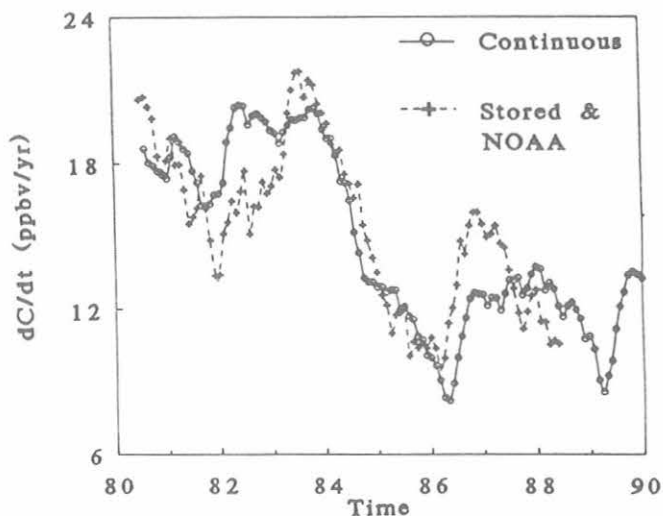


Fig. 3. Trends of methane over 3-year overlapping periods of time. The graph shows the slowdown of methane trend during the course of the experiment.

and the composite data (CMDL and stored air) agree very well, showing that CH_4 has probably decreased from about 20 ppbv yr^{-1} down to 10 ppbv yr^{-1} . The somewhat abrupt timing of this change is also supported by both data sets. These results lend support to the accuracy of the continuous data from Cape Meares, which are, as mentioned earlier, extremely detailed and contain much more information than the composite data or the flask sampling data in general.

4. HOW TO GET THE DATA

The data are archived at the Carbon Dioxide Information and Assessment Center (CDIAC) and may be obtained from CDIAC, Oak Ridge National Laboratory, Oak Ridge, TN 37831-9984. The data at CDIAC are in three tables that can be directly retrieved into the computer. Table 1 contains time and continuous data in ASCII format. Table 2 contains the time, daily average concentration, standard deviations (of daily concentrations), number of data during each day, and a column with interpolated data. The interpolation is used to fill gaps when samples were not collected. Table 3 contains monthly average data. The primary references for this data set are Khalil and Rasmussen [1993] and Khalil *et al.* [1993].

Acknowledgments. We thank D. Pierotti, D. Joseph, S. Crawford, J. Mohan, D. Stearns, and R. Dalluge for experimental work and D. Joseph, P. Turner, and M. Shearer for data management. There has been no continuous or systematic financial support for this project. During some periods grants have provided either full or partial financial support to the CH_4 measurements program at Cape Meares Station. These grants were: National Science Foundation (ATM-8109047), National Aeronautics and Space Administration (NAGW-1348, NAG-1-35, NAG-1-160), and Department of Energy (DE-FG06-85ER6031). Some recent work was supported by the Environmental Protection Agency through a contract to Andarz Company for modeling and data analysis (contract no. 1D3216NASA). Additional support was provided by the resources of the Biospherics Research Corporation and the Andarz Co.

5. REFERENCES

- Khalil, M.A.K., and R.A. Rasmussen, Decreasing trend of methane: Unpredictability of future concentrations, *Chemosphere*, 27, 803-814, 1993.
- Khalil, M.A.K., R.A. Rasmussen, and F. Moraes, Atmospheric methane at Cape Meares: Analysis of a high resolution data base and its environmental implications, *J. Geophys. Res.*, in press, 1993.
- Khalil, M.A.K., and R.A. Rasmussen, Atmospheric methane, carbon monoxide and carbon dioxide at Cape Meares, Oregon: Data analysis, interpretation and experimental design, U.S. EPA, Research Triangle Park North Carolina, in press, 1993.
- Rasmussen, R.A., and M.A.K. Khalil, Atmospheric methane: Trends and seasonal cycles, *J. Geophys. Res.*, 86, 9826-9832, 1981.
- Steele, L.P., E.J. Dlugokencky, P.M. Lang, P.P. Tans, R.C. Martin, and K.A. Masarie, Slowing down of the global accumulation of atmospheric methane during the 1980s, *Nature*, 358, 313-316, 1992.

Radioactivity in the Surface Air at BRW, MLO, SMO, and SPO During 1992

RICHARD J. LARSEN AND COLIN G. SANDERSON

Environmental Measurements Laboratory, U.S. Department of Energy, New York, New York 10014-3621

1. INTRODUCTION

Hi-volume air filter samples are routinely collected by CMDL personnel at BRW, MLO, SMO, and SPO for EML's Surface Air Sampling Program (SASP). The primary objective of this program is to identify and study the temporal and spatial distribution of specific anthropogenic and natural radionuclides in the lower troposphere. Of the radionuclides that are analyzed by gamma-ray spectrometry, only the naturally occurring radioisotopes ^7Be and ^{210}Pb are still readily measured in most of the filter samples. Beryllium-7 ($T_{1/2} = 53.2\text{d}$) is produced by cosmic-ray interactions in the upper troposphere and the

stratosphere and ^{210}Pb ($T_{1/2} = 22.3$ years) is a decay product of ^{222}Rn , a noble gas that diffuses from soils. Because of their distinctly different source regions, these radioisotopes may serve as excellent tracers for air masses of upper and lower tropospheric origin. Therefore, they are quite useful in studies of atmospheric transport processes.

2. MATERIAL AND METHODS

Weekly air filter samples are continuously collected using Dynaweb filter material. The air samplers move $\sim 1700\text{ m}^3$ of air per day through a 20.3-cm diameter filter. The weekly filter samples collected at BRW and MLO are

TABLE 1. Monthly Surface Air Concentrations of Radionuclides at BRW, MLO, SMO, and SPO During 1992

Site	Nuclide	Jan.	Feb.	March	April	May	June	July	Aug.	Sept.	Oct.	Nov.	Dec.
BRW	Gamma (cpm m ⁻³)	<0.01	<0.01	<0.01	<0.01	<0.01	<0.01	<0.01	<0.01	<0.01	<0.01	<0.01	<0.01
MLO	Gamma (cpm m ⁻³)	<0.01	<0.01	<0.01	<0.01	<0.01	<0.01	<0.01	<0.01	<0.01	<0.01	<0.01	<0.01
SMO	Gamma (cpm m ⁻³)		<0.01	<0.01	<0.01	<0.01	<0.01	<0.01	<0.01	<0.01	<0.01	<0.01	<0.01
SPO	Gamma (cpm m ⁻³)	<0.01	<0.01	<0.01	<0.01	<0.01	<0.01	<0.01	<0.01	<0.01	<0.01	<0.01	<0.01
BRW	^7Be (mBq m ⁻³)	2.0	2.2	2.0	2.3	1.7	<0.4	0.8	0.7	0.7	1.0	1.2	2.2
MLO	^7Be (mBq m ⁻³)	5.8	6.6	7.3	9.2	5.8	8.3	6.8	4.0	3.3	4.1	4.8	4.3
SMO	^7Be (mBq m ⁻³)	*	1.4†	1.5	1.2	2.6	2.7	2.2	1.8	2.8	3.1	1.8	1.6
SPO	^7Be (mBq m ⁻³)	5.5	4.2†	2.5	2.0†	3.3	2.4	1.9	1.8	2.0	2.6	3.5	4.7
BRW	^{95}Zr (μBq m ⁻³)	<4.5	<7.0	<8.9	<20.	<8.4	<30.	<8.6	<3.4	<19.	<19.	<8.0	<12.
MLO	^{95}Zr (μBq m ⁻³)	<20.	<9.4	<11.	<16.	<14.	<13.	<7.0	<15.	<18.	<59.	<76.	<20.
SMO	^{95}Zr (μBq m ⁻³)	*	<38.	<11.	<13.	<13.	<28.	<7.0	<24.	<18.	<14.	<2.9	<9.1
SPO	^{95}Zr (μBq m ⁻³)	<100.	<100.	<100.	<75.	<87.	<69.	<40.	<20.	<15.	<12	<10.	<6.1
BRW	^{137}Cs (μBq m ⁻³)	<1.2	<1.1	<1.2	<1.5	<1.1	<2.5	<0.7	<0.6	<2.1	<1.1	<0.7	<1.5
MLO	^{137}Cs (μBq m ⁻³)	<2.9	<2.1	<1.0	<2.3	<2.4	<2.1	<1.4	<2.2	<3.0	<3.8	<5.7	<4.2
SMO	^{137}Cs (μBq m ⁻³)	*	<3.0	<2.3	<1.5	<1.3	<1.7	<0.8	<1.4	<2.3	<1.4	<0.6	<2.8
SPO	^{137}Cs (μBq m ⁻³)	<3.7	<1.3	<2.4	<1.8	<1.8	<2.7	<1.9	<1.2	<1.2	<1.8	<2.0	<1.7
BRW	^{144}Ce (μBq m ⁻³)	<5.2	<5.5	<6.1	<8.2	<5.4	<13.	<3.9	<2.7	<11.	<5.6	<3.3	<7.7
MLO	^{144}Ce (μBq m ⁻³)	<12.	<11.	<4.0	<13.	<12.	<11.	<5.3	<11.	<12.	<23.	<30.	<18.
SMO	^{144}Ce (μBq m ⁻³)	*	<17.	<11.	<5.1	<5.4	<10.	<3.9	<8.2	<12.	<7.5	<2.1	<11.
SPO	^{144}Ce (μBq m ⁻³)	<24.	<8.0	<18.	<9.6	<13.	<18.	<12.	<5.5	<5.1	<8.5	<9.2	<7.9
BRW	^{210}Pb (mBq m ⁻³)	0.78	1.07	0.78	0.48	0.27†	0.08†	0.07†	0.06†	0.08†	0.29	0.38	1.27
MLO	^{210}Pb (mBq m ⁻³)	0.31	0.36‡	0.56	0.63	0.43	0.48	0.39	0.16	0.20	0.15	0.19	0.13†
SMO	^{210}Pb (mBq m ⁻³)	*	0.04‡	0.02‡	0.04	0.07	0.09†	0.04†	0.06	0.09†	0.11	0.06	0.05†
SPO	^{210}Pb (mBq m ⁻³)	0.05†	0.02†	0.01†	0.01‡	0.03†	0.03‡	0.02‡	0.01‡	0.01‡	0.01§	0.01§	0.03‡

*No data

Uncertainty is <20% except:

†Uncertainty is between 20% and 50%

‡Uncertainty is between 50% and 100%

§Uncertainty is greater than 100%

analyzed by gamma-ray spectrometry using a high-purity germanium (HPGe) detector with a 1.5 cm diameter well. The individual weekly samples from SMO and SPO are not routinely analyzed. A monthly composite sample for each site was formed by adding together one half of each of the weekly filter samples. These monthly composite samples are compressed into 45-cm³ plastic planchets and are routinely analyzed for several gamma-ray emitting radionuclides using either n-type low-energy coaxial, high-purity germanium (HPGe) detectors or p-type coaxial high-resolution, germanium lithium or HPGe detectors. Detailed information on SASP is periodically published [Larsen and Sanderson, 1991].

3. RESULTS

The results of the analyses of several radionuclides and the total gamma-ray activities for the monthly composite samples from filters collected at BRW, MLO, SMO, and SPO during 1992 are reported in Table 1. The total gamma-ray activities are reported in units of counts per minute (cpm) per cubic meter of sampled air referenced to 15°C and 1 Atm. The surface air concentrations of ⁷Be and ²¹⁰Pb are reported in millibecquerels (mBq) per standard cubic meter of air, and ⁹⁵Zr, ¹³⁷Cs, and ¹⁴⁴Ce are reported in microbecquerels (μBq) per cubic meter of air referenced

to 15°C and 1 Atm. The concentrations are reported as corrected for radioactive decay to the midpoint of the month of collection. The results of the analyses on the weekly samples from BRW and MLO are presently being prepared for publication as an EML report.

4. DISCUSSION

There were no reported significant releases of radioactive materials into the atmosphere during 1992, and the concentrations of fission products such as ⁹⁵Zr, ¹³⁷Cs, and ¹⁴⁴Ce were at or below the lower limits of detection for the analytical and sampling techniques that we currently use to measure them. The seasonal cycles of ⁷Be and ²¹⁰Pb continue to follow those observed in previous years.

Acknowledgment. We wish to thank the NOAA CMDL staff at BRW, MLO, SMO, and SPO for the collection of air filter samples for the SASP.

5. REFERENCE

Larsen, R.J., and C.G. Sanderson, EML surface air sampling program, 1989 data, August 1991, *U.S. DOE Rep. EML-541*, U.S. Dept. of Energy, Environmental Measurement Laboratories, New York, 1991.

Tomsk-7 Debris at BRW: Detection and Transport

H. N. LEE, R. J. LARSEN, AND C. G. SANDERSON

Environmental Measurements Laboratory, U.S. Department of Energy, New York, New York 10014-3621

1. INTRODUCTION

On April 6, 1993, radioactivity was accidentally released into the atmosphere during an explosion and fire at a reprocessing plant in the Tomsk-7 military nuclear complex located 16 km north of the Siberian city of Tomsk. About 40 Ci (19.9 TBq) of beta-gamma radionuclides were released into the atmosphere. The isotopic composition of the beta-gamma radionuclides at the time of the accident was reported by the IAEA [1993] to be 43.2% ^{95}Nb , 35.3% ^{106}Ru , 18.7% ^{95}Zr , 2.7% ^{103}Ru , <0.1% ^{137}Cs , with traces of ^{90}Sr .

2. MATERIAL AND METHODS

Week-long, high-volume air filter samples are routinely collected by CMDL personnel at BRW, MLO, SMO, and SPO for EML's Surface Air Sampling Program. The primary purpose of this program is to study the temporal and spatial distribution of specific natural and anthropogenic radionuclides in the surface air. Following notification of the accident, air filter samples collected at BRW were express mailed to EML and were immediately analyzed for gamma-ray emitting isotopes. The samples were collected on Dynaweb filters, which have an effective exposure area of about 266 cm², at a flow rate of ~1.5 m³ min⁻¹. A 65.3 cm² section of each filter was removed and compressed into a 1-2 cm³ cylinder and analyzed by gamma-ray spectrometry using a 320 cm³ high-purity germanium well detector.

3. RESULTS AND DISCUSSION

The fission products ^{95}Nb and ^{106}Ru were first detected in the BRW sample collected from April 15-21. The surface air concentrations of these isotopes inferred from this sample were 2.2 and 15 $\mu\text{Bq m}^{-3}$, respectively, at the midpoint of collection. In the sample collected from April 21-30, ^{95}Zr and ^{103}Ru were detected in addition to ^{95}Nb and ^{106}Ru . The surface air concentrations of ^{95}Zr , ^{103}Ru , ^{95}Nb , and ^{106}Ru inferred from this sample were 1.2, 0.8, 2.8, and 16 $\mu\text{Bq m}^{-3}$, respectively, with counting uncertainties at 1 sigma, between 10% and 30%. No fission products were detected in the sample collected from April 30-May 8. These results have been submitted for publication [Larsen *et al.*, 1993].

To understand the global transport of these isotopes, a three-dimensional trajectory model was developed to calculate the transport paths of the radionuclides released

during the accident. The trajectories were calculated based on the wind forecast generated by the global model operated at the National Meteorological Center, Camp Springs, Maryland. The 12-hr analysis wind data at grid intervals of 2.5 degrees for the 1000-, 850-, 700- and 500-mb in the northern hemisphere were used in this study. Figure 1 presents two trajectories, computed at each 3-hr interval, showing the transport paths, from April 6-30, for radionuclide particles released near the Tomsk-7 site on April 6. The computations start at 875-mb (solid line) and 835-mb (dotted line). This figure shows that the debris initially moved in a northeastern direction. Then, the debris meandered around at 80 degree latitude above the Arctic Ocean before finally moving southward, passing near the sampling station at BRW. The estimated arrival times for these trajectories at BRW, April 17 (835-mb) and April 27 (875-mb) are consistent with the arrival times estimated from the measurements. The debris followed different trajectories, depending on the initial time and location assumed for the released radionuclide particles.

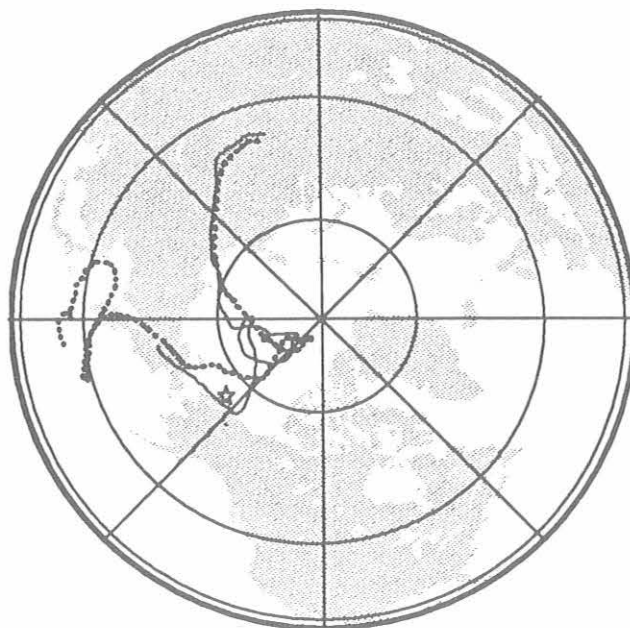


Fig. 1 Trajectories of radionuclides released at the Tomsk-7 site. The release heights are 875- and 835-mb for solid and dotted lines, respectively. The star represents the sampling site at Barrow, Alaska.

We have computed additional trajectories showing the transport of the Toms-7 debris to Greenland and to central and eastern Canada, where we also have detected traces of Toms-7 debris.

The concentrations of these fission products are extremely low and are of no dosimetric significance to the residents of Barrow. For example, we estimate the maximum increase in the daily external radiation exposure rate resulting from these fission products was less than 1/100th of a percent.

Acknowledgment. We wish to thank Dan Endres for coordinating the collection and mailing air filter samples to EML.

REFERENCES

- IAEA, Toms-7 caused minimal radiation hazards, *Nuclear Waste News*, 13, 157, 1993.
- Larsen, R.J., C.G. Sanderson, H.N. Lee, K.M. Decker, and H.L. Beck, Fission products detected in Alaska following the Toms-7 accident, submitted, *J. Environ. Radioactivity*, 1993.

Ultrahigh Resolution Infrared Solar Spectra from Mauna Loa Observatory

FRANK J. MURCRAY, SHELE J. DAVID, RONALD D. BLATHERWICK, AARON GOLDMAN, AND DAVID G. MURCRAY
University of Denver, Department of Physics, Denver, Colorado 80208

1. INTRODUCTION

An ultrahigh resolution (0.0035 cm^{-1}) FTIR system was installed at the Mauna Loa Observatory (MLO) in May 1991. It was run routinely once per week by the MLO staff since November 1991. This instrument is serving as a prototype for the solar absorption FTIR instrument that will be used in the Network for Detection of Stratospheric Change. The instrument and analysis procedure were described in last year's Summary Report (*Ferguson and Rosson, 1992*).

During 1992, University of Denver (DU) personnel operated and adjusted the equipment during a 1-week period in January. In May and June, the quality of the data slowly degraded until it was not usable. DU personnel returned to MLO and found that a set screw holding the solar tracker in position had become loose. The screw was tightened and the system ran fine. In October, one of the instrument's power supplies failed. A new power supply was installed in December. Throughout the rest of the year when everything was running properly, MLO staff operated the instrument on a once-per-week basis (usually Wednesdays), weather permitting.

This instrument currently measures the spectrum in the 750 to 1250 cm^{-1} (8 to 13 micron) band and the 2500 to 3100 cm^{-1} (3 to 4 micron) band. Total column amounts of HCl, HNO_3 , O_3 and N_2O are currently processed routinely. Retrieval software for many of the other gases are under development. Last year we presented results pertaining to HCl and HNO_3 . This year we will focus on our O_3 and N_2O results.

2. ANALYSIS

The procedure for analyzing data is the same as described last year. A small section of a MLO spectrum fitted to a calculated spectrum, around 1163 cm^{-1} , is shown in Figure 1. The ozone spectral lines were chosen to be isolated and only weakly temperature dependent. The fitted spectral region includes two prominent ozone absorptions and a strong line due to N_2O . The difference between the observed and calculated spectra is shown below the spectra on an expanded scale. The residuals appear to be random, indicating that the fit is good down to the noise level of the instrument. The initial profile used in fitting the ozone was based on an average of the ozone sonde data provided by S. Oltmans (personal communication).

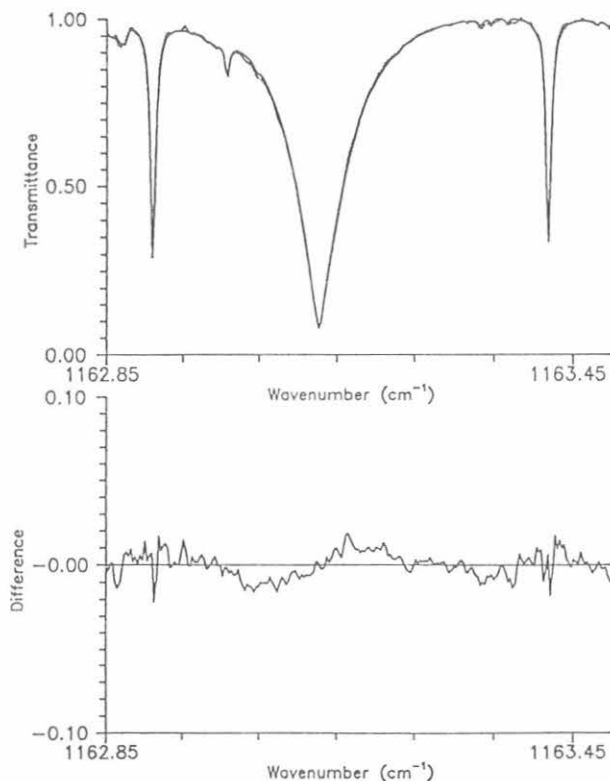


Fig. 1. The top panel shows a portion of the spectrum in the 750 to 1250 cm^{-1} band, which is analyzed for O_3 and N_2O . The N_2O line is the broader line near the center of the region, sharper O_3 lines are on either side. The observed spectrum is the dotted line, the best fit calculated spectrum is the solid line. The bottom panel shows the difference between the observed and calculated on an expanded scale.

3. DISCUSSION

Figure 2 shows the total column ozone measured by FTIR and by the Dobson for January 1992-January 1993. Except when the instrument was down, there is FTIR data for almost every week. The data are plotted to show the natural variability as well as to compare the FTIR and Dobson results. Using only the days where measurements were made using both techniques (29 days), the mean total ozone column determined by the FTIR is 4.6% lower than the Dobson. After raising the FTIR results by 4.6%, the RMS difference between FTIR and Dobson is 2.7%. Considering the two techniques differ widely in instrumentation, analysis and spectroscopy, the agreement between them is extremely good.

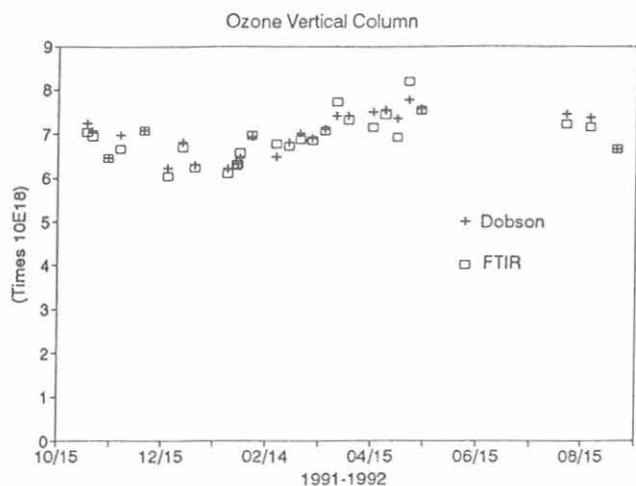


Fig. 2. Total column ozone on days with both FTIR and Dobson measurements (Dobson data are taken from the WMO World Ozone Data Center).

Figure 3 shows the total column of N_2O measured by FTIR. We have not yet carried out a detailed study of the error budget in this analysis; however, retrievals of N_2O are consistent within about 2.5% (RMS).

We are still trying to understand the remaining differences between the Dobson and FTIR, even though the agreement is already very good. Possible systematic differences include different response to tropospheric ozone.

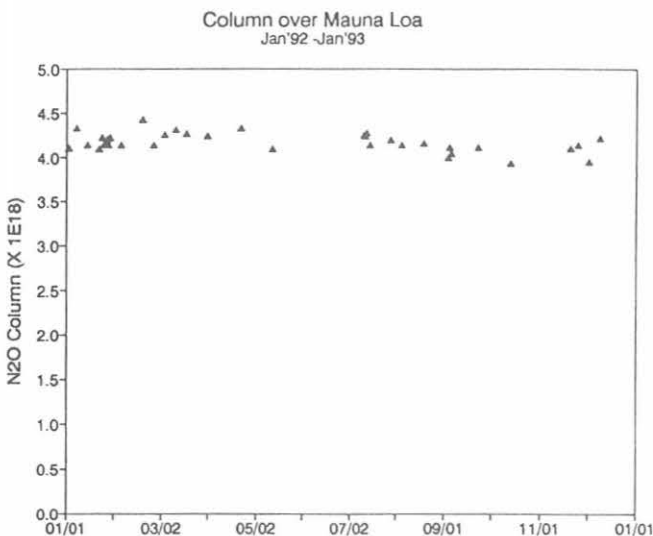


Fig. 3. Total column N_2O as measured by the FTIR. There is a slight indication of a possible seasonal effect, possibly related to the tropopause height.

Acknowledgments. We wish to thank the staff of MLO for their kind support. Russell Schnell has been very helpful. We are particularly indebted to Bob Uchida for collecting most of the data every week and letting us know when problems arise with the instrument.

4. REFERENCE

Ferguson, E.E., and R.M. Rosson (Eds.), *Climate Monitoring and Diagnostics Laboratory No. 20: Summary Report 1991*, pp. 115-116, NOAA Environmental Research Laboratories, Boulder, CO, 1992.

Advanced Global Atmospheric Gases Experiment (AGAGE)

R.G. PRINN

Massachusetts Institute of Technology, Cambridge, Massachusetts 02139

R.F. WEISS

Scripps Institution of Oceanography, University of California, La Jolla, California 92093

F.N. ALYEA AND D.M. CUNNOLD

Georgia Institute of Technology, Atmospheric Sciences, Atlanta, Georgia 30332

P.J. FRASER AND L.P. STEELE

CSIRO, Division of Atmospheric Research, Victoria, Australia 3195

P.G. SIMMONDS

University of Bristol, School of Chemistry, Bristol, United Kingdom BS8 ITS

1. INTRODUCTION

In this global network program, continuous high-frequency gas chromatographic measurements of two biogenic/anthropogenic gases (CH_4 , N_2O) and five anthropogenic gases (CFCl_3 , CF_2Cl_2 , CH_3CCl_3 , $\text{CF}_2\text{CICFCl}_2$, CCl_4) are carried out at globally distributed sites in order to quantitatively determine the source and sink strengths and circulation of these chemically and radiatively important long-lived gases. The program that started in 1978 is conveniently divided into three parts associated with three changes in instrumentation: the Atmospheric Lifetime Experiment (ALE) that utilized Hewlett-Packard HP5840 gas chromatographs, the Global Atmospheric Gases Experiment (GAGE) that utilizes HP5880 gas chromatographs, and the Advanced (AGAGE) phase that has recently started using a new fully automated system from the Scripps Institution of Oceanography (SIO) containing a custom-designed sample module and HP5890 and Carle Instruments gas chromatographic components.

The current station locations are Cape Grim, Tasmania (41°S , 145°E); Point Matatula, American Samoa (14°S , 171°E), Ragged Point, Barbados (13°N , 59°W), and Mace Head, Ireland (53°N , 10°W). Stations also previously existed at Cape Meares, Oregon (45°N , 124°W) and Adrigole, Ireland (52°N , 10°W). The current Mace Head station replaced the Adrigole station, and a station is planned at Trinidad Head, California, (41°N , 124°W) to replace Cape Meares.

2. 1992-1993 UPDATE

The data for the seven long-lived gases measured in GAGE during 1992-1993 continue to generally be of good quality. Two publications have appeared or are about to appear describing and analyzing the data. First, measurements made between 1978 and 1990 of the anthropogenic chemical compound 1,1,1-trichloroethane (methyl chloroform, CH_3CCl_3) show it increasing at a

global average rate of $4.4 \pm 0.2\%$ per year (1σ) over this later time period. The measured trends combined with industrial emission estimates, are used in an optimal estimation inversion scheme to deduce a globally averaged CH_3CCl_3 tropospheric (and total atmospheric) lifetime of 5.7 (+0.7, -0.6) years (1σ) and a weighted global average tropospheric hydroxyl radical (OH) concentration of $8.7 \pm 1.0 \times 10^5$ radical cm^{-3} (1σ). Inclusion of a small loss rate to the ocean for CH_3CCl_3 of $1/85$ year $^{-1}$ does not affect the stated lifetime but lowers the stated OH concentration to $8.1 \pm 0.9 \times 10^5$ radical cm^{-3} (1σ). The rate of change of the weighted global average OH concentration over this time period is determined to be $1.0 \pm 0.8\%$ per year (1σ) which has major implications for the oxidation capacity of the atmosphere and more specifically for methane (CH_4), which like CH_3CCl_3 is destroyed primarily by OH radicals. The CH_3CCl_3 measurements at Samoa show remarkable sensitivity to the El Niño-Southern Oscillation (ENSO) that is attributable to modulation of cross-equatorial transport during the northern hemisphere winter by the interannually varying upper tropospheric zonal winds in the equatorial Pacific. Thus measurements of this chemical compound have led to the discovery of a previously unappreciated aspect of tropical atmospheric tracer transport [Prinn *et al.*, 1992].

Second, 13 years of ALE/GAGE CCl_3F and CCl_2F_2 measurements have also been analyzed. Comparisons are made against shipboard measurements by the SIO group and archived air samples collected at Cape Grim, Tasmania, since 1978. CCl_3F in the lower troposphere was increasing at an average rate of 9.1 ppt yr $^{-1}$ over the period July 1978 to June 1988. CCl_2F_2 was increasing at an average 17.4 ppt year $^{-1}$ in the lower troposphere over the same period. However, between July 1988 and June 1991 the increases of CCl_3F and CCl_2F_2 in this region have averaged just 6.9 ppt year $^{-1}$ and 15.7 ppt year $^{-1}$ respectively. The rate of increase has been decreasing 2.4 ppt year $^{-2}$ and 2.9 ppt year $^{-2}$ over this 3-year period. On the basis of recent scenarios of the worldwide releases of

these compounds and using the calibration scale SIO 1986, the equilibrium lifetimes are estimated to be 49^{+20}_{-11} years and 150^{+540}_{-67} years for CCl_3F and CCl_2F_2 respectively. Using these lifetime estimates and a two-dimensional model, it is estimated that global releases of these two chlorofluorocarbons in 1990 were $242 \pm 20 \times 10^6$ kg for CCl_3F and $367 \pm 29 \times 10^6$ kg for CCl_2F_2 . It is also estimated that combined releases of these chlorofluorocarbons in 1990 were $21 \pm 4\%$ less than those in 1986. Slightly different estimates of lifetimes and emissions are obtained using new SIO 1993 calibrations [Cunnold *et al.*, 1993].

Operations at the American Samoa CMDL Observatory will soon make the transition from the GAGE instrument to the new AGAGE system. During 1992 the GAGE HP5880 continued to be operated by the CMDL station personnel in collaboration with the SIO group. Operations were generally smooth and uneventful except for two significant problem periods. In the aftermath of Hurricane Val (December 1991), the island electrical power was extremely unreliable and the station's generating system was severely taxed. Although the GAGE instrument operates on an uninterruptible power supply, the island power is so unreliable that we have decided not to risk uncontrolled shutdowns by operating the GAGE instrument when the station generator is not working. Station generator problems resulted in the suspension of operations for 11 days in early January and again for 9 days at the end of January. The second major problem was the erratic performance of the GAGE air sampling system between August and October. During this period there were several problems with failures of the metal bellows air sampling pump that were ultimately traced to a clogged inlet filter and approximately 2 months of data were lost.

The new instrument systems for AGAGE represent a significant technological advance. All operations and data acquisition are by a Sun Microsystems workstation computer using custom runfile architecture, signal processing and integration routines, and storing all the data and chromatograms digitally. The instrument measures its own non-linearity for all the AGAGE gases on a regular basis using a pressure-programmed constant-volume injection system and a single gas standard. All channels of

the instrument are fitted with precolumns to avoid column contamination by late-eluting gases, and as a result the frequency of measurement was increased three-fold versus GAGE. Precision is also greatly improved over the GAGE instruments, with 1σ relative precisions on the order of 0.05% for the rapidly eluting gases CH_4 , CCl_2F_2 , N_2O , and CCl_3F . The system works interactively with its uninterruptible power supply so that controlled shutdown and startup of the entire instrument and sampling system are assured when there are extended power outages. The first AGAGE field instrument is now in operation at Cape Grim, and the instruments for Samoa and the other stations will be installed during the coming year.

3. DATA ACCESS

The ALE/GAGE/AGAGE data are archived at the Georgia Institute of Technology and are available to interested scientists. Potential users of the data should contact Fred Alyea (Internet: alyea@eas.gatech.edu, telephone: 404-894-3815). Generally, monthly means and standard deviations can be immediately transferred electronically. Transmission of the full data set (4-12 measurements day^{-1} for each compound at each station for all years beginning 1978) will require consultation.

Acknowledgments. The AGAGE is supported by NASA Grants NAGW-732 and NAGW-2034, NOAA Contract NA85-RAC05103, CSIRO, Australian Bureau of Meteorology, and the U.K. Department of Environment. We thank the NOAA staff at Samoa for their continued excellent local support for our instrumentation there.

4. REFERENCES

- Cunnold, D.M., P.J. Fraser, R.F. Weiss, R.G. Prinn, P.G. Simmonds, B.R. Miller, F.N. Alyea, and A.J. Crawford, Global trends and annual releases of CCl_3F and CCl_2F_2 estimated from ALE/GAGE and other measurements from July 1978 to June 1991, *J. Geophys. Res.*, in press, 1993.
- Prinn, R., D. Cunnold, P. Simmonds, F. Alyea, R. Boldi, A. Crawford, P. Fraser, D. Gutzler, D. Hartley, R. Rosen, and R. Rasmussen, Global average concentration and trend for hydroxyl radicals deduced from ALE/GAGE trichloroethane (methyl chloroform) data, *Geophys. Res. Lett.*, 97, 2445-2461, 1992.

The $^{13}\text{C}/^{12}\text{C}$ of Atmospheric Methane

PAUL QUAY, JOHN STUTSMAN AND DAVID WILBUR

School of Oceanography, University of Washington, Seattle, Washington 98195

1. INTRODUCTION

For the past 5 years we have been measuring the $^{13}\text{C}/^{12}\text{C}$ of atmospheric CH_4 on air samples collected at three CMDL sites (BRW at 71°N 156°W , MLO at 19°N 155°W , and SMO at 14°S 170°W) and on the Washington coast at 48°N 126°W .

The $^{13}\text{C}/^{12}\text{C}$ of atmospheric CH_4 is a tracer that can distinguish between CH_4 input from bacterial and non-bacterial CH_4 sources. Bacterial CH_4 is microbially produced in anoxic environments like swamps, bogs, rice paddies, and the rumens of cows. Non-bacterial CH_4 sources include thermogenically produced natural gas and CH_4 produced during the incomplete oxidation of plant material during biomass burning. Bacterial CH_4 has a $\delta^{13}\text{C}$ of about -60‰ (versus PDB) whereas the $\delta^{13}\text{C}$ of natural gas and CH_4 produced from biomass burning are about -40 and -27‰ , respectively [Quay *et al.*, 1991].

The spatial and temporal variations in the $^{13}\text{C}/^{12}\text{C}$ of atmospheric CH_4 depend on the variations in the relative strength and $^{13}\text{C}/^{12}\text{C}$ of the CH_4 sources and sinks. Over interannual time scales, the change in the $^{13}\text{C}/^{12}\text{C}$ of atmospheric CH_4 indicates changes in the source composition, i.e., the relative strength of bacterial versus non-bacterial CH_4 sources. Because CH_4 will likely contribute about 15% of the radiative forcing during the next century [Wigley and Raper, 1992], it is important to quantify the strength of the individual CH_4 sources, currently known to about $\pm 50\%$, and to determine whether the CH_4 source strengths are changing with time. This latter point has been underscored by the recently observed slow down in the rate of CH_4 increase in the atmosphere [Steele *et al.*, 1992].

2. METHODS

The air samples are collected, at approximately 2-week intervals, using pre-evacuated stainless-steel flasks either 15 or 30 L in volume. The CH_4 is extracted from air in our laboratory using the procedure developed by Stevens and Rust [1982]. Briefly, the air is metered into a high vacuum extraction line through a series of liquid nitrogen traps to remove H_2O , CO_2 , and N_2O . The air then passes through a bed of Schutze's reagent, I_2O_5 on silica, to oxidize CO to CO_2 that is trapped cryogenically. Then the CH_4 in the air is combusted over platinumized silica at 800°C to CO_2 which is then trapped cryogenically. The yield of the procedure, determined from standards, is $100 \pm 2\%$ ($n = 114$). The $^{13}\text{C}/^{12}\text{C}$ of the CO_2 derived from CH_4 is measured on a Finnigan MAT 251 gas ratio isotope mass spectrometer.

The overall measurement precision is about $\pm 0.1\text{‰}$. We obtain a $\delta^{13}\text{C}$ of -41.73‰ (versus PDB) for NBS-16.

3. RESULTS AND DISCUSSION

The seasonal cycle in the $\delta^{13}\text{C}$ of CH_4 is greatest at 71°N (BRW), with an amplitude of $\sim 0.6\text{‰}$ and decreases southward to 14°S (SMO) where we measure no significant seasonal trend, i.e., $< 0.1\text{‰}$ (Figure 1). The seasonal trends at 71°N and 48°N can be approximated roughly by a single harmonic with an annual period. Episodes of high CH_4 concentrations associated with very depleted $\delta^{13}\text{C}$ values occur at these two sites in September-October of each year. Generally at the northern hemisphere sites the lowest $\delta^{13}\text{C}$ values occur in the fall and the highest values occur in the summer. This trend toward enriched summertime $\delta^{13}\text{C}$ values is expected if CH_4 oxidation by OH primarily controls the seasonal cycle because the $^{12}\text{CH}_4$ molecules react at a slightly faster rate (1.005x) than the $^{13}\text{CH}_4$ molecules [Cantrell *et al.*, 1990]. The annual mean $\delta^{13}\text{C}$ values increase southward from about -47.8‰ at 71°N to -47.3‰ at 14°S .

We calculate a global average $\delta^{13}\text{C}$ of CH_4 of about -47.5‰ . The mean global $\delta^{13}\text{C}$ value, when combined with the ^{14}C content of atmospheric CH_4 , yields an estimate of the proportion of bacterial versus non-bacterial CH_4 source strengths [Quay *et al.*, 1991]. We estimate that bacterial CH_4 sources contribute $\sim 70\%$, fossil CH_4 sources $\sim 20\%$, and biomass burning $\sim 10\%$ of the total CH_4 input.

Although the seasonal cycle in $\delta^{13}\text{C}$ dominates the time series measurements, there is evidence for a slight interannual trend. Measurements at all four time series locations indicate an increase in $\delta^{13}\text{C}$, and when combined, yield an average rate of approximately $0.04 \pm 0.02\text{‰}$ per year. Measuring the interannual change in the $\delta^{13}\text{C}$ of atmospheric CH_4 over the longer term will be a useful indicator of changes in the proportion of bacterial and non-bacterial CH_4 inputs.

4. REFERENCES

- Cantrell, C.A., R.E. Shetter, A.H. McDaniel, J.G. Calvert, J.A. Davidson, D.C. Lowe, S.C. Tyler, R.J. Cicerone and J.P. Greenberg, Carbon kinetic isotope effect in the oxidation of methane by the hydroxyl radical, *J. Geophys. Res.*, 95, 22455-22462, 1990.
Quay, P.D., S.L. King, J. Stutsman, D.O. Wilbur, L.P. Steele, I. Fung, R.H. Gammon, T.A. Brown, G.W. Farwell, P.M. Grootes, and F.H. Schmidt, Carbon isotopic composition of atmospheric methane: Fossil and biomass burning source strengths, *Global Biogeochem. Cycles*, 5, 25-47, 1991.

Steele, L.P., E.J. Dlugokencky, P.M. Lang, P.P. Tans, R.C. Martin, and K.A. Maseric, Slowing down of the global accumulation and atmospheric methane during the 1980s, *Nature*, 358, 313-316, 1992.

Stevens, C.M., and F.E. Rust, The carbon isotopic composition of atmospheric methane, *J. Geophys. Res.*, 87, 4879-4882, 1982.
 Wigley, T.M.L., and S.C.B. Raper, Implications for climate and sea level of revised IPCC emission scenarios, *Nature*, 357, 293-300, 1992.

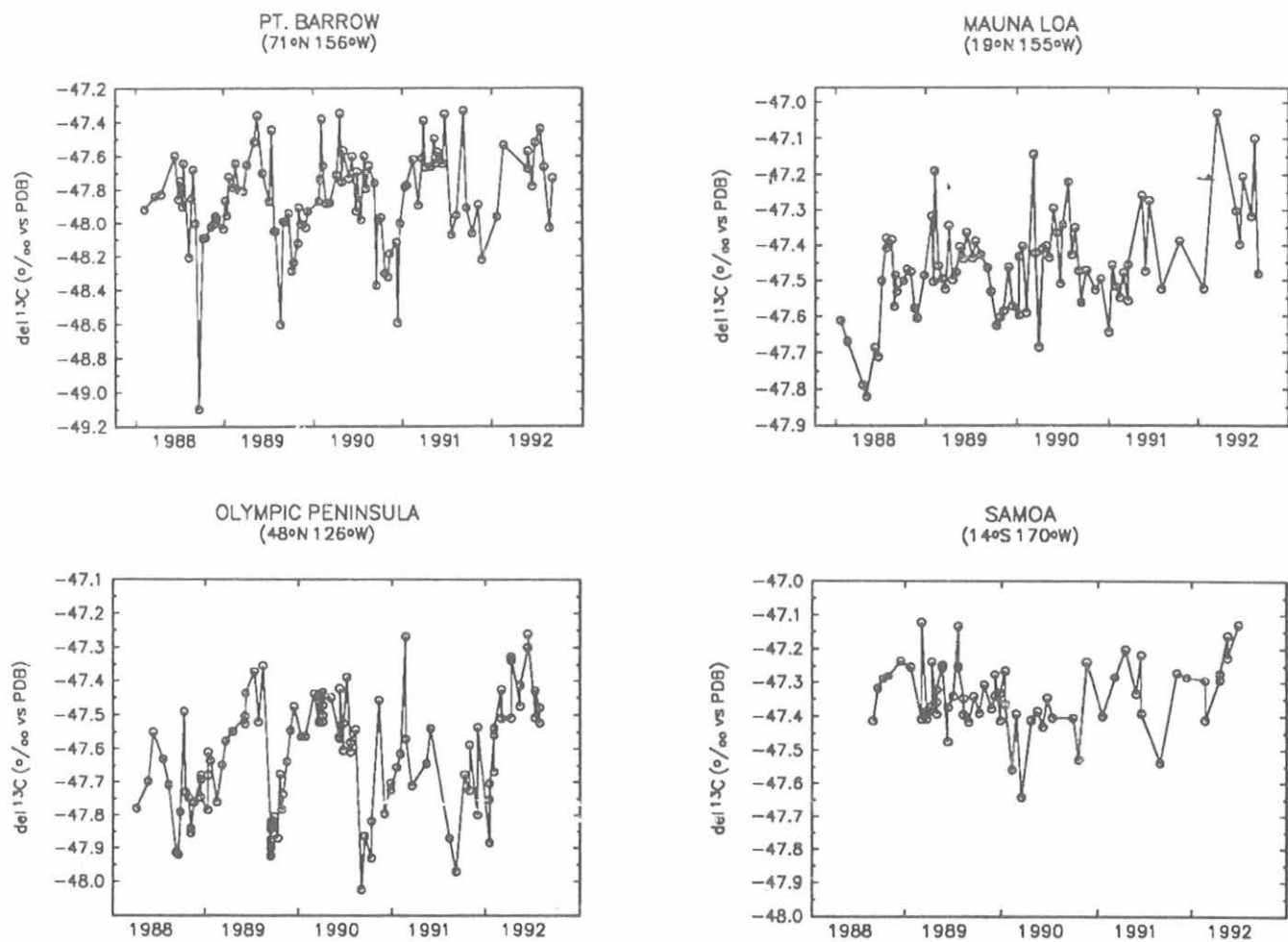


Fig. 1. The time series of the $\delta^{13}\text{C}$ of atmospheric CH_4 measured at Pt. Barrow, Alaska; Olympic Peninsula, Washington; Mauna Loa, Hawaii; and American Samoa since 1988.

Non Seasalt Sulfate to Methanesulfonate Ratios at American Samoa

DENNIS L. SAVOIE AND JOSEPH M. PROSPERO

*University of Miami, Rosenstiel School of Marine and Atmospheric Sciences
Division of Marine and Atmospheric Chemistry, Miami, Florida 33149-1098*

1. INTRODUCTION

A major goal of our cooperative work at SMO is to more rigorously define the sources, atmospheric transport pathways, and fluxes of particulate nitrogen and sulfur species in the remote marine atmosphere. As a major component of aerosols, non seasalt (nss) SO_4^- is believed to play an important role in the radiation balance of the atmosphere as well as in the acidity of atmospheric particles and precipitation. Estimates of the absolute and/or relative contributions of the marine and continental sources to the total nss SO_4^- concentration require an independent estimate of the amount of nss SO_4^- derived from at least one of these two sources. Methanesulfonate (MSA) has frequently been used as a tracer for the marine biogenic component because its dominant source over the ocean is believed to be the oxidation of dimethylsulfide (CH_3SCH_3 , DMS). However, there has been some concern that the (DMS) derived nss SO_4^- /MSA ratio may vary significantly in both time and space. The best locations to assess the variation in the DMS-derived nss SO_4^- /MSA ratio are those in regions that are minimally impacted by continentally-derived material either anthropogenic or natural; SMO appears to be one such location. In this report, we use the results from 149 more recent samples in addition to the original 22 of *Saltzman et al.* [1985] to assess the variations in the relative concentrations of MSA and nss SO_4^- at SMO. The more recent data are from 96 weekly samples collected from January 3, 1990, through May 6, 1992, and from 53 daily samples collected in conjunction with the NASA GLOBE aircraft missions of November 1989 and May 10 to June 10, 1990.

The aerosol samples were collected by drawing air through 20×25 -cm Whatman-41 filters at a nominal flow rate of $1.1 \text{ m}^3 \text{ min}^{-1}$. The sampling pumps are controlled by wind sensors that activate the pumps only when the wind is off the ocean at speeds greater than 1 m s^{-1} . Milli-Q water extracts of quarter-sections of the filters were analyzed for SO_4^- and MSA (1σ uncertainties = 5%) using suppressed ion chromatography and for N_a^+ (1σ uncertainty = 2%) using flame atomic absorption. Nss SO_4^- is the difference between total SO_4^- and seasalt SO_4^- , the latter being calculated as total N_a^+ times 0.2516, the $\text{SO}_4^-/\text{N}_a^+$ mass ratio in bulk seawater. The results from an intensive study of concurrent samples collected on Barbados indicate that the uncertainties in a given interspecies ratio are about 2-5% and are attributable almost exclusively to the imprecisions in the chemical analyses.

2. RESULTS

The mean concentrations of nss SO_4^- and MSA for a variety of periods are presented in Table 1. A similar mean nss SO_4^- concentration, $0.36 \mu\text{g m}^{-3}$, was reported by *Savoie et al.* [1989a,b] for 215 samples. Even the comparatively small data set ($n = 22$) used by *Saltzman et al.* [1985] provided comparable means: $0.41 \mu\text{g m}^{-3}$ for nss SO_4^- and 26 ng m^{-3} for MSA. The seasonal cycles of nss SO_4^- and MSA are indicated by the seasonal averages listed in Table 1. The nss SO_4^- seasonal cycle is virtually identical to that which was based on the 1983 through 1987 samples [*Savoie et al.*, 1989b]. Perhaps partially as a consequence of the more limited data set, there is no clearly coherent pattern in either the monthly or the seasonal averages for MSA.

The coefficients of determination (r^2) between MSA and nss SO_4^- are clearly significant: 0.66 for all of the weekly averages; 0.64 for November 1989 daily samples; and 0.83 for May-June 1990 daily samples. Using a least-squares regression technique that takes into account the errors in both variables, the 127 weekly averages for nss SO_4^- and MSA yield the following equation:

$$\text{nss SO}_4^- = 15.6 (\pm 3.5) \text{ MSA} + 0.047 (\pm 0.089) \quad (1)$$

where all concentrations are in $\mu\text{g m}^{-3}$ and \pm indicates the 95% confidence intervals. Excluding the intercept (which is not significantly different from zero) yields the following relationship:

$$\text{nss SO}_4^- = 17.9 (\pm 2.7) \text{ MSA} \quad (2)$$

For the 127 weekly averages, the geometric mean (GM) ratio (18.1 ± 0.9) is virtually identical to the MSA regression coefficient in eq. (2) and to the results obtained if all of the daily samples are considered separately rather than combined into weekly averages. The results from the composited seasonal data sets clearly indicate that there is no consistent seasonal variation in the nss SO_4^- /MSA ratio. Moreover, the GM ratio for all of the 53 daily samples considered collectively (GM = 17.4; standard geometric deviation (SGD) = 1.346; median = 17.3) does not differ significantly from those for the overall or seasonal data sets even though there appear to be differences between the two daily sets.

The overall variance in the measured nss SO_4^- /MSA ratio includes two principal components: (1) the variance due to

TABLE 1. Mean Concentrations (Standard Deviation, N) of Nonsea-Salt (nss) SO_4^- and MSA and Statistics of the nss SO_4^-/MSA Ratio at American Samoa for Various Time Periods.

Data Set	NSS SO_4^- $\mu\text{g m}^{-3}$	MSA ng m^{-3}	NSS N	SO_4^-/MSA GM	Ratio SGD
All weekly averages	0.371 (0.160, 393)	22.9 (10.6, 128)	127	18.07	1.328
All individual samples, 1983-1992			171	18.06	1.373
Seasonal Using Weekly Averages					
Dec., Jan., Feb.	0.411 (0.174, 78)	22.9 (8.0, 21)	21	17.46	1.230
March, April, May	0.340 (0.165, 99)	21.9 (11.6, 36)	36	18.14	1.306
June, July, Aug.	0.320 (0.133, 107)	22.8 (12.1, 33)	32	17.50	1.382
Sept., Oct., Nov.	0.421 (0.148, 109)	23.8 (9.9, 38)	38	18.84	1.354
Daily Samples					
Nov. 1989	0.366 (0.177, 25)	17.7 (8.0, 25)	25	20.13	1.373
May-June 1990	0.444 (0.227, 28)	29.9 (16.5, 28)	28	15.25	1.229

N = Number of data, GM = geometric mean, SGD = standard geometric deviation

the random errors in the measured concentrations of SO_4^- , N_a^+ , and MSA; and (2) the variance in the actual nss SO_4^-/MSA ratio in the atmosphere. Because the frequency distribution of the ratio is lognormal, we assess the variance in the natural logarithm of the ratio ($\ln R$) which exhibits a normal distribution. In this case, the appropriate equation is:

$$\ln R = \ln (\text{nss } \text{SO}_4^-) - \ln (\text{MSA}) \quad (3)$$

and propagation of errors yields the following estimate for the variance in $\ln R$ that arises solely as a consequence of the analytical variance (a) of SO_4^- , N_a^+ , and MSA:

$$\sigma^2[\ln R, a] = \sigma^2[\ln (\text{nss } \text{SO}_4^-), a] + \sigma^2[\ln (\text{MSA}), a] \quad (4)$$

which can be calculated from the following:

$$\begin{aligned} \sigma^2[\ln(\text{MSA}), a] &= \sigma^2[(\text{MSA}), a]/(\text{MSA})^2 = \\ & (0.05 * \text{MSA})^2 / (\text{MSA})^2 = 0.0025 \end{aligned} \quad (5)$$

$$\sigma^2[\ln(\text{nss } \text{SO}_4^-), a] = \sigma^2[(\text{nss } \text{SO}_4^-), a]/(\text{nss } \text{SO}_4^-)^2 \quad (6)$$

$$\sigma^2[(\text{nss } \text{SO}_4^-), a] = (0.05 * \text{SO}_4^-)^2 + (0.02 * 0.2516 * \text{N}_a^+)^2 \quad (7)$$

where the constants 0.05 and 0.02 represent the analytical uncertainties for MSA, SO_4^- , and N_a^+ , respectively.

For all sample sets that were examined, the variance of the measured $\ln R$ is comparable to the variance that would be expected from the uncertainties in the measured atmospheric concentrations alone. For the 171 individual

samples, $\sigma^2[\ln R, m]$ was 0.085 which is virtually identical to the estimated analytical variance, $\sigma^2[\ln R, a] = 0.083$. For all 127 weekly averages, $\sigma^2[\ln R, m]$ is similar, 0.080, and only 10% higher than $\sigma^2[\ln R, a]$, 0.073. For all 53 daily averages, $\sigma^2[\ln R, m]$, 0.090, is 14% lower than $\sigma^2[\ln R, a]$, 0.104. Even for the May-June 1990 daily samples for which the geometric mean ratio was statistically significantly different from that in the other sets, $\sigma^2[\ln R, m]$ and $\sigma^2[\ln R, a]$ were within 14% of one another (0.073 and 0.063, respectively). The largest difference between the two variances was for the November 1989 daily samples for which $\sigma^2[\ln R, m]$, 0.112, was about 28% less than would have been predicted from the uncertainties in the concentrations, $\sigma^2[\ln R, a] = 0.155$.

3. CONCLUSIONS

Several fundamental conclusions can be drawn from the results of this research. A nss SO_4^-/MSA ratio of 18.1 (± 0.9) appears to be applicable at Samoa throughout the year. This value is only 7% higher than the GM ratio of 16.9 (± 1.1) in the much smaller data set used by *Saltzman et al.* [1985]. Since the observed variances from this value can be attributed solely to the random errors in the measurements, there is no evidence that this ratio varies to any significant extent. Hence measurement uncertainties would have to be reduced substantially in order to observe any variations that could be attributed to actual changes in the ambient atmosphere. The ratio at Samoa is consistent with the biogenic nss SO_4^-/MSA ratios that were estimated for Bermuda and Barbados from the results of multiple variable regression analyses, 19.6 (± 2.1) and 18.8 (± 2.2), respectively [*Savoie et al.*, 1993].

Acknowledgments. We thank T. Snowdon, F. Huang, T. Huang, M. Izaguirre, and L. Custals (University of Miami) for their technical assistance; B. Mendonca and CMDL Boulder for their continued cooperation; and C. Farmer and M. Winey (SMO) for maintaining and operating our sampling systems. The research was supported by NSF grants ATM8703411 and ATM9013125, and NASA contracts NAG8-621 and NAG8-841.

4. REFERENCES

Saltzman, E.S., D.L. Savoie, J.M. Prospero, and R.G. Zika, Atmospheric methanesulfonic acid and non-seasalt sulfate at Fanning and American Samoa, *Geophys. Res. Lett.*, 12, 437-440, 1985.

Savoie, D.L., J.M. Prospero, and E.S. Saltzman, Nitrate, non-seasalt sulfate and methanesulfonate over the Pacific Ocean, in *Chemical Oceanography, Vol. 10, SEAREX: The Sea/Air Exchange Program*, pp. 219-250, edited by J. P. Riley, R. Chester, and R. A. Duce, Academic, San Diego, CA, 1989a.

Savoie, D.L., J.M. Prospero, J.T. Merrill, and M. Uematsu, Nitrate in the atmospheric boundary layer of the tropical South Pacific: Implications regarding sources and transport, *J. Atmos. Chem.*, 8, 391-415, 1989b.

Savoie, D.L., R. Arimoto, J.M. Prospero, R.A. Duce, W.C. Graustein, K.K. Turekian, J.N. Galloway, and W.C. Keene, Oceanic and anthropogenic contributions to non-seasalt sulfate in the marine boundary layer over the North Atlantic Ocean, *J. Geophys. Res.*, submitted, 1993.

USGS Barrow Observatory

JACK TOWNSHEND

U.S. Geological Survey, College Observatory, Fairbanks, Alaska 99775-5160

The USGS Barrow Observatory is the northernmost of this agency's 13 continuously recording, digital magnetic observatories. As such, it serves as a singularly important site in a global network of observing stations, whose combined data define the planetary magnetic field and track its secular change. Ground stations such as at the Barrow Observatory are controls for field modeling by harmonic analysis, essential reference stations for airborne and satellite surveys, and absolute calibration locations for field survey instrumentation. The observatory is operated from the USGS College Observatory at the University of Alaska in Fairbanks as a satellite station. Staff scientists from the College Observatory visit the site bimonthly to make absolute observations, perform routine equipment maintenance, and retrieve data on magnetic tape. Staff personnel from NOAA CMDL make weekly visits to the site to check equipment operation and occasionally

perform emergency service when there is a problem and a College Observatory staff person is not available to make repairs.

The primary equipment used to acquire the magnetic data is an EDA FM-100-BR Triaxial fluxgate magnetometer, an EDA PPM-105 proton free-precession magnetometer, an observatory magnetometer interface system, and several pier-mounted instruments for absolute control observations. Data are retrieved by telephone periodically through a computer modem by the USGS office in Golden, Colorado. A seismograph is operated on site in a vault located 6.1 m beneath the ground surface. The present seismic program is operated in cooperation with the Geophysical Institute at the University of Alaska, Fairbanks.

The USGS Barrow Observatory has been in continuous operation since 1949.

Separation of Local From Distant Pollution at MLO Using Pb-212

S. WHITTLESTONE

Australian Nuclear Sciences & Technology Organisation, Menai, N.S.W. 2234, Australia

S.D. SCHERY AND YANXIA LI

New Mexico Tech., Socorro, New Mexico 87801

1. INTRODUCTION

At MLO there are several means of deciding whether an air mass can be considered "baseline." Wind direction, dew point, CN, and radon are the most important parameters on which to base selection of baseline samples. Combined, they can be used with a high success rate to select air samples that represent a large volume of the atmosphere and are free from recent pollution [Gras *et al.*, 1992]. They cannot, however, be used to distinguish between local and distant sources.

Some observers need to know if the air parcel has been in contact with Hawaiian soil. Asian contact a few days before is not always important. Some short-lived gases such as isoprene have shown that it is possible to have entrainment of Hawaiian air into the down-slope flow. But isoprene has complex generation and transport, and a more quantitative, or at least a complementary indicator of local influence is needed.

Pb-212 has the potential to fulfill this role. It is the decay product of thoron gas (radon 220) that is emitted from all soils along with radon-222. Thoron has a 55-second half life and that of Pb 212 is 10.6 hours. After 4 days, only 0.2% of the original Pb-212 remains, which means that it has virtually disappeared from the fastest Asian air flows. However it lasts long enough to be present in 1-day scale circulation. Pb-212 has been used by others for indication of close land contact [Heimann *et al.*, 1990]. Hutter *et al.*, [1990] have measured Pb-212 at MLO, and shown the expected result that Pb-212 tends to be present in up-slope air, but not in downslope.

This report describes a 5-week study of Pb-212 concentration at MLO to assess its potential for detecting local land influence on air samples. The measurements were carried out at the invitation of NCAR in July-August 1992 to coincide with the last phase of MLOPEX II. Brief mention is made of some measurements of Pb-212 and thoron emanation from lava in April 1993 because the preliminary results clarify the MLOPEX measurements.

2. EXPERIMENTAL METHOD

The method employed to measure the concentration of Pb-212 required three steps. First, air was drawn from a mast 3 m above ground at a rate of 250 L min⁻¹ through a filter (Gelman versipore, 1.2 micron pore size) with diameter 115 mm. This stage lasted 2 hours, and was synchronized with even hours local time. Next, the filter

was left for 4 hours; long enough to allow any radon-222 decay products to decay. Finally, the filter was exposed to a screen coated with zinc sulfide, the scintillation's of which were detected by a photomultiplier.

This process was fully automated and permitted measurement of Pb-212 averaged over precisely defined 2-hour periods. Extraction of the Pb-212 concentration was simple in principle, requiring only subtraction of background events from the raw count and multiplication by a calibration factor.

3. RESULTS

At MLO influence of Hawaiian land is most strongly felt during the day when the synoptic winds are light and there is no heavy cloud above the mountain. Under these conditions convective northerly upslope winds become established. At night the same cloud and wind conditions lead to southerly downslope winds that are subject to the least island contact. Synoptic flows and clouds result in more complex sampling conditions.

The week starting July 16 (Figure 1) was so variable that most conditions of interest occurred. On July 16, CN, water, Pb-212, and radon concentrations varied as expected for upslope and downslope conditions: concentrations elevated in upslope winds compared to concentrations in downslope winds. On other days most possible combinations of tracer concentrations occurred: high CN

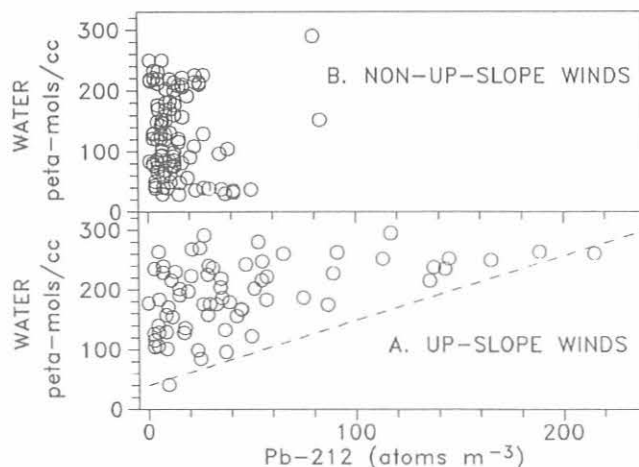


Fig. 1. Pb-212 versus water concentration.

and water with low Pb-212 and radon on July 20, low CN and water with high Pb-212 and radon on July 18, and so on. It is of particular note that elevated Pb-212 does occur in dry downslope winds when land contact should be a minimum.

The data for 5 weeks were sorted into groups in which the wind had persisted in the upslope (315° through north to 67°) and non-upslope sectors for 2 hours. Upslope conditions are easiest to understand. A high proportion of radon in upslope wind is from Hawaii, rather than from remote land, and correlation analysis indicated that the correlation of Pb-212 with radon is quite high (0.76). The sources of Pb-212 and CN tend to be differently distributed on the island, so this correlation is modest (0.48). In the case of water, the data are stronger than would appear from the modest correlation coefficient of 0.45. This is illustrated in Figure 1a. It is not unusual to have moist boundary layer air transported to the observatory with a minimal contact with Pb-212 producing land, so there will be times when Pb-212 is low but water concentration high: at low Pb-212 concentrations it is possible to have a wide range of water concentrations. However, if the Pb-212 concentration is high, the air path must have been close to land and therefore, from the moist boundary layer. Pb-212 thus provides clear discrimination of moist air into parcels with and without contact with Hawaiian soil.

In non-upslope winds, the proportions of non-Hawaiian radon and CN are higher and the correlations with Pb-212 weaker as expected. The relationship between Pb-212 and water (Figure 1b) was markedly different from that in the upslope sector and the correlation coefficient was slightly negative (-0.2). This suggests that some of the down-slope Pb-212 may not have come from the moist boundary layer.

The origin of non-upslope Pb-212 was investigated in a number of ways. First, correlations were carried out for data from a wind sector close to directly downslope. These winds tend to occur when the skies are clear and the synoptic winds light and should accentuate any direct effects of the mountain above MLO. Table 1 shows correlations of Pb-212 with radon, CN, water, wind speed, and differential temperature. The number of events in this sector was only 20, 17% of all non-upslope, so not too much weight should be given to the correlations.

TABLE 1. Correlations between Pb-212 and wind speed, radon, CN, and water concentrations, for winds persisting in the downslope sector, south $\pm 16^\circ$, for at least 2 hours at more than 2 ms^{-1}

	PB-212	Radon	CN	Water	Wind Speed
Radon	0.81				
CN	0.82	0.90			
Water	0.03	0.17	0.27		
Wind speed	-0.47	-0.44	-0.66	-0.52	
DT*	-0.64	-0.36	0.34	0.38	0.25

*DT - Differential temperature 2-40 m.

The correlations in the downslope sector are very much stronger than in the broader non-upslope sector. Taking them at face value, it would seem that Pb-212 is higher when wind speed is less and the differential temperature is more negative: conditions favoring a smaller mixing depth and a larger contribution from the lava above MLO. There are also strong correlations, not seen in the rest of the non-upslope sector between Pb-212 and species that can be imagined to come from volcanic vents: CN and radon. It is somewhat confusing that the correlation of differential temperature is weakly positive with CN but moderately negative with Pb-212.

A second approach to assessing the origin of non-upslope Pb-212 was to compare the average concentrations in the three wind sectors. From Table 2 it is evident that Pb-212 responds more strongly to Hawaiian land contact than the other species: the ratio of non-upslope to upslope is 0.2. This proportion is small enough for it to be reasonable to attribute it to either lava above MLO or re-circulated air from below MLO. Data in Table 2 support the indication above that a significant proportion of non-upslope radon is from above MLO: the Pb-212 concentration in the broad non-upslope sector is only half that in the downslope sector.

Thirdly, Pb-212 was compared to another natural tracer, isoprene. Both the source distributions and evolution with time of these species are somewhat different. Even so, there is close correlation between the means of groups selected on the basis of Pb-212 concentration ranges as shown in Figure 2. Isoprene has no source above MLO or distant from Hawaii. Figure 2 therefore supports the evidence from wind sector averages that most Pb-212 comes from below MLO.

The final evidence for location of Pb-212 sources comes from a set of measurements specifically designed to set limits on the amount from above MLO. From preliminary analysis of this experiment three conclusions are suggested: (1) The thoron emanation from lava above MLO is sufficient to produce Pb-212 concentrations of the order of those observed in downslope winds with reasonable mixing depths. (2) In ideal downslope winds, Pb-212 concentrations close to the top of Mauna Loa, directly upwind of MLO have been observed to be close to the limit

TABLE 2. Ratios between concentrations of PB-212, radon, CN, water, and wind speed in three wind sectors. The non-upslope sector excludes the downslope, south $\pm 16^\circ$, sector.

Wind Sectors	Ratio				
	PB-212	Radon	CN	Water	Wind Speed
Non-upslope	0.21	0.67	0.54	0.66	1.58
Upslope					
Non upslope	0.50	1.14	0.94	1.02	1.07
Downslope					

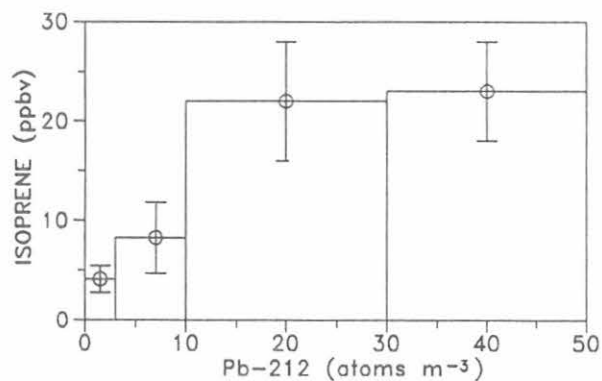


Fig. 2. Average isoprene concentration in each Pb-212 concentration range. Bars are errors on the means.

of detection (2 atoms m^{-3}) while the level at MLO was up to 17 atoms m^{-3} . This may have come from the lava in the path of the air flow. (3) When a moderate southeasterly synoptic wind de-coupled the boundary layer from MLO, the Pb-212 concentration in the saddle below MLO was lower than the concentration at MLO. This is strong evidence for a Pb-212 source above the saddle where the terrain is similar to that above MLO.

4. CONCLUSIONS

Continuous measurements of Pb-212 with 2-hour time resolution have established that levels at MLO over a wide range of conditions could be made by a relatively simple instrument with sufficient sensitivity at 1-hour time resolution.

The presence of Pb-212 is unequivocal evidence of passage of an air parcel close to the Hawaiian land, and it is feasible to detect concentrations as small as 2% of the highest levels observed in upslope winds. Pb-212 is, therefore, an excellent supplement to radon, which detects land contact, but not necessarily with Hawaii.

Interpretative difficulties arise because some Pb-212 enters air from even relatively recent lava above MLO. The total amount of Pb-212 in non-upslope winds is generally small compared with that in upslope winds, being less by a factor of 5 on average. Most of the Pb-212 in a narrow downslope sector appears to come from the lava above MLO. Further analysis is required to decide whether there is any Pb-212 recirculated from below MLO to the broad non-upslope sector.

Acknowledgments. CMDL provided some equipment and preliminary meteorological data. The practical assistance of S. Ryan was most valuable. J. Greenburg of NCAR supplied preliminary isoprene data. The automatic Pb-212 detector was built by B. Stenhouse of ANSTO. S. Schery's and Y. Li's research is funded in part by the U.S. D.O.E.

5. REFERENCES

- Gras, J.L., and S. Whittlestone, Radon and CN: Complementary tracers of polluted air masses at coastal and island sites, *J. Radioanalytical and Nuclear Chem.*, 161, 293-306, 1992.
- Heimann, M., P. Monfray, and G. Polian, Modeling the long-range transport of ^{222}Rn to subantarctic and antarctic areas, *Tellus*, 42B, 83-99, 1990.
- Hutter, A.R., A.C. George, M.L. Maiello, I.M. Fisenne, R.J. Larsen, H.L. Beck, and F.C. Wilson, ^{222}Rn , ^{222}Rn progeny and ^{220}Rn progeny as atmospheric tracers of air masses at the Mauna Loa Observatory, EML-522., 26 pp., Environmental Measurements Laboratory, U.S. Dept. of Energy, New York, 1990.

Recent Interannual Variations in CO₂ in Both Hemispheres

T. P. WHORF, C. D. KEELING, AND D. M. WAHLEN
Scripps Institution of Oceanography, La Jolla, California 92093-0220

1. INTRODUCTION

Cooperative programs of CO₂ measurements between the Scripps Institution of Oceanography (SIO) and CMDL continued through 1992 at Point Barrow, Alaska (PTB), Mauna Loa Observatory (MLO), Cape Kumakahi (KUM), Samoa (SAM), and the South Pole (SPO). Air samples were collected in 5-L glass flasks several times per month since the 1950s at MLO and SPO, and since the mid 1970s to early 1980s at the other three stations. SIO also collects flask samples at a few other stations, including La Jolla (LJO) since 1969. In addition, SIO continues to monitor atmospheric CO₂ concentrations at MLO on a continuous basis using the non-dispersive infrared (NDIR) gas analyzer installed on site in 1958. Furthermore, since 1978 at some stations the ¹³C/¹²C isotopic ratio of atmospheric CO₂ was determined from samples collected in flasks. Measurements before 1992 were made at the laboratory of Willem Mook at Groningen University [Keeling *et al.*, 1989, and unpublished data]. Subsequent measurements were made at SIO. Recent data indicate that the persistent rise in atmospheric CO₂ has anomalously slowed since 1989 on a global basis. The anomalous departures at MLO and SPO are the largest ever seen at these stations in over 30 years of record. Nevertheless, as with previously observed anomalies in atmospheric CO₂, this anomaly appears to be associated with an El Niño event. It may also be related to the eruption of the Pinatubo volcano. In either case, the anomaly is expected to be transient and not an indication that the global carbon cycle has become more efficient in sequestering CO₂ produced by the combustion of fossil fuels.

2. DATA AND ANALYSIS

All flask samples were analyzed for their CO₂ concentration with an NDIR gas analyzer of the same design as that installed at MLO. Calibrations have continued with reference gases similar to those used at MLO [Keeling *et al.*, 1986]. Air samples were rejected if pairs did not agree within 0.40 ppm (0.60 ppm for Point Barrow), i.e., singlets were rejected also, or if found to be outliers having a residual greater than three standard deviations from a smooth curve fit describing the seasonal and interannual variations. The function chosen in the fitting process uses a sum of four harmonics to describe the seasonal variations, and a cubic spline [Reinsch, 1967] to describe the interannual variations. A gain factor is used to model an approximately linearly increasing seasonal amplitude variation [Keeling *et al.*, 1989, pp. 167, 176]. This simple model of increasing annual CO₂ cycles was

introduced when it became clear in our longer CO₂ records that there were significant increases in the seasonal amplitude of CO₂ concentration.

Figure 1 shows the results of such fits made to the CO₂ observations selected from a subset of the stations where we sample air. Point Barrow data were augmented to include continuous CO₂ data measurements made by Kelley [Kelley, 1969] during the period 1961-1967. Data at five additional sites are shown in the figure: La Jolla, California (33°N, 117°W), MLO (19°N, 155°W), Christmas Island (2°N, 157°W), SMO (14°S, 171°W) and SPO (90°S). A cooperative program at Alert between SIO and the Atmospheric Environment Service of Canada has existed since 1985. The Alert CO₂ record is, however, relatively

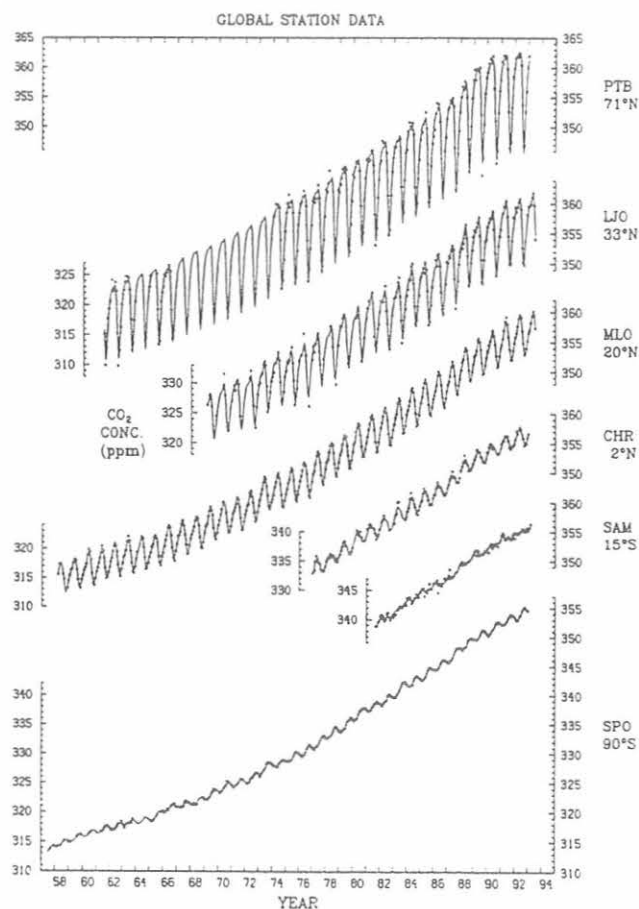


Fig. 1. Monthly average CO₂ concentration (in ppm) at six SIO stations spanning the globe and fit by the function prescribed in the text. Early Point Barrow data are from Kelley [1969] and Mauna Loa data from the continuous data record.

short and thus in this analysis provides only supporting evidence to the results from the longer stations. The Christmas Island data record shown in Figure 1 was extended back from 1976 to 1972 by using data from nearby Fanning Island in the computation of CO₂ anomalies discussed in the next section.

3. RESULTS

Plots of CO₂ anomalies were prepared from seasonally-adjusted monthly average CO₂ data at each station by subtracting a constant fraction of the CO₂ produced by industrial processes, as described by Keeling *et al.*, [1989,

p. 179-180]. This airborne fraction (58.6%) was chosen so that the anomaly is zero on January 1, 1959, and 1986 for MLO in the northern hemisphere and for SPO in the southern hemisphere. Figures 2 and 3 show the results for selected northern and southern hemisphere stations, respectively. A strong negative anomaly is seen to have developed at all stations in 1992. At many of the stations it began immediately following the eruption of Mt. Pinatubo in the Philippine Islands. It is more pronounced in the northern hemisphere, but is global in scope.

To determine the cause of this anomaly, we have computed global terrestrial vegetative and oceanic fluxes of CO₂ that explain the recent trends in both atmospheric CO₂

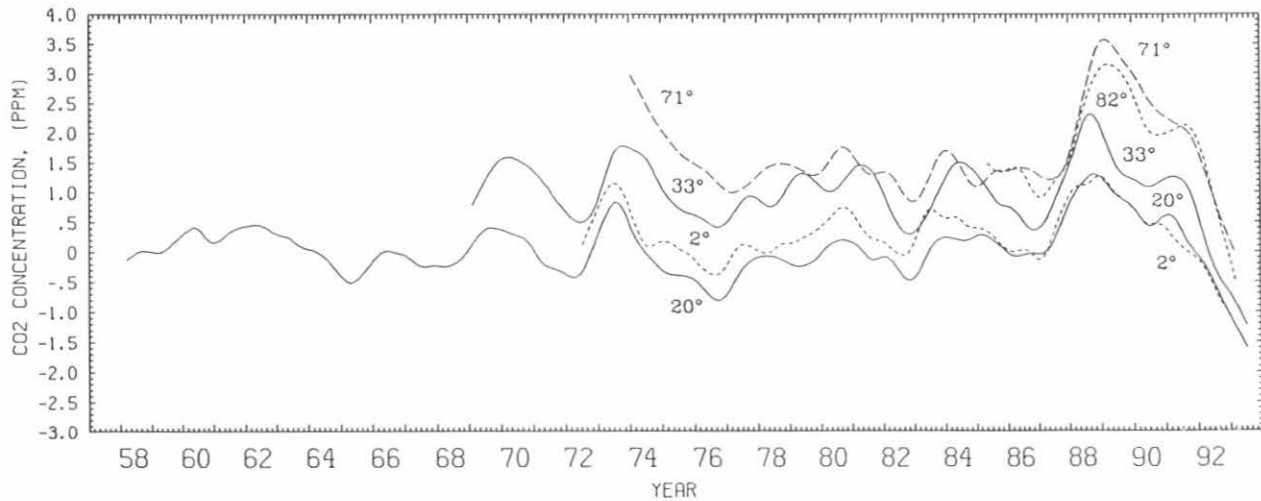


Fig. 2. CO₂ anomalies for northern hemisphere stations obtained by seasonally adjusting the data and then subtracting a constant airborne fraction of the CO₂ released to the atmosphere by industrial processes, calculated to agree with the Mauna Loa CO₂ record (58.58%). The latitude of each station is indicated: Alert 82°N, Pt. Barrow 71°N, La Jolla 33°N, Mauna Loa 20°N, Christmas Island 2°N.

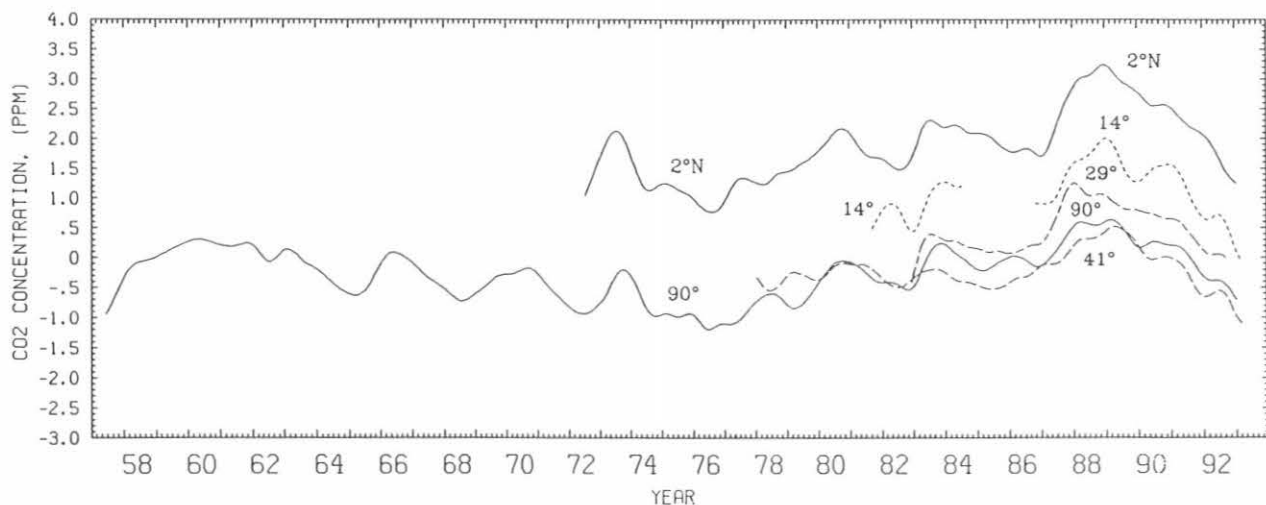


Fig. 3. CO₂ anomalies for southern hemisphere stations obtained as in Figure 2, except that the constant airborne fraction is calculated for the South Pole (55.94%). Stations plotted are Samoa 14°S, Kermadec 29°S, New Zealand 41°S, and South Pole 90°S. Christmas Island is repeated from Figure 2 but with the airborne fraction calculated for the South Pole.

concentration and its $^{13}\text{C}/^{12}\text{C}$ ratio. First we combined data for MLO and SPO to obtain estimates of the global trends in both the concentration and $^{13}\text{C}/^{12}\text{C}$ ratio. Then with a one-dimensional model of the oceanic carbon cycle [Siegenthaler, 1983] we estimated the rate at which the oceans have absorbed CO_2 injected into the atmosphere by industrial processes.

The calculated rate is a function of the rate of industrial emissions [Marland, 1991 and personal communication] and of the observed atmospheric concentration variation since preindustrial times. The concentration variation used in the calculation, as described by Keeling *et al.*, [1989, pp. 186] combines estimates of CO_2 concentration from air trapped in ice cores with the CO_2 data from MLO and SPO. We then calculated the variations in CO_2 concentration not accounted for by oceanic absorption of industrial CO_2 . For the period commencing with the isotopic record in 1978, these anomalous variations were further partitioned into oceanic and terrestrial components consistent with the observed $^{13}\text{C}/^{12}\text{C}$ ratio of atmospheric CO_2 . This computation was done by a "double deconvolution" as described by Keeling *et al.*, [1989, pp 229-230]. The oceanic and terrestrial fluxes implied by this double deconvolution are plotted in Figures 4 and 5, respectively. Fluxes in gigatons of carbon (GtC) are shown as integrals over intervals defined by episodes of persistently positive and negative oceanic anomalies. The anomalies are expressed with respect to the average trend in each flux from the beginning of 1978 until May 1991, when the most recent negative anomaly began. Since May 1991, the oceans are computed to have taken up 0.7 GtC, in addition to 4.5 GtC absorbed primarily in response to the increase in atmospheric CO_2 from industrial emissions, but partially owing to long-term changes in the carbon cycle reflected in the average trend in each anomalous flux component from

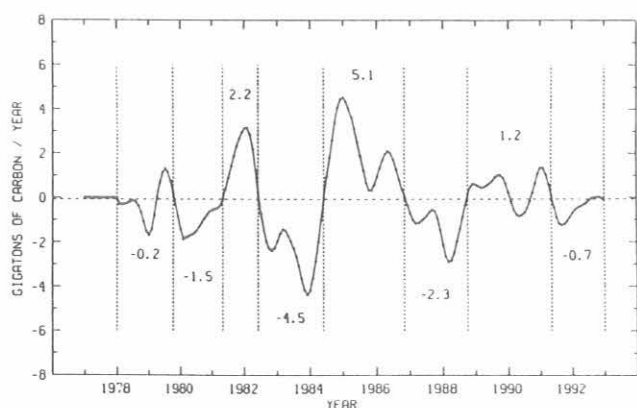


Fig. 4. Time trend of the anomalous release of CO_2 by the oceans shown as a solid curve in units of GtC yr^{-1} . Vertical lines separate persistently positive and negative anomalies with amounts integrated over each interval expressed in GtC. A dashed curve indicates the long-term trend evaluated as the mean of the anomaly over the isotopic record period up to May 1991 (0.08 GtC yr^{-1}).

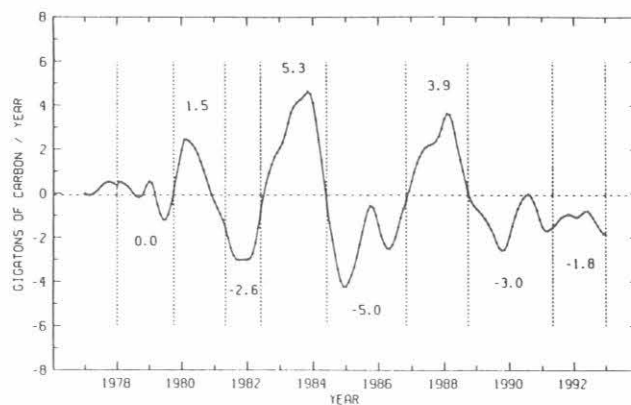


Fig. 5. Same as Figure 4 except showing the time trend of the net release of CO_2 by the biosphere. The vertical lines are those used in Figure 4, and the mean of the anomaly over the isotopic record up to May 1991 is $-0.08 \text{ GtC yr}^{-1}$.

1978 to 1991. During the same time period, the terrestrial vegetation is computed to have anomalously taken up 1.8 GtC. These two estimated amounts are, however, more uncertain than those for previous periods of persistent anomalies, because the isotopic measurements of the final period were made on a different mass spectrometer, not yet fully calibrated.

The computations, if correct, indicate that the oceanic and terrestrial flux components, since May 1992, have both involved withdrawals of CO_2 from the air, contrary to all previously documented episodes shown in Figures 4 and 5, in which the fluxes were in opposite directions with respect to the atmosphere. Thus they have evidently produced a prominent anomaly in CO_2 concentration, even though they are not particularly striking when viewed separately. We caution that these conclusions could be altered if the isotopic calibrations turn out later to need adjustment.

In our calculations, we have taken into account the influence of temperature at the sea surface on the air-sea flux. The oceans cooled since May 1991 by about 0.5°C as judged from a cooling trend in global air temperature [Dutton and Christy, 1992]. According to calculations using the one-dimensional model as cited previously, this cooling accounts for an additional absorption of only about 01 GtC CO_2 by the oceans. Thus the principal cause of the anomalous oceanic sink of 0.7 GtC is evidently an increase in photosynthesis of marine plants that decreased the pressure of CO_2 gas dissolved in the water by converting inorganic carbon to organic carbon.

4. CONCLUDING REMARKS

Until the present event terminates with a return to a positive CO_2 concentration anomaly, it is difficult to assess the extent to which this anomaly is actually synchronous with the climatic impacts of the Mt. Pinatubo eruption. The El Niño event that began in 1991 in the eastern half of the equatorial Pacific, then waned in late 1992, and had a

short re-emergence in early 1993 [*Climatic Analysis Center*, 1993], is a further complicating factor in deciding the cause of the anomaly. Before carrying the interpretation any further, the question of the isotopic calibration needs to be resolved. Improvements in modeling the isotopic aspects of the carbon cycle would also add confidence to our tentative findings.

Acknowledgments. This work was supported by Grants ATM91-21986 and DPP91-96095 of the National Science Foundation, Grant DE-FGO3-90ER60940 of the U.S. Department of Energy and Grants NAGW-2542 and NAGW-2987 of the U.S. National Aeronautics and Space Administration. In addition NOAA, through Contract 50RANR100090, provided for the cost of maintaining our primary standard reference gases used to maintain accuracy in our measurements of atmospheric CO₂. We are grateful to CMDL for providing assistance in our sampling program and for maintenance of our continuous recording instrument at MLO.

5. REFERENCES

- Climate Analysis Center, *Climate Diagnostics Bulletin*, NOAA, National Meteorological Center, Camp Springs, MD, 5-9, August 1993.
- Dutton, E.G., and J.R. Christy, Solar Radiative Forcing at Selected Locations and Evidence for Global Lower Tropospheric Cooling Following the Eruptions of El Chichon and Pinatubo, *Geophys. Res. Lett.*, 19, 2313-2316, 1992.
- Keeling, C.D., P.R. Guenther, and D.J. Moss, Scripps reference gas calibration system for carbon dioxide-in-air standards: Revision of 1985, *Report No. 4 of the Environmental Monitoring Programme of the World Meteorological Organization*, Geneva, 34 pp. and Addendum, 43 pp., 1992.
- Keeling, C.D., R.B. Bacastow, A.F. Carter, S.C. Piper, T.P. Whorf, M. Heimann, W.G. Mook, and H. Roeloffzen, A three-dimensional model of atmospheric CO₂ transport based on observed winds: 1. Analysis of observational data, in *Aspects of Climate Variability in the Pacific and the Western Americas*, edited by D.H. Peterson, Geophysical Monograph, American Geophysical Union, 165-236, Washington, D.C., 1989.
- Kelley, J.J., Jr., An analysis of carbon dioxide in the arctic atmosphere near Barrow, Alaska 1961 to 1967, Contract N00014-67-A-0103-0007 NR, 307-252, 172 pp., Scientific Report of the United States Office of Naval Research, 1969.
- Marland, G., Global CO₂ Emissions, in *Trends '91: A Compendium of data on global change*, ORNL/CDIAC-46, T.A. Boden, J.R. Sepanski, and F.W. Stoss, (Eds.), Carbon Dioxide Information Analysis Center, Oak Ridge National Laboratory, Oak Ridge, TN, pp. 389, 1991.
- Reinsch, C.H., Smoothing by spline functions, *Numerische Mathematik*, 10, 177-183, 1967.
- Siegenthaler, U., Uptake of excess CO₂ by an outcrop-diffusion model of the ocean, *J. Geophys. Res.*, 88, 3599-3608, 1983.

8. International Activities, 1992

In September-October, E. Ferguson visited the University of Paris-South to interact with former colleagues in the Physical Chemistry Department to discuss current research there. He attended the NATO Advanced Study Institute program on The Role of the Stratosphere in Global Change where he lectured on the subject of "Stratospheric Homogeneous Chemistry." Also during this visit he participated in a round-table discussion regarding collaborations on sampling at the Centre des Faibles Radioactivities, and he presented a lecture in the Atomic and Molecular Physics Laboratory at Orsay on "Chemistry of Stratospheric Ozone and the Ozone Hole."

E. Ferguson was in Germany in December to attend the World Meteorological Organization (WMO) Global Atmospheric Watch (GAW) Quality Assurance Program meeting that involved experts on global atmospheric monitoring. The purpose of the meeting was to devise procedures and protocols for assuring high-quality data acquisition at the present and contemplated WMO/GAW global sites. During this time, he also presented a seminar on recent CMDL results at the Max Planck Institute for Chemistry.

J. Peterson traveled to Toronto, Canada, in February to participate in a WMO/GAW meeting on the developing Chinese baseline stations in Qinghai Province. The meeting focused on potential Canadian, Australian, and United States cooperative support with the Chinese to further development of their baseline station.

R.C. Schnell traveled to Siberia from Nome, Alaska, in April to assist in initiating the Bennett Island Project and to recover samples. The Bennett Island Project was a Joint NOAA/Russia Academy of Sciences airborne project (using a Russian AN-26) to sample the Bennett Island plume. These plumes periodically originate from an isolated, uninhabited island in the New Siberian chain and can last for 10-36 hours. It was thought the plumes may be produced by releases of methane from ocean floor clathrate decomposition. The sampling showed the plumes to be natural, post-frontal orographic clouds.

The 5th International Symposium on Arctic Air Chemistry, Copenhagen, Denmark, September 8-10, 1992, was attended by P.J. Sheridan, I. Sokolik, and R.C. Schnell, AGASP members. Seven of the twenty-four core papers presented at the conference were authored by AGASP scientists.

R.C. Schnell attended the Cape Grim Baseline Station annual meeting, Aspendale, Australia, November 25-27, 1992, and visited a number of CSIRO and university facilities both prior to and subsequent to the meeting. Each year CMDL and the Australian Bureau of Meteorology host one scientist from the other's institution at their respective baseline station's annual meeting.

In January, B. Mendonca was a participant and organizer of the first planning meeting for the establishment of a GAW station in Algeria, sponsored by the WMO. In Paris

and Geneva, he met with the research specialists from France and Algeria to define and plan for the GAW station in Algeria. A location for the station and a measurement and instrumentation list was decided on and a time schedule for the initiation of the program was established and agreed upon.

Munich, Germany, was the site of the second Programs and Technical Advisory Group (PTAG) for the Harmonization of Environmental Measurement (HEM) program in May. B. Mendonca was an invited member to review this United Nations Environment Programme (UNEP). As a member of the advisory group, the past year's work and accomplishments were reviewed, and the future direction and goals of the program were formulated and agreed upon.

The University of La Laguna (Tenerife, Spain) sponsored a course on global climate and its relationship with the subtropical region of the globe. B. Mendonca participated as an invited guest lecturer. The course was structured for graduate students and offered advanced study in environmental issues. The lecture was based on the monitoring and research effort in CMDL and with the GAW stations and their programs. A full course brochure was prepared and distributed as a course aid for the students.

In February, L. Haszpra, Institute for Atmospheric Physics, Budapest, Hungary, came to Boulder for 2 weeks. The purpose of the visit was to compare CO₂ data from the Hungarian site at K-Puszta and the CMDL flask network. Discussions were held regarding NOAA-provided gas standards to the Hungarian program and for possible collaboration with CMDL on-tower and aircraft measurements. These discussions lead directly to the preparation and delivery of four carbon dioxide/methane standards and plans for setting up a NOAA flask sampling network site in Hungary.

From March 10 to 13, Pieter Tans presented a paper and participated in the Workshop for Trace Gas Measurement in Both Hemispheres that was held at Aspendale, Australia. The conference was sponsored by the Center for Global Environment Research, National Institute for Environmental Studies (Japan).

The program to bring flask-sampling network personnel to Boulder was continued. In preparation for establishing a sampling site at Sal, Cape Verde, E. Fernando from the Servico Meteorológico Nacional visited Boulder between May 6 and 13. Following training in the use of the MAKS and discussions on methodology and logistics, he hand-carried a MAKS unit back to Sal.

In August 1992, L. Waterman traveled to Warsaw and Gdynia, Poland, to initiate twice-weekly sampling on the *Balanga Queen*, a Baltic Sea ferry operating between Poland and Sweden. Arrangements were made at the U.S. Embassy to receive boxes of flasks sent from Boulder and to dispatch boxes of samples sent from Gdynia by way of

diplomatic post. Arrangements were made with the Morski Instytut Rybacki (MIR) [Sea Fisheries Institute] to operate the sampling program from Gdynia. Samples are collected by the deck officers of the *Balanga Queen* on scheduled voyages between Gdynia and Karlskrona, Sweden. The initial Poland-to-Sweden voyage for the CMDL sampling network site was made on August 31 by L. Waterman and M. Pustuszek (MIR). The Master and several mates were briefed on the program, demonstrations were given, and practice samples collected. Three days later (September 3) on the return voyage to Poland, the second crew was briefed and trained to collect samples. While in Karlskrona, meetings were held with G. Sella and L. Lundahl of the Fiskeriverket Östersjölaboratoriet, the Swedish counterpart of Poland's MIR.

Following completion of the Baltic work, L. Waterman traveled to Oslo and Kristiansund, Norway. Meetings were held with A. Grammelvendt, Director, Det Norske Meteorologiske Institutt, University of Oslo, and other staff members. It was learned that the meteorological institute has reasonably secure funding to operate the *W/S Polarfront* (STM) for at least 2 years (1993-1994). Logistics were discussed and the institute will continue paying some costs associated with the domestic transfer of sample boxes.

L. Waterman visited the *W/S Polarfront* on September 8 and presented the crew with a plaque commemorating 10 years of collecting samples for the CMDL Worldwide Flask Sampling Network. Discussions were held with both sample collectors, and the sample flushing apparatus (P3) was inspected.

On September 10 and 11, L. Waterman visited Blue Star Ship Management Ltd. (London) and the British Antarctic Survey (Cambridge). The reorganization of the Blue Star Line in the Pacific and the plan to replace both the *Southland Star* and the *Wellington Star* were discussed. At the British Antarctic Survey, a meeting was held with the liaison with CMDL for Halley Bay and Bird Island, South Georgia.

On September 12 to 14, L. Waterman visited the AEROCE Mace Head Station at Carna, County Galway, Ireland, and met with G. Spain, Station Manager. A new flask sampling procedure using a Dekabon line attached to the AEROCE tower was initiated.

On September 15, L. Waterman traveled to Reykjavik, Iceland, to initiate a new flask sampling site at Storhofdi Lighthouse, Heimaey, Westman Islands, including sending flask boxes to and from Iceland by diplomatic post. Regular sampling began on October 2.

In September, P. Tans visited the Chinese Academy of Meteorological Sciences (CAMS) in Beijing. The purpose of the trip was to inspect the Mt. Waliguan baseline station that is a part of the CMDL air sampling network, and to investigate the possibilities for a cooperative effort to monitor trace gas fluxes in China's agricultural heartland. Talks were presented at CAMS on the CMDL global methane monitoring program and on the carbon dioxide program. A talk on global climate change was also given

at the State Oceanographic Administration. Hubei Province was visited to inspect radio transmission towers in the vicinity of Jingzhou. The highest towers are about 125 m and not tall enough for the type of concentration measurements currently being made in North Carolina. It would be useful to obtain experimental data on regional greenhouse gas fluxes in this region of China. Discussions were held on setting up such an experiment with focus on communication, maintenance, and training. The realization of this program depends on finding new funding sources, however. Qinghai Province was visited with a group driving to the Mt. Waliguan baseline station. The site and conditions appear to be excellent for atmospheric background monitoring activities, and when fully equipped and staffed as currently envisioned, this observatory can become a first-class facility.

From September 21 to 28, P. Bakwin visited László Haszpra, Hungarian Meteorological Service, to determine the feasibility of using an existing television transmitter tower as a platform for trace gas monitoring. The trip was sponsored by the U.S. Hungarian Joint Fund. Three towers were considered and inspected: Tokaj in northwest Hungary, Komádi in western Hungary near the Romanian border, and Hegyhátsál, 7 km southwest of Körmen.

In October, E. Dlugokencky visited Prof. Y.S. Chung at the Korean National University of Education (KNUE) and the CMDL flask sampling network site at Tae-ahn Peninsula, Korea. Seminars were given at KNUE and for the Department of Oceanography, College of Natural Sciences, Seoul National University. Discussions were held with Prof. Chung on joint publication results of collaborative air sampling.

Two sets of three cylinders each containing CO₂ standard gases (341, 348, 375 ppm) were provided by NIST for international "round robin" intercomparisons. Both sets were analyzed by NIST and the CMDL Carbon Cycle Division prior to starting the circuits. Set A was circulated among European laboratories in Germany, France, Spain (Canary Islands), Italy, and Hungary. Set B was sent to the U.S. (SIO), Canada, Japan, New Zealand, and Australia. Altogether, 16 laboratories in 10 countries participated. J. Peterson acted as referee for the experiment.

E. Dlugokencky and P. Lang conducted comparisons with two laboratories in 1992. A standard prepared at Niwot Ridge, Colorado, in 1988 and calibrated periodically in Boulder, was used for both experiments. During July and August, the cylinder was sent to the Geochemical Research Laboratory, Meteorological Research Institute (Japan), and in September, to the Atmospheric Environment Service (Canada).

P. Novelli conducted intercomparisons of standards with the Fraunhofer Institute, Garmisch, Germany. Six mixtures in the 50-200 ppb range made in Boulder by the NOAA Division [Novelli, *et al.*, 1991] were used. The results of five calibrations agreed to within 3%; the sixth standard agreed to within 5%. This project was carried out over a 2-year period. An experiment involving eight laboratories will be next in this series.

In January, D. Hofmann and F. Polacek III, conducted correlative water vapor and aerosol balloon flights in support of the NASA UARS program at Lauder, New Zealand. The aerosol and water-vapor measurement data from these balloon flights were presented at a meeting (June 27-July 3) in Aix-en Provence, France, sponsored by the NASA Upper Atmosphere Research Satellite (UARS) Correlative Measurement program. S. Oltmans and D. Hofmann attended the Aix-en-Provence meeting, where S. Oltmans presented a paper and participated in the Investigators Workshop and Science Team Meeting. D. Hofmann presented the aerosol data. After the meeting, D. Hofmann participated in cooperative atmospheric research involving the effects on the stratosphere of the Mt. Pinatubo eruption with colleagues at the Institute for Atmospheric Environmental Research in Garmisch, Federal Republic of Germany.

D. Hofmann returned to Lauder in May to participate in a joint meeting with scientists from the NOAA Aeronomy Laboratory and six other research groups in an international intercomparison of nitrogen dioxide measurement instruments. Again in November, D. Hofmann traveled to Lauder, New Zealand, to conduct water vapor and aerosol balloon flights in support of the NASA UARS program.

B. Bodhaine, J. Ogren, and J. Wendell spent 2 weeks in August setting up an aerosol monitoring station at the Canadian Atmosphere Environment Services station on Sable Island, Nova Scotia. Sable Island is a remote site and all the instrumentation that was installed had to be shipped by boat and unloaded to a beach without a dock on motorized rubber rafts. The measurements recorded so far at Sable Island reveal it to be an excellent site for obtaining data of aerosols affected by polluted areas. J. Ogren traveled to Montreal, Canada, to attend the 11th International Conference on Clouds and Precipitation to present a paper. At that time, he also participated in the meeting of the executive committee of the International Commission on Clouds and Precipitation.

In January, J. Ogren was invited to the University of Stockholm where he presented a seminar "Measurements of the size-dependence of the scavenging efficiency of aerosol

particles by fog droplets." He also worked on evaluation of aerosol and cloud chemical and microphysical measurements obtained during a 1990 field experiment in Germany.

In August, S. Oltmans was invited to Wolfville, Canada, by the NATO Scientific Affairs Division to attend the NATO Advanced Research Workshop on Tropospheric Chemistry of Ozone in the Polar Regions where he presented a paper. In September, he traveled to Heimaey on the Westman Islands of Iceland to set up an ozone monitor. Further, he serviced and calibrated the ozone monitor at Reykjavik, Iceland.

J. Eason of the Australian Bureau of Meteorology and T. Uebuko of the Japanese Aerological Observatory visited Boulder in June and July to calibrate their respective country's secondary standard Dobson spectrophotometers relative to World Primary Standard Dobson Instrument 83. During the summer of 1992, an Argentine Dobson instrument was received in Boulder for repair and calibration.

A program to check on the calibration status of Dobson spectrophotometers throughout the world by means of traveling calibrated standard lamps was continued. This is the third such international activity conducted since the program was first implemented in 1981.

To use CFC tracers to determine the ocean circulation and age of water mass, J.M. Lobert, J.H. Butler, and T.J. Baring participated in the World Ocean Circulation Experiment (WOCE-16) starting from Long Beach, California, on August 4 and ending at Noumea, New Caledonia, on October 22 (see Figure 5.20).

J.W. Elkins, T.J. Baring, G.A. Holcomb, T.M. Gilpin, J.H. Butler, T.M. Thompson, and W.T. Sturges participated on the continuation in 1992 of the NASA Airborne Arctic Stratospheric Expedition II (AASE II) based out of Bangor, Maine. The purpose of the participation was to continue to measure CFC-11 and -113 using the ACATS instrument, aboard the NASA ER-2 aircraft for the January through March polar mission. The science investigators included scientists from Canada, United Kingdom, Australia, New Zealand and Iceland.

9. Publications and Presentations by CMDL Staff, 1992

- Barrie, L.A., B.A. Bodhaine, R.C. Schnell, G.A. Shaw, and J.K. McKie, Symposium on the Tropospheric Chemistry of the Antarctic Region, *Tellus*, 44B, 250-251, 1992.
- Bodhaine, B.A., and J.M. Harris, Aerosol measurements at the South Pole during 1987, *NOAA DR ERL CMDL-9*, 120 pp., 1992.
- Bodhaine, B.A., J.M. Harris, J.A. Ogren, and D.J. Hofmann, Aerosol optical properties at Mauna Loa Observatory: Long-range transport from Kuwait? *Geophys. Res. Lett.*, 19(6), 581-584, 1992.
- Butler, J.H., Calculation of air-sea transfer velocity from anthropogenic halocarbon distributions in the surface oceans, paper presented at Biogeochemical Ocean-Atmosphere Transfer, NATO Advanced Research Workshop, Bermuda, January 27-31, 1992.
- Butler, J.H., The ocean as a source of atmospheric N₂O, paper presented at the American Society for Limnology and Oceanography Aquatic Sciences Meeting, Santa Fe, NM, February 9-14, 1992.
- Butler, J.H., J.W. Elkins, B.D. Hall, S.O. Cummings, and S.A. Montzka, A decrease in the growth rates of atmospheric halon concentrations, *Nature*, 359, 403-405, 1992.
- Cahill, T.A. K. Wilkinson, and R.C. Schnell, Compositional analyses of size-resolved aerosol samples taken from aircraft down wind of Kuwait, Spring 1991, *J. Geophys. Res.*, 97(D13), 14,513-14,520, 1992.
- Cantrell, C.A., J.A. Lind, R.E. Shetter, J.G. Calvert, P.D. Goldan, W. Kuster, F.C. Fehsenfeld, S.A. Montzka, D.D. Parish, E.J. Williams, M.P. Buhr, H.H. Westberg, G. Allwine, and R. Martin, Peroxy radicals in the ROSE experiment: measurement and theory, *J. Geophys. Res.*, 97(D18), 20,671-20,686, 1992.
- Charlson, R.J., S.E. Schwartz, J.M. Hale, R.D. Cess, J.A. Coakley, Jr., J.E. Hansen, and D.J. Hofmann, Climate forcing by anthropogenic aerosols, *Science*, 255, 423-430, 1992.
- DeFoor, T.E., S. Ryan, J.J. DeLuisi, E. Dutton, D.J. Hofmann, P.B. Russell, and J.M. Livingston, A comparison of El Chichon and Mt. Pinatubo stratospheric aerosols as measured at Mauna Loa Observatory, paper presented at the AGU Chapman Conference on Climate Volcanism and Global Change, Hilo, Hawaii, March 1992.
- DeFoor, T.E., E. Robinson, and S. Ryan, Early lidar observations of the June 1991 Pinatubo eruption plume at Mauna Loa Observatory, Hawaii, *Geophys. Res. Lett.*, 19(2), 187-190, 1992.
- DeLuisi, J.J., J. Wendell, and F. Kreiner, An examination of the spectral response characteristics of seven Robertson-Berger meters after long-term field use, *Photochem. Photobio.*, 56(1), 115-122, 1992.
- Deshler, T., and D.J. Hofmann, Measurements of unusual aerosol layers in the upper troposphere over Laramie, Wyoming, in the spring of 1991: Evidence for long-range transport from the oil fires in Kuwait, *Geophys. Res. Lett.*, 19(4), 385-388, 1992.
- Deshler, T., D.J. Hofmann, B.J. Johnson, and W.R. Rozier, Balloonborne measurements of the Pinatubo aerosol size distribution and volatility at Laramie, Wyoming during the summer of 1991, *Geophys. Res. Lett.*, 19(2), 199-202, 1992.
- Deshler, T., A. Adriani, G.P. Gobbi, D.J. Hofmann, G. DiDonfrancesco, and B.J. Johnson, Volcanic aerosol and ozone depletion within the Antarctic polar vortex during the austral spring of 1991, *Geophys. Res. Lett.*, 19(18), 1819-1822, 1992.
- DeLuisi, J.J., K. Dehne, R. Vogt, T. Konzelmann, and A. Ohmura, First results of the Baseline Surface Radiation Network (BSRN) broadband infrared radiometer intercomparison at Fire II, in *IRS '92*, S. Keevallik and O. Kärner (Eds.), Deepak, Hampton, VA, 559-564, 1992.
- Dlugokencky, E.J., and A.R. Ravishankara, Laboratory measurements of direct ozone loss on ice and doped-ice surfaces, *Geophys. Res. Lett.*, 19(A), 41-44, 1992.
- Dutton, E.G., and J.R. Christy, Solar radiative forcing at selected locations and evidence for global lower tropospheric cooling following the eruptions of El Chichon and Pinatubo, *Geophys. Res. Lett.*, 19(23), 2313-2316, 1992.
- Elkins, J.W., Flying high into the Arctic stratosphere: CFC measurements from a spy plane, after dinner speech at the CMDL Annual Meeting, Boulder, CO, March 4, 1993.
- Elkins, J.W., Slowdown of the atmospheric growth rates of CFC-11 and CFC-12: The result of the Montreal Protocol, paper presented at the Center for Analytical Chemistry Seminar, NIST, Gaithersburg, MD, June 4, 1992.
- Elkins, J.W., Distributions of two chlorofluorocarbons in the polar and mid-latitude stratosphere from August 1991 through March 1992, invited talk for the NOAA Aeronomy Laboratory Seminar, Boulder, CO, October 21, 1992.
- Elkins, J.W., Slowdown of the atmospheric growth rates of CFC-11 and CFC-12: The result of the Montreal Protocol, paper presented at the Center for Analytical Chemistry Seminar, NIST, Gaithersburg, MD, June 4, 1992.
- Elkins, J.W., J.H. Butler, S.A. Montzka, J.M. Lobert, and W.T. Sturges, The impact of the ocean on atmospheric methyl bromide, paper presented at the Methyl Bromide Workshop sponsored by the Methyl Bromide Global Coalition, Arlington, VA, June 2-3, 1992.
- Elkins, J.W., D.W. Fahey, T.M. Gilpin, M.H. Proffitt, S. Solomon, M. Loewenstein, C.R. Webster, and K.R. Chan, Fast response CFC-11 and CFC-113 measurements from the NASA ER-2 aircraft during AASE-II, paper presented at the NASA High-Speed Research Project (HSRP) Meeting, Virginia Beach, VA, May 18-22, 1992.
- Elkins, J.W., D.W. Fahey, S. Solomon, W.H. Pollock, L.E. Heidt, T.M. Gilpin, C.R. Webster, R.D. May, M. Loewenstein, A. Weaver, J.R. Podolske, K.R. Chan, S.C. Wofsy, and R.J. Salawitch, The evolution of the total organic and inorganic chlorine in the Arctic polar stratospheric vortex, poster presentation at the Fall American Geophysical Union Meeting, San Francisco, CA, December 10, 1992.
- Facchini, M.C., S. Fuzzi, M. Kessel, W. Wobrock, W. Jaeschke, B.G. Arends, J.J. Möls, A. Berner, I. Solly, C. Kruisz, G. Reischl, S. Pahl, A. Hallberg, J.A. Ogren, H. Fierlinger-Oberlinninger, A. Marzorati, and D. Schell, The chemistry of sulfur and nitrogen species in a fog system—a multiphase approach, *Tellus*, 44B, 505-521, 1992.
- Fahey, D., J.W. Elkins, T.M. Thompson, R.C. Myers, J.H. Butler, W.C. Kuster, T.L. Thompson, R.H. Winkler, S.A. Montzka, T.M. Gilpin, T.J. Baring, G.A. Holcomb, W.T. Sturges, J.M. Lobert, and B.D. Hall, The distribution of CFC-11 and CFC-113 in the Arctic polar stratospheric vortex, poster presentation at the Fall American Geophysical Union Meeting, San Francisco, December 9, 1992.
- Ferguson, E.E., A personal history of the early development of the flowing afterglow technique for ion-molecule reaction studies, *J. Am. Soc. Mass Spectrom.*, 3, 479-486, 1992.
- Ferguson, E.E., and R.M. Rosson (eds.), *Climate Monitoring and Diagnostics Laboratory No. 20 Summary Report 1991*, 131 pp., NOAA Environmental Research Laboratories, Boulder, CO, 1992.

- Ferguson, E.E., J.M. Van Doren, A.A. Viggiano, R.A. Morris, J.F. Paulson, J.D. Stewart, L.S. Sunderlin, and P.B. Armentrout, Internal and translational energy effect on the charge-transfer reaction of CO_2^+ with O_2 , *Int. J. Mass Spectrom. Ion Proc.*, 117, 261-282, 1992.
- Fiocco, G., M. Cacciani, P. DiGirolamo, D. Fuà, and J. DeLuisi, Stratospheric clouds at South Pole during 1988, 1, Results of lidar observations and their relationship to temperature, *J. Geophys. Res.*, 97(D5), 5939-5946, 1992.
- Foster, J.L., J.W. Winchester, and E.G. Dutton, The date of snow disappearance on the Arctic tundra as determined from satellite, meteorological station and radiometric in situ observations, *IEEE Transactions on Geoscience and Remote Sensing*, 30(4), 793-798, 1992.
- Fuzzi, S., C. Facchini, G. Orsi, J.A. Lind, W. Wobrock, M. Kesel, R. Maser, W. Jaeschke, B.G. Arends, A. Berner, I. Solly, C. Kruisz, G. Reischl, U. Kaminski, P. Winkler, J.A. Ogren, A. Hallberg, H. Fierlinger-Oberlininger, H. Puxbaum, A. Marzorati, H.-C. Hansson, A. Wiedensohler, I.B. Svenningsson, B.G. Martinsson, D. Schell, and H.W. Georgii, The Po Valley fog experiment 1989: an overview, *Tellus*, 44B, 448-468, 1992.
- Hahn, C.J., J.T. Merrill, and B.G. Mendonca, Meteorological influences during MLOPEX, *J. Geophys. Res.*, 97(D10), 10,291-10,309, 1992.
- Hallberg, A., J.A. Ogren, K.J. Noone, J. Heintzenberg, A. Berner, I. Solly, C. Kruisz, G. Reischl, S. Fuzzi, C. Facchini, H.-C. Hansson, A. Wiedensohler, and I.B. Svenningsson, Phase partitioning for different aerosol species in fog, *Tellus*, 44B, 545-555, 1992.
- Hansen, A.D.A., R.C. Schnell, A.V. Polissar, and G.S. Golitsyn, Aerosol measurements over the East Siberian Sea, paper presented at the 5th Symposium on Arctic Air Chemistry, Copenhagen, Denmark, September 8-10, 1992.
- Harris, J.M., An analysis of 5-day midtropospheric flow patterns for the South Pole: 1985-1989, *Tellus*, 44B, 409-421, 1992.
- Harris, J.M., P.P. Tans, E.J. Dlugokencky, K.A. Masarie, P.M. Lang, S. Whittlestone, and L.P. Steele, Variations in the atmospheric methane at Mauna Loa Observatory related to long-range transport, *J. Geophys. Res.*, 97(D5), 6003-6010, 1992.
- Harriss, R.C., G.W. Sachse, G.F. Hill, L. Wade, K.B. Bartlett, J.E. Collins, L.P. Steele, and P.C. Novelli, Carbon monoxide and methane in the North American Arctic and subarctic troposphere: July-August 1988, *J. Geophys. Res.*, 97(D15), 16,589-16,599, 1992.
- Hofmann, D.J., and S.J. Oltmans, The effect of stratospheric water vapor on the heterogeneous reaction rate of ClONO_2 and H_2O for sulfuric acid aerosol, *Geophys. Res. Lett.*, 19(22), 2211-2214, 1992.
- Hofmann, D.J., E.F. Ferguson, P.V. Johnston, and W.A. Matthews, Tropospheric ozone variation in the Arctic during January 1990, *Planet. Space Sci.*, 40, 203-210, 1992.
- Hofmann, D.J., S.J. Oltmans, J.M. Harris, S. Solomon, T. Deshler, and B.J. Johnson, Observation and possible causes of new ozone depletion in Antarctica in 1991, *Nature*, 359, 283-287, 1992.
- Hubler, G., D.D. Montzka, R.B. Norton, P.C. Murphy, F.C. Fehsenfeld, S.C. Liu, B.A. Ridley, J.G. Walega, E. Atlas, F.E. Grahek, L.E. Heidt, J. Merrill, B.J. Huebert, and B.A. Bodhaine, Total reactive oxidized nitrogen (NO_y) in the remote Pacific troposphere and its correlation with O_3 and CO: Mauna Loa Observatory Photochemistry Experiment 1988, *J. Geophys. Res.*, 97, 10,427-10,447, 1992.
- Kahl, J.D., M.C. Serreze, and R.C. Schnell, Tropospheric low-level temperature inversions in the Canadian Arctic, *Atmos.-Ocean*, 39(4), 511-529, 1992.
- Kahl, J.D., M.C. Serreze, S. Shiotani, S.M. Skony, and R.C. Schnell, In situ meteorological sounding archives for Arctic studies, *Bull. Am. Meteorol. Soc.*, 73(11), 1824-1830, 1992.
- Kahl, J.D., D.J. Charlevoix, R.C. Schnell, and N.A. Zaitseva, Lower tropospheric temperature trends over the Arctic Ocean: 1950-1990, *Preprints, Third Conference on Polar Meteorology and Oceanography*, Portland, OR, September 29-October 2, 1992, pp.141-144, American Meteorological Society, Boston, 1992.
- Lang, P.M., L.P. Steele, L.S. Waterman, R.C. Martin, K.A. Masarie, and E.J. Dlugokencky, NOAA/CMDL atmospheric methane data for the period 1983-1990 from shipboard flask sampling, *NOAA TM ERL CMDL-4*, 88 pp., 1992.
- Luria, M., J.F. Boatman, J.M. Harris, J. Ray, T. Straube, J. Chin, R.L. Gunter, G. Herbert, T.M. Gerlach, and C.C. Van Valin, Atmospheric sulfur dioxide at Mauna Loa, Hawaii, *J. Geophys. Res.*, 97(D5), 6011-6022, 1992.
- Mateer, C.L., and J.J. DeLuisi, A new Umkehr inversion algorithm, *J. Atmos. Terr. Phys.*, 54(5), 537-556, 1992.
- Martinsson, B.G., E. Swietlicki, H.-C. Hansson, A. Wiedensohler, K.J. Noone, J.A. Ogren, and A. Hallberg, Elemental composition of fog interstitial particle size fractions and hydrophobic fractions related to fog droplet nucleation scavenging, *Tellus*, 44B, 593-603, 1992.
- Noone, K.J., J.A. Ogren, A. Hallberg, H.-C. Hansson, A. Wiedensohler, and E. Swietlicki, A statistical examination of the chemical differences between interstitial and scavenged aerosol, *Tellus*, 44B, 581-592, 1992.
- Noone, K.J., J.A. Ogren, A. Hallberg, J. Heintzenberg, J. Strom, H.-C. Hansson, B. Svenningsson, A. Wiedensohler, S. Fuzzi, M.C. Facchini, B.G. Arends, A. Berner, Changes in aerosol size- and phase-distributions due to physical and chemical processes in fog, *Tellus*, 44B, 489-504, 1992.
- Novelli, P.C., L.P. Steele, and P.P. Tans, Mixing ratios of carbon monoxide in the troposphere, *J. Geophys. Res.*, 97(D18), 20,731-20,750, 1992.
- Ogren, J., Size-dependent scavenging efficiencies of aerosol particles in a polluted fog, paper presented at the 11th International Conference on Clouds and Precipitation, Montreal, Canada, August 1992.
- Ogren, J.A., and R.J. Charlson, Implications for models and measurements of chemical inhomogeneities among cloud droplets, *Tellus*, 44B, 208-225, 1992.
- Ogren, J.A., K.J. Noone, A. Hallberg, J. Heintzenberg, D. Schell, A. Berner, I. Solly, C. Kruisz, G. Reischl, B.G. Arends, and W. Wobrock, Measurements of the size dependence of the concentration of non-volatile material in fog droplets, *Tellus*, 44B, 570-580, 1992.
- Oltmans, S.J., Balloon water vapor correlative measurements for UARS, paper presented at a meeting sponsored by the NASA Upper Atmosphere Research Satellite (UARS) Correlative Measurement Program, in Aix-en Provence, France, June 27-July 3, 1992.
- Oltmans, S.J., Climatology of Arctic and Antarctic tropospheric ozone, paper presented at the NATO Advanced Research Workshop on Tropospheric Ozone, Wolfville, Canada, August 1992.
- Oltmans, S.J., and H. Levy, II, Seasonal cycle of surface ozone over the western North Atlantic, *Nature*, 358, 392-394, 1992.
- Parungo, F., B. Kopcewicz, C. Nagamoto, R. Schnell, P. Sheridan, Z. Zhu, and J. Harris, Aerosol particles in the Kuwait oil fire plumes: Their morphology, size distribution, chemical composition, transport, and potential effect on climate, *J. Geophys. Res.* 97(D14), 15,867-15,882, 1992.

- Ridley, B.A., and E. Robinson, The Mauna Loa Observatory photochemistry experiment, *J. Geophys. Res.*, 97(D10), 10,285-10,290, 1992.
- Rosen, J., B.A. Bodhaine, J.F. Boatman, J.J. DeLuisi, M.J. Post, Y. Kim, R.C. Schnell, P.J. Sheridan, and D.M. Garvey, Measured and calculated optical property profiles in the mixed layer and free troposphere, *J. Geophys. Res.*, 97, 12,837-12,850, 1992.
- Russell, P.B., R.F. Pueschel, S.A. Kinne, J.M. Livingston, E. Dutton, T. DeFoor, J. Reagan, and M. Box, Pinatubo optical depth spectra; temporal and spatial evolution of inferred particle size, areas and backscatter, with radiative implications, paper presented at the Fall American Geophysical Union Meeting, San Francisco, CA, December 7-11, 1992.
- Ryan, S., and J.F.S. Chin, Quiescent CO₂ outgassing of Mauna Loa volcano, paper presented at the Fall American Geophysical Union Meeting, San Francisco, CA, December 7-11, 1992.
- Savoie, D.L., J.M. Prospero, S.J. Oltmans, W.C. Graustein, K.K. Turekian, J.T. Merrill, and H. Levy II, Sources of nitrate and ozone in the marine boundary layer of the tropical North Atlantic, *J. Geophys. Res.*, 97(D11), 11,575-11,589, 1992.
- Schnell, R.C., G.A. Allen, and A.D.A. Hansen, Black carbon aerosol output from a photocopier, *Proceedings, 85 Annual Meeting and Exhibition*, June 21-26, Kansas City, Kansas, 9 pp., Air and Waste Management Association, Pittsburgh, PA, 1992.
- Schnell, R.C., E. Dlugokencky, T.J. Conway, A. Polissar, and G.S. Golitsyn, Airborne investigation of the Bennett Island plume, *Proceedings, 5th Symposium on Arctic Air Chemistry*, Copenhagen, Denmark, September 8-10, 1992.
- Serreze, M.C., J.A. Maslanik, R.S. Stone, and R.C. Schnell, Predicted heights of buoyant convection above leads in the winter Arctic pack ice cover, *Preprints, Third Conference on Polar Meteorology and Oceanography*, Portland, OR, September 29-October 2, 1992, pp. J45-J48, American Meteorological Society, Boston, 1992.
- Sheridan, P.J., R.C. Schnell, D.J. Hofmann, and T. Deshler, Electron microscope studies of Mt. Pinatubo aerosol layers over Laramie, Wyoming during summer 1991, *Geophys. Res. Lett.*, 19(2), 203-206, 1992.
- Sheridan, P.J., R.C. Schnell, and J.D. Kahl, Individual particle analysis of the springtime Arctic aerosol, 1983-1989, *Proceedings, International Conference on the Role of the Polar Regions in Global Change*, June 11-15, 1990, University of Alaska, Fairbanks, edited by G. Well, C.L. Wilson, and B.A.B. Severin, pp. 708-715, Geophysical Institute, Univ. of Alaska Fairbanks and Center for Global Change and Arctic System Research, 1992.
- Sheridan, P.J., R.C. Schnell, D.J. Hofmann, J. M. Harris, and T. Deshler, Electron microscope studies of aerosol layers with likely Kuwaiti origins over Laramie, Wyoming during spring 1991, *Geophys. Res. Lett.*, 19(4), 389-392, 1992.
- Sokolik, I.N., and R. Schnell, Comparison of data on physical properties of Arctic aerosols, *Proceedings, 5th Symposium on Arctic Air Chemistry*, Copenhagen, Denmark, September 8-10, 1992, National Environmental Research Institute, Copenhagen, 1992.
- Steele, L.P., E.J. Dlugokencky, P.M. Lang, P.P. Tans, R.C. Martin, and K.A. Masarie, Slowing down of the global accumulation of atmospheric methane during the 1980s, *Nature*, 358, 313-316, 1992.
- Stone, R.S., J.D. Kahl, M.C. Serreze, and R.C. Schnell, Trend analyses of tropospheric temperatures in the Arctic—Is there evidence of greenhouse warming?, *Preprints, Third Conference on Polar Meteorology*, Portland, OR, September 29-October 20, 1992, American Meteorology Society, Boston, 137-140, 1992.
- Strom, J., J. Heintzenberg, K.J. Noone, K.B. Noone, J.A. Ogren, F. Albers, and M. Quante, CVI measurements on small crystals in cirrus clouds, *Proceedings, 11th International Conference on Clouds and Precipitation*, Montreal, Canada, 1992, International Commission on Clouds and Precipitation, International Assoc. of Met. and Atmos. Physics, Innsbruck, Austria, 471-472, 1992.
- Sturges, W.T., G.F. Cota, and P.T. Buckley, Bromoform emission from Arctic ice algae, *Nature*, 358, 660-662, 1992.
- Svenningsson, I.B., H.-C. Hansson, A. Wiedensohler, J.A. Ogren, K.J. Noone, and A. Hallberg, Hygroscopic growth of aerosol particles in the Po Valley, *Tellus*, 44B, 556-569, 1992.
- Tans, P., U.S. baseline station network, paper presented at the Workshop for Trace Gas Measurements in Both Hemispheres, Aspendale, Australia, March 10-13, 1992.
- Walega, J.G., B.A. Ridley, S. Madronich, F.E. Grahek, J.D. Shetter, T.D. Sauvain, C.J. Hahn, J.T. Merrill, B.A. Bodhaine, and E. Robinson, Observations of peroxyacetyl nitrate, peroxypropionyl nitrate, methyl nitrate, and ozone during the Mauna Loa Observatory photochemistry experiment. *J. Geophys. Res.*, 97(D10), 10,311-10,330, 1992.
- Whittlestone, S., E. Robinson, and S. Ryan, Radon at the Mauna Loa Observatory: Transport from distant continents, *Atmos. Environ.* 26A(2), 251-260, 1992.
- Yamato, M., Y. Iwasaka, R.C. Schnell, P.J. Sheridan, M. Nishikawa, T. Mizoguchi, and N. Nakai, Chemical composition and physical characteristics of aerosols in the smoke plume from the Kuwaiti oil fires, *Proceedings, Japan Meteorological Society, Annual Meeting, Tokyo, Japan*, October 23-25, 1991, Japan Met. Soc., Tokyo, 121-122, 1992.

10. Acronyms and Abbreviations

AASE	Airborne Arctic stratospheric Expedition
ACATS	Airborne Chromatograph for Atmospheric Trace Species
AEROCE	Atmosphere/Ocean Chemistry Experiment
AEC	Atomic Energy Commission
AES	Atmospheric Environment Service, Canada
AGASP	Arctic Gas and Aerosol Sampling Program
AGL	above ground level
AL	Aeronomy Laboratory, Boulder, Colorado (ERL)
ALE/GAGE	Atmospheric Lifetime Experiment/Global Atmospheric Gases Experiment
AMIE	Automated Methane Instrument Evaluation
ANSTO	Australian Nuclear Science and Technology Organization
AOML	Atlantic Oceanographic and Meteorological Laboratory, Miami, Florida (ERL)
ARL	Air Resources Laboratory, Silver Spring, Maryland (ERL)
ARM	Atmospheric Radiation Measurement program
ASA	Antarctic Support Associates, Inc.
ASASP	Active Scattering Aerosol Spectrometer Probe
ASCII	American Standard Code For Information Interchange
ASL	above sea level
ASR	aerosol solar radiation
ATS	Application Technology Satellite
ATMOS	Atmospheric Trace Molecule Spectroscopy
BAO	Boulder Atmospheric Observatory
BC	black carbon
BSRN	Baseline Surface Radiation Network
BRW	Barrow Observatory, Barrow, Alaska (CMDL)
CAF	Clean Air Facility
CAMS	Control and Monitoring System
CART	Cloud And Radiation Testbed
CFC	chlorofluorocarbon
CFC-11	trichlorofluoromethane
CFC-12	dichlorodifluoromethane
CGO	Cape Grim, Tasmania, baseline station
CIRES	Cooperative Institute for Research in Environmental Sciences, University of Colorado, Boulder
CMDL	Climate Monitoring and Diagnostics Laboratory (ERL)
CN	condensation nuclei
CNC	condensation nucleus counter
CSIRO/DAR	Commonwealth Scientific and Industrial Research Organization/Division of Atmospheric Research, Australia
CSU	Colorado State University, Fort Collins, Colorado
DB	direct-beam [irradiance]
DEW	distant early warning
DMS	dimethyl sulfide
DOE	Department of Energy
DOY	day of year
DU	Dobson units
ECC	electrochemical concentration cell
ECD	electron capture detector
EC-GC	electron capture-gas chromatograph
ECMWF	European Center for Medium-Range Weather Forecasts
EML	Environmental Measurements Laboratory
ENSO	El Niño/Southern Oscillation
EPA	Environmental Protection Agency

ERL	Environmental Research Laboratories, Boulder, Colorado (NOAA)
FID	flame ionization detector
FPD	flame photometric detector
FRLAB	Front Range Lidar, Aircraft, and Balloon experiment
FSSP	Forward Scattering Spectrometer Probe
FTIR	Fourier transform infrared (spectroscopy)
FW	filter wheel
GAGE	Global Atmospheric Gases Experiment
GC	gas chromatograph
GCRP	Global Climate Change Program
G.E.	General Electric
GMT	Greenwich Mean Time
GONG	Global Oscillation Network Group
GR	growth rate
GSA	General Services Administration
HAO	High Altitude Observatory
HCFC	hydrochlorofluorocarbon
HFC	hydrofluorocarbon
HP	Hewlett-Packard
HST	Hawaii standard time
INSTAAR	Institute for Arctic and Alpine Research, University of Colorado, Boulder
IR	infrared
ISWS	Illinois State Water Survey
LAN	local area network
LEADEX	Leads Experiment
LEAPS	Low Electron Attachment Potential Species
LES	Lincoln Experimental Satellite
LPM	liters per minute
LST	local standard time
MAKS	Martin and Kitzis Sampler (portable air sampler)
MASC	Mountain Administration Support Center (NOAA)
MLO	Mauna Loa Observatory, Hawaii (CMDL)
MLOPEX	MLO Photochemical Experiment
MRI	Meteorology Research, Inc.
MS	mass spectrometer
MSL	mean sea level
NADP	National Atmospheric Deposition Program
NARL	National Arctic Research Laboratory, Barrow, Alaska
NASA	National Aeronautics and Space Administration
NAVSWC	Naval Surface Warfare Center, Department of Defense
NCAR	National Center for Atmospheric Research
NDSC	Network for the Detection of Stratospheric Change
NDIR	non-dispersive infrared analyzer
NIP	normal incidence pyrheliometer
NOAA	National Oceanic and Atmospheric Administration (U.S. Department. of Commerce)
NOAH	Nitrous Oxide And Halocarbons Division (CMDL)
NSF	National Science Foundation
NWR	Niwot Ridge, Colorado
NWS	National Weather Service
OAXTC	Ocean Atmosphere Exchange of Trace Compounds
OGIST	Oregon Graduate Institute of Science and Technology
OH	hydroxyl radical
PBL	planetary boundary layer
PC	personal computer

PMEL	Pacific Marine Environmental Laboratory (ERL)
PMOD	Physikalisch-Meteorologisches Observatorium Davos (World Radiation Center)
QBO	quasi-biennial oscillation
RITS	Radiatively Important Trace Species
RGA	reduction gas analyzer
RSD	residual standard deviation
SBUV	solar backscattered ultraviolet (satellite ozone instrument)
SCS	Soil Conservation Service, Anchorage, Alaska
s.d.	standard deviation
SEAREX	Sea-Air Exchange Experiment
SEASPAN	SEAREX South Pacific Aerosol Network
SIO	Scripps Institution of Oceanography
SMO	Samoa Observatory, American Samoa (CMDL)
SOI	Southern Oscillation Index
SPADE	Stratospheric Photochemistry, Aerosols, and Dynamics Expedition
SPO	South Pole Observatory, Antarctica (CMDL)
SRB	surface radiation budget
SRF	Solar Radiation Facility (CMDL)
SRF	spectral response function
SST	sea-surface temperature
STP	standard temperature and pressure (0° and 1 atm)
TOMS	Total Ozone Mapping Spectrometer
TSI	Thermo Systems Incorporated
UARS	Upper Atmosphere Research Satellite
UCI	University of California, Irvine
UIC	Ukpeaguik Inupiat Corporation
UPS	uninterruptable power supply
URAS	[a commercial CO ₂ analyzer]
URI	University of Rhode Island
USDA	United States Department of Agriculture
USGS	United States Geological Survey
UT	universal time
UV	ultraviolet
UVB	ultraviolet B spectral band
WHOI	Woods Hole Oceanographic Institute
WMO	World Meteorological Organization

